INTELLIGENT CONTROL OF AN INTERIOR PERMANENT MAGNET SYNCHRONOUS MOTOR DRIVE

MOHAMMAD NASIR UDDIN

Intelligent Control of an Interior Permanent Magnet Synchronous Motor Drive

by

© Mohammad Nasir Uddin

A thesis submitted in partial fulfillment
of the requirements for the degree of
Doctor of Philosophy

Faculty of Engineering and Applied Science
Memorial University of Newfoundland

St. John's Newfoundland Canada

October 2000

Abstract

Novel speed control techniques using intelligent computation algorithms for the interior permanent magnet synchronous motor (IPMSM) to be used in high performance drive (HPD) systems are presented. In HPD systems, fast and accurate speed response and quick recovery of speed from any uncertain disturbance are of critical importance. The vector control technique is used in this work to obtain the highest torque response for the IPMSM drive. In the vector control scheme, both the current and the speed controllers play an important role for the drive performance.

In order to select a suitable current controller, a current controlled voltage source inverter (VSI) fed IPMSM drive is developed and implemented in real-time. The performance of various current controllers, particularly hysteresis and ramp comparator controllers for the IPMSM drive, are investigated both theoretically and experimentally. A comparison is also made among the current controller performances for the IPMSM drive.

In this work, the control of the IPMSM over a wide speed range incorporating the flux weakening operation is also presented. The scheme incorporates the maximum torque per ampere operation in the constant torque region and the flux-weakening operation in the constant power region. The performance of this proposed technique is evaluated by simulation results as well as by experimental re-

sults. A comparison between the flux-weakening control technique and the conventional constant flux control scheme is also presented.

An integral part of this work is directed to develop and implement a fuzzy logic controller (FLC) for the IPMSM drive in order to overcome the unknown and/or nonlinear disturbances such as sudden load change, parameter variations, step change of command speed and system noise, etc. A specific FLC for the IPMSM is developed from the motor dynamics and nonlinear load characteristics. The complete vector control scheme incorporating the FLC is successfully implemented in real-time using the digital signal processor (DSP) board DS1102 for the laboratory 1 hp interior type permanent magnet motor. In order to achieve the better switching performance for the current controlled VSI, an insulated gate bipolar transistor (IGBT) inverter module and its associated drive circuits are also built in the Power Research Laboratory of Memorial University of Newfoundland. Numerous tests are carried out for the IPMSM drive at different dynamic operating conditions to evaluate the efficacy of the fuzzy logic controller. The experimental results validate the robustness and hence justify the applicability of the FLC for the IPMSM drive to be used in high performance drive applications. In order to prove the superiority of the FLC over the conventional controllers a comparison between the proposed FLC based system and the conventional proportional-integral (PI) controller-based system is made based on experimental results at different dynamic operating conditions. There is an excellent agreement between the simulated and the experimental results for the FLC based system.

Acknowledgements

I would like to express my most sincere gratitude and appreciation to my supervisor Professor M. Azizur Rahman for his guidance, advice and encouragement throughout of this program. My sincerest thanks to Canadian Commonwealth Scholarship and Fellowship Program for sponsoring me, which provided me the opportunity to pursue my Doctoral Study at Memorial University of Newfoundland. I wish to thank Dr. G. H. George and Dr. S. O' Young, the members of my supervising committee for their useful suggestions. My special thanks go to Dr. T. S. Radwan for helping me to work on the DSP board. I would also like to thank Dr. B. Jeyasurya and Dr. J. Quaicoe for their useful discussions.

I would like to acknowledge the assistance from the School of Graduate Studies, all Faculty members, graduate fellows and staff members especially, Mr. Richard Newman, Mr. Don Guy, Mr. Dennis Johnson, Mr. Tom Pike, Mr. Philip Van Ulden and Mr. Glenn Crewe. My sincere thanks to Dr. Amol Kulkarni, University of Washington, Seattle for his helpful suggestions.

Finally, I express my sincere appreciation to my wife Shahida Pervin, my parents Mr. Md. Arshed Ali and Mrs. Sajeda Arshed, as well as other family members, relatives and friends without whose support and encouragement it would not have been possible to complete this study.

DEDICATED TO:

My Parents ***Mr. Md. Arshed Ali*** and ***Mrs. Sajeda Arshed***

&

My wife ***Mrs. Shahida Pervin***

Contents

List of Figures

List of Symbols

v_a, v_b and v_c	a, b and c, phase voltages, respectively
i_a, i_b and i_c	Actual a, b and c, phase currents, respectively
i_a^*, i_b^* and i_c^*	Command a, b and c, phase currents, respectively
v_d	d-axis voltage
v_q	q-axis voltage
i_d	d-axis current
i_q	q-axis current
r_s	stator resistance per phase
L_d	d-axis inductance
L_q	q-axis inductance
L_l	leakage inductance
L_{md}	d-axis magnetizing inductance
L_{mq}	q-axis magnetizing inductance
ω_s	stator angular frequency
ω_r	actual rotor speed
ω_r^*	motor command speed
$\Delta\omega_r$	error between actual and command speeds
Δe	change of speed errors

θ_r	rotor position
$\theta_r(0)$	initial rotor position
p	differential operator (d/dt)
P	number of pole pairs
ζ	damping ratio
ω_n	undamped natural oscillation
T_e	electromagnetic developed torque
T_L	load torque
J_m	rotor inertia constant
B_m	friction damping coefficient
Ψ_m	magnet flux linkage
V_B	dc bus voltage for the inverter

List of Acronyms

ANN	Artificial neural network controller
BJT	Bipolar junction transistor
BLDC	Brushless dc
DSP	Digital signal processor
FFT	Fast Fourier transform
FLC	Fuzzy logic controller
FWC	Flux-weakening control
HPD	High performance drive
IGBT	Inverted gate bipolar transistor
IPMSM	Interior permanent magnet synchronous motor
MOSFET	Metal-oxide-semiconductor field-effect transistor
MRAC	Model reference adaptive controller
MUN	Memorial University of Newfoundland
PI	Proportional-integral
PID	Proportional-integral-derivative
PM	Permanent magnet
PMSM	Permanent magnet synchronous motor
PWM	Pulse width modulation

RTI	Real-time interface
SMC	Sliding mode controller
STR	Self tuning regulator
THD	Total harmonic distortion
TI	Texas Instruments
VSC	Variable structure controller
VSI	Voltage source inverter

Chapter 1

Introduction

1.1 A General Description of Electric Motors

Conventional direct current (dc), induction and synchronous machines are the three basic electric machines that serve daily needs, from small household appliances to large industrial plants, year after year. The application demand of electric motors is increasing rapidly with increasing technological advancement. Due to increasing demands of electric motors, researchers have been continuing their efforts to develop new machines like the brushless dc (BLDC) machine, the switched reluctance machine, the permanent magnet hysteresis machine and the permanent magnet synchronous machine [1-7]. After developing these new types of special machines, researchers are working on the control of these motors to optimize the design performance and cost. These developmental activities are now in a revolutionary stage due to the recent development of semiconductor and microprocessor technologies.

For many decades, dc motors, particularly separately excited dc motors, have been used extensively for variable speed and high performance drive systems, be-

cause the separately excited dc motor can be controlled in a simple way due to the decoupled nature of its field and armature. However, the dc motor has some disadvantages, which include limited range of speed operation, lack of overload capability, robustness, the frequent maintenance requirement as well as high cost due to brush-gear, and commutators and power loss in the field circuit. Due to these drawbacks of dc motors, researchers have developed ac motors such as induction and synchronous motors to use for high performance variable speed drives, where robustness and maintenance free operations are the main concern. The ac motors are suitable for constant speed operation, but due to recent development of power electronic devices, very large scale integrated (VLSI) technologies and efficient use of microprocessors, ac motors can also be used for variable speed drives. The ac motors can be used for high performance drive (HPD) systems using closed loop vector control techniques [8].

Among the ac motors, induction motors (IM) have been widely used and considered as a workhorse in the industry due to some of their advantageous features like good efficiency, low cost, reliability and ruggedness. However, there are some limitations of the induction motor. One of the limitations is that it always runs at a lagging power factor because the rotor field voltage is induced from the stator side. Another limitation is that the IM drive system is not highly efficient due to slip power loss. As the IM runs at a speed always less than the synchronous speed, the control of these motors is very complex. Moreover, the real time implementation of these motor drives needs accurate estimation of motor parameters and sophisticated modeling with complex control circuitry. Due to the above mentioned limitations, researchers have looked into the synchronous motors for easier control in high performance variable speed drives.

There are some advantages of synchronous motors over the induction motors which are as follows. As the synchronous motor runs at synchronous speed, its control is less complex. It also removes the slip power loss. However, the conventional wire wound excited synchronous motors have some drawbacks such as the requirement of extra power supply, slip ring and brush gears at the rotor side to supply the dc field excitation.

Due to the limitations of the conventional wire-wound synchronous motors, more recently different kinds of special motors have been developed. Among them, the permanent magnet (PM) motor is becoming popular due to some of its advantageous features, which include high torque to current ratio as well as high power to weight ratio, high efficiency, low noise and robustness. Unlike in the wire-wound synchronous motor, the excitation is provided by the permanent magnets in a PM synchronous motor. Thus, there is no need for any extra power supply or field windings. Hence, the cost is reduced and the power loss due to the excitation windings is eliminated.

1.1.1 A general description of PM motors

The development of the PM motor is directly related to the recent achievement in high-energy permanent magnet material like neodymium-boron-iron (Nd-B-Fe), samarium-cobalt (Sm-Co), etc. The fast digital signal processor (DSP) board with built-in interface provisions and artificial intelligent algorithms provide advanced starting and control means for a PM motor drive. Permanent magnets have been used for both the dc and ac motors. In the case of dc motors, PM dc motors are separately excited dc motors with the permanent magnets as the field excitation source. The PM dc motor is widely used in industry for control purposes.

The permanent magnet ac motors are usually considered as synchronous motors according to the operational point of view. Permanent magnet ac synchronous motors are commonly known as PM motors. We can classify the PM motors in different ways. Depending on the position of the magnets on the rotor, the permanent magnet synchronous motors can be broadly classified into three categories: (a) interior type PM synchronous motors, where the permanent magnets are buried within the rotor core; (b) surface mounted type, where the permanent magnets are mounted on the surface of the rotor; and (c) inset type, where the permanent magnets are fully or partially inset into the rotor core [3]. The cross section of interior, surface mounted and inset type PM synchronous motors are shown in Figs. 1.1, 1.2 and 1.3, respectively. Depending on the orientation of the magnets, the PM motors can be classified into three types: (a) radial type, (b) circumferencial type and (c) axial type. For the surface mounted type, the orientation of magnetization is only radial. For the interior and inset types, the orientation of magnetization can be either radial or circumferential. The PM motors shown in Figs. 1.1-1.3 are radial. Depending on the rotor cage winding, the PM motors may be classified as: (a) cageless, where the rotor has no cage winding and (b) cage type, where the rotor is provided with a cage winding. In the case of the cage type motor, the cage winding provides the starting torque and hence this type of motor is capable of self-starting with a rated supply voltage and frequency. To use the motor as a variable speed drive from a controlled voltage source inverter (VSI), the proper control strategy should enable the drive so that the motor can start smoothly up to synchronous speed from standstill. Thus, there is no need of cage winding. Depending on the control strategy, the PM synchronous motors may be classified into two types: (a) brushless dc (BLDC) motor, which is an electronically commutated three-phase

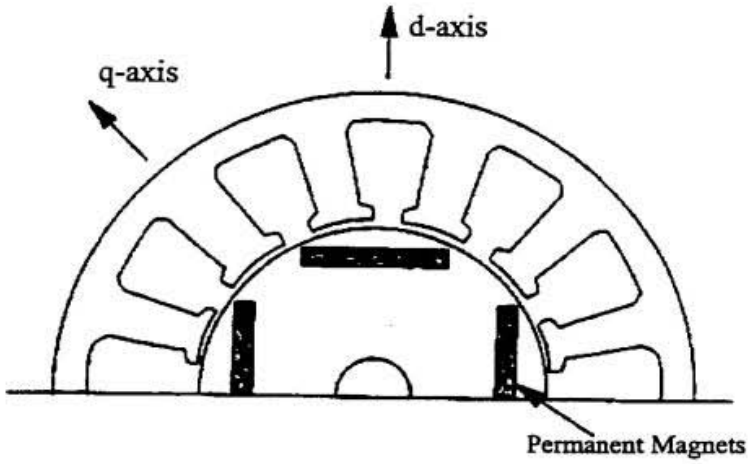

Fig. 1.1 Cross section of the interior type PM motor.

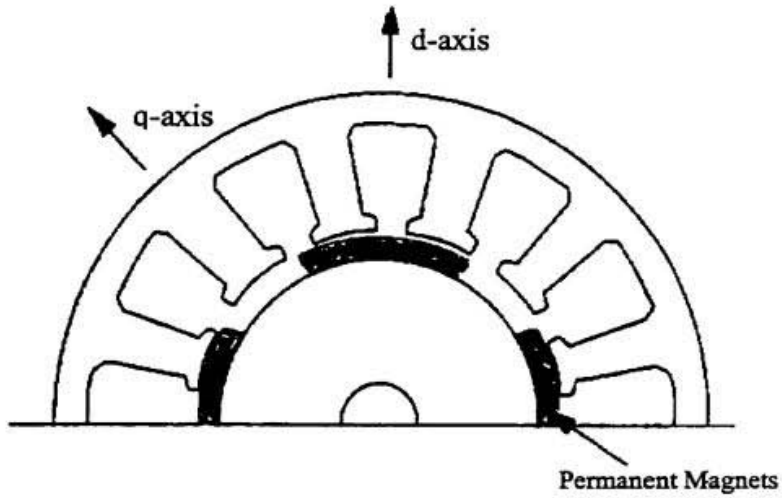

Fig. 1.2 Cross section of the surface mounted type PM motor.

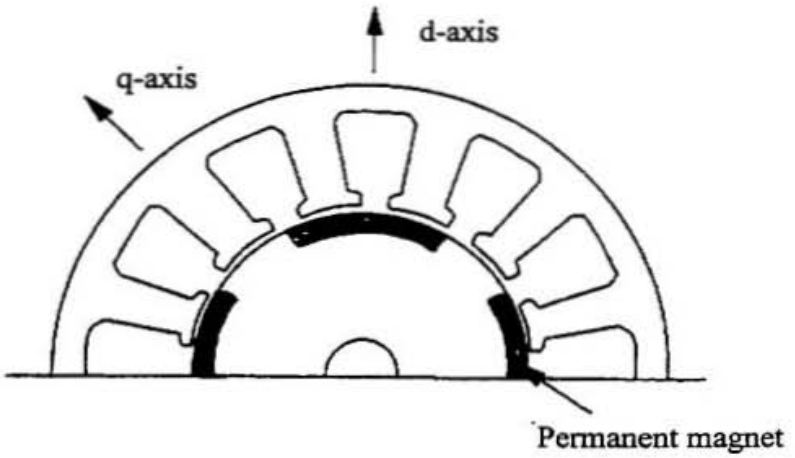

Fig. 1.3 Cross section of the inset type PM motor.

synchronous motor with surface mounted permanent magnet excitation and (b) conventional PM synchronous motor, which is a sinusoidal wave fed PM motor. The BLDC motor is sometimes classified as a brushless PM dc motor. In the case of the brushless dc motor, the induced emf is usually trapezoidal. A discrete position feedback signal is used every 60° electrical and the current is required to be held constant for at least 120° in order to generate a ripple free torque. Brushless dc motors are widely used as the hard disk drive in computers. They are also widely used as precision control motors. In the case of a permanent magnet synchronous motor (PMSM), the induced emf is ideally sinusoidal and it uses continuous rotor positions to force the current in order to generate a ripple free torque. Usually various current controllers like hysteresis, ramp comparator and predictive current controllers are used for pulse width modulated (PWM) control of the PMSM drives. Depending on the use of a sensor, the PM synchronous motor may be classi-

fied as: (a) sensorless and (b) with sensor. In the sensorless scheme, no sensor is used to detect the rotor position but the rotor position is detected by some other techniques such as observer or computation techniques using stator currents, voltages and motor parameters. In the case of the PMSM drive with sensor, the rotor position is continuously detected by the use of an absolute or differential incremental encoder. Hall effect sensors are used to detect the actual currents. It is to be noted that the implementation of a sensorless scheme for the PMSM is difficult because the PMSM needs continuous position detection. This may not always be correct from the computation, as the motor parameters also undergo variation at different steady-state and dynamic operating conditions.

Among the various types of PM motors discussed above, the interior type PM motor with radial magnetization is the most economical to manufacture. Moreover, as the permanent magnets are buried within the rotor core, it provides a smooth rotor surface and reduced air gap. As a result, this type of motor can be used for high speed with quiet operation and better dynamic performance, which are the major concerns for high performance drive systems. In order to take all of these advantages without the lack of generality, the interior permanent magnet synchronous motor (IPMSM) has been considered as a working model in this thesis. The IPMSM saves up to 50% of the energy for split air conditioners. Use of IPMSM for air-conditioner compressor pumps up to 3.7 kW has been the industrial standard of the Japanese air conditioner manufacturers like Mitsubishi, Daiken, Toshiba and Carrier.

In the following section, a review of the existing PMSM drives for high performance applications such as robotics, rolling mills, traction, spindle drives, air compressors and conditioners and machine tools has been given.

1.2 The Current State of PMSM Drive

Due to the increased technological advancements and versatile use of interior permanent magnet synchronous motors (IPMSM), it is essential to develop a robust controller for IPMSM to be used in a high performance drive (HPD) system in order to overcome various uncertainties like sudden change of command speed, abrupt load change and parameter variations. The controllers used in motor drive systems can be broadly classified into three categories such as: (a) fixed gain types, (b) adaptive types and (c) artificial intelligent types. The conventional fixed gain types are proportional-integral (PI), proportional-integral-derivative (PID) and pseudo-derivative-feedback (PDF) controllers. The adaptive types are model reference adaptive controller (MRAC), sliding mode controller (SMC), self tuning regulator (STR) and variable structure controller (VSC). The artificial intelligent types are artificial neural network (ANN) controller, fuzzy logic controller (FLC), and neuro-fuzzy controller. Major reported works on the interior permanent magnet synchronous motor (IPMSM) drive will be briefly discussed below.

1.2.1 PMSM drives with conventional PI, PID and various adaptive controllers

Many researchers have reported their work on the development of high performance IPMSM drives. Basically, the researchers initiated their work during study of the performance of the IPMSM fed by a voltage source or current source inverter. A typical closed loop vector control scheme of the IPMSM is shown in Fig. 1.4. Gumaste and Slemon [9] have proposed a vector control scheme to analyze the steady state performance of a voltage source inverter fed permanent

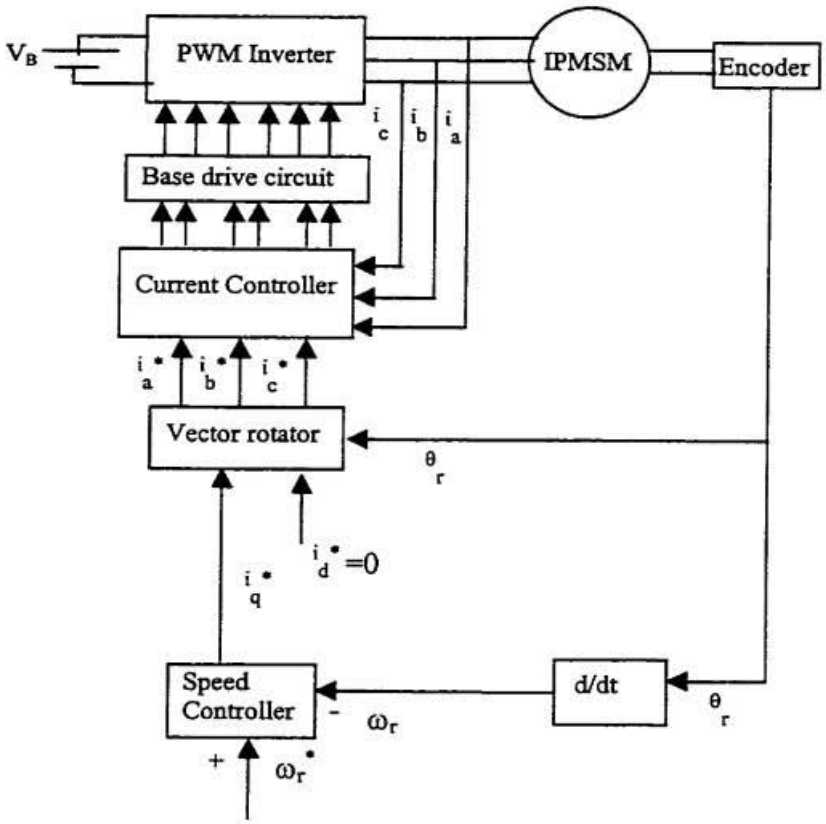

Fig. 1.4. Block diagram of the vector control scheme of the IPMSM drive.

magnet synchronous motor (PMSM) drive. The same authors have reported another similar work on the current source inverter fed PMSM drive [10]. For both schemes they have used a position feedback control from a shaft position sensor so that the inverter can operate in self-control mode. The constant torque mode and the constant power mode operations have been investigated. The control strategies have been developed for torque control. They have suggested removing the damper (cage) winding for the voltage source inverter (VSI) fed PMSM drive in order to operate the motor with stability. The damper winding also provides a path for the flow of harmonic currents induced for non-sinusoidal voltage output of the inverter.

However, for the current source inverter (CSI) fed PMSM drive, the damper windings are helpful in reducing the commutating inductance. An analysis of a PMSM drive supplied from a 180° inverter with phase control provision has been presented by Krause et. al., [11]. In their work, the current is changed by shifting the phase of the applied voltage and thus the average torque is maximized. Phase shifting also provides a means of speed control which should be used in conjunction with pulse width modulation (PWM) control. Liu et. al., [12] have presented a microprocessor-based implementation of the PMSM drive. In this work, the motor is fed by the hysteresis current controlled VSI. They have proposed a method to improve the performance of the current controller at low speed by utilizing the freewheeling period. However, this method reduces the average torque and the performance is not much better. Pillay and Krishnan [13-16] have reported a number of results on modeling, simulation, analysis and the design of controllers for a high performance vector controlled PMSM drive using a state space model. They have investigated the transient and steady state performance of the drive using a d-q axis model of the PMSM. They have also investigated the performance of the hysteresis and ramp comparator controller for the PMSM drive. In these works, a PID type speed controller has been used. To design the speed controller, the authors have used the linear model of the PMSM. But in real time, it is very difficult to predict the performance of the drive accurately using this linear model. The performance of the drive has been limited to a certain command speed. Moreover, because of the PID controller, the performance of the drive is sensitive to the motor parameters and to the load. In another work, Pillay et. al., [17] have proposed a digital signal processor (DSP) based hysteresis current controller scheme for a PMSM drive. They have implemented their scheme using TMS320E15/C15 and TMS320E17/C17 DSPs.

The TMS320E15/C15 has been used to implement the current controller algorithm and the other DSP has been used to implement the vector control algorithm. The performance of the drive is affected due to the slow speed of DSPs. In this work, although the experimental results show the effectiveness of the controller, comprehensive tests of the drive at different dynamic operating conditions have not been done. A look-up table was used to generate the command currents. This is not suitable for a wide range of speed operation. Hence, there is a lack of the robustness of the drive. Bose [18] has reported a high performance inverter fed IPMSM drive system. In this work, a closed loop torque control has been implemented using a feedback torque estimation and taking into accounts the effect of saturation, temperature variations and non-linearity. The drive system has incorporated the constant torque as well as constant power regions. The performance of the drive system has been investigated only for a fixed speed. However, in order to test the efficacy of the drive, it is essential to investigate the performance of the drive over a wide speed range at different dynamic operating conditions. Huy and Dessaint [19] have proposed an adaptive current control scheme for the PM synchronous motor drive. The controller uses two modes, namely hysteresis current control for transient operation and predictive current control for steady state operation. However, the performance of the drive at a low speed condition has not been investigated. Huy et. al., [20] have presented an analysis and implementation of real time predictive current controller for a PM synchronous motor servo drive. High performance can be obtained from this controller but its implementation needs hardware design using an EPROM based approach. The flexibility of this approach is less than the microprocessor-based approach. Bose and Szczesny [21] have proposed a microcontroller based control of an IPMSM drive for electric vehicle propulsion. The

control system incorporates both the constant torque region as well as the constant power region where the flux weakening operation is used. As the drive system has been implemented on a multiprocessor architecture, the system becomes costly and the possibility of fault tolerance is also present.

Jahns et. al., [22] have proposed an adjustable speed drive of IPMSM using a torque control technique. The smooth torque control has been achieved by providing a control of the magnitude and phase angle of the sinusoidal phase currents with respect to the rotor orientation. Although the paper has taken into account the effects of rotor configuration and current regulator saturation, the performance of the drive system has not been investigated over a wide speed range. Moreover the method cannot provide a smooth transition from the constant torque mode to the constant power mode while the motor is in operation. In another work, Jahns [23] has proposed a flux-weakening operation of an IPMSM to investigate the performance of the drive over an extended speed range. In this method, the direct axis rotor current is obtained from the available phase currents of the motor and the d-axis reference current.

Recently, Morimoto et. al., [24-29] have done some work to design and control an IPMSM drive using the flux-weakening control method. They have accounted and compensated for the magnetic saturation and demagnetization effects of permanent magnets to achieve high torque and high efficiency operation within the maximum voltage and current limit of the inverter and the motor. They have studied different control methods such as i_d=0, unity power factor ($\cos \phi = 1.0$) and constant flux linkage control methods. Then a comparison has been made among the various methods. The drive performance has been investigated over a wide speed range. However, all the control schemes use the ramp comparator controller

either in the voltage reference frame or the current reference frame. Regarding the current controlled VSI, this controller has drawbacks such as magnitude and phase errors, especially at high speed operation. In these works, a compensating technique based on the calculated value of q-axis inductance L_q from the actual q-axis current has been used. In order to overcome the effects of saturation, the d-axis command current is generated from the calculated value of L_q. However, in these works the effects of parameter variations due to noise, temperature, etc. are not considered. Therefore the drive system suffers from instability unless an on-line adaptive scheme is incorporated. Rahman et. al. [30] have reported a torque control of the IPMSM drive incorporating the field weakening operation exceeding the speed above the base speed. They have also considered the maximum voltage and current capabilities of the motor and the inverter during motor operation. The performance of the drive has not been investigated for variable speed operation. Vaez et. al. [31] have proposed a vector control strategy of the IPMSM drive to provide a minimum loss operation. They have used a PI controller as a speed controller, which is parameter sensitive. Radwan et. al. [32] have developed an hybrid current controller for the interior permanent magnet synchronous motor drive. In the hybrid controller, they have used the ramp comparator controller for low speed operation and the hysteresis current controller for high speed operation. They have investigated the performances and shown that the controller works very well and is stable. However, the speed controller is a PI controller, which is sensitive to parameter variations, load variations, etc.

Some other investigations [33-36] of the performance of the PMSM drive have also been reported while the flux-weakening method is used. The conventional PI and PID have been used as the speed controller for the PMSM drive for the last few

decades, because of their simplicity and ease to implement in real time. However, these controllers are very sensitive to parameter variations due to saturation, temperature variation, sudden change of command speed, load disturbances and other uncertainties. Moreover, it is very difficult to tune the controller parameters exactly both for on-line and off-line implementations. Therefore, these types of controllers are not always suitable for high performance applications. As a result, researchers [37-44] have developed adaptive control schemes for PMSM drive systems so that the controller can adapt the controller parameters to system parameter variations and load disturbances. The availability of relatively inexpensive and powerful digital signal processors (DSP) has encouraged researchers to apply these adaptive controllers for PMSM drives.

Recently [37-44], adaptive controllers have been used for PMSM drives to achieve fast transient response, parameter insensitivity, nonlinear load handling capability and high adaptability to other types of uncertainties. Among various adaptive schemes, the model reference adaptive controller (MRAC) scheme is one in which the drive forces the response to follow the output of a reference model regardless of the drive parameter changes. MRAC may be used with a PI controller to adapt the controller gains as a compensation to the system parameter changes. It is impossible to adapt the controller gains exactly, so the parameters are adapted by trial and error such that the error between the actual and the desired responses remains within the specified limit. The reference model is designed by considering the worst case system parameters so that the drive can physically track the reference model. Choy et. al., [37] have reported a vector control position servo PMSM drive system using MRAC. In that work, an MRAC controller is used in the outer loop and a PI controller is used in the inner loop. The steady state error gain com-

ponent of the PI controller is used to compensate for the chattering problem that occurs due to discontinuous control inputs. However, this still does not completely rid the drive of the chattering problem. Cerruto et. al., [38] have proposed a model reference adaptive controller based PM motor drive for robotic applications. The MRAC has been used to compensate for variation in such system parameters as the inertia and torque constants. The error between the reference model speed and the actual speed is used to adjust the parameters. However, the proposed model suffers from increased on-line computational burden for increased robustness of the drive.

Sozer and Torrey [39] have proposed an adaptive flux weakening control of the PMSM drive. They have developed an adaptive technique to adjust the d-axis current, i_d. In order to make the scheme adaptive, they have used a direct model reference adaptive controller. They have not demonstrated the response at variable speed conditions. Moreover, they have investigated the response of the drive using simulation only.

There are other types of adaptive controllers namely, sliding mode controller (SMC) and variable structure controller (VSC) which have also been used for the PMSM drive system. Namudri and Sen [40] have proposed an SMC based self-controlled synchronous motor drive system. The scheme uses a vector control strategy for a position servo drive. A phase-controlled chopper and a gate turn-off (GTO) inverter are used for the drive to provide the torque-producing current component. In that work, a controller was designed taking into account the parameter variations and load disturbances.

Consoli and Antonio [41] have proposed a DSP based vector control scheme for an interior PMSM drive using a sliding mode controller for torque control. The simulation results have been presented to investigate the performance of the drive

above the base speed using the field-weakening technique. Both the actual motor currents and the terminal voltages are used as feedback signals to generate the feedback torque and flux. The effects of constant acceleration, constant speed and constant deceleration have been accounted for designing the sliding mode controller. The chattering problem has been reduced by considering a variable bandwidth. However, the drive system has not been investigated in real-time where the unknown and unavoidable parameter variations and the chattering problem exist.

Ghirby and Le-Huy [42] have reported an ac servo drive for PMSM using a variable structure controller (VSC). They have used two control loops: the inner loop is used for predictive current controllers and the outer loop is used for a position or speed controller. The predictive current controller has been used to improve the robustness of the drive. They have implemented the complete system using the digital signal processor TMS320C30. However, the performance of the drive has not been investigated for wide variable speed condition. Moreover, the drive is not completely rid of the chattering problem even in the steady state.

El-Samahy et. al. [43] have proposed high performance tracking control for the brushless dc motor using a self tuning regulator. They have used generalized minimum variance theory for the single layer self-tuning regulator. A multi layer self-tuning regulator consisting of a self-tuning control layer and a supervisory control layer has also been developed. The supervisory control layer continuously monitors the system parameters, the structure of the controller and motor performance.

Sepe and Lang [44] have proposed an adaptive speed control for the PMSM drive system. Their work is very similar to the self-tuning regulator case. The mechanical system parameters of the motor have been estimated in real-time to redes-

ign the gain of the controller. The complete drive system is composed of two loops. The inner loop of the drive system consists of the motor, inverter, current controller, speed controller and filter. The slower outer loop consists of the motor parameter estimator and the control algorithm. They have implemented the complete drive using a Motorola 68020 microprocessor. Because of the computational limitation of the microprocessor, the performance of the drive has been affected. As a result, significant noise is introduced in steady state speed responses.

The adaptive controllers show better performance regarding insensitivity to parameter variations, load disturbances and other uncertainties as compared to the conventional fixed gain PI and PID controllers. However, the major drawback of the adaptive controller is the high computational burden. For real-time implementation, the high computational burden needs large memory space and high speed DSPs or microprocessors, which may not be available. As the number of the system state variables increases, undesirable observation noise also increases. Additionally, almost all of the adaptive controller based systems suffer from chattering, overreaching and steady state errors due to finite switching. Moreover, the unavailability of the exact system mathematical model results in a cumbersome design approach for these types of controllers.

1.2.2 PMSM drives with artificial intelligent controllers

Due to the above mentioned shortcomings of the fixed gain PI, PID and various adaptive controllers, researchers [45-67] have recently looked into the intelligent controllers such as artificial neural network (ANN), fuzzy logic and neuro-fuzzy controllers to handle the unknown and/or nonlinear dynamics of the system, where one parameter depends on the other parameters or the operating conditions.

Intelligent controllers are basically self optimized and adaptive with the system nonlinearity. Intelligent controllers may not need any information about the system nonlinearity. Recently, significant efforts have been made on the use of intelligent algorithms to develop controllers for motor drives. Intelligent controllers are sometimes called artificial intelligence (AI) controllers, as they involve software programming, where the computer will be the interface between the software and the dedicated hardware so that the controller can mimic human thinking.

Some work has already been reported on the use of artificial neural networks (ANNs) for dc motor drives [45-47] and induction motor drives [48-52]. Weerasooriya and El-Sharkawi [45] have developed an ANN based dc motor drive. They have used the back propagation training algorithm. In this work, two types of controller topologies are developed. For both topologies two artificial neural networks are used. However, the investigation is based on simulation results only. In real time, the controller performance may not be acceptable where the motor parameter changes with dynamic operating conditions. Some other works [46-52] have reported the use of the ANN in motor drive systems with the aim of achieving the characteristics of adaptive controllers by exploiting the inherent non-linear input and output mapping property of the ANN.

Recently, researchers have also reported some initial work on the use of artificial neural networks for PMSM drive systems [53-55]. El-Sarkawi et. al., [53], have proposed a high performance brushless dc motor drive using the artificial neural network. They have used a model reference adaptive controller to implement a multi layer neural network. The inputs of the neural network are the estimated speed from the reference model, three consecutive past samples of actual speed, a past sample of the converter input voltage and the error between the reference

model speed and the actual speed. The back propagation algorithm has been used to train the network. Because of off-line training of the ANN, the speed control is not precise and may not be useful for different dynamic operating conditions like load changes, parameter variations and system disturbances. Shigou et. al., [54] have proposed an off-line trained ANN-based digital control of a brushless dc servo motor drive system. In order to obtain better servo performance, they have used an analog speed controller. In this work, they have discussed various training issues for the ANN to be used in the servo drive. However, they have not looked into precise and detailed speed control. Recently, Rahman and Hoque [55] have proposed an on-line adaptive ANN based PMSM drive. The back propagation training algorithm has been used in this work. There are two artificial neural networks: the output of one network is the command signal and the output of the other network is the estimated signal. Depending on the error between the two outputs, the weights and biases are updated. The combined off-line and on-line trainings have been used for the work. In their work, for the complete vector control scheme they used an extra analog circuit to implement the hysteresis current controller, which makes the system more complex and also not reliable for robust operation as compared to the fully digital drive system. Moreover, they took an assumption that the d-axis command current i_d^* is zero, so it is not possible to control the motor above base speed.

In order to obtain a more flexible and effective capability of handling and processing the uncertainties of a complicated and ill-defined nonlinear system like IPMSM, Zadeh [56] proposed a linguistic approach, which introduced the fuzzy set and fuzzy logic theory. Thus, a fuzzy logic controller (FLC) is developed. Human thinking is often qualitative rather than quantitative, involving the ideas like high, low, medium, etc. Presently, researchers [46,57-71] have developed fuzzy logic

controllers for motor drives to mimic human thinking as closely as possible. Some work has already been reported on the use of a FLC for the conventional dc motor [46,57-59], switched reluctance motor [60-62] and induction motor drives [63-67]. In almost all cases, the FLC is used as a speed controller. FLCs show encouraging simulation performances for those drives.

Researchers have just started focusing their work on the use of FLCs for PMSM drive systems [68-71]. Inoue et. al., [68] have proposed a fuzzy algorithm for the brushless dc servo motor drive. The fuzzy algorithm is used to tune the gain of the PI controller with load changes, parameter changes and system disturbances. The actual speed, reference speed and the output of the reference filter are used to generate the membership functions. They have implemented the complete drive using the DSP board ADSP-2101. The experimental results show optimum response after several auto tuning calculations. However, the drive system incorporates a reference generator, the observer and fuzzy interferencers with two PI controllers. This makes the system complex. Hence, the design of the complete system becomes time consuming. Moreover, the system suffers from a high computation burden due to the system complexity.

Erenay et. al., [69] have proposed a fuzzy logic approach for the brushless dc motor drives used in washing machines. They have made a comparison among various controller techniques namely, the conventional PI, fuzzy PI, fuzzy reset rate and fuzzy gain scheduled PI. In this work, the error between the set point and the process output, and the change in error between the present and past samples are used as input linguistic variables, and the control variable is used as the output linguistic variable for a fuzzy logic based algorithm. Triangular membership functions have been used for both the input and output linguistic variables. In the reset rate

technique, a resetting factor whose value is determined by the fuzzy algorithms has been used. In the fuzzy gain scheduled PI controller, fuzzy algorithms have been used to adapt the gains of the PI controller with changing operating conditions. For real time implementation they have used an 8-bit micro-controller, which is not flexible and reliable for high performance drives. They have investigated the speed response only for a fixed speed condition. Because of an excessive computational burden arising from a number of fuzzy rules used in this work, the algorithms may not be useful for a high speed condition where high sampling frequency in real-time is essential. Moreover, in experimental results it is shown that the motor cannot follow the command speed smoothly.

Koviac et. al., [70] have proposed a fuzzy logic based model reference adaptive controller (MRAC) for the PMSM drive. The inputs of the fuzzy logic based adapter are the error between the MRAC output and the actual system output and the change in error between the previous and current samples. The system output consists of reference input, feedback output, and fuzzy adapted output. A linearized model of the PMSM has been used to develop the control algorithm. The simulation results verify the effectiveness of the proposed algorithm, but the algorithm may not be suitable for a real-time application where the motor has nonlinear characteristics, nonlinear load changes and parameter variations that exist with different operating conditions. Moreover, the reference model is parameter dependent. Thus the unavailability of the accurate values of the motor parameters may lead to unstable operation of the system for unknown system behaviours.

Lin et. al. [71] have proposed a position controller for the PMSM using fuzzy neural network controller. However, the fuzzy neural network controller has been used only for making correction of the q-axis command current i_q^*, which is the

output of the IP controller used as a main position controller. Thus, the principal purpose of the FLC is not served as it is used as a secondary controller.

It is found from the above discussions that the recent trends of research are to use artificial intelligent controllers like the ANN, Fuzzy Logic and Neuro Fuzzy algorithms for ac motors used in high performance drive applications. However, the application of FLC has been facing some disadvantages during hardware and software implementation due to its high computational burden [72]. That is why so far the reported works [60-62,64-66] are mainly theoretical and based on simulation results only. Although some works [58,59,63,69,71] are reported with experimental results, these are at low speed conditions due to high computational burden and hence the low sampling frequency. In most cases, the researchers [46,57,58,61,64,66,69] have used FLC to get a control output which is the rate of change of actual output. In order to get the actual output, another integrator has been added following the FLC, which may accumulate the steady-state error. Hence, instability can occur. Previously, it was suggested that the off-line fuzzy logic controller is the effective solution. However, this method has some disadvantages as it depends on the look-up table and, for implementation, it needs standard microprocessors [72].

Although some research work has been reported on the use of ANN in the IPMSM drive [55], the successful real-time application of the fuzzy logic controller for the high performance drive IPMSM system has not yet been reported. Therefore, there exists a need to provide systematic research on the vector control of the IPMSM drive incorporating the FLC. The FLC is used as a speed controller. In a vector control scheme, it is also important to determine the nature of various current controllers for the IPMSM motor drive, as the current controller also plays a

critical role for drive performance. The detailed performance analysis of various current controllers, especially hysteresis with fixed band, sinusoidal band and mixed band, and ramp comparator with conventional and improved controllers, remains unexplored. These kinds of research demand special attention to take advantage of various current controllers. The possibility of combining hysteresis and a ramp comparator in a single controller scheme over the entire range of motor speed needs to be explored in order to overcome the various drive uncertainties such as unknown nonlinear load characteristics, parameter changes and other system disturbances.

1.3 Problem Identification and Thesis Objectives

On the basis of the literature review, it is concluded that the interior type PM synchronous motor possesses many appealing characteristics. It is emerging as one of the most efficient motors in adjustable speed drive applications. The major advantages of the interior permanent magnet synchronous motor (IPMSM) include high torque to inertia ratio, high power to weight ratio, high efficiency, low noise, robustness and high speed operation with better dynamic performance as compared to the conventional ac motors. Fast speed response, quick recovery of speed from unknown and sudden disturbances and insensitivity to parameter variations are some of the main criteria for high performance drive (HPD) systems used in rolling mills, robotics, air conditioners, tractions, spindle drives and machine tools. In spite of the various advantages of the IPMSM, the operation of the motor is strongly affected by the rotor magnetic saliency, saturation and armature reaction effects [73]. Particularly, the saturation of the rotor iron portion around the magnet produces a significant distortion of the air-gap flux that affects the reactance parameters and

hence the performance of the drive at different dynamic and steady-state operating conditions. Therefore, the control of the IPMSM for high performance drive applications needs complex structure and becomes an engineering challenge. The vector control scheme incorporating the speed controller and the current controller is used for the IPMSM drive. This decouples the torque and flux, thus providing faster transient response and making the control task easier. Both the current and the speed controllers play an important role in meeting all the requirements of the HPD systems.

The main emphasis of this work is directed to develop and implement a complete IPMSM drive system for HPD applications. The first objective is to investigate the performance of various current controllers, namely hysteresis and ramp comparator controllers for IPMSM drives at various operating speed conditions. Based on the performances of various current controllers the selection of the current controller has to be made. The second objective is to develop an efficient speed controller for the high performance IPMSM drive.

As discussed in the literature survey, the design of conventional controllers such as fixed gain PI, PID and other adaptive types of controllers, such as the MRAC, VSC, SMC and STR, depend on accurate system model parameters. Moreover, the fixed gain PI and PID controllers are sensitive to parameter variations, load changes and other system disturbances. Intelligent controllers such as the FLC usually do not need any information on the accurate system mathematical model. It can handle non-linearity of arbitrary complexity and it is self-adaptive to uncertainties [56].

Therefore, an integral part of this work is the real time implementation of the IPMSM complete drive incorporating an intelligent controller. As one of such in-

telligent controllers, the FLC is proposed. In this work, based on motor dynamics and nonlinear load characteristics a specific FLC for the IPMSM is developed which removes the integrator and gives the actual output directly. The real-time implementation of the complete vector control scheme of IPMSM incorporating the FLC is carried out using a DSP controller board, DS-1102, through both hardware and software on a laboratory 1 hp interior type permanent magnet motor. The real-time implementation technique used in this thesis overcomes the high computational burden and hence a suitable sampling frequency of 5 kHz is achieved which is adequate for successful real-time implementation. In order to operate the motor above the base speed, the flux weakening operation is also considered in this work. By using this technique, the motor can be used for both constant torque and constant power modes and hence the operating speed range of the motor can be increased significantly.

1.4 Organization of the Thesis

The organization of the remaining chapters of this thesis is as follows. As the current controlled voltage source inverter is one of the main parts of the drive and also plays an important role in drive performance, a new voltage source insulated gate bipolar transistor (IGBT) inverter as well as the base drive circuit have been designed and built at Memorial University of Newfoundland Power Research Laboratory. Details of the IGBT inverter system and the base drive circuit are given in Appendix-C. The performance of various current controllers for the IPMSM drive has been analyzed and a comparison is made in chapter 2. There, special attention is paid to the various hysteresis and ramp comparator controllers. The various hysteresis current controllers are fixed band, sinusoidal band and mixed band

controllers. The various ramp comparator controllers are the conventional and the improved ramp comparator controllers. The systematic mathematical formulations are presented. The experimental implementation incorporating both hardware and software of the complete drive has also been presented in that chapter. DSP based vector control of a laboratory 1 hp IPMSM drive has been successfully implemented and tested. The comparison among various current controllers is based on both theoretical and experimental results. Finally, a hybrid current controller is proposed. The motor parameters used in simulation are given in Appendix-A. The Simulink model used for the complete drive simulation is given in Appendix-B.

The control of the IPMSM over a wide speed range incorporating the flux weakening operation is presented in chapter 3. The scheme includes the maximum torque per ampere operation in the constant torque region (i.e., below the base speed) and the flux-weakening operation in the constant power region (i.e., above the base speed). Finally a comparison between the proposed flux-weakening ($i_d \neq 0$) control technique and the conventional $i_d = 0$ control technique, is made and presented.

The fundamental idea of the FLC related to motor control application is presented briefly in chapter 4. The fuzzy logic includes linguistic variables, membership functions, fuzzification, rule evaluation and defuzzification.

In chapter 5, a novel speed control scheme of the IPMSM drive using a fuzzy logic algorithm is presented. A new specific FLC for the IPMSM drive is developed based on motor dynamics and nonlinear load characteristics. In order to predict the performances of the proposed FLC, an extensive simulation is carried out and the simulation results are presented in this chapter.

In chapter 6, a step-by-step real-time implementation of the complete vector control scheme of the IPMSM incorporating the new FLC is presented. The complete drive is successfully implemented in real-time using a DS1102 DSP board on a prototype 1 hp interior permanent magnet motor. The detailed hardware and software required for real-time implementation are provided in this chapter. Various experimental results of the proposed FLC-based IPMSM drive carried out at different dynamic operating conditions are presented. The experimental results validate the simulations presented in chapter 5. Also, a comparison between the conventional PI controller and the new FLC for the IPMSM drive is made. These have been verified based on experimental results carried out under the same operating conditions. The comparative results show that the FLC is more robust and it is found as a suitable replacement of the conventional controller.

Finally, a summary of the major contributions of this work, suggestions for future study in this area, and the conclusions of this thesis are highlighted in chapter 7. After that all pertinent references and appendices are listed.

Chapter 2

Performance Analysis of Current Controllers for PWM VSI-Fed IPMSM Drive

This chapter presents the development of a complete current-controlled voltage source inverter (VSI) fed IPMSM drive. In the vector control scheme, both the current and the speed controllers play important roles for the drive to follow the command speed accurately at different operating conditions. First, in order to select a suitable current controller for the IPMSM drive to be used in high performance industrial applications, it is important to analyze the performance of various current controllers. The d-q axis model of the IPMSM has been used to analyze the performance of various current controllers for the IPMSM drive. Particularly, attention is paid to the hysteresis current controller and the ramp comparator controller. The various hysteresis current controllers such as the fixed band, sinusoidal band and mixed band controllers, and various ramp comparator controllers such as the con-

ventional and the improved ramp comparator controller have been considered in this work. In order to operate the vector control scheme, a PI type speed controller is used. The real time implementation of the complete drive using a DSP has also been presented in this chapter. The Fast Fourier Transform (FFT) is used to get the frequency spectrum of the experimental current waveforms. A comparison is made among the performances of various current controllers based on both simulation and experimental results. Finally, a hybrid current controller scheme is proposed based on performance analysis of ramp and hysteresis current controllers.

2.1 Mathematical Modeling of IPMSM

The IPMSM is similar to the conventional wire-wound excited synchronous motor with the exception that the excitation is provided by the permanent magnets instead of a wire-wound dc rotor field. Therefore, the d-q axis model of the IPMSM can be derived from the standard model for synchronous machines by removing the equation related to the field current and associated dynamics. The flux linkages in the three-stator phase windings due to the permanent magnets of the rotor are given in matrix form as [74]:

$$\begin{bmatrix} \psi_{am} \\ \psi_{bm} \\ \psi_{cm} \end{bmatrix} = \psi_m \begin{bmatrix} \sin\theta_r \\ \sin\left(\theta_r - \frac{2\pi}{3}\right) \\ \sin\left(\theta_r + \frac{2\pi}{3}\right) \end{bmatrix} \tag{2.1}$$

where ψ_{am}, ψ_{bm} and ψ_{cm} are the a, b and c phase stator flux linkages due to permanent magnet alone, respectively, ψ_m is the constant flux supplied by the permanent magnets and θ_r is the rotor position angle.

The three-phase air gap flux linkage equations are given in matrix form as:

$$\begin{bmatrix}\psi_a\\ \psi_b\\ \psi_c\end{bmatrix}=\begin{bmatrix}L_{aa} & M_{ab} & M_{ac}\\ M_{ba} & L_{bb} & M_{bc}\\ M_{ca} & M_{cb} & L_{cc}\end{bmatrix}\begin{bmatrix}i_a\\ i_b\\ i_c\end{bmatrix}+\psi_m\begin{bmatrix}\sin\theta_r\\ \sin\left(\theta_r-\frac{2\pi}{3}\right)\\ \sin\left(\theta_r+\frac{2\pi}{3}\right)\end{bmatrix} \tag{2.2}$$

where ψ_a, ψ_b and ψ_c are the three-phase air gap flux linkages, L_{aa}, L_{bb}, L_{cc} are the self inductances and M_{ab}, M_{bc}, M_{ca} are the mutual inductances.

Now, the voltage equations of the three phases of the IPMSM can be defined as:

$$v_a = r_a\, i_a + \frac{d\psi_a}{dt} \tag{2.3}$$

$$v_b = r_b\, i_b + \frac{d\psi_b}{dt} \tag{2.4}$$

$$v_c = r_c\, i_c + \frac{d\psi_c}{dt} \tag{2.5}$$

where v_a, v_b, v_c are the three-phase voltages, i_a, i_b, i_c are the three-phase currents and r_a, r_b, r_c are the three-phase stator resistances.

In matrix form Eqn. (2.5) can be written as,

$$\begin{bmatrix}v_a\\ v_b\\ v_c\end{bmatrix}=\begin{bmatrix}r_a & 0 & 0\\ 0 & r_b & 0\\ 0 & 0 & r_c\end{bmatrix}\begin{bmatrix}i_a\\ i_b\\ i_c\end{bmatrix}+p\begin{bmatrix}\psi_a\\ \psi_b\\ \psi_c\end{bmatrix} \tag{2.6}$$

where p is the differential operator, $\frac{d}{dt}$. Equation (2.2) indicates that the flux linkages as well as the machine inductances are functions of rotor position and hence functions of rotor speed. Therefore, the coefficients of the voltage equations are time varying except when the motor is stationary. In order to avoid the complexity of calculations, all the equations have to be transformed to the synchronously rotating rotor reference frame where the machine equations are no longer dependent

on the rotor position. These transformations can be accomplished in two steps using the Park's transformation equations [74]. In the first step, the machine equations are to be transformed from the stationary a-b-c frame into the stationary d-q frame and in the second step, from the stationary d-q frame to the synchronously rotating d^r-q^r frame. The phase variables in terms of d-q variables can be written in matrix form as,

$$\begin{bmatrix} x_a \\ x_b \\ x_c \end{bmatrix} = \begin{bmatrix} \cos\theta_r & \sin\theta_r & 1 \\ \cos\left(\theta_r - \frac{2\pi}{3}\right) & \sin\left(\theta_r - \frac{2\pi}{3}\right) & 1 \\ \cos\left(\theta_r + \frac{2\pi}{3}\right) & \sin\left(\theta_r + \frac{2\pi}{3}\right) & 1 \end{bmatrix} \begin{bmatrix} x_q \\ x_d \\ x_o \end{bmatrix} \tag{2.7}$$

where x_a, x_b and x_c are the a, b and c phase quantities, respectively, x_d, x_q and x_o are the d-axis, q-axis and zero sequence components, respectively. The matrix element x may represent either voltage or current.

Eqn. (2.7) can be written in compact form as,

$$[x_{abc}] = [C]^{-1}\,[x_{qdo}] \tag{2.8}$$

where C is the coefficient matrix.

The corresponding inverse relation can be written as,

$$\begin{bmatrix} x_q \\ x_d \\ x_o \end{bmatrix} = \frac{2}{3} \begin{bmatrix} \cos\theta_r & \cos\left(\theta_r - \frac{2\pi}{3}\right) & \cos\left(\theta_r + \frac{2\pi}{3}\right) \\ \sin\theta_r & \sin\left(\theta_r - \frac{2\pi}{3}\right) & \sin\left(\theta_r + \frac{2\pi}{3}\right) \\ \frac{1}{2} & \frac{1}{2} & \frac{1}{2} \end{bmatrix} \begin{bmatrix} x_a \\ x_b \\ x_c \end{bmatrix} \tag{2.9}$$

or in compact form as,

$$[x_{qdo}] = [C]\,[x_{abc}] \tag{2.10}$$

The rotor position angle θ_r is defined as,

$$\theta_r = \int_0^t \omega_r(t)dt + \theta_r(0) \tag{2.11}$$

Equations (2.7) and (2.9) are both in a stationary reference frame, so θ_r is only the initial rotor position, $\theta_r(0)$, which is also the angle difference between the q-axis and a-phase. For balanced 3-phase, x_o does not exist, and it is also convenient to set $\theta_r(0) = 0$ so that the q-axis coincides with a-phase. Under these conditions Eqns. (2.7) and (2.9) can be written, respectively, as

$$\begin{bmatrix} x_a \\ x_b \\ x_c \end{bmatrix} = \begin{bmatrix} 1 & 0 \\ \frac{-1}{2} & \frac{-\sqrt{3}}{2} \\ \frac{-1}{2} & \frac{\sqrt{3}}{2} \end{bmatrix} \begin{bmatrix} x_q \\ x_d \end{bmatrix} \tag{2.12}$$

and

$$\begin{bmatrix} x_q \\ x_d \end{bmatrix} = \begin{bmatrix} \frac{2}{3} & \frac{-1}{3} & \frac{-1}{3} \\ 0 & \frac{-1}{\sqrt{3}} & \frac{1}{\sqrt{3}} \end{bmatrix} \begin{bmatrix} x_a \\ x_b \\ x_c \end{bmatrix} \tag{2.13}$$

The relative position of the stationary d-q axis and the rotating $d^r - q^r$ axis is shown in Fig. 2.1. Now the quantities in the stationary d-q frame can be converted to the synchronously rotating $d^r - q^r$ frame with the help of Fig. 2.1 as:

$$\begin{bmatrix} x_q^r \\ x_d^r \end{bmatrix} = \begin{bmatrix} \cos\theta_r & -\sin\theta_r \\ \sin\theta_r & \cos\theta_r \end{bmatrix} \begin{bmatrix} x_q \\ x_d \end{bmatrix} \tag{2.14}$$

The inverse relation can be written as,

$$\begin{bmatrix} x_q \\ x_d \end{bmatrix} = \begin{bmatrix} \cos\theta_r & \sin\theta_r \\ -\sin\theta_r & \cos\theta_r \end{bmatrix} \begin{bmatrix} x_q^r \\ x_d^r \end{bmatrix} \tag{2.15}$$

In order to derive the d^r–q^r model of the IPMSM drive, the following assumptions are made:

(a) The eddy current and hysteresis losses are negligible.

(b) The induced emf is sinusoidal.

(c) The saturation is neglected.

(d) The stator resistances of the three phases are balanced.

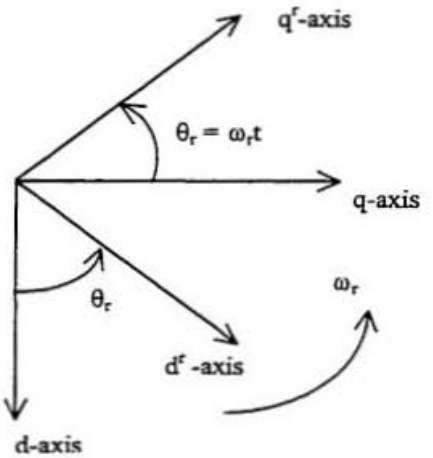

Fig. 2.1 Relative positions of stationary d-q axes and rotating d^r-q^r axes.

With the above assumptions and using Eqns. (2.6), (2.7) and (2.15), the d^r-q^r axis model of the IPMSM can be written as,

$$v_q^r = r_s i_q^r + p\psi_q^r + \omega_s \psi_d^r \tag{2.16}$$

$$v_d^r = r_s i_d^r + p\psi_d^r - \omega_s \psi_q^r \tag{2.17}$$

where v_d^r and v_q^r are d and q axis voltages, i_d^r and i_q^r are d and q axis currents, ψ_d^r and ψ_q^r are d and q axis flux linkages, respectively, r_s is the stator resistance per phase and ω_s is the stator frequency.

ψ_q^r and ψ_d^r can be written as,

$$\psi_q^r = L_q i_q^r \tag{2.18}$$

$$\psi_d^r = L_d i_d^r + \psi_m \tag{2.19}$$

where,

$$L_q = L_l + L_{mq} \tag{2.20}$$

$$L_d = L_l + L_{md} \tag{2.21}$$

L_d and L_q are d and q axis inductances, L_{md} and L_{mq} are d and q axis magnetizing inductances and L_l is the leakage inductance per phase. The stator frequency ω_s is related to the rotor frequency ω_r as,

$$\omega_s = P\omega_r \tag{2.22}$$

where P is the number of pole-pairs. Therefore, Eqns. (2.16) and (2.17) can be re-written as,

$$\begin{bmatrix} v_q^r \\ v_d^r \end{bmatrix} = \begin{bmatrix} r_s + pL_q & P\omega_r L_d \\ -P\omega_r L_q & r_s + pL_d \end{bmatrix} \begin{bmatrix} i_q^r \\ i_d^r \end{bmatrix} + \begin{bmatrix} P\omega_r \psi_m \\ 0 \end{bmatrix} \tag{2.23}$$

According to Eqn. (2.23), the permanent magnet synchronous motor can be represented by the d^r and q^r axis equivalent circuit diagrams as shown in Fig. 2.2. The torque developed by the machine can be obtained by considering the power entering the two sources as shown in Fig. 2.2. The permanent magnet is represented as a current source, I_m, [75] in Fig. 2.2(a).

The total average power entering the sources which is also the developed power per phase is given by,

$$P_{phase} = \left(-P\omega_r L_q i_q^r i_d^r + P\omega_r L_d i_d^r i_q^r + P\omega_r \psi_m i_q^r\right)\left(\frac{1}{2}\right) \tag{2.24}$$

Therefore, the total power developed by the machine is,

$$P_{mach} = \frac{3P\omega_r}{2}\left\{\psi_m i_q^r + \left(L_d - L_q\right) i_d^r i_q^r\right\} \tag{2.25}$$

Now the developed electromagnetic torque is given by,

$$T_e = \frac{P_{mach}}{\omega_r} = \frac{3P}{2}\left[\psi_m i_q^r + \left(L_d - L_q\right) i_d^r i_q^r\right] \tag{2.26}$$

The motor dynamics can be represented by the following equation:

$$T_e = T_L + B_m\omega_r + J_m p\,\omega_r \tag{2.27}$$

where T_L is the load torque (in Nm), B_m is the friction damping coefficient (in Nm/rad./sec.) and J_m is the rotor inertia constant (in kg-m^2).

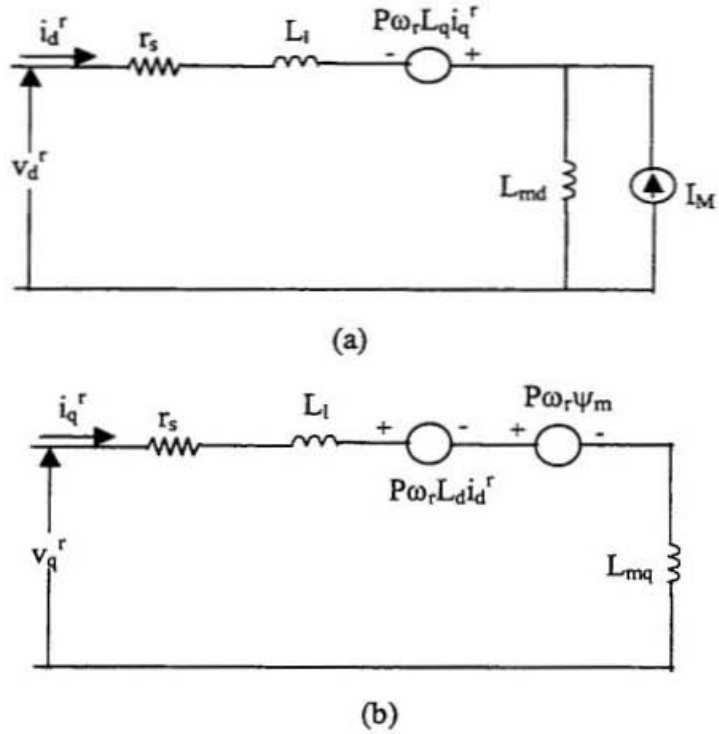

Fig. 2.2. Equivalent circuit model of the IPMSM: (a) d-axis, (b) q-axis.

For dynamic simulation the IPMSM model equations may be expressed as follows:

$$pi_q^r = (v_q^r - R\, i_q^r - P\omega_r L_d\, i_d^r - P\omega_r \psi_m)/ L_q \quad (2.28)$$

$$pi_d^r = (v_d^r - R\, i_d^r + P\omega_r L_q\, i_q^r)/ L_d \quad (2.29)$$

$$p\omega_r = (T_e - T_L - B_m \omega_r)/J_m \quad (2.30)$$

The motor parameters used in the simulation are given in Appendix A.

2.2 Vector Control Strategy for IPMSM Drive

As mentioned earlier, the vector control technique is one of the most effective techniques for use with ac motors in high performance drives. The IPMSM can be vector controlled when the machine equations are transformed from the a-b-c frame to the synchronously rotating d^r-q^r frame where the sinusoidal quantities become

constant. In the case of dc motor control, the developed torque T_e can be expressed as,

$$T_e = K_t' I_a \psi_f = K_t I_a I_f \tag{2.31}$$

where K_t', K_t are constants, I_a is the armature current, I_f is the field current and ψ_f is the field flux linkage. Both I_a and I_f are orthogonal and decoupled vectors. Hence the control task becomes much easier for the separately excited dc motor. In the case of the permanent magnet synchronous motor (PMSM), the torque Eqn. (2.26) has two terms: the first term represents the magnet torque produced by the permanent magnet flux ψ_m and the torque producing current component i_q^r; the second term represents the reluctance torque produced by the complex interaction of inductances L_d and L_q and also the currents i_d^r and i_q^r. In the case of the surface mounted permanent magnet synchronous motor, $L_d \cong L_q$ so the contribution of the second term in Eqn.(2.26) is negligible. Therefore, the torque equation of the surface mounted permanent magnet synchronous motor becomes linear and hence the control task is easier. However, in the case of the interior permanent magnet synchronous motor (IPMSM), L_q is larger than L_d. Moreover, it is also known that the excitation voltage due to permanent magnets, and the values of the inductances L_d and L_q undergo significant variations in an interior type permanent magnet motor under different steady state and dynamic loading conditions [71]. Thus, the complexity of the control of the IPMSM drive arises due to the nonlinear nature of the torque Eqn.(2.26). In order to operate the motor in a vector control scheme avoiding the complexity, i_d^r is set to zero. Then the torque equation becomes linear and is given by,

$$T_e = \frac{3P}{2} \psi_m i_q^r = K \psi_m i_q^r \tag{2.32}$$

where the constant $K = \frac{3P}{2}$. It is to be noted that the torque expressions of Eqns.(2.31) and (2.32) are identical and decoupled. Using phasor notations and taking the d^r axis as a reference phasor, the steady state phase voltage V_a can be derived from the steady state d^r-q^r axis voltage Eqn. (2.23) as,

$$V_a = v_d^r + j\, v_q^r$$

$$= r_s I_a - \omega_s L_q i_q^r + j\omega_s L_d i_d^r + j\omega_s \psi_m \qquad (2.33)$$

where the phase current, $I_a = -i_d^r + j\, i_q^r$ (2.34)

In the case of the IPM motor, the d^r-axis current is negative and it demagnetizes the main flux provided by the permanent magnets. Thus, in order to take only the absolute value of i_d^r we can re-write the Eqn.(2.33) as follows:

$$V_a = r_s I_a - \omega_s L_q i_q^r - j\omega_s L_d i_d^r + j\omega_s \psi_m \qquad (2.35)$$

According to Eqn.(2.33) the basic vector diagram of IPMSM is shown in Fig. 2.3(a). The vector control scheme can be clearly understood by this vector diagram. It is shown in the vector diagram that the stator current can be controlled by controlling the d^r and q^r axis current components. In the vector control scheme, when i_d^r is set to zero then all the flux linkages are oriented in the d^r-axis as shown in Fig. 2.3(b). After setting $i_d^r = 0$, Eqn. (2.32) shows that the torque is a function of only the quadrature axis current component, and hence a constant torque can be obtained by ensuring i_q^r constant. With the $i_d^r = 0$ control technique, the dynamic Eqns. (2.28) to (2.30) of IPMSM can be rewritten as,

$$p i_q^r = (v_q^r - R i_q^r - K_b \omega_r)/ L_q \qquad (2.36)$$

$$v_d^r = -P \omega_r L_q I_q^r \qquad (2.37)$$

$$p\omega_r = (K_T i_q^r - T_L - B_m \omega_r)/J_m \qquad (2.38)$$

where $K_T = (3/2)K_b$ and $K_b = P\psi_m$.

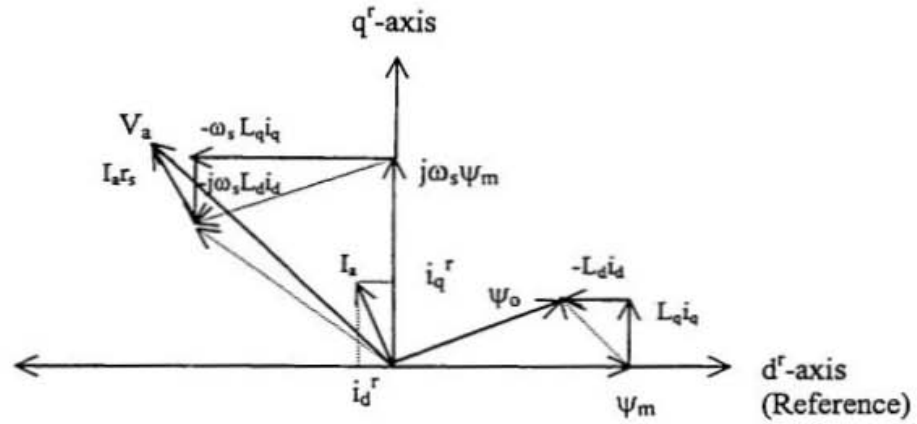

(a)

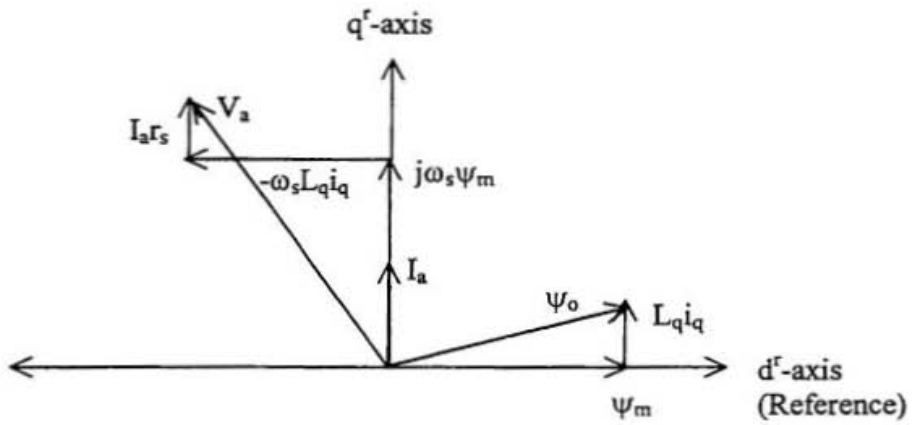

(b)

Fig. 2.3 Basic vector diagram of IPMSM: (a) general; (b) modified with i_d=0.

2.3 Implementation Technique for Vector Control Strategy of IPMSM

In the vector control scheme, the IPMSM is controlled in such a way that the q-axis current provides the desired torque. The complete control scheme for the current controlled VSI fed IPMSM drive is shown in Fig. 2.4. In this figure V_B is the dc bus voltage for the inverter. The IPMSM drive consists of the current controller and the speed controller. The speed controller generates the torque command and hence the q-axis current command i_q^{r*} from the error between the command speed and the actual speed. As mentioned earlier, in the vector control scheme the d-axis command current i_d^{r*} is set to zero to simplify the nonlinear dynamic model

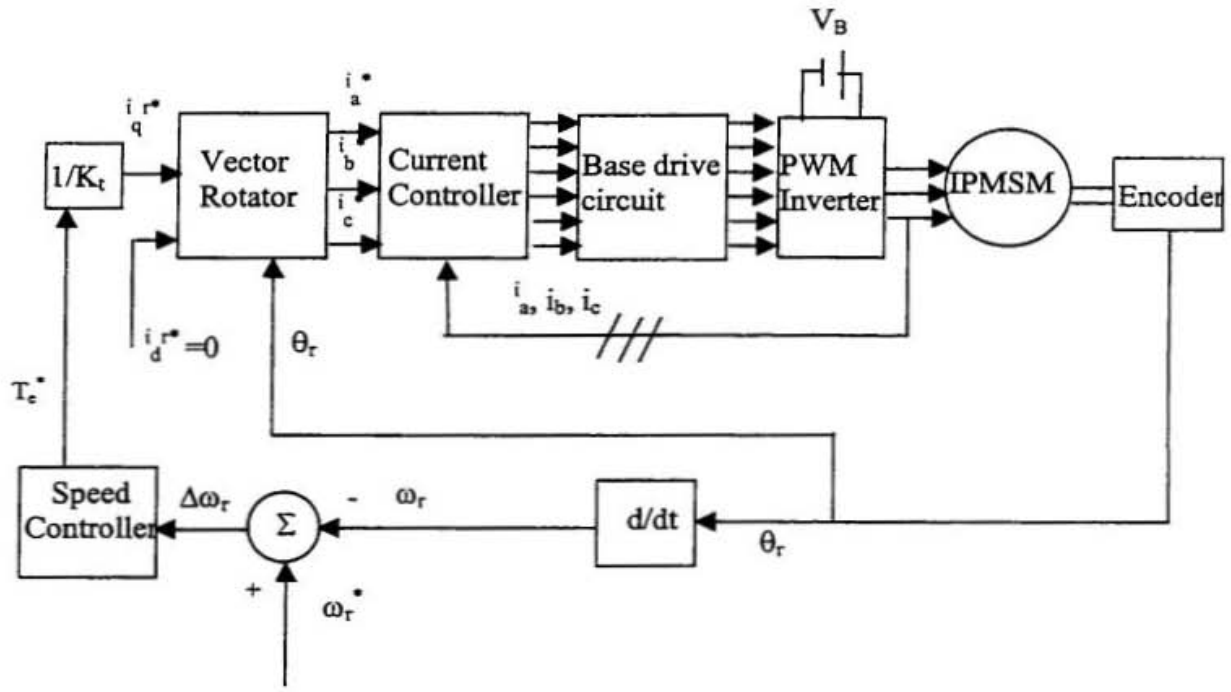

Fig. 2.4. Block diagram of complete current-controlled VSI-fed IPMSM drive.

of the IPMSM. The command phase currents i_a^*, i_b^* and i_c^* are generated from the d and q axis command currents using Park's transformation described earlier. The current controller forces the load current to follow the command current as closely as possible and hence forces the motor to follow the command speed due to the feedback control. Therefore, in order to operate the motor in a vector control scheme the feedback quantities will be the rotor angular position and the actual motor currents. The current controlled voltage source pulse width modulated (PWM) inverter is usually preferred for the IPMSM drive because of its quick response and accurate control, compared to the conventional voltage control scheme. In the control scheme, the torque is maintained constant up to the base speed and hence the constant voltage to frequency ratio (V/f) control technique is used. The (V/f) is maintained constant by using PWM operation of the VSI. The designs of the speed controller, vector rotator, current controller and voltage source inverter to perform their specific functions are given in the following sub-sections.

2.3.1 Speed Controller

The speed controller processes the error between command and actual speeds and generates the command torque. The small change in speed $\Delta\omega_r$ produces a corresponding change in torque ΔT_e and taking the load torque T_L as a constant, the motor dynamic Eqn.(2.27) becomes,

$$\Delta T_e = J_m \frac{d(\Delta\omega_r)}{dt} + B_m \Delta\omega_r \tag{2.39}$$

Integrating Eqn.(2.39) gives us the total change of torque as,

$$T_e = J_m \Delta\omega_r + B_m \int_0^t \Delta\omega_r(\tau) d\tau \tag{2.40}$$

Eqn.(2.40) represents the PI algorithm for the speed controller that may be rewritten as,

$$T_e^* = K_p \Delta\omega_r + K_i \int_0^t \Delta\omega_r(\tau)d\tau \qquad (2.41)$$

where K_p is the proportional constant, K_i is the integral constant and $\Delta\omega_r = \omega_r^* - \omega_r$ is the speed error between the command speed ω_r^* and the actual motor speed ω_r. In Laplace domain Eqn. (2.41) can be written as,

$$T_e^* = \left(K_p + \frac{K_i}{s}\right)\Delta\omega_r(s) \qquad (2.42)$$

Substituting for $s = \frac{2}{T_s}\left(\frac{1-z^{-1}}{1+z^{-1}}\right)$ in Eqn. (2.42) where z^{-1} represent one sample delay and T_s is the sampling period, or by differentiating Eqn. (2.41) and then replacing the continuous terms by their finite differences, the discrete form of the PI algorithm can be written as,

$$T^*(k) = T^*(k-1) + K_p[\Delta\omega_r(k) - \Delta\omega_r(k-1)] + K_i T_s \Delta\omega_r(k) \qquad (2.43)$$

where $T^*(k)$ is the present sample of command torque, $T^*(k-1)$ is the past sample of command torque, $\Delta\omega_r(k)$ is the present sample of speed error and $\Delta\omega_r(k-1)$ is the past sample of speed error. Equation (2.43) can be easily implemented using a DSP if the values of K_p, K_i, T_s and the command speed are chosen properly.

2.3.2 Vector Rotator

The function of this block is to transform the rotating rotor reference frame quantities into the stator reference frame. The inputs of this block are the d-q axis command currents i_d^{r*} and i_q^{r*}, respectively, and the rotor position θ_r. The outputs are the three-phase command currents i_a^*, i_b^* and i_c^*. The transformation is done in

two steps: first the synchronously rotating d^r –q^r axis quantities are transformed to the stationary d-q axis quantities and then the stationary d-q axis quantities are transformed to the a-b-c phase quantities.

2.3.3 Current Controller and Voltage Source Inverter

The current controller is used to force the motor currents to follow the command currents and hence forces the motor to follow the command speed due to the feedback control. The outputs of the current controller are the firing pulses for the inverter switches. The current control principle for the voltage source inverter is given in section 2.4. Among the various current controller schemes, the hysteresis and the ramp comparator are the most commonly used current controllers for high performance drive applications. These controllers are getting more attention due to their simplicity and wide spread use. The detailed analysis of these current controllers is given in section 2.5.

2.4 Current Control of the Voltage Source Inverter

The current controller forces the load current to follow the command current as closely as possible. In the case of the IPMSM drive, the command currents are generated from the error between the command speed and the actual motor speed. Therefore, the current controller indirectly also forces the motor to follow the command speed. The operation of the current controlled VSI can be analyzed by considering the circuit as shown in Fig. 2.5(a). In this figure, each stator phase of the motor load is connected to each leg of the three phase transistorized inverter. The center point of the two equal capacitors is considered as ground. The neutral of the stator is not connected to the ground. The actual motor currents are compared to

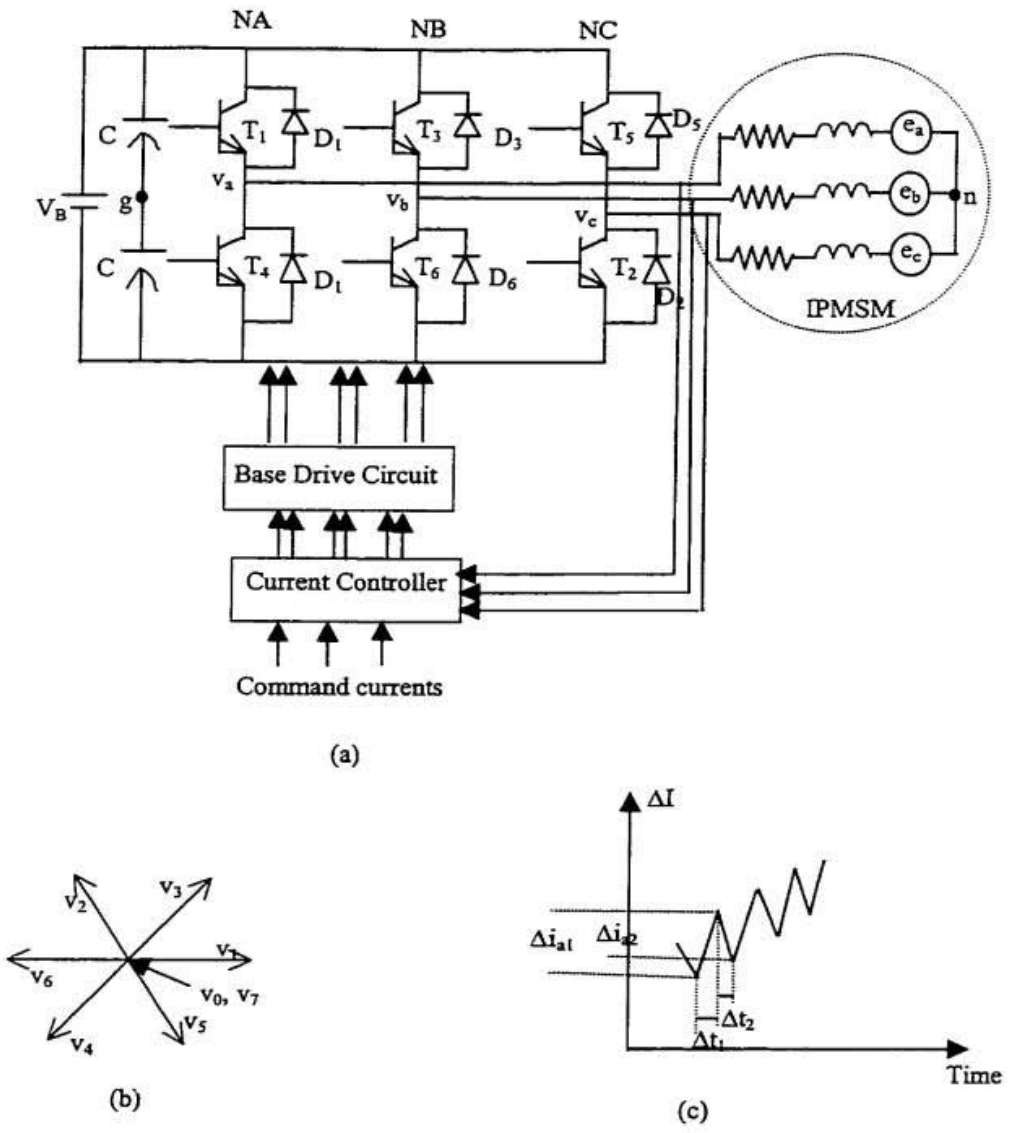

Fig. 2.5. (a) Current controlled voltage source inverter of the IPMSM drive, (b) Inverter voltage vectors and (c) Switching current waveform.

the command currents and the error signals are processed by the current controllers to generate the firing pulses for six transistors of the inverter. In this figure NA, NB and NC represent three logic variables of the three legs of the inverter, respectively.

These logic variables determine the conduction state of the inverter. When the logic NA is 1 then T_1 is conducting and when it is 0 then T_4 is conducting. The concept of voltage and current space vectors are used to analyze the current controllers because it simplifies the representation of a set of three phase voltages or currents. The inverter voltage vector is defined in [76] as

$$v = (2/3)\,(v_a + av_b + a^2 v_c) \tag{2.44}$$

where $a=e^{j2\pi/3}$ and v_a, v_b, and v_c are phase voltages. Similarly, the inverter current vector is defined as

$$i = (2/3)\,(i_a + ai_b + a^2 i_c) \tag{2.45}$$

Table 2.1 Conduction modes of the VSI under current control

State, L	Leg 'a'		Leg 'b'		Leg 'c'		Operating modes	Voltage phasor
	T_1	T_4	T_3	T_6	T_5	T_2		
0	0	1	0	1	0	1	Freewheeling	v_o
1	1	0	0	1	0	1	Active	v_1
2	0	1	1	0	0	1	Active	v_2
3	1	0	1	0	0	1	Active	v_3
4	0	1	0	1	1	0	Active	v_4
5	1	0	0	1	1	0	Active	v_5
6	0	1	1	0	1	0	Active	v_6
7	1	0	1	0	1	0	Freewheeling	v_7

The phase voltages v_a , v_b and v_c are expressed as a function of bus voltage V_B and logic variables as

$$\begin{bmatrix} v_{an} \\ v_{bn} \\ v_{cn} \end{bmatrix} = \frac{1}{3}\begin{bmatrix} 2 & -1 & -1 \\ -1 & 2 & -1 \\ -1 & -1 & 2 \end{bmatrix}\begin{bmatrix} NA \\ NB \\ NC \end{bmatrix} V_B \qquad (2.46)$$

There are eight switch combinations for the six switches of the inverter. Using Eqn.(2.44) the inverter voltage vector can be written as

$$\begin{aligned} v_L &= (2/3)\, V_B\, e^{j(L-1)\pi/3} \quad \text{for } L = 1,2,\ldots,6 \\ &= 0 \quad \text{for } L = 0,7 \end{aligned} \qquad (2.47)$$

The logic operation of the voltage source inverter under current control is shown in Table 2.1. The voltage vectors corresponding to the six active states are shown in Fig. 2.5(b). The magnitude of each voltage vector is $(2/3)V_B$. The magnitudes of voltage vectors v_0 and v_7 corresponding to the freewheeling states are zero. In these instances no voltage is applied to the motor because then either all the high side or all the low side transistors of the inverter are on.

2.4.1 Effect of unconnected neutrals

If the neutral of the load is not connected at the dc bus mid point, the switching of one phase depends on the states of the other two phases. Thus, the individual line to neutral voltages are dependent on each other and each line current will depend not only on the corresponding inverter phase but also on the state of the other two phases. Therefore, a current controller experiences interaction between the phases of the inverter. Hence, the actual current may not follow the command current properly.

2.4.2 Limitation of dc bus voltage and inverter switching frequency

For a current controller to operate the IPMSM properly, the dc voltage must be sufficient to force the line currents in the desired direction and follow the command. In the case of a low counter emf, the dc voltage is not critical, but as the counter emf is increased a point is reached where the line to neutral voltage becomes a six step quasi-square wave and then the current is not able to follow the command current. This happens due to saturation of the current controller. However, the inverter switching frequency depends on the type of current controllers used. In the case of the ramp controller, the switching frequency is measured by the ramp signal frequency. In the case of the hysteresis controller, the switching frequency depends on several factors which can be described by the following equation that represents one phase of a motor:

$$L\frac{di_a}{dt} = v_a - Ri_a - e_a \tag{2.48}$$

where L is the leakage inductance per phase, v_a, i_a and e_a are the 'a' phase applied voltage, current and back emf, respectively. The actual switching pattern is shown in Fig.2.5(c). Let Δt_1 be the time during which the line current will increase by Δi_{a1}, and let Δt_2 be the time during which the current will decrease by Δi_{a2}. Assuming v_a and e_a are constant during the interval, one can write the equation for Δt_1 and Δt_2 as

$$\Delta t_1 = \frac{L\Delta i_{a1}}{V_B - Ri_a - e_a};\quad \Delta t_2 = \frac{L\Delta i_{a2}}{V_B - Ri_a - e_a} \tag{2.49}$$

$$f = 1/(\Delta t_1 + \Delta t_2) \tag{2.50}$$

Therefore, the inverter switching frequency depends on dc bus voltage, inductance, as well as magnitude of motor current and its ripple content. As the line to neutral

fundamental voltage varies periodically, the inverter switching frequency will vary over the fundamental period.

2.5 Analysis of Current Controllers

The block diagram of a general current controller scheme is shown in Fig. 2.6. The same scheme can be used as hysteresis controller with switch SW off and ramp comparator controller with switch SW on and by reducing the hysteresis band block H to zero or to a small value, if required.

2.5.1 Hysteresis controller

The hysteresis controller is widely used to control the current in such a way that it can follow the command current with a hysteresis band. A typical three-phase hysteresis current controller is shown in Fig. 2.6 with switch SW turned off. This type of controller is extensively used because of its simplicity and excellent dynamic response. However, in this controller, the switching frequency of the inverter varies over the fundamental period. This results in an irregular operation of the inverter with time and hence the switching losses are increased. Based on the hysteresis band conventionally there are two types of hysteresis controllers, namely, fixed band and sinusoidal band hysteresis controllers. The waveform of the fixed band controller is shown in Fig. 2.7(a). In this scheme, the maximum switching frequency of the inverter is reduced but the harmonic current is increased. In the sinusoidal band, the hysteresis band varies sinusoidally over the fundamental period as shown in Fig. 2.7(b). The advantage of this scheme is that the harmonic content of the current is low. The disadvantage is that the switching frequency near the zero crossing is very high. As a result, the maximum switching frequency of the

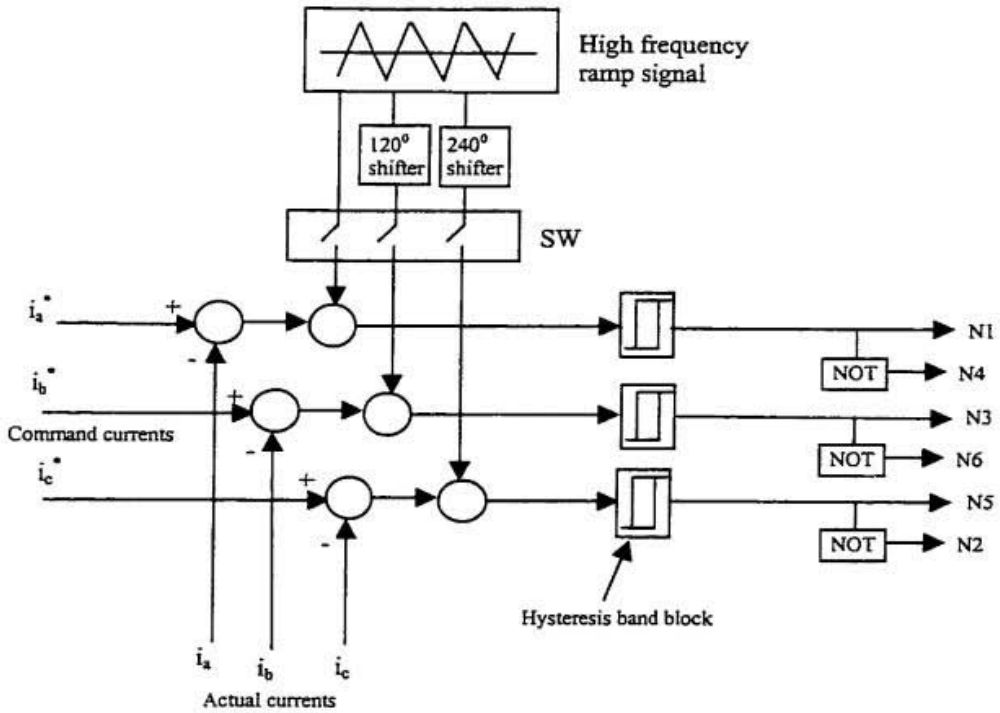

Fig.2.6. General current controller scheme.

inverter increases. In order to compromise between the maximum inverter switching frequency and harmonic content of the current, the mixed band hysteresis controller is used. In the mixed band controller, the hysteresis band varies sinusoidally around the reference and a constant value as shown in Fig. 2.7(c).

Consider that N1, N3 and N5 are the logic signals for the high transistors of the inverter and N4, N6 and N2 are the logic signals for the low transistors of the inverter, respectively. When the logic signal N1 is 1 then the transistor T_1 is on and when it is 0 then T_1 is off. Similar logic is valid for other five logic signals. The control logic of the hysteresis controller can be described as follows:

(i) For $i_a^* > 0$: $N_4=0$, if $i_a > i_{up}$, then $N_1=0$, else if $i_a < i_{lo}$, then $N_1 = 1$.

(ii) For $i_a^* < 0$: $N_1=0$, if $i_a > i_{up}$, then $N_4=1$, else if $i_a < i_{lo}$, then $N_4=0$.

where i_a is actual 'a' phase current, i_a^* is command current, $i_{up}=i_a^* + H$ is the upper band and $i_{lo}=i_a^* - H$ is the lower band, and H is the hysteresis band. For fixed band $H=\alpha_1$; for sinusoidal band $H=\beta_1\sin(\omega t)$; and for mixed band $H=\alpha_2+\beta_2\sin(\omega t)$ where α_1, α_2, β_1 and β_2 are constants.

2.5.2 Conventional ramp comparator controller

The typical three-phase conventional ramp comparator controller is also shown in Fig.2.6 with switch SW 'on' and by omitting the phase shifters. In the ramp comparator controller, the error signals between the actual motor currents and the

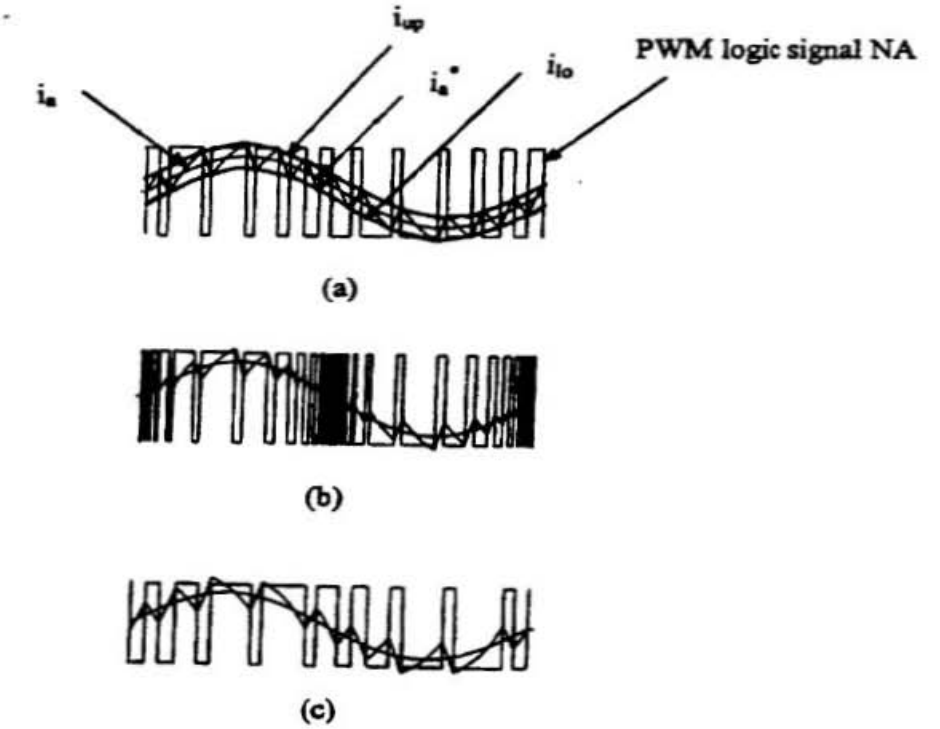

Fig. 2.7. Current waveforms for the hysteresis controller: (a) fixed band, (b) sinusoidal band and (c) mixed band.

respective command currents are compared to a high frequency triangular waveform of fixed frequency and amplitude. If the error signal is positive and greater than the triangular wave, then the upper transistors of the inverter will be activated to apply $+V_B$ to the motor terminal. If the current error signal is positive and less than triangular wave, the lower transistors will be activated to apply $-V_B$ to the motor terminal. In order to prevent multiple crossings of error signals with the triangular waveform, some hysteresis band has been added to the controller. Because of the fixed frequency of the triangular wave, the switching frequency of the inverter remains fixed. This is the advantage of this controller. However, the disadvantages of this controller are that the actual current has amplitude and phase errors, which become acute with high speed operation. Moreover, sometimes the motor is disconnected from the supply over the fundamental period when a zero voltage vector is applied to the motor. These drawbacks result in poor dynamic performance, and hence this type of controller has limitations for the IPMSM drive when used at high speed in high performance drive applications.

2.5.3 Improved ramp comparator controller

In order to overcome the previously mentioned difficulties of the conventional ramp controller, an improved ramp comparator controller is used. The schematic diagram of this controller is shown in Fig.2.6. In this controller, the current error signals are compared to three 120° phase shifted triangular waveforms having the same fixed frequency and amplitude. The performance is identical to three independent single-phase ramp comparator controllers. As there is no interaction between the three phases, it removes the zero voltage vector for balanced operation.

2.6. Simulation of the Complete Current-Controlled VSI-Fed IPMSM drive

The dynamic of the IPMSM is very complex because of its nonlinear nature and also the discrete time nature of the inverter and motor system. Therefore, after developing the control strategy of the complete drive it is usual practice to simulate the drive system on the computer and predict the performances before real-time implementation. The complete drive as shown in Fig. 2.4 has to be simulated using suitable software. There is much dedicated software, which can be helpful in simulating the dynamics of the system, such as electromagnetic transient program (EMTP), simulation of nonlinear systems (SIMNON) and Simulink. The simulation of the proposed complete drive has been carried out using SIMULINK software [77]. The simulation allows investigation of both transient and steady state performance of the drive. For simulation, the inputs are all the motor parameters, sampling frequency and command speed. The outputs are the instantaneous currents, voltages, speed and torque. In simulation, the inverter transistors are modeled as ideal controlled switches with zero turn-on and turn-off time and hence the switches of each inverter leg have a complementary switching state. The following steps have been carried out to simulate the drive in Simulink format:

- The equations describing the IPMSM are rearranged in state-space form.
- The inverter is represented by the real-time switching model of Simulink.
- The system performances are obtained using a built-in Runge-Kutta algorithm.
- The logic of the current controllers is represented by a combination of digital and analog modes.

The schematic diagram of the complete drive system using Simulink is shown in Fig. 2.8. This figure contains different blocks such as command-current generator, current controller, inverter etc. These are known as the subsystems. Each subsystem consists of many blocks, which perform specific functions. The details of these subsystems are given in Appendix B.

2.7. Simulation Results

An extensive simulation has been done to predict the performance of the drive. Some sample results are presented here. The speed response at no load and rated speed (188.5 rad./sec.) is shown in Fig. 2.9(a) for the fixed band hysteresis current controller. The corresponding command phase current, q-axis command current, and actual motor current are shown in Figs. 2.9(b)-(d), respectively. It is shown that the drive follows the command speed without any steady-state error although there is a small overshoot in the transient condition. The actual motor current also follows the command current with a hysteresis band. The similar transient responses for the same controller at full load condition are shown in Figs. 2.10(a)-(d). This time the drive follows the command speed with a smaller overshoot as compared to the no load condition and the actual motor current also follows the command current. The responses including speed, PWM logic signal NA, q-axis command current and the actual motor current at low speed (50rad./sec.) and rated load conditions are shown in Figs. 2.11(a)-(d). It is shown from Fig. 2.11(a) that, although the drive follows the command speed, the speed response was not so smooth even at steady-state condition. Therefore, the drive response of the hysteresis controller is not so good at low speed condition.

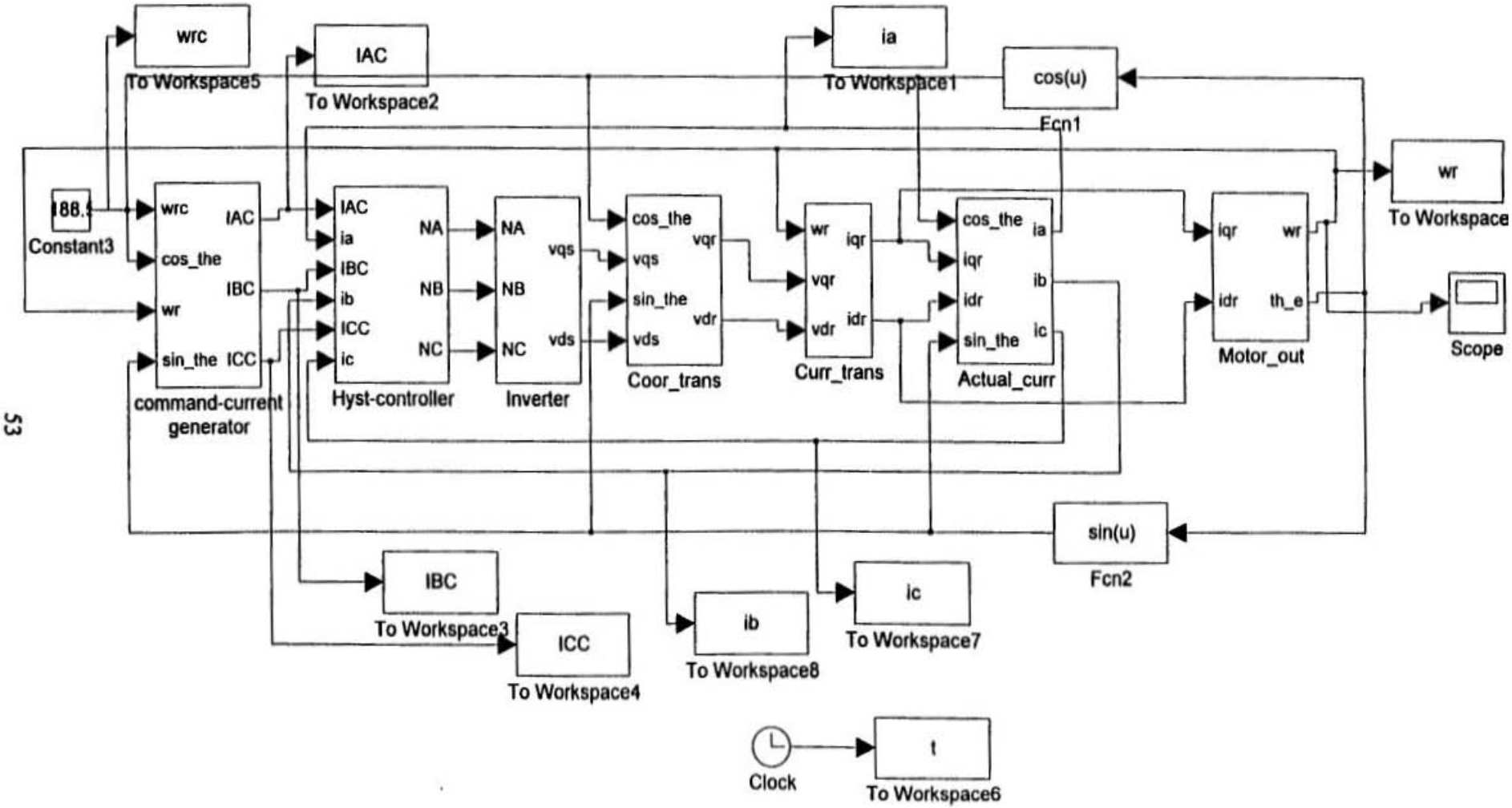

Fig. 2.8. Simulink schematic of the complete current-controlled VSI-fed IPMSM drive system.

The speed, actual a-phase current, q-axis command current and the actual a, b and c-phase currents are shown in Figs. 2.12(a)-(d), respectively for step change of speed (100 rad./sec.→188.5 rad./sec) at the rated load for the fixed band hysteresis controller. It is shown that the motor can follow the command speed very quickly even after an abrupt change of command speed. For the same controller, the similar responses of the drive are shown in Figs. 2.13(a)-(d), respectively for a sudden increase of load at the rated speed. It is also shown that the motor can follow the command speed even after some disturbances of load.

The drive performances for a step increase of speed at rated load for the conventional ramp comparator controller are shown in Figs. 2.14(a)-(d). The rotor of the IPMSM drive also follows the command speed accurately even after a sudden change of command speed for the ramp comparator controller. However, it is observed from Fig. 2.14(d) that the actual current has magnitude and phase errors. Figs. 2.15 (a)-(d) show the speed, command phase current, command q-axis current and the actual phase current, respectively for the ramp comparator controller at low speed (50rad./sec.) and rated load conditions. It is also observed that the motor can follow the command speed smoothly for the conventional ramp comparator controller when the command speed is low. Also the actual phase current follows the command current without any phase and magnitude errors as noted in Fig. 2.15(d). Comparing Fig. 2.12(a) for the hysteresis controller and Fig. 2.14(a) for the ramp controller, it is found that the speed response of the hysteresis controller is faster than that of the ramp comparator controller. The simulation results show that the hysteresis current controller works well at high speed conditions and the ramp comparator controller works well at low speed conditions. The simulation results show encouraging performances of the controllers for the drive.

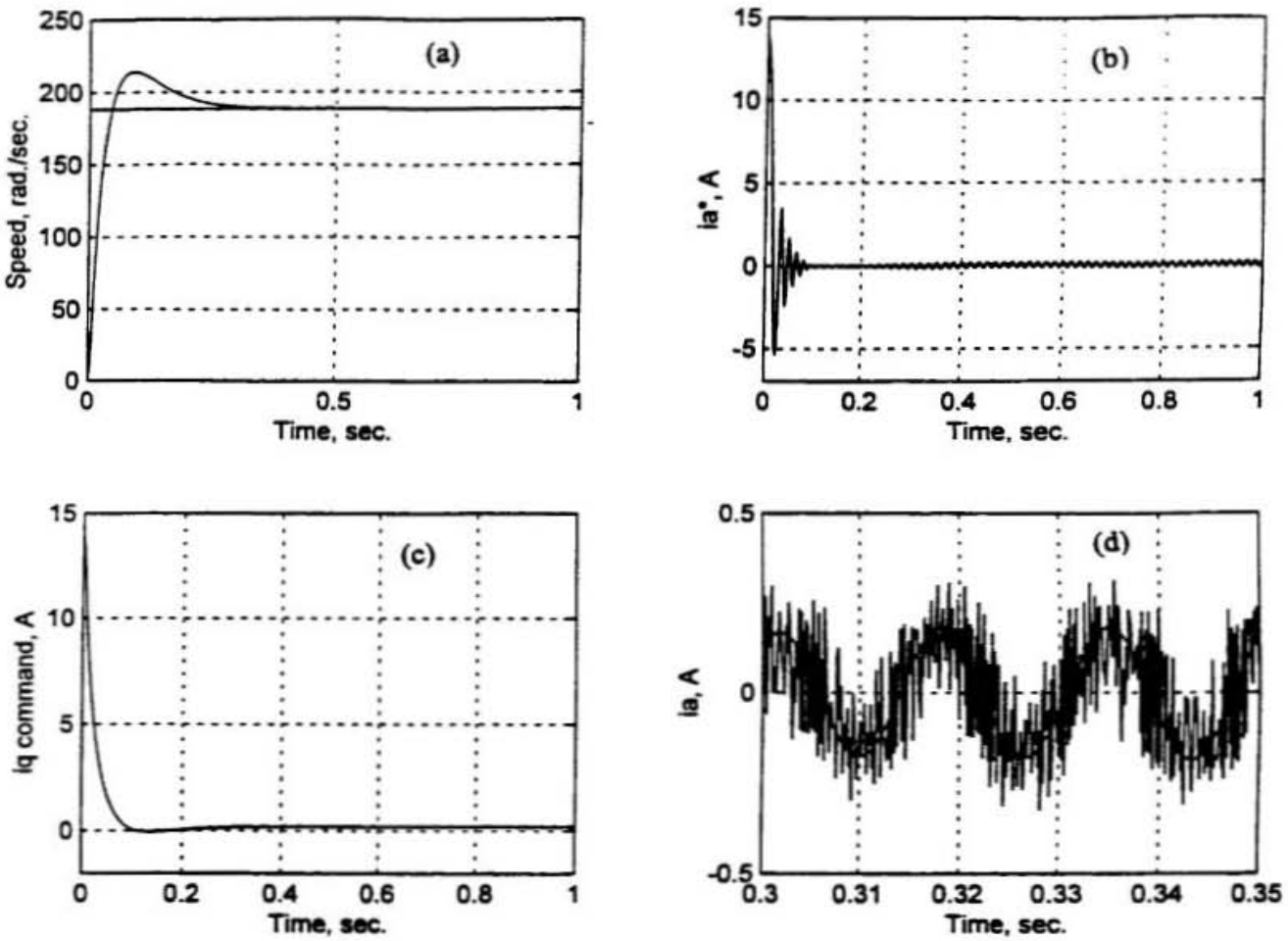

Fig.2.9. Simulated responses of the drive at no load and rated speed (188.5 rad./sec.) conditions for the fixed band hysteresis current controller: (a) speed, (b) command phase current, (c) command q-axis current, and (d) actual phase current.

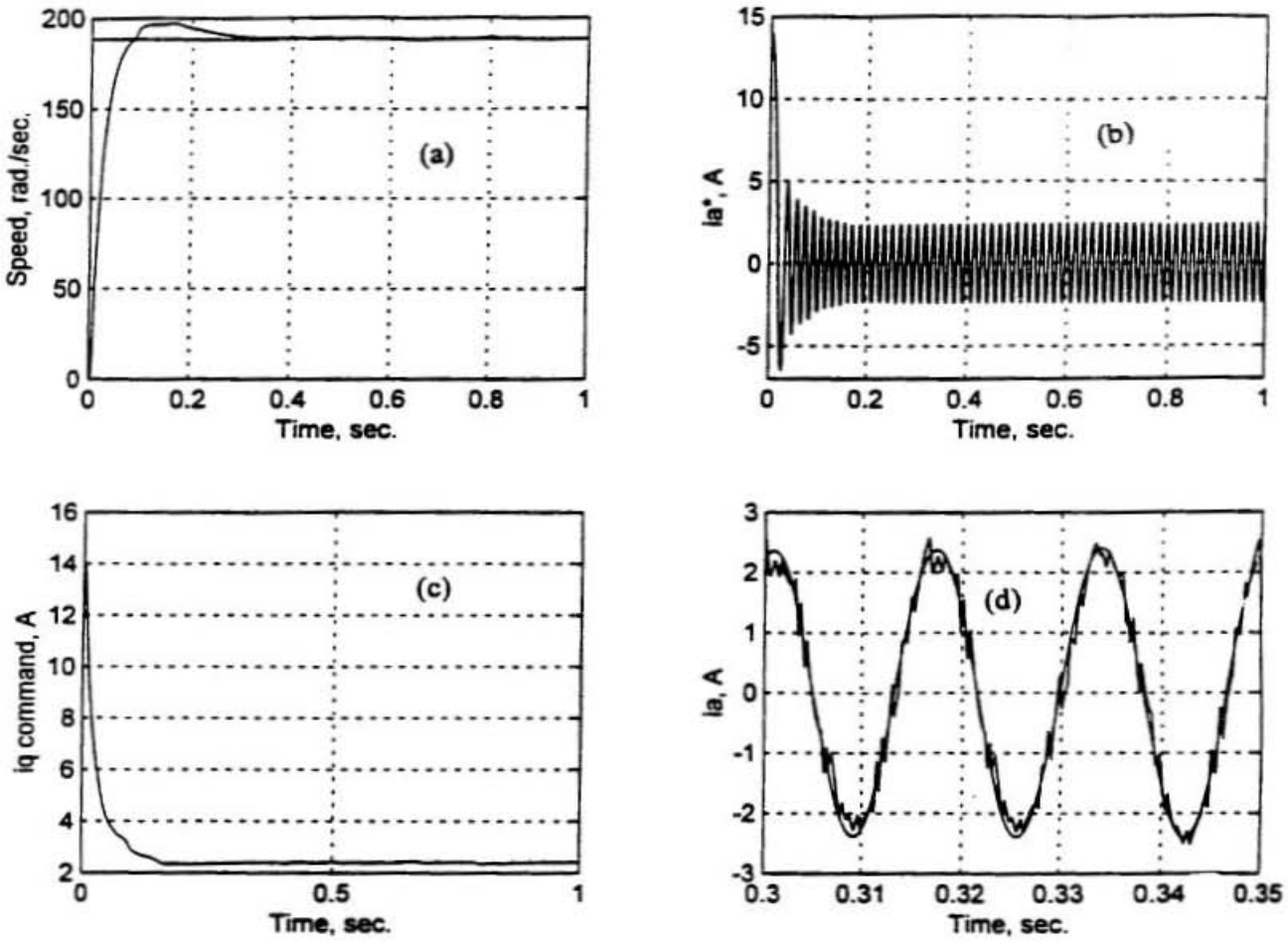

Fig.2.10. Simulated responses of the drive at full load and rated speed (188.5 rad./sec.) conditions for the fixed band hysteresis current controller: (a) speed, (b) command phase current, (c) command q-axis current, and (d) actual phase current.

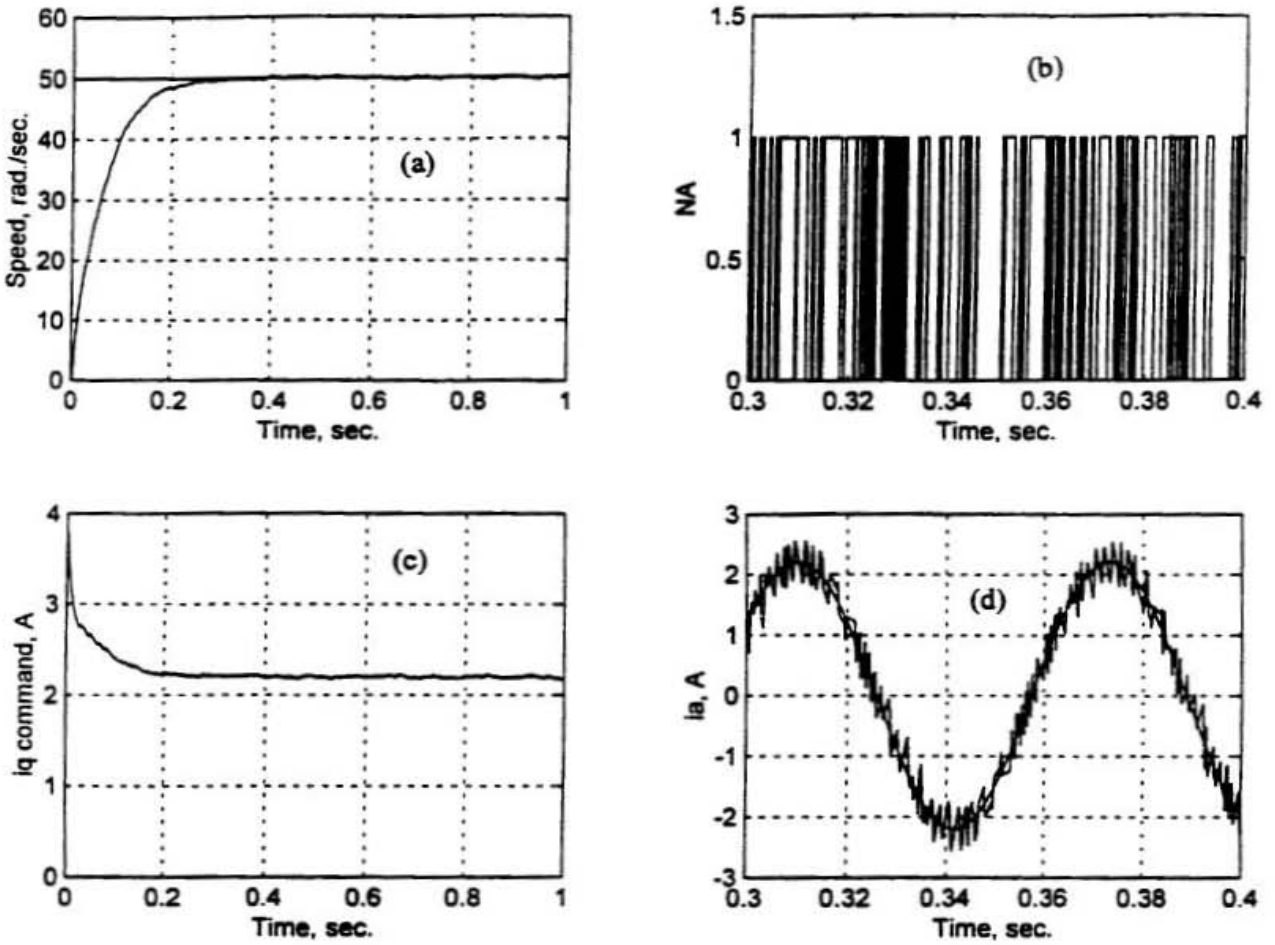

Fig.2.11. Simulated responses of the drive at full load and low speed (50rad./sec.) conditions for the fixed band hysteresis current controller: (a) speed, (b) PWM logic signal NA, (c) command q-axis current, and (d) actual phase current.

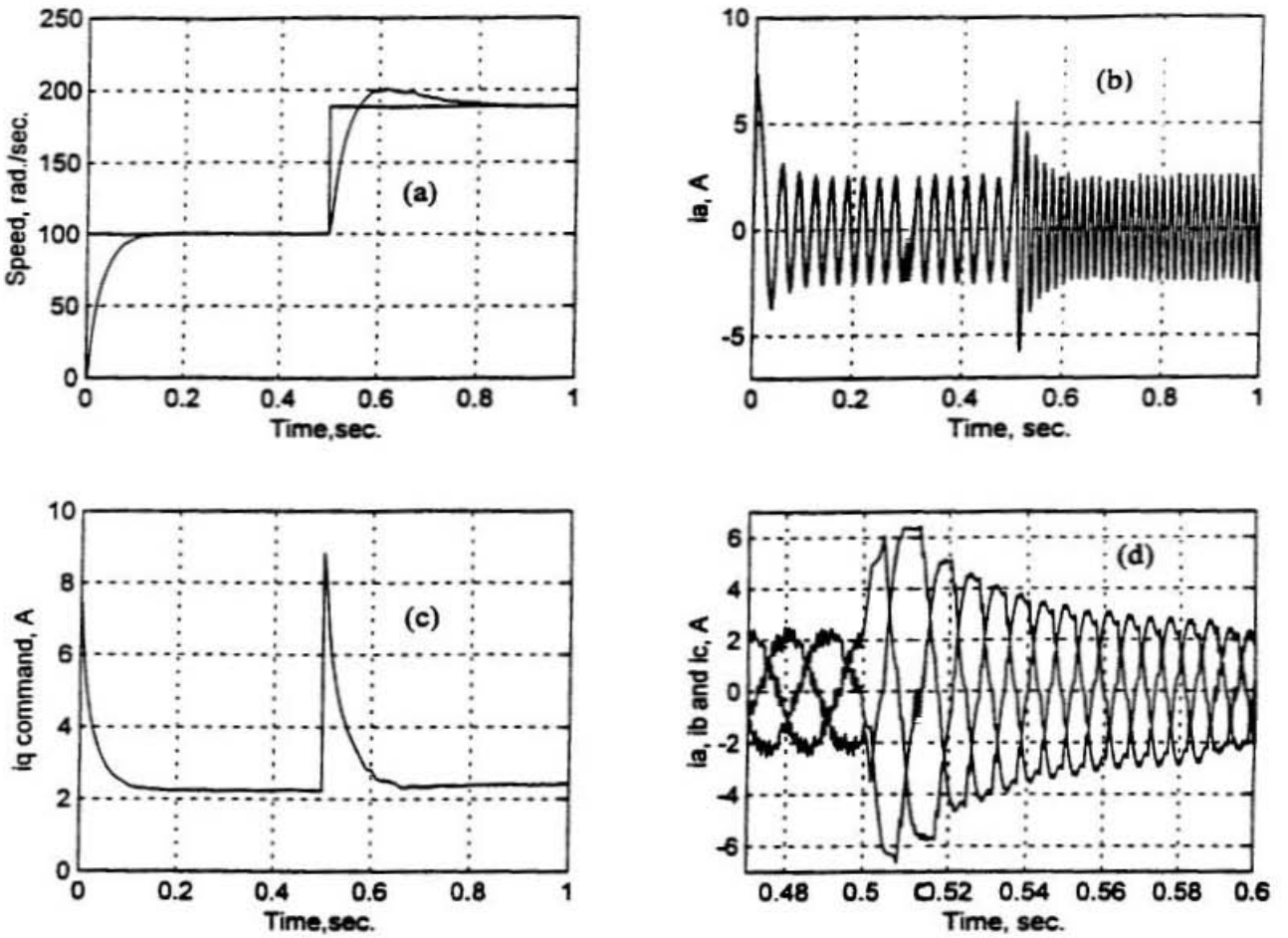

Fig.2.12. Simulated responses of the drive at a step change of speed (100rad./sec.→ 188.5rad./sec.) and full load conditions for the fixed band hysteresis current controller: (a) speed, (b) actual a-phase current, (c) command q-axis current, and (d) actual a, b and c-phase currents.

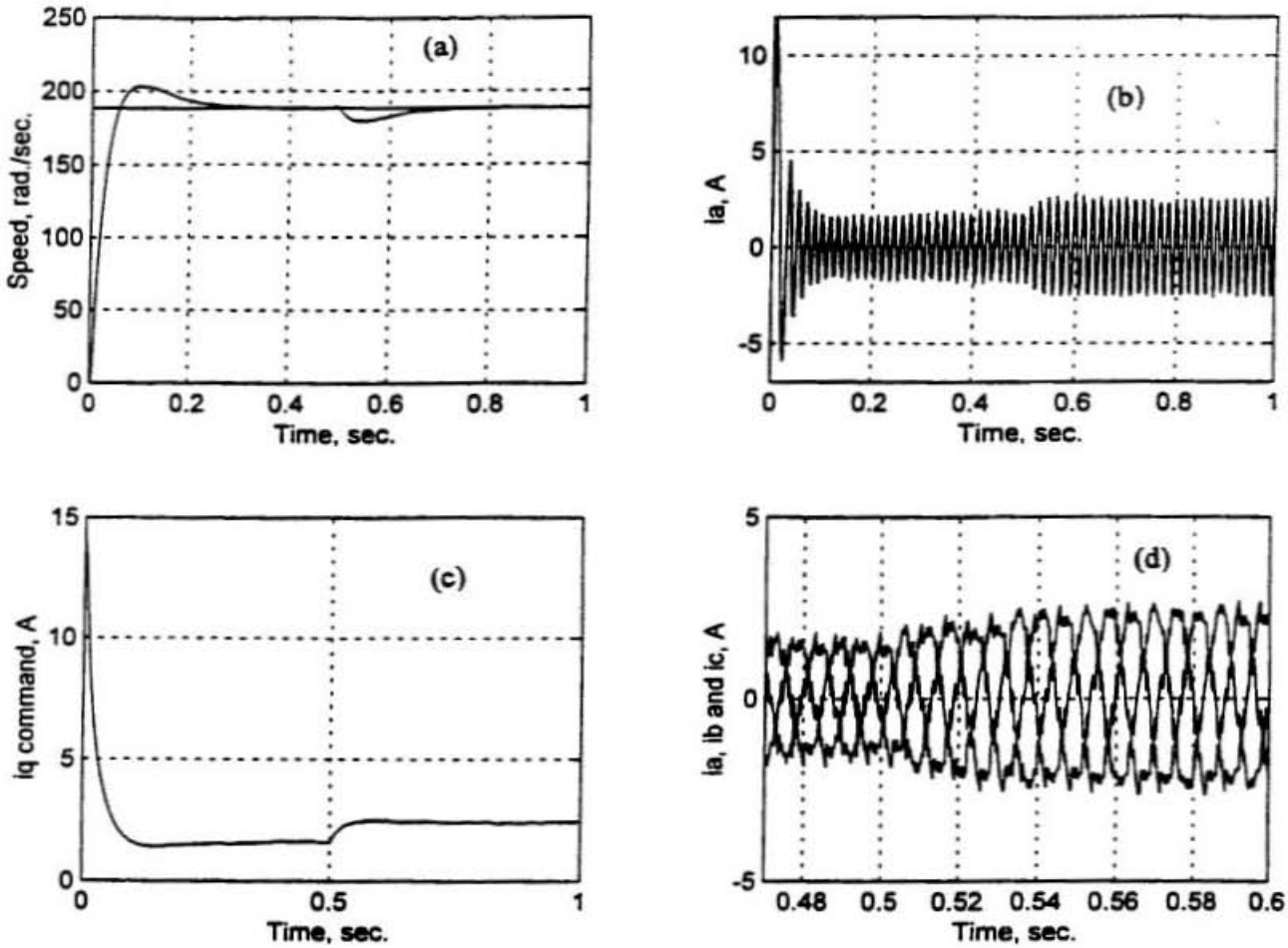

Fig.2.13. Simulated responses of the drive at a step increase of load (half load→ full load) and rated speed conditions for the fixed band hysteresis current controller: (a) speed, (b) actual a-phase current, (c) command q-axis current, and (d) actual a, b and c-phase currents.

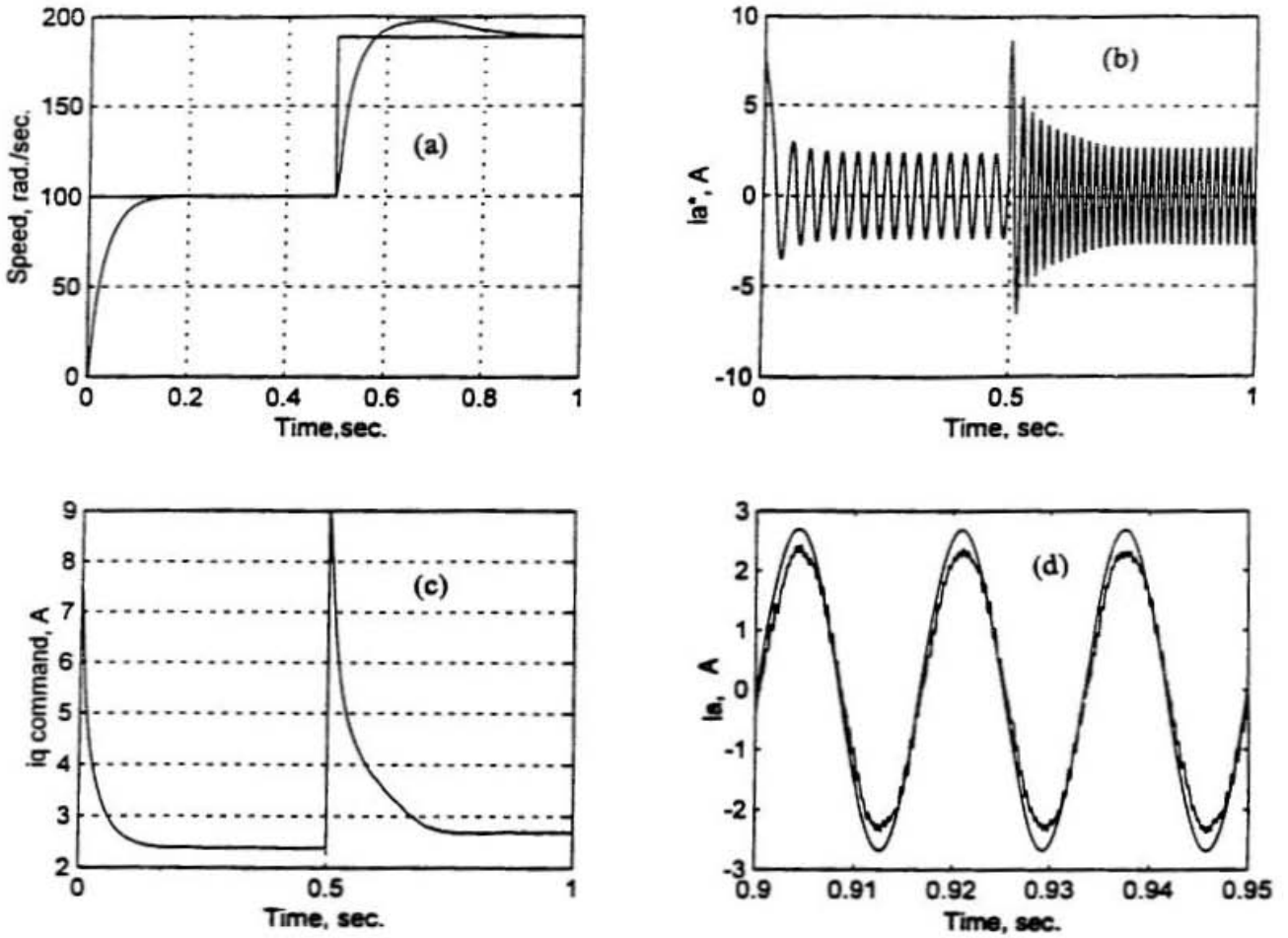

Fig.2.14. Simulated responses of the drive at a step change of speed (100rad./sec.→ 188.5rad./sec.) and full load conditions for the conventional ramp comparator controller: (a) speed, (b) command phase current, (c) command q-axis current, and (d) actual phase current at high speed (188.5 rad./sec.) condition.

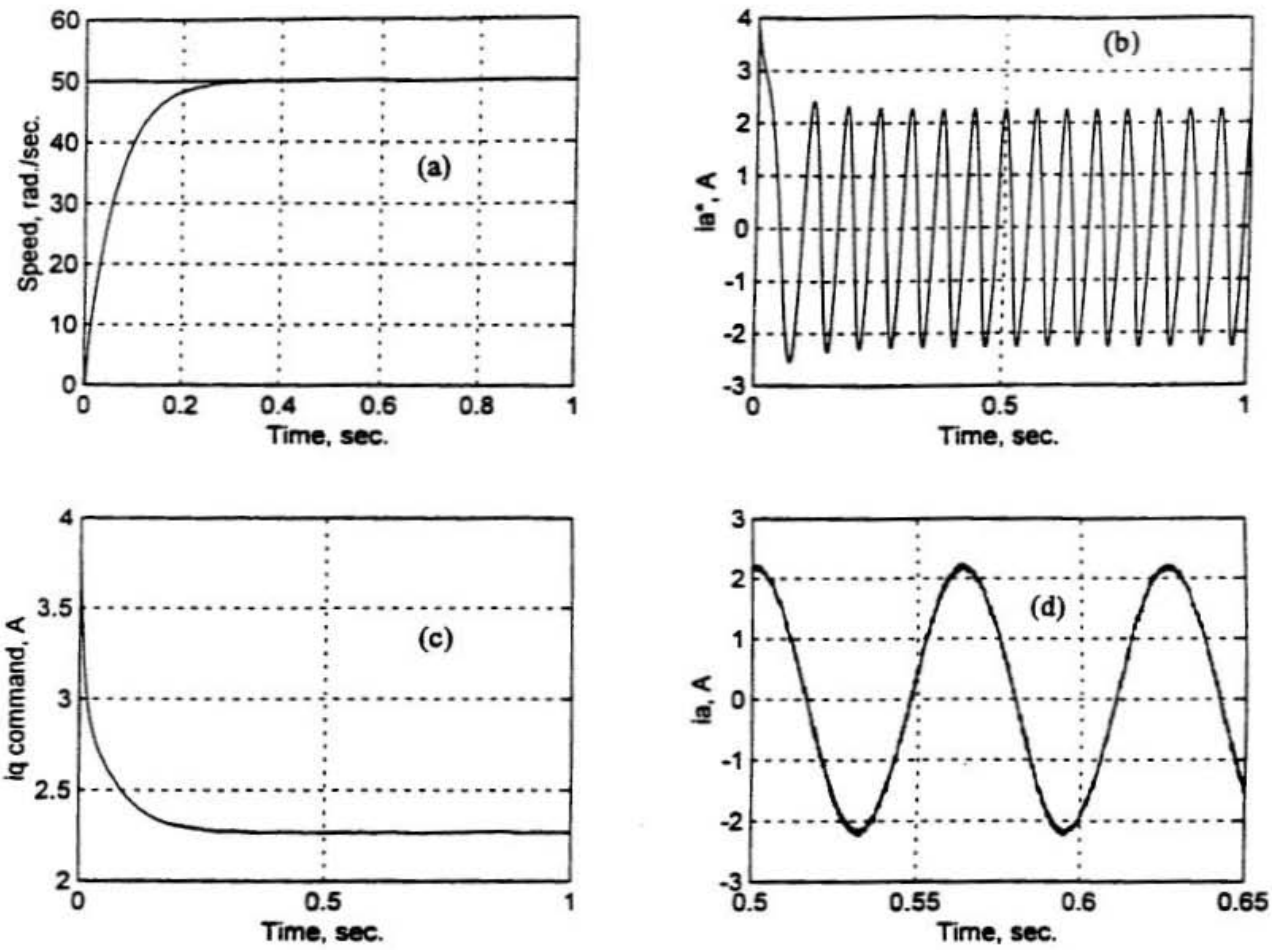

Fig.2.15. Simulated responses of the drive at full load and low speed (50rad./sec.) conditions for the ramp comparator controller: (a) speed, (b) command phase current, (c) command q-axis current, and (d) actual phase current at low speed condition.

From simulation results, it was found that the speed responses for all other current controllers were almost similar but there exist some discrepancies. These occur due to the current responses of various current controllers at different operating speed conditions that may affect the system dynamic performances and stability. In simulation, the real-time motor parameter variations and the limitations of inverter switching frequencies are absent so those discrepancies of current responses are not a matter of fact in simulation. Therefore, the speed and current responses of various current controllers need to be investigated in real-time. In experiments, it was observed that some current controllers do not follow the command speed with stability at some operating speed ranges. This happens due to the current waveforms for those controllers at that speed range.

2.8. Real-Time Implementation of the Current-Controlled VSI-Fed IPMSM Drive.

In order to implement the control scheme in real time the DSP board DS1102 has been used [78]. The board is installed in a PC-AT computer with uninterrupted communication through dual port memory. The DS1102 board is mainly based on a Texas Instrument TMS320C31 32 bit floating point digital signal processor. The DSP has been supplemented by a set of on-board peripherals used in digital control systems including analog to digital (A/D), digital to analog (D/A) converters and incremental encoder interfaces. The DS1102 is also equipped with a TI TMS320P14 16 bit micro controller DSP that acts as a slave processor and provides the necessary digital I/O ports and powerful timer functions such as input capture, output capture and PWM generation. The block diagram of the hardware schematic

is shown in Fig.2.16. The actual motor currents and the rotor position angle are fed back to the DSP board through the A/D channel and the encoder interface, respectively. The actual currents are sensed by the Hall-effect transducers with good frequency response. The rotor position angle is sensed by an optical incremental encoder mounted at the rotor shaft. The encoder generates 4096 pulses per revolution and by using a 4-fold pulse multiplication the output of the encoder is increased to 4x4096 pulses per revolution. A 24-bit position encoder is used to count the encoder pulses. The counter is reset once per revolution by the index pulse generated from the encoder. The outputs of the DSP board are six PWM signals that are sent directly to the base drive circuit of the transistorized inverter.

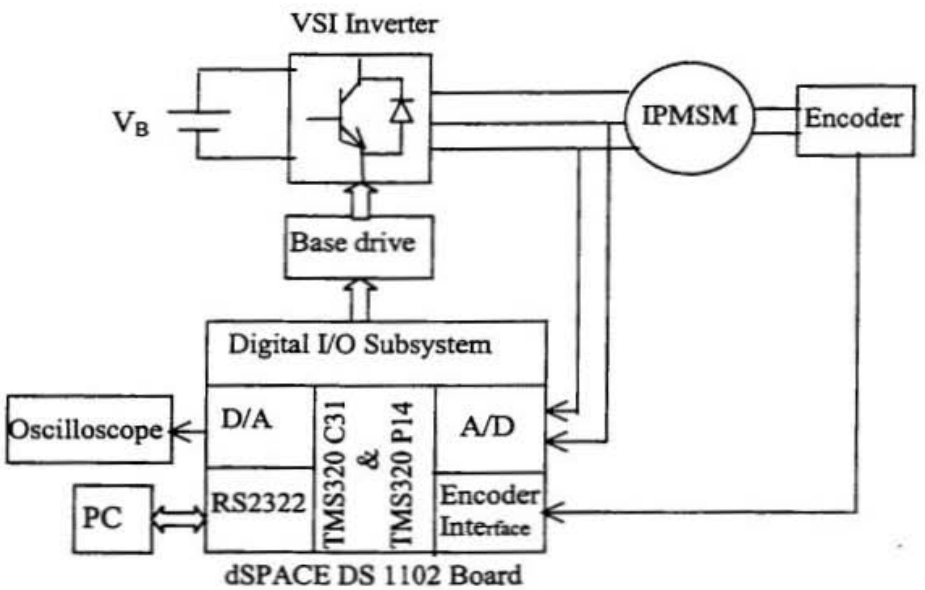

Fig. 2.16. Block diagram of the hardware schematic of current-controlled VSI Fed-IPMSM drive.

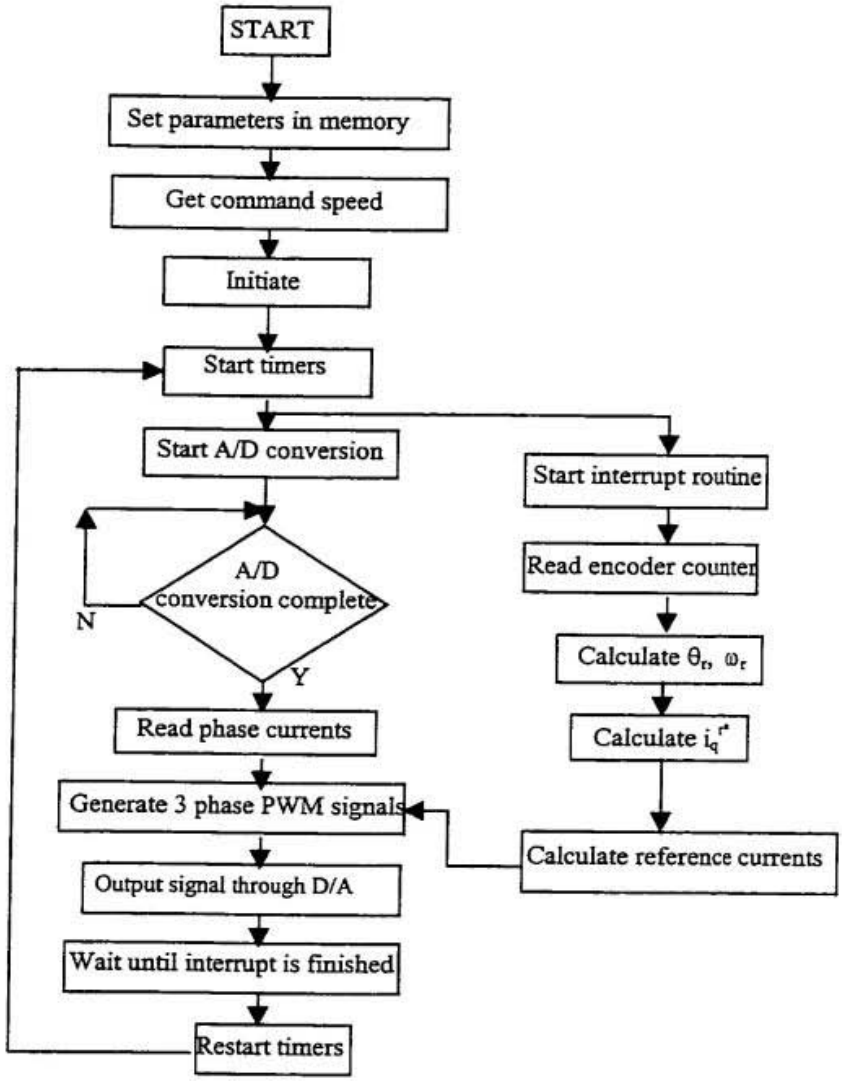

Fig. 2.17. The flow chart of the software for real-time implementation of current-controlled VSI Fed-IPMSM drive.

The control algorithm has been implemented in real time by developing a program in the high level 'C' programming language and is compiled by the Texas Instrument 'C' code generator. Then, the program is down loaded to the DSP board with the help of the dSPACE loader program. The flow chart of the software for real-time implementation of the complete drive is shown in Fig. 2.17. A timer interrupt service routine is set up to read the values of the terminal currents and rotor position angle every 100 μsec. After initializing all the required variables, the speed is calculated from the present and past samples of feedback rotor position angle. The error between the command and actual speeds is then utilized to generate the command currents using a PI controller. In the case of a hysteresis current controller, these command currents are compared to the actual feedback currents to generate the PWM signals for the BJT or IGBT switches of the inverter. In the case of a ramp comparator controller, the error signals between the actual and the command currents are compared to the high frequency carrier signals to generate the PWM signals for the inverter switches. The sampling frequency used to implement the above algorithm is 10 kHz.

2.9 Experimental Results and Discussions

Numerous experimental tests have been completed to evaluate the performance of various current controllers at various speeds. Some sample results have been presented in this thesis. Figures 2.18(a) and (b) show the speed and the corresponding current responses of the drive, respectively, in the case of the sinusoidal band controller at rated speed and no load conditions. The speed responses of the drive at the rated load are shown in Figs. 2.19(a) and 2.19(b) for high speed (188.5 rad./sec.) and low speed (50 rad./sec.) conditions, respectively for the same current

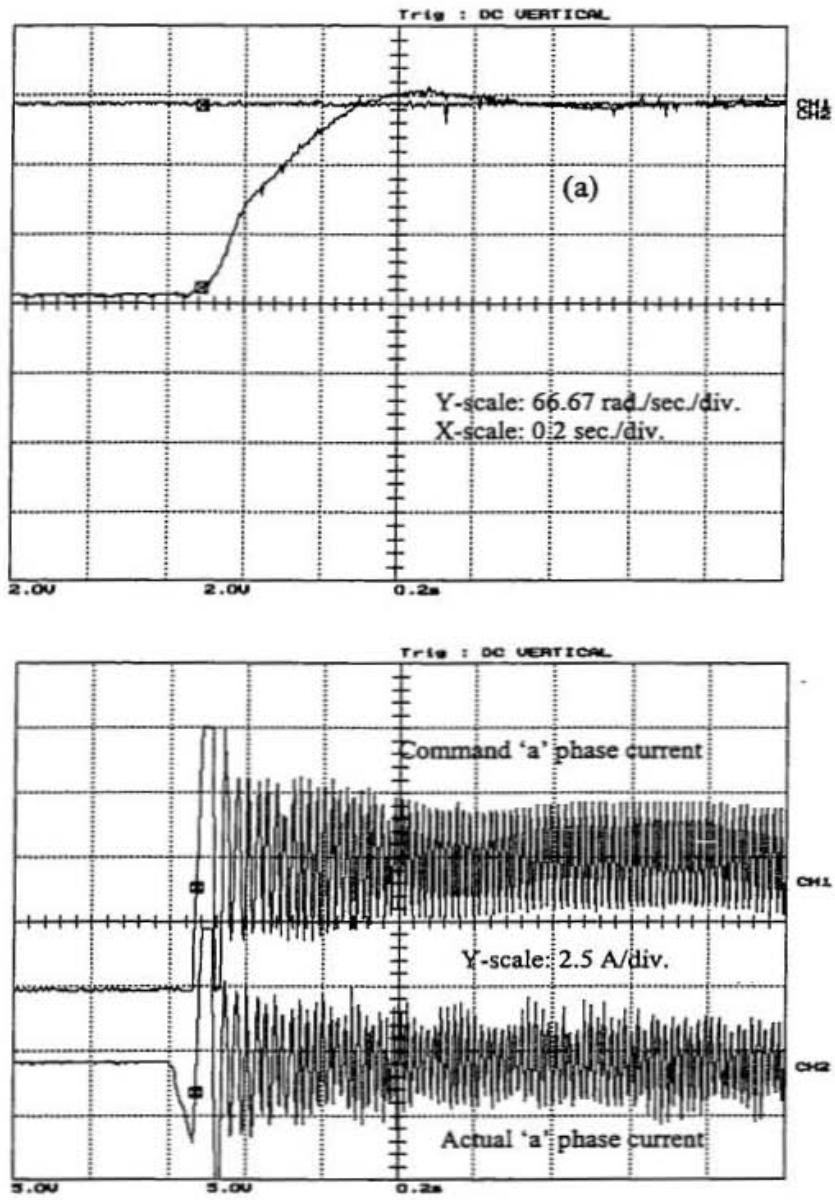

Fig. 2.18. Experimental responses of the drive for the sinusoidal band hysteresis current controller at no load and rated speed: (a) speed, and (b) corresponding 'a' phase actual and command currents.

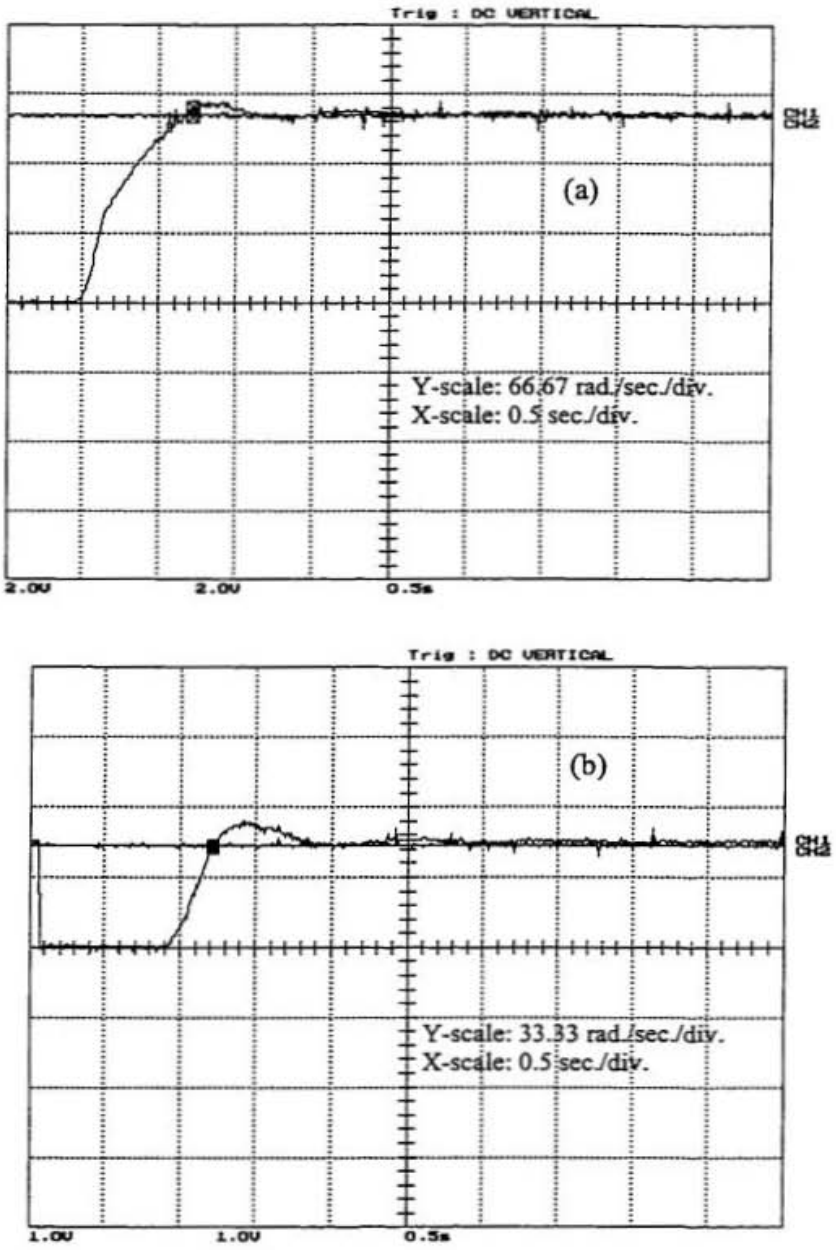

Fig. 2.19. Experimental speed responses of the drive for the sinusoidal band hysteresis current controller at rated load: (a) at rated high speed (188.5 rad./sec.), and (b) at low speed (50 rad./sec.).

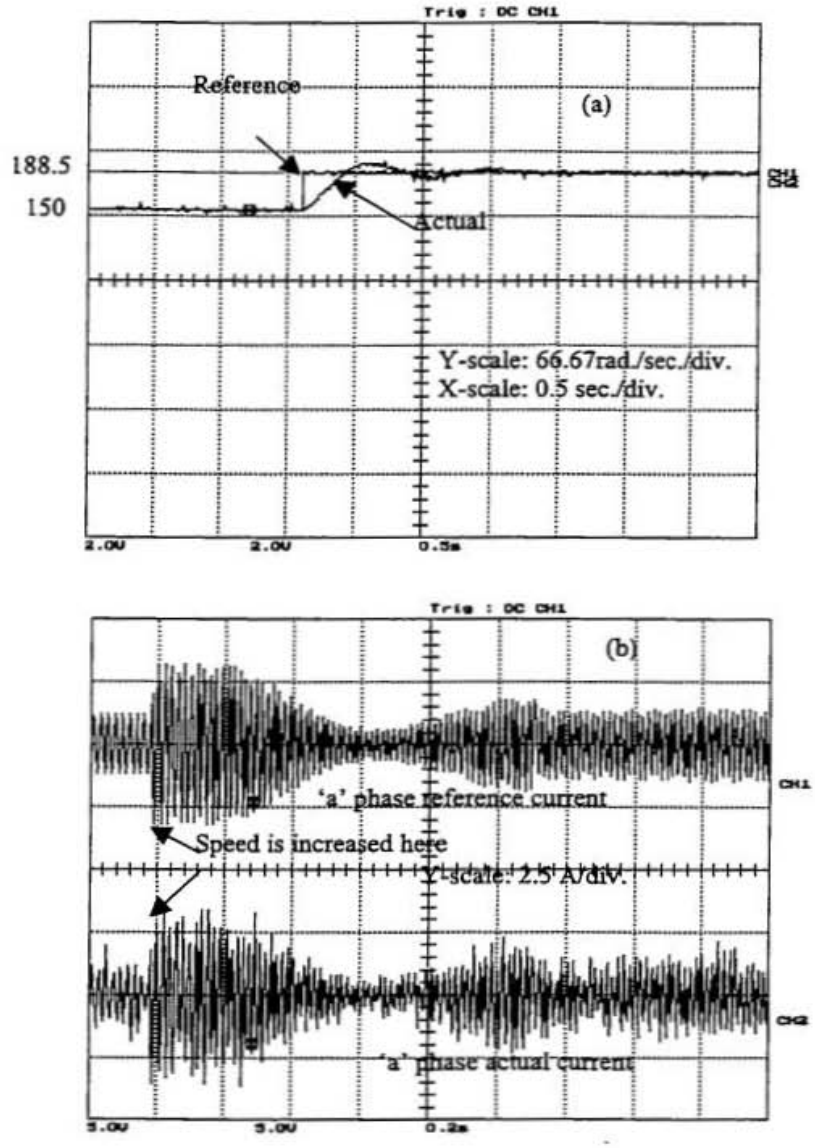

Fig. 2.20. Experimental responses of the drive for the sinusoidal band hysteresis controller: (a) speed, and (b) current responses for a step change of speed at the half load condition.

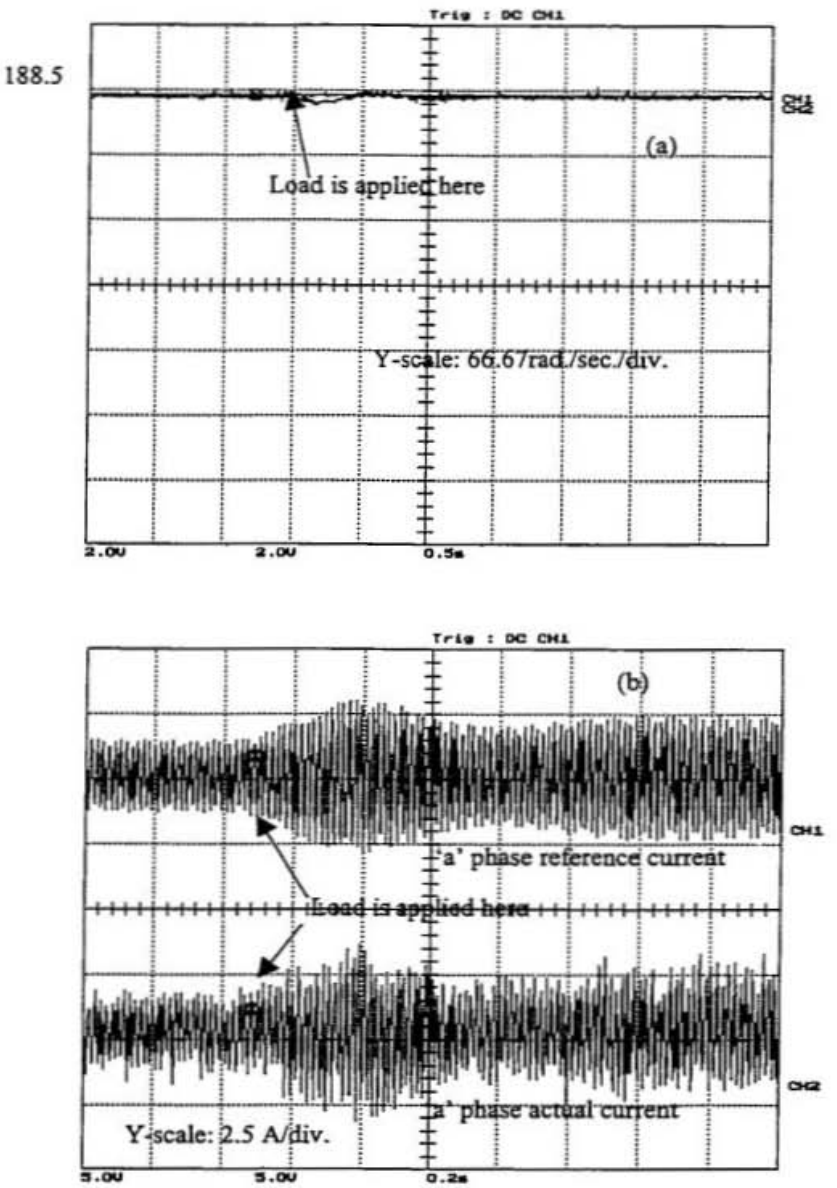

Fig. 2.21. Experimental responses of the drive for the sinusoidal band hysteresis controller: (a) speed response, and (b) current response for a sudden change of load (50%→75%) at the rated speed condition.

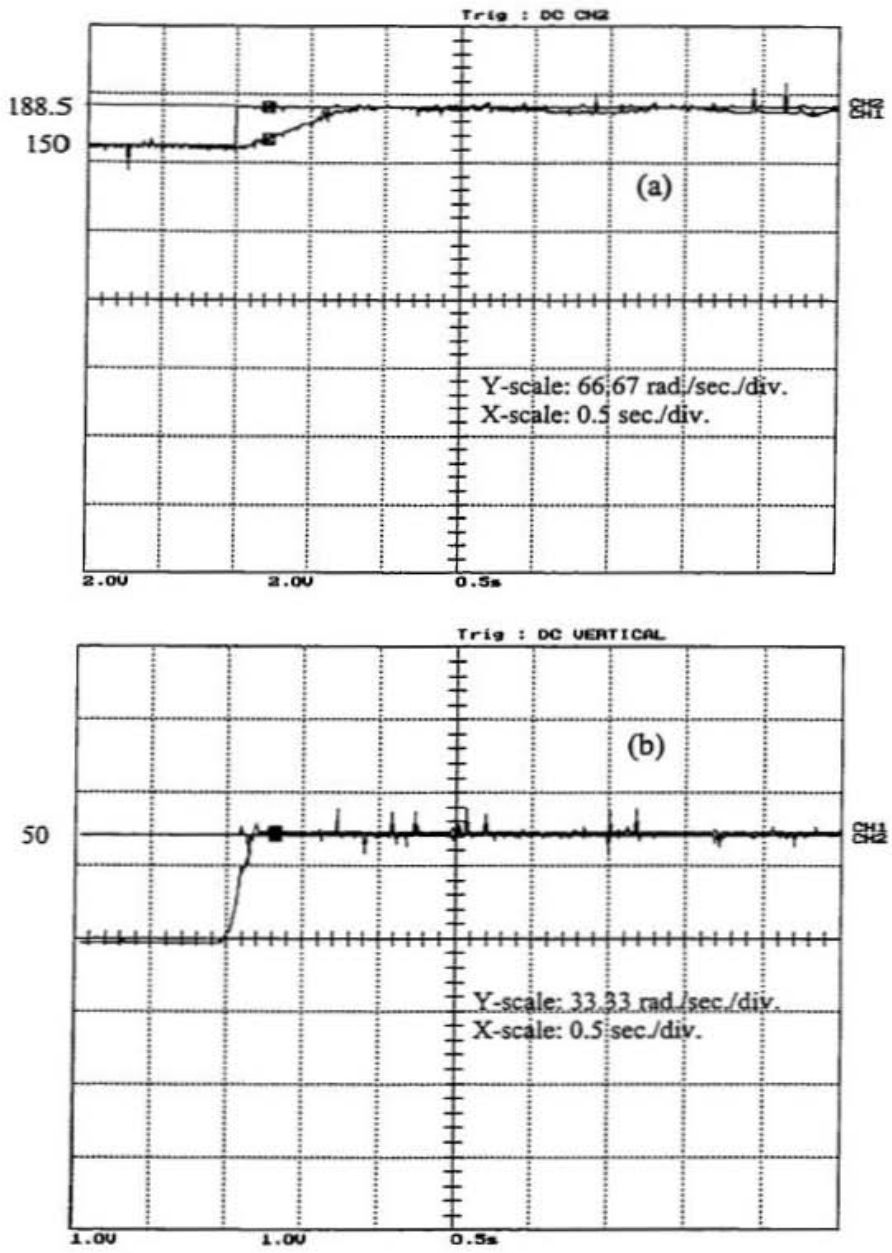

Fig. 2.22. Experimental speed responses of the drive for the conventional ramp comparator controller at half load: (a) at a step change of command speed (150→188.5 rad./sec.), and (b) at low speed (50 rad./sec.).

controller. These results show that the sinusoidal band hysteresis current controller follows the high command speed smoothly without steady state error. However, it follows the low command speed with a small steady-state error as shown in Fig. 2.19(b). Although the error was not measured exactly but the HPD systems will not allow any steady-state error for the drive. Figures 2.20(a) and (b) show the speed and the corresponding current responses for a step change of reference speed, respectively, in the case of the sinusoidal band hysteresis controller. Figures 2.21(a) and (b) show the speed and the corresponding current responses, respectively, at rated speed for a sudden increase of load for the same controller. In both cases, it is shown that the drive can follow the command speed accurately and the actual motor current also follows the command current very quickly even after a sudden change of command speed and load disturbance, as the command speed is high. However, at low command speed with those disturbances the drive may not follow the command speed accurately as it shows error in steady-state where there is no disturbance.

Figures 2.22(a) shows the speed response of the IPMSM drive at a step change of command speed (150→188.5 rad./sec.) for the conventional ramp comparator controller. It is shown that the speed response has a steady-state error at high speed (188.5 rad./sec.). However, the drive follows the low command speed (50 rad./sec.) without any steady state error, as shown in Fig. 2.22(b) for the same controller. It is evident from these figures that the ramp comparator controller can follow the low command speed more accurately than that of the high command speed. From the experimental results, it is observed that the speed responses of the drive at different command speeds for various current controllers show some discrepancies. In the experiment it was also found that the hysteresis controller can follow the low speed

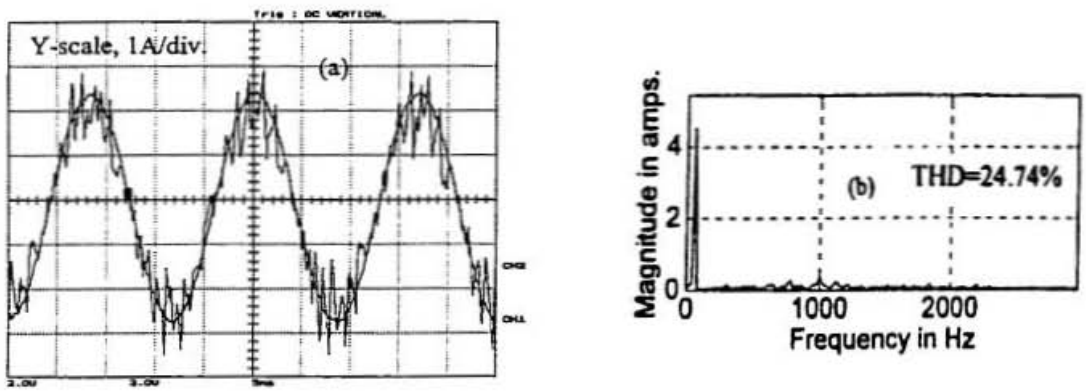

Fig. 2.23. Drive responses for the sinusoidal band controller at high speed (188.5 rad./sec.), H=0.55sin(ωt) A: (a) current; (b) corresponding harmonic spectrum at rated load.

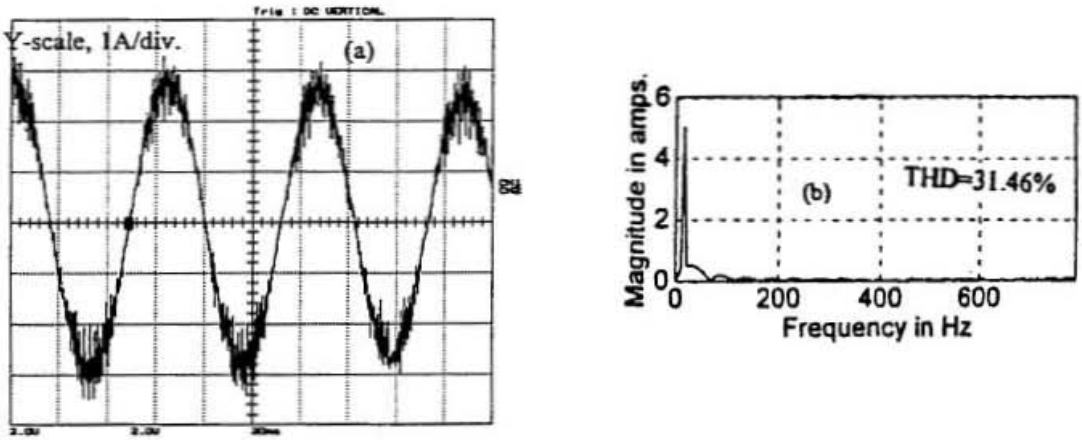

Fig. 2.24. Drive responses for the sinusoidal band controller at low speed (50 rad./sec.), H=0.55sin(ωt) A: (a) current; (b) corresponding harmonic spectrum at rated load.

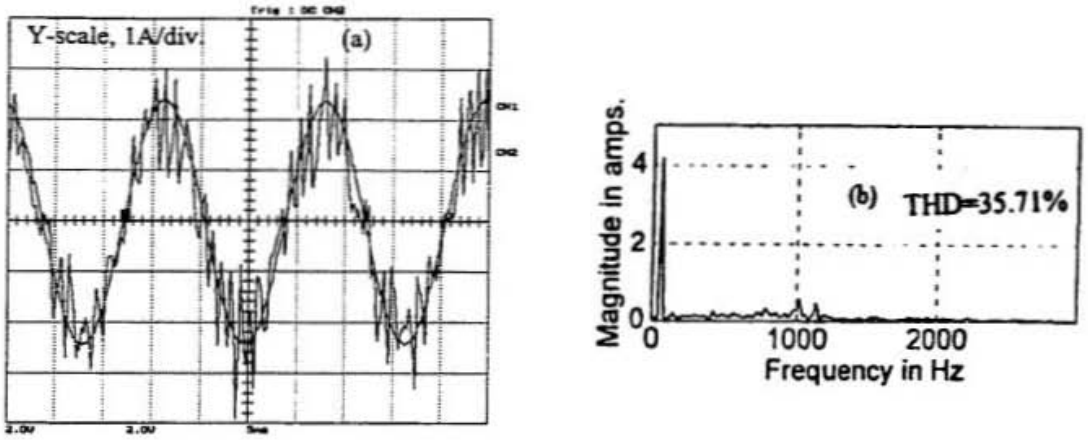

Fig. 2.25. Drive responses for the fixed band controller at high speed (188.5 rad./sec.), H=0.55A: (a) current; (b) corresponding harmonic spectrum at rated load.

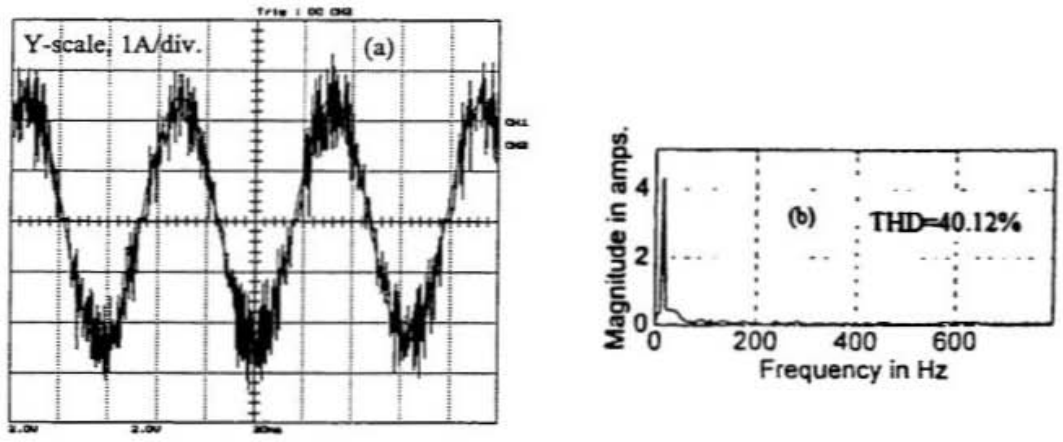

Fig. 2.26. Drive responses for the fixed band controller at low speed (50 rad./sec.), H=0.55A: (a) current; (b) corresponding harmonic spectrum at rated load.

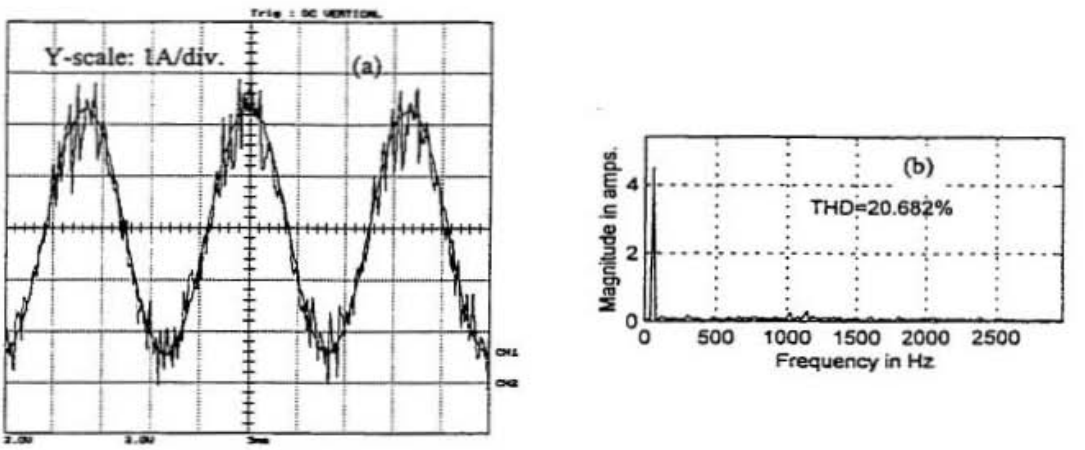

Fig. 2.27. Drive responses for the mixed band controller at high speed (188.5 rad./sec.), H=0.275+0.275sin(ωt) A: (a) current; (b) corresponding harmonic spectrum at rated load.

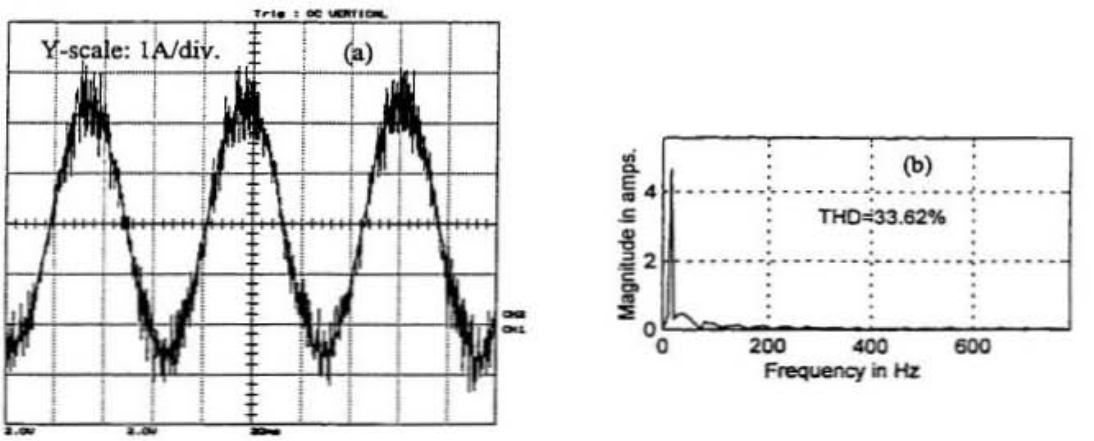

Fig. 2.28. Drive responses for the mixed band controller at low speed (50 rad./sec.), H=0.275+0.275sin(ωt) A: (a) current; (b) corresponding harmonic spectrum at rated load.

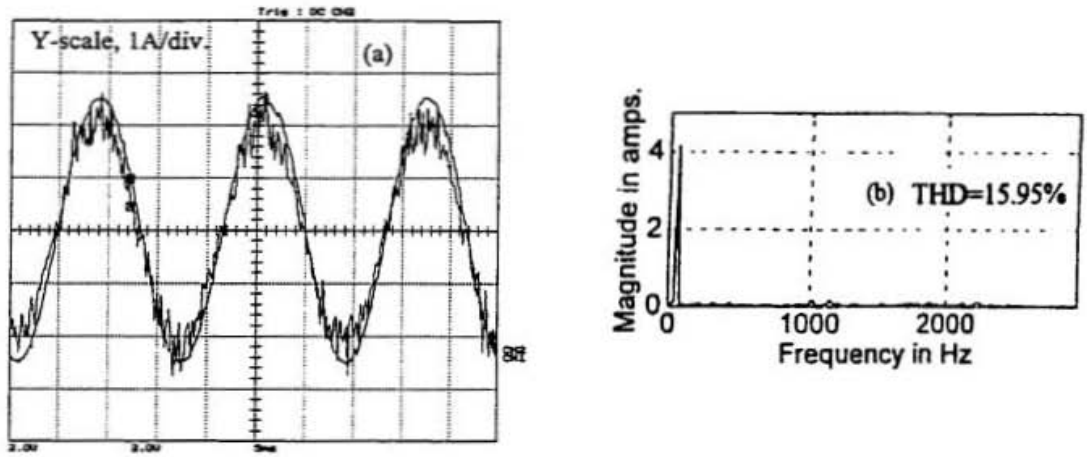

Fig. 2.29. Drive responses for the conventional ramp comparator controller at high speed (188.5 rad./sec.), f=2.5 KHz: (a) current; (b) corresponding harmonic spectrum at rated load.

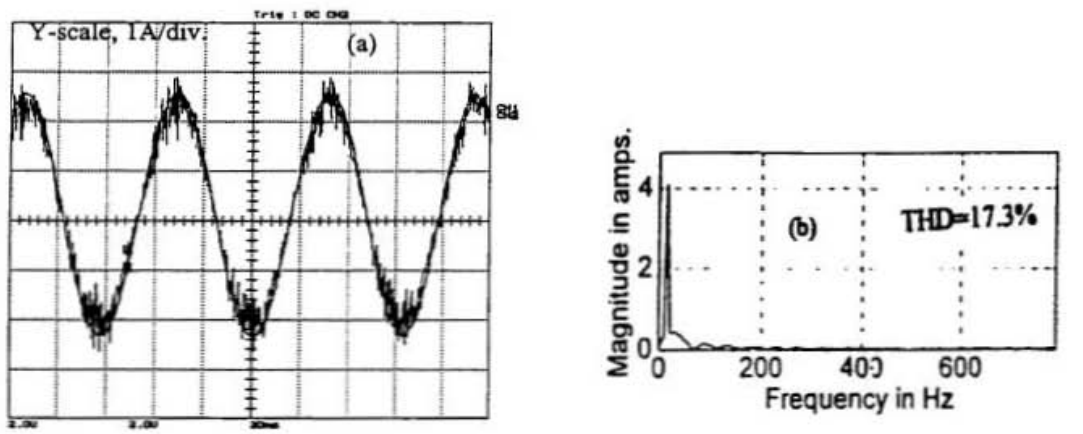

Fig. 2.30. Drive responses for the conventional ramp comparator controller at low speed (50 rad./sec.), f=2.5 KHz: (a) current; (b) corresponding harmonic spectrum at rated load.

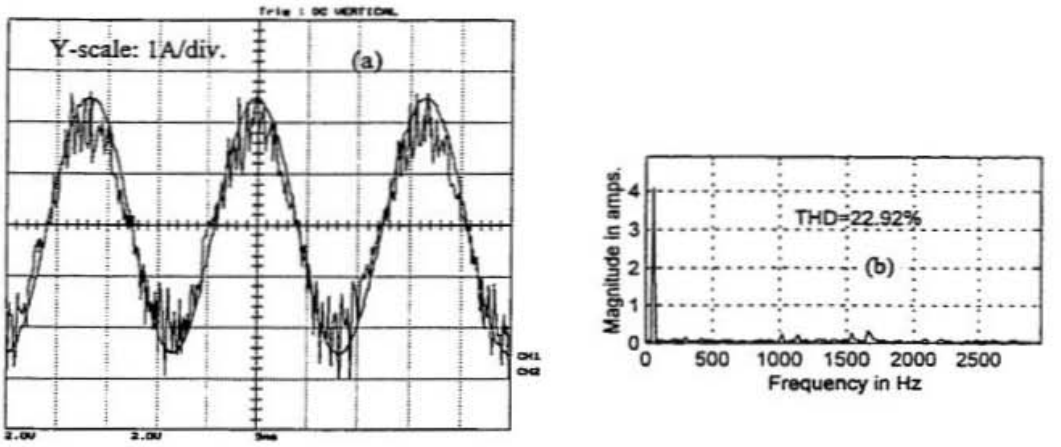

Fig. 2.31. Drive responses for the improved ramp comparator controller at high speed (188.5 rad./sec.), f=2.5KHz: (a) current; (b) corresponding harmonic spectrum at rated load.

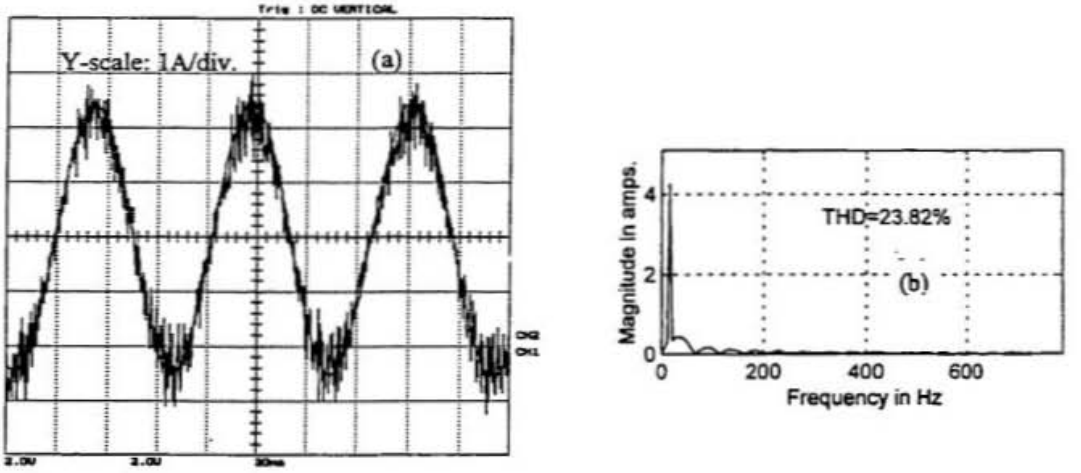

Fig. 2.32 Drive responses for the improved ramp comparator controller at low speed (50 rad./sec.), f=2.5KHz: (a) current; (b) corresponding harmonic spectrum at rated load.

commands and the ramp comparator controller can follow the high speed commands. However, if one runs the motor for a long time they may not even follow the speed commands. Therefore, the hysteresis controller is not stable for low speeds and the ramp controller is not stable for high speeds. The speed discrepancy occurs due to the different nature of actual motor currents for various current controllers at different speed conditions [79]. Therefore, one needs to pay special attention to the analysis of current responses for various current controllers. The frequency spectrum of the current waveform has been obtained by using the Fast Fourier Transform (FFT) after getting the data of the actual motor currents. In the analysis only the 'a' phase current is considered. Figures 2.23 and 2.24 show the current responses at high speed (188.5 rad./sec.) and low speed (50 rad./sec.), respectively, in the case of the sinusoidal band hysteresis controller. It is shown that the total harmonic distortion (THD) is less at high speed. As the motor neutral was not connected to the dc bus mid point, the voltage vector of each leg of the inverter was dependent not only on the state of the corresponding leg but also on the state of the other two legs. As a result, sometimes the motor current cannot follow the command current accurately within the band. Figures 2.25 and 2.26 show the corresponding results for the fixed band hysteresis controller. It is also observed that the THD of the fixed band controller at high speed is smaller than that at low speed. From the above mentioned results it is also observed that, in the case of the sinusoidal band controller, the THD is lower than that of the fixed band controller. However, the maximum inverter switching frequency is very high in the case of the sinusoidal band controller near zero crossing. In the fixed band controller the maximum inverter switching frequency is reduced as compared to the sinusoidal band controller. Figs. 2.27 and 2.28 show the corresponding responses for the

mixed band controller. The results show a compromise between the THD and the inverter switching frequency as compared to the previous two controllers. From the analysis it is shown that the hysteresis controller works well at high speeds. In the experiment it was also found that the hysteresis current controller could not follow the low command speed with stability. This validates the high THD at the low speed condition. Figures 2.29 and 2.30 show the corresponding responses for the conventional ramp comparator controller. It is shown that the motor current has magnitude and phase errors at high speed with the ramp controller, and hence the motor cannot follow the high command speed with stability. Therefore, the ramp comparator is not suitable at high speed in high performance applications. However, at low speed the motor current can follow the command current without significant magnitude and phase errors. Figures 2.31 and 2.32 show the responses for the improved ramp comparator controller. It is shown that the motor current can follow the command current even at the high speed condition without significant magnitude and phase errors. The performance comparison of various current controllers at different operating speeds is summarized in Table II. The Inverpower transistorized inverter module has been used for the experiment. The dc supply was applied through a variac for safe operation.

TABLE II
Performance Comparison of Various Current Controllers

Controller types	Maximum inverter switching frequency	%THD at high speed (188.5 rad./sec.)	%THD at low speed (50 rad./sec.)	Performance at high speed (188.5rad./sec.)	Performance at low speed (50rad./sec.)
Sinusoidal band	high	24.74	31.46	acceptable	acceptable but instability may occur
Fixed band	low	35.71	40.12	acceptable but instability may occur	not acceptable
Mixed band	medium	20.68	33.62	acceptable but instability may occur	not acceptable
Conventional ramp	fixed as ramp signal	15.95	17.3	not acceptable	acceptable but sluggish speed response
Improved ramp	fixed as ramp signal	22.92	23.82	acceptable but sluggish speed response	acceptable but sluggish speed response

The performance analysis of various current controllers establishes that the hysteresis controller is suitable for high speed and the ramp comparator controller is suitable for low and medium speeds. In order to take advantage of both types of controllers, a hybrid controller is proposed for the IPMSM drive. The switching from one controller to another has been done in software.

2.10 Proposed Hybrid Current Controller

In the hybrid current controller, the hysteresis controller scheme for high speed operation and ramp comparator controller scheme for low speed operation are combined in software in order to obtain the best performance over the entire speed range. The principle of operation for the hybrid current controller scheme is

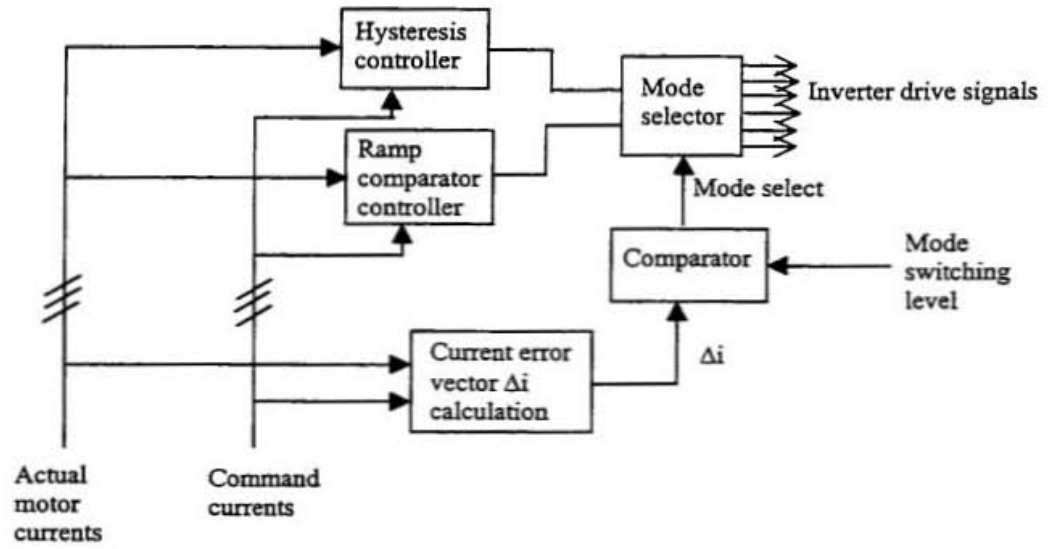

Fig.2.33. Schematic diagram of the proposed hybrid current controller.

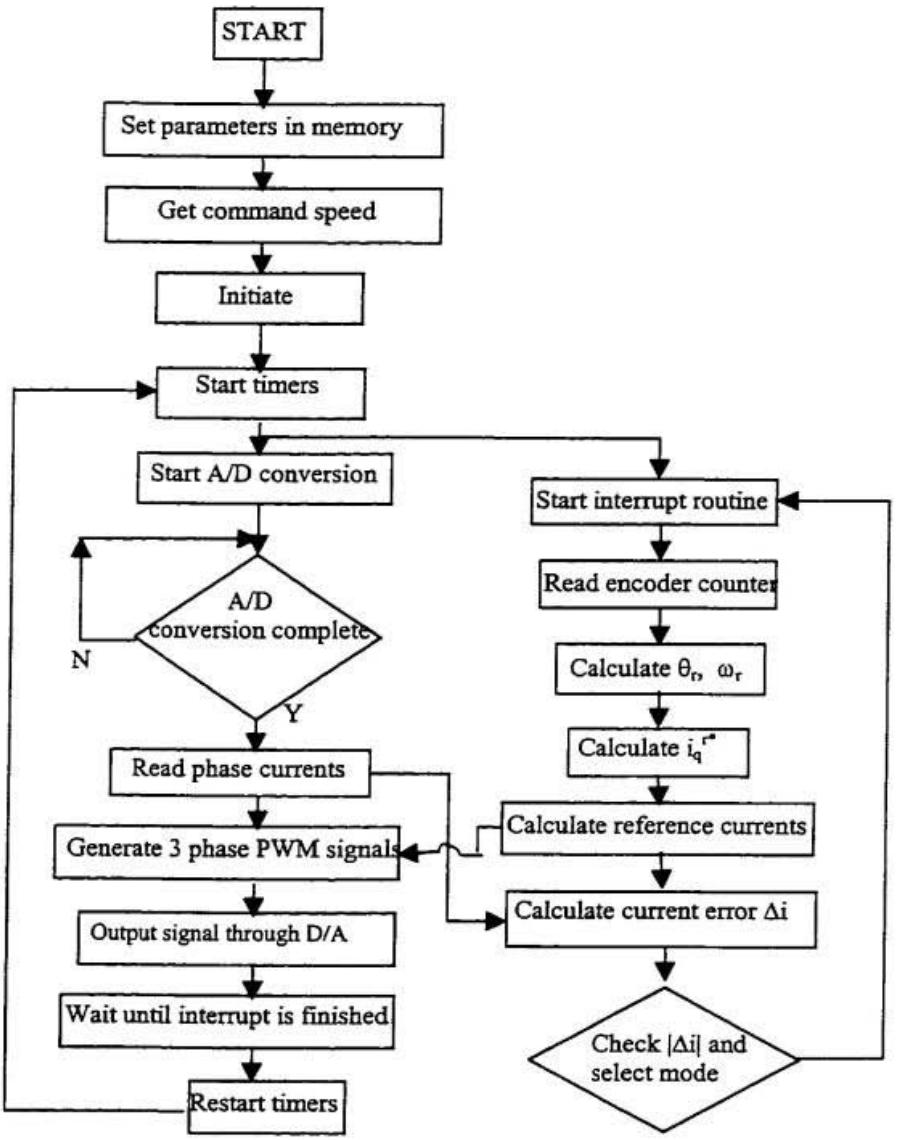

Fig.2.34. Flow chart of the software for real time implementation of the hybrid current controller.

shown in Fig.2.33. The mode switching level between the hysteresis and ramp comparator modes depends on the magnitude of the current error Δi. When |Δi| is greater than the mode switching level the ramp comparator mode is selected. When |Δi| is less than the mode switching level the hysteresis mode is selected to reduce the amplitude and phase errors introduced by the ramp comparator controller. During large current transients such as starting or load variations, etc., the controller will operate in hysteresis mode to achieve fast dynamic responses. The current error vector Δi is given as [80],

$$\Delta i = (2/3)\,[\,(i_a^* + a i_b^* + a^2 i_c^*) - (i_a + a\, i_b + a^2\, i_c)\,] \qquad (2.51)$$

where operator $a = 1\angle 120^\circ$. The mode selection depends on the magnitude of the current error vector Δi which is given by,

$$|\Delta i| = \sqrt{\Delta i_a^* + \frac{1}{3}(\Delta i_b - \Delta i_c)^2} \qquad (2.52)$$

With the assumption that the neutral is not connected, $|\Delta i|$ is given by,

$$|\Delta i| = \sqrt{\Delta i_a^* + \frac{1}{3}(\Delta i_a + 2\Delta i_b)^2} \qquad (2.53)$$

where i_a, i_b and i_c are the measured values of the line currents and their corresponding command values are i_a^*, i_b^* and i_c^*. In order to minimize the switching back and forth between the modes, the value of the mode switching level is chosen to be equal to the ripple current in the ramp comparator controller but within the limit of the hysteresis band. It is found that this criterion ensures stable operation between the operating modes. The flowchart of the software for real-time implementation of the hybrid current controller is shown in Fig. 2.34. In the experimental laboratory 1 hp test IPMSM motor, it was observed that the switching speed from ramp to hysteresis controller was 70 rad./sec.

2.11 Concluding Remarks

The complete current-controlled VSI-fed IPMSM drive has been successfully implemented in real-time in a laboratory 1 hp PM motor. The drive performances have been investigated both in simulation and experimentally. The experimental results validate the simulations. A detailed comparison of various current controller performances for the IPMSM drive has been presented. It is shown that the hysteresis current controller gives better performance at high speeds and the ramp comparator controller gives better performance at low and medium speeds. The performance of the improved ramp comparator controller is better than that of the conventional ramp controller but it increases the computational burden. A hybrid current controller has also been proposed in order to take advantage of the good features of both the ramp and hysteresis controllers. However, the computational burden of the hybrid current controller is also increased. If the inverter is made of fast switching devices like the IGBT then the switching frequency will not be a major problem and hence one can use a sinusoidal band hysteresis controller for optimum performances over the entire speed range.

Chapter 3

Control of IPMSM over Wide Speed Range

Precise control of the high performance IPMSM over a wide speed range is an engineering challenge. In the previous chapter the performance of such motor has been investigated up to the base speed. In the design of the controller the assumption of $i_d = 0$ has been taken and hence the flux supplied by the permanent magnet remains constant. Moreover, the assumption of $i_d = 0$ leads to a non-optimum efficiency and sometimes instability of the IPMSM even below the base speed. As the speed is inversely proportional to the flux due to permanent magnet and proportional to the back emf, in order to operate the motor above the base speed within the rated voltage capacity of the motor and the inverter, the field flux must be decreased. In the case of the IPMSM, direct control of the field flux is not possible. However, the field flux can be weakened by the demagnetizing effect of the d-axis stator current i_d [29]. Above the base speed as the voltage and the current remain fixed to their maximum value, the power remains constant. The operation

above the base speed is called the constant power mode. Some systems like spindle drives and tractions need the constant power mode of operation. Recently, researchers [23,29,30,35,36,81] have reported some work in the flux weakening control technique of the IPMSM. However, the investigation of the flux weakening control technique is in its initial stage as compared to the $i_d = 0$ control technique. So there exists a need for thorough investigation of the flux-weakening control of the IPMSM drive. The performance of the IPMSM drive over a wide speed range for high precision industrial applications is presented in this chapter. The scheme incorporates the maximum torque per ampere (MTPA) operation in the constant torque region i.e., below the base speed and the flux-weakening operation in the constant power region i.e., above the base speed. The power capacities of the motor and the inverter are also considered. The efficacy of the above mentioned control techniques of IPMSM drive system is evaluated by both experimental and computer simulation results. Finally, a comparison between the conventional $i_d = 0$ control and the proposed flux-weakening control technique is presented in this chapter.

3.1 Flux-Weakening Control Principle

The mathematical models of an IPMSM in the d^r-q^r synchronously rotating rotor reference frame for assumed sinusoidal stator excitation are briefly summarized [74] as

$$\begin{bmatrix} v_q^r \\ v_d^r \end{bmatrix} = \begin{bmatrix} r_s + pL_q & P\omega_r L_d \\ -P\omega_r L_q & r_s + pL_d \end{bmatrix} \begin{bmatrix} i_q^r \\ i_d^r \end{bmatrix} + \begin{bmatrix} P\omega_r \psi_m \\ 0 \end{bmatrix} \tag{3.1}$$

The electromagnetic developed torque is given by,

$$T_e = \frac{3P}{2}\left[\psi_m i_q^r + (L_d - L_q) i_d^r i_q^r\right] \tag{3.2}$$

The motor dynamics can be represented by the following equation:

$$T_e = T_L + B_m\omega_r + J_m p\, \omega_r \tag{3.3}$$

The symbols are defined in chapter 2. The first term of Eqn. (3.2) represents the magnet torque component due to the rotor permanent magnet flux ψ_m and the second term represents the reluctance torque due to the complex interaction of d-q axis currents and inductances of the IPMSM. In the case of the IPMSM, i_d^r is negative and the q-axis inductance L_q is greater than the d-axis inductance L_d, so the reluctance torque component is an additional advantage for the IPMSM in terms of performance and cost. The complexity of the control arises due to the nonlinear nature of the torque Eqn. (3.2) for the IPMSM drive system. To make the torque equation linear and the control task easier, usually i_d^r is set to zero. However, in an actual IPMSM nonlinear drive, the assumption of $i_d^r = 0$ leads to erroneous results due to the saturation of the current regulator particularly at high speeds. In the proposed technique i_d^r is not considered zero. The value of i_d^r is calculated from i_q^r maintaining the armature voltage and current within the capacity of the motor and the inverter. This improves the performance of the drive system as compared to the $i_d = 0$ technique.

The stator phase voltage and current can be related to the d-q axis voltages and currents as,

$$V_a = v_d^r + jv_q^r \tag{3.4}$$

$$I_a = i_d^r + ji_q^r \tag{3.5}$$

The maximum value of the stator phase voltage and current are V_m and I_m, respectively. Below the base speed, with the assumption of keeping the absolute value of stator current I_a constant at its maximum value I_m, i_d^r can be calculated in terms of

i_q^r for maximum torque per ampere (MTPA). This is obtained by differentiating Eqn. (3.2) with respect to i_q^r and setting the differentiating result to zero [82] as

$$i_d^r = \frac{\psi_m}{2(L_q - L_d)} - \sqrt{\frac{\psi_m^2}{4(L_q - L_d)^2} + (i_q^r)^2} \tag{3.6}$$

Above the base speed, the steady-state current i_d^r can be calculated in terms of i_q^r in order to maintain the absolute value of stator voltage V_a constant at its maximum value of V_m. This is obtained from Eqns. (3.1) and (3.4) by neglecting the voltage drop across the stator resistance [82] as

$$i_d^r = -\frac{\psi_m}{L_d} + \frac{1}{L_d}\sqrt{\frac{(V_m')^2}{P^2\omega_r^2} - L_q^2(i_q^r)^2} \tag{3.7}$$

where V_m' is the corresponding maximum stator phase voltage.

$$V_m' = \sqrt{(v_{do}^r)^2 + (v_{qo}^r)^2} \tag{3.8}$$

$$v_{do}^r = -P\omega_r i_q^r L_q \tag{3.9}$$

$$v_{qo}^r = P\omega_r i_d^r L_d + P\omega_r \psi_m \tag{3.10}$$

Based on the above algorithm the block diagram of the complete IPMSM drive is shown in Fig.3.1. The typical torque-speed characteristic curve over a wide range of speed is shown in Fig.3.2. Equation (3.7) represents an ellipse in the d-q plane, which indicates that an increase in rotor speed results in smaller ranges for the current vector. By appropriately controlling i_d^r, the amplitude of the terminal voltage is

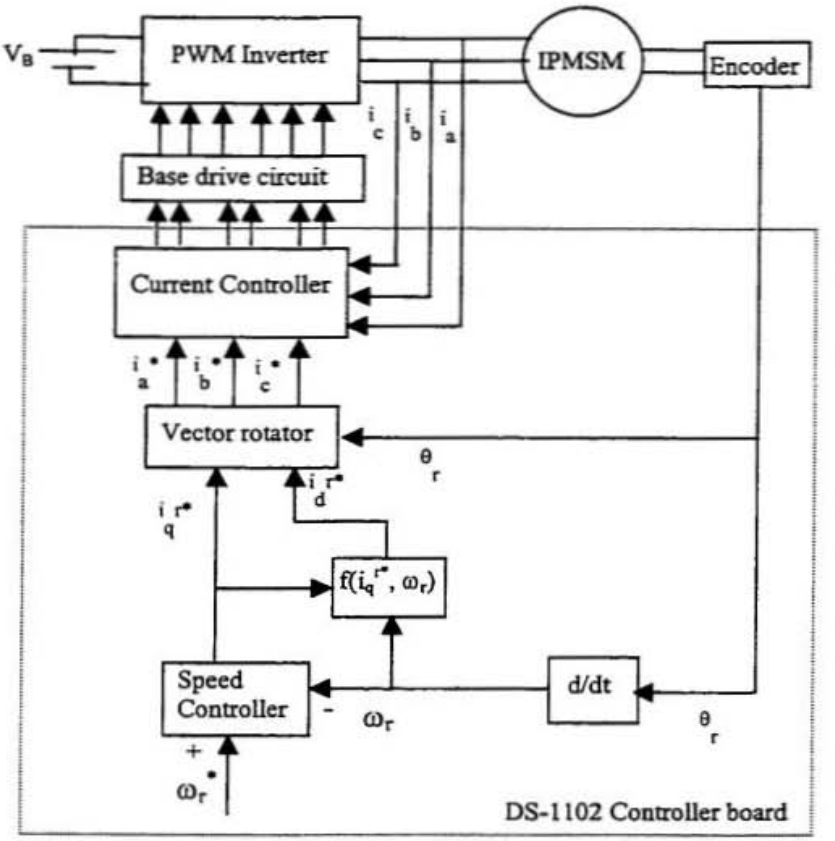

Fig.3.1 Block diagram of the complete IPMSM drive incorporating the flux-weakening operation.

adjusted to V_m. Above the base speed i.e., in constant power region, the voltage remains constant as the magnet flux is weakened by the armature reaction of i_d^r in order to decrease the total air gap flux. The flux-weakening control not only extends the operating limits of the IPMSM drive but also relieves the current regulator from saturation that occurs at high speed operation. The maximum amplitude of the phase voltage V_m, which can be sustained by the inverter without saturation of the current regulator, is given as a function of the dc bus voltage V_B as,

$$V_m = (2 / \pi)\, V_B \tag{3.11}$$

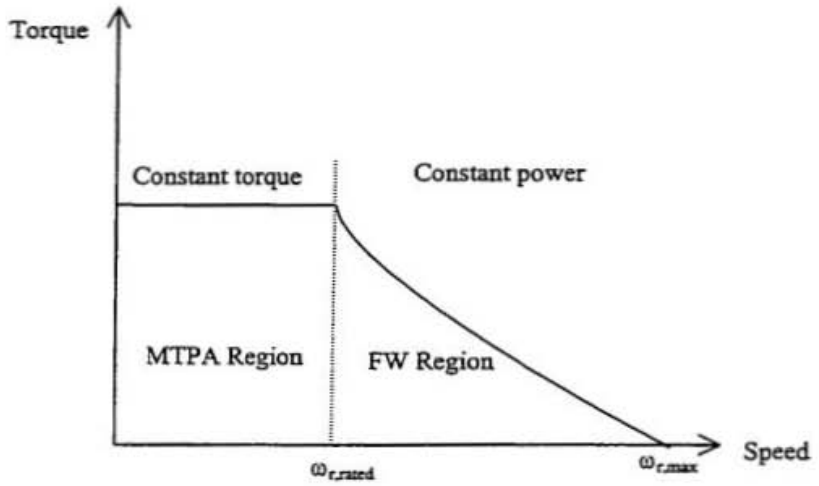

Fig. 3.2 Typical torque-speed characteristic curve over wide range of speed.

It is seen from Eqns. (3.1) and (3.4) that in case of $i_d^r = 0$, the magnitude of the terminal voltage V_a increases with an increase in motor speed ω_r or the q-axis current i_q. Therefore, the saturation of the current regulator occurs at high speeds for a given torque when the motor terminal voltage approaches V_m. This may cause instability of the drive for $i_d^r = 0$ control. From Eqn. (3.7) the maximum attainable speed for a given set of maximum stator voltage and current can be calculated as,

$$\omega_{r\,max} = \frac{\sqrt{V_m^2 - r_s^2 I_m^2}}{P(\psi_m - L_d I_m)} \tag{3.12}$$

In the case of the conventional i_d=0 control technique, the maximum attainable speed can be calculated in order to maintain the maximum voltage limitation of the inverter as,

$$\omega_{r\,max} = \frac{V_m}{P\psi_m} \tag{3.13}$$

3.2 Implementation of the Flux-Weakening Control

The complete IPMSM drive has been implemented in real-time using a digital signal processor (DSP) controller board DS-1102 on a laboratory 1 hp IPMSM drive. The general implementation procedure is the same as described in chapter 2. For real-time implementation of the control algorithm, a program has been developed in the high level ANSI 'C' programming language. The flow chart of the software for real-time implementation of the proposed flux-weakening control algorithm is shown in Fig. 3.3.

3.3 Results and Discussions

The performances of the drive system have been investigated both experimentally and in simulation. Fig.3.4 shows the steady-state developed torque against the 'a' phase current I_a at a constant speed of 100 rad./sec. for both the conventional i_d=0 control technique and the flux-weakening control (FWC) technique where i_d is not zero. It is shown that in the case of the flux-weakening control, the motor can develop more torque for the same stator current as compared to the i_d=0 control technique. This feature exhibits that for the proposed control the motor can carry the higher load while maintaining stability. It is also observed that for the same stator current the motor develops more torque at high speed operation. The simulated transient and steady-state responses for a step change of speed at rated load for the flux-weakening control technique are shown in Fig.3.5. This figure demonstrates that the motor can follow the speed without any steady-state error in both the constant torque and constant power regions. In the constant torque region, i_q^{r*} is almost constant and i_d^{r*} is nearly zero but in the constant power region, i_q^{r*} decreases with the increase of speed and i_d^{r*} becomes more negative to demagnetize

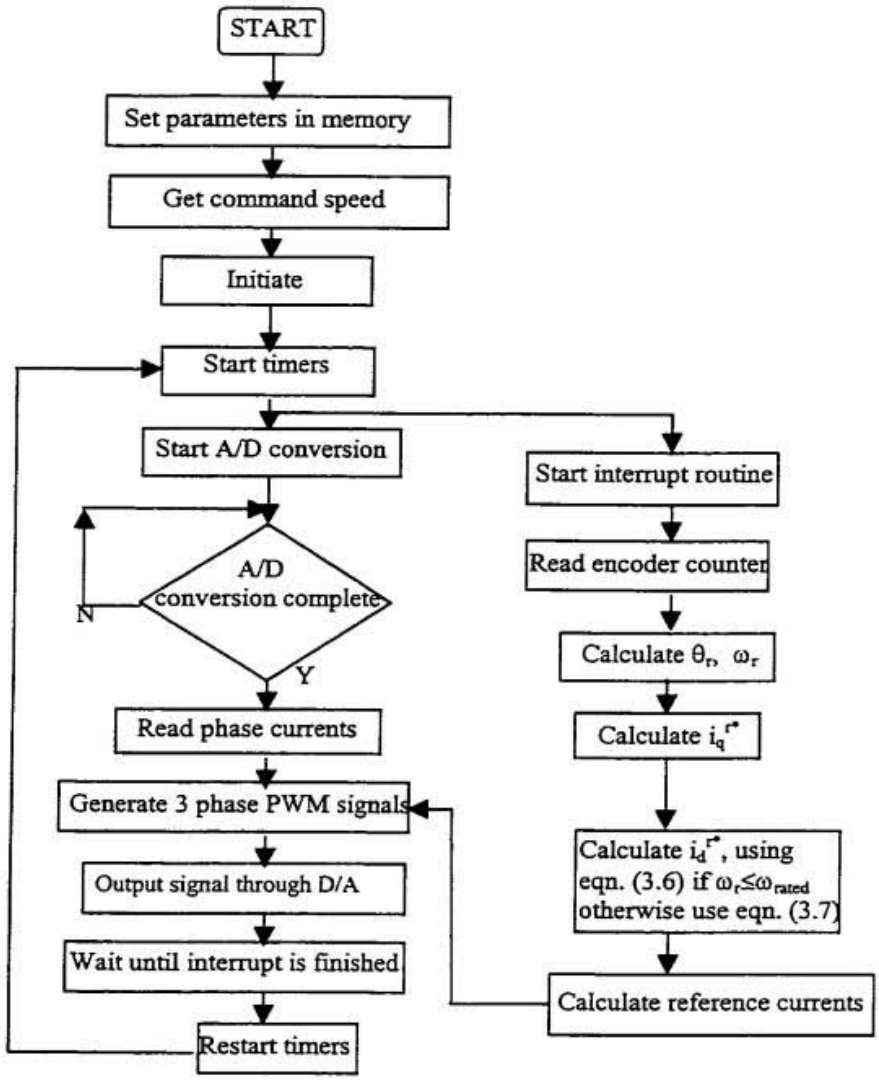

Fig.3.3 Flow chart of the software for real-time implementation of the proposed flux-weakening control algorithm of IPMSM drive.

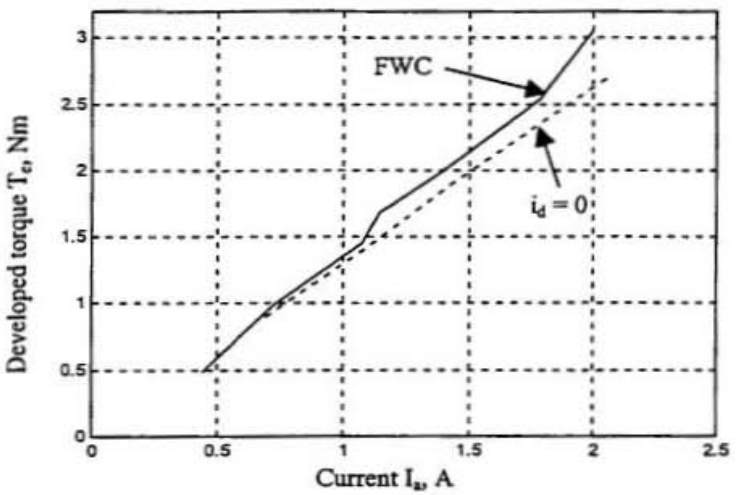

Fig.3.4. Experimental torque-current relation for both flux weakening control (FWC) and i_d=0 control techniques at a speed of 100 rad./sec.

the field flux. Above the base speed, i_q^{r*} decreases with increase of speed. This means that the torque decreases with the increase of speed in order to maintain the constant power. Figs. 3.6(a) and (b) show the experimental speed responses for a step change of speed for i_d=0 and the flux-weakening control (FWC) techniques, respectively. It is shown that for the FWC technique the motor reaches the steady-state speed earlier without any oscillation. Figs. 3.7(a) and (b) show the experimental speed response for a sudden change of load for i_d=0 and the flux weakening control techniques, respectively in the constant power region. It is observed that the FWC technique is relatively insensitive for sudden changes of load over a wide speed range. While for i_d=0 control there is a significant drop in speed and the actual motor speed cannot follow the command speed smoothly. In experiment it has been observed that for i_d=0 control above the base speed, the experimental motor was vibrating even at steady state condition. This is shown by the spikes in

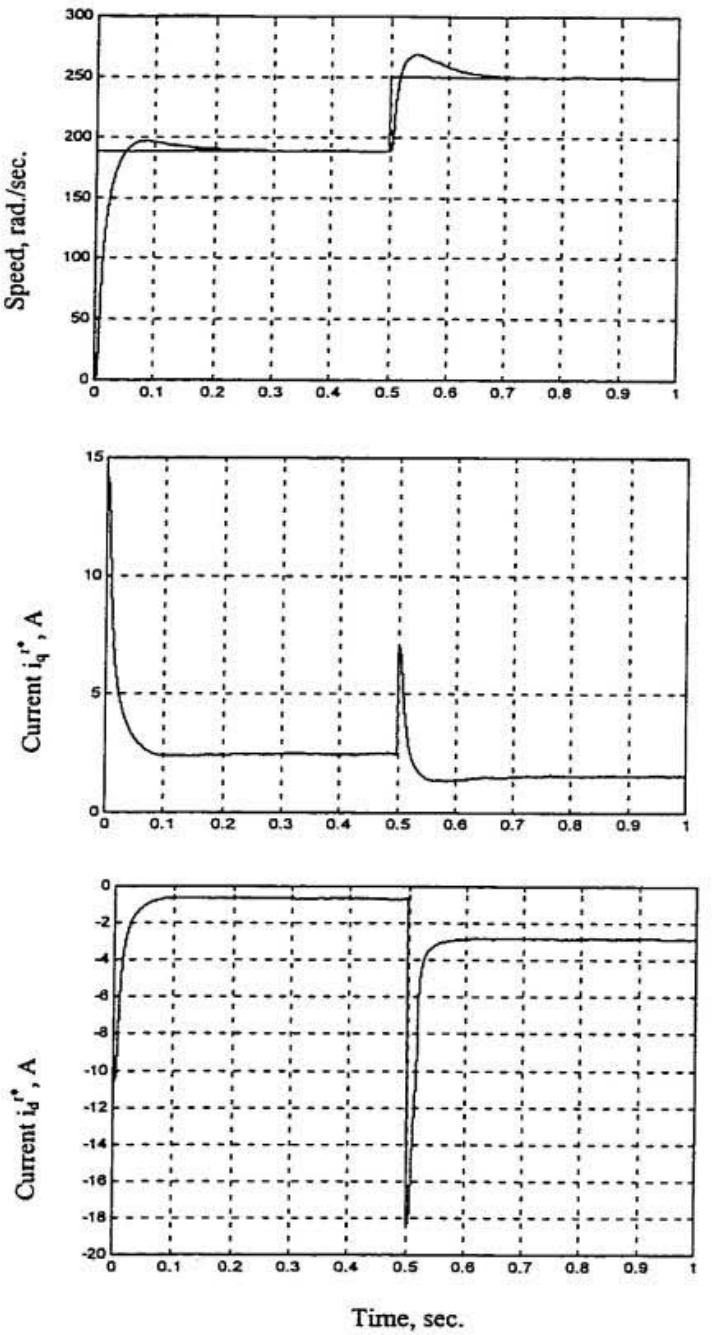

Fig. 3.5. Simulated transient responses of the drive for step change of speed at rated load using the flux weakening control technique: (a) speed, (b) q-axis command current and (c) d-axis command current.

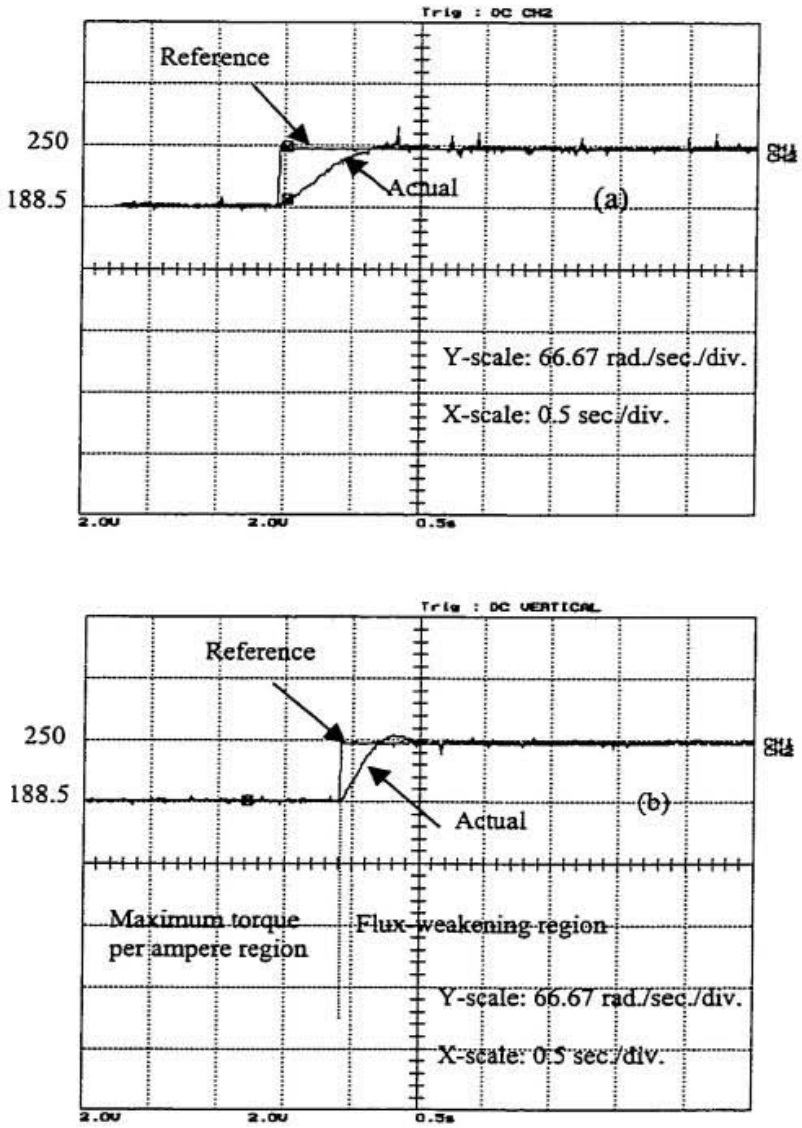

Fig.3.6. Experimental speed responses for a step change of command speed, (a) i_d =0; (b) flux-weakening control technique.

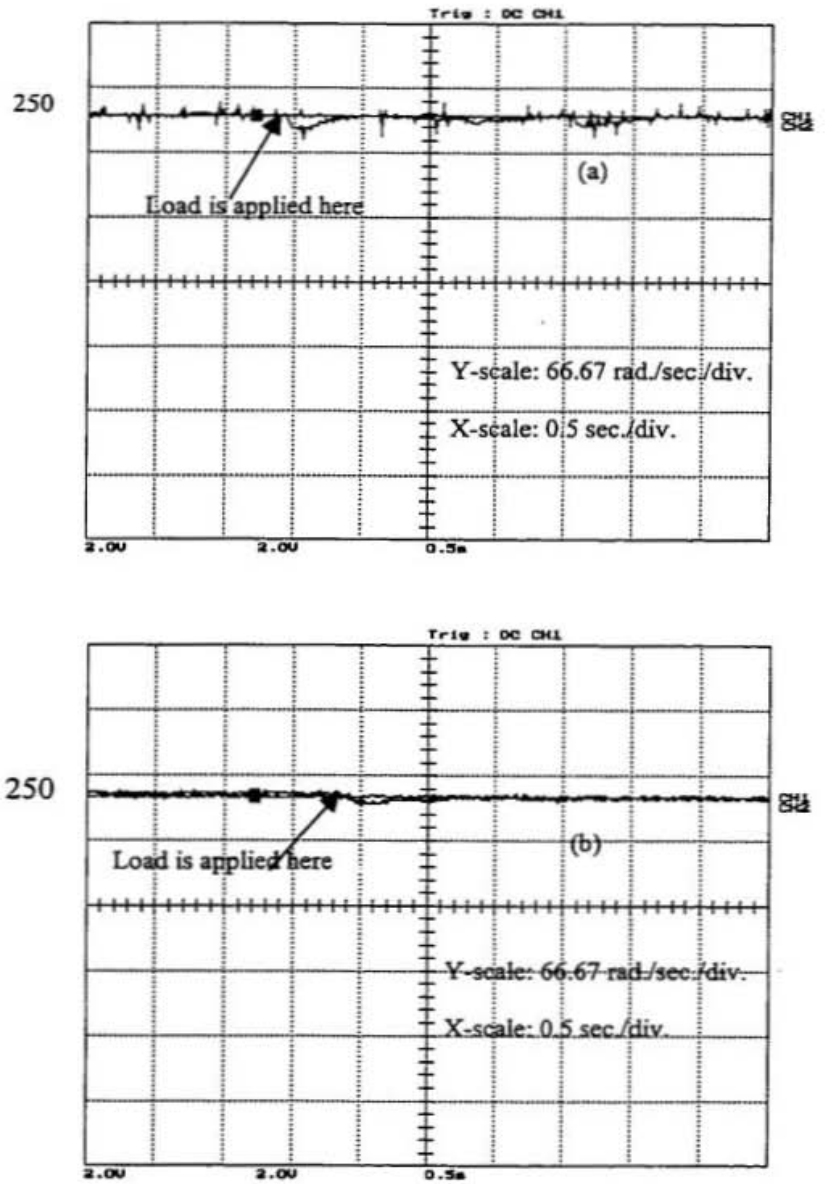

Fig.3.7. Experimental speed responses for sudden increase of load (50%→75%), (a) i_d =0; (b) flux-weakening control techniques.

Figs. 3.6(a) and 3.7(a). But in the case of the flux weakening control technique, the motor was running smoothly even after some disturbances in the constant power region. The almost negligible spikes in Figs. 3.6(b) and 3.7(b) show these smooth operations. Therefore, it is found that the proposed FWC technique is more robust as compared to the conventional i_d=0 control technique over a wide speed range.

3.4 Concluding Remarks

The complete drive system has been implemented successfully for the laboratory 1 hp motor incorporating the flux weakening operation. The performances of the drive system have been investigated for both i_d=0 and the flux-weakening control techniques by computer simulation and experimental results. The simulation has been carried out using the Matlab Simulink software [75]. From the results it is shown that the drive system for the flux-weakening control technique is more robust than the conventional i_d=0 control technique in the case of a sudden change of speed or load disturbances over a wide speed range. Moreover, for the i_d=0 control technique, the maximum attainable speed is limited. In the case of the flux-weakening control, the operating speed range of the drive has been increased significantly as the motor was running smoothly up to 400 rad./sec.

Chapter 4

Fuzzy Logic Based Speed Controller

In a FLC, the system control parameters are adjusted by a fuzzy rule based system, which is a logical model of the human behavior for process control. Presently, fuzzy logic is being used for many engineering applications such as image processing, pattern recognition, load forecasting, power scheduling and cost estimation in power systems, power electronic equipment controls and also for motor control to be used in HPD systems. The advantages of FLCs over the conventional fixed gain PI, PID and some adaptive controllers such as MRAC, SMC, etc. are:

(1) The design of FLC does not need the exact mathematical model of the system. This is a great advantage in motor drive applications where the motor and the load dynamics are described by nonlinear and/or unknown differential equations.

(2) The FLC is better than the conventional controllers in terms of insensitivity to parameter and load variations, response time, settling time and robustness.

(3) It can handle nonlinear functions of arbitrary complexity.

(4) It is based on the linguistic control rules (LCRs) which are also the basis of human logic.

In motor drive applications, the FLC is mainly used as a speed controller. The speed is a linguistic variable if its values are high, low, medium, etc. As the fuzzy logic controller is based on linguistic variables and fuzzy rules, the control system is easily understandable even to non-expert users. Therefore, the fuzzy logic controller is a new approach to make the process control automotive.

4.1 Fundamentals of Fuzzy Logic Related to Control Applications

Fuzzy logic controllers are based on fuzzy set and fuzzy logic theory introduced by Zadeh [56]. The fuzzy set (subset) A on the universe (set) X is defined by a membership function, μ_A, from X to the real interval [0,1], which associates a number $\mu_A(x) \in [0,1]$ to each element x of universe X. The membership function $\mu_A(x)$ represents the grade of the membership function of x to A, i.e., a subjective value for the degree of A-ness of x. The equation $\mu_A(x)=0.5$ means x has A-ness of about 50%. A fuzzy singleton $S(x_o) = \mu(x)|_{x_o}$ is a fuzzy set that supports only one element x_o. Therefore, the fuzzy set is a union of fuzzy singletons of its constituents. In the fuzzy set theory, the boundaries of the fuzzy sets can be vague and ambiguous, just to make it useful for approximate systems. Fuzzy sets are represented graphically by means of their membership functions.

There are numerous choices for the membership functions. Fig.4.1 shows some possible choices of membership functions for a fuzzy set associated with the linguistic value ZE (zero) in the universe X=[-1, 1]. From Fig.4.1 it is shown that the number 0 fully belongs to the fuzzy sets while the numbers –1 and +1 do not

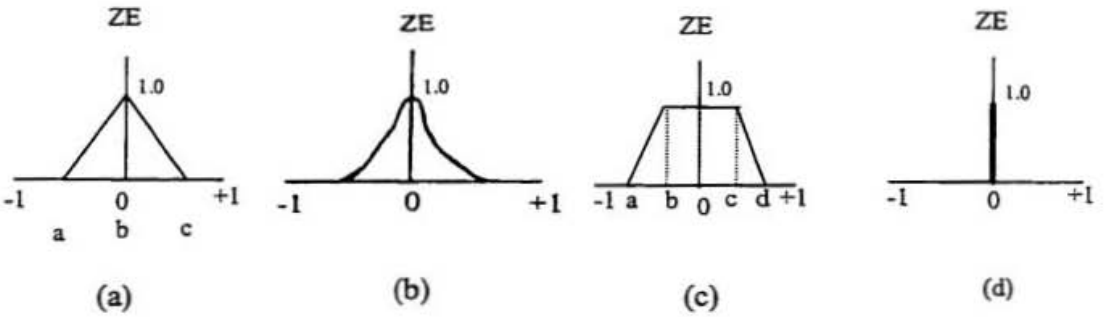

Fig.4.1. Membership functions of linguistic value zero: (a) triangular, (b) Gaussian function, (c) trapezoidal and (d) singleton

Mathematically the above membership functions can be defined as,

a) triangular: $$f(x;a,b,c)=\begin{cases}0, & x\le a\\ \dfrac{x-a}{b-a}, & a\le x\le b\\ \dfrac{c-x}{c-b}, & b\le x\le c\\ 0, & x\ge c\end{cases}$$

b) Gaussian function: $$f(x;\sigma,c)=e^{\frac{-(x-c)^2}{2\sigma^2}}$$

c) trapezoidal: $$f(x;a,b,c,d)=\begin{cases}0, & x\le a\\ \dfrac{x-a}{b-a}, & a\le x\le b\\ 1 & b\le x\le c\\ \dfrac{d-x}{d-c}, & c\le x\le d\\ 0, & x\ge d\end{cases}$$

d) singleton: $$f(x)=\begin{cases}1, & x=x_o\\ 0, & x\ne x_o\end{cases}$$

belong to the fuzzy sets at all. The choice of fuzzy logic membership functions depends on the designer's preference and/or experience. In fuzzy logic there are not only the standard membership functions but also the designer can generate his/her own membership functions. Fuzzy logic implements human experiences and preference via membership functions and fuzzy rules. The complete process of formulating the mapping from a given input to an output using fuzzy logic is known as fuzzy inference. There are two types of fuzzy inference methods: the Mamdani type and the Sugeno type. The difference between the two methods is only in the way the output is defined. In control applications, Mamdani type fuzzy inference is the most commonly used method. In the Mamdani method the output is defined by the centroid of a two-dimensional function. Fuzzy inference is mainly based on three components which are: (1) fuzzification, (2) fuzzy inference engine (rule base) and, (3) defuzzification. These are described briefly in following sub-sections.

4.1.1 Fuzzification

The first step of fuzzy inference is to take inputs and determine the degree to which they belong to each of the appropriate fuzzy sets via membership functions. The process of converting a numerical variable (real or crisp value) into a linguistic variable (fuzzy value) is called fuzzification. In the FLC, the input is a numerical value limited to the universe of the input variable and the output is fuzzy degree of membership in the qualifying linguistic set (between 0 and 1 inclusive). Mathematically, the fuzzification of an input can be obtained using a singleton fuzzifier according to the equations of pre-selected membership functions of various fuzzy sets of that input.

4.1.2 Fuzzy inference engine (Rule base)

In a fuzzy logic controller, the fuzzy inference engine is composed of a set of conditional statements like "if-then" control rules to obtain the results of all applicable rules, where both the antecedent (if...) and the consequent (then...) parts are expressed in linguistic form. It computes the fuzzy value of the output using a composition of two fuzzy inputs through a fuzzy rule base matrix. The fuzzy inference engine, i.e., the rule evaluation, includes two processes: first the application of the fuzzy operator (AND or OR) in the antecedent and then implication from the antecedent to the consequent. A typical rule can be written as follows:

$$\text{Rule } R_k : \text{If } \Delta\omega \text{ is } A_k \text{ and } \Delta e \text{ is } B_k \text{ then i is } C_k \qquad (4.1)$$

where speed error $\Delta\omega$ and change of speed error Δe are the input linguistic variables, current i is the output linguistic variable; and A_k, B_k, and C_k are the labels of linguistic variables $\Delta\omega$, Δe and i, respectively. If the antecedent is true to some degree of membership, the consequent is also true to that same degree. The fuzzy operators used for fuzzy rules are AND ($\cap$), OR ($\cup$) and NOT ($\overline{\ }$) which can be defined as follows:

a) AND means classical intersection: $\mu_{A\cap B} = \min\{\mu_A(x), \mu_B(x)\}$

b) OR means classical union: $\mu_{A\cup B} = \max\{\mu_A(x), \mu_B(x)\}$ (4.2)

c) NOT means classical complement: $\bar{\mu}_A = 1 - \mu_A(x)$.

Therefore, according to rule R_k, $\mu_{ck}(x)=\min(\mu_{Ak}(x), \mu_{Bk}(x))$. The fuzzy rules can be derived by using the following approaches:

a) from expert experience and control engineering knowledge

b) from the behavior of human operators

c) from a fuzzy model of a process

d) from a learning process.

With respect to fuzzy control, Mamdani implication is the most important implication known in the literature [83]. The graphical representation of Mamdani implication in order to interpret the meaning of a rule is shown in Fig.4.2. This figure shows the firing of a rule "if $\Delta\omega$ is PS (positive small) the output 'i' is NS (negative small)". In this figure, $\Delta\omega^*$ is the crisp input and the deep solid lines in the output membership function $\mu_{NS}(i)$ indicates the modified (clipped) membership function $\mu_{CNS}(i)$. Thus according to Mamdani implication,

$$\mu_{CNS}(i) = \min(\mu_{PS}(\Delta\omega^*), \mu_{NS}(i)) \qquad (4.3)$$

The process described by this equation is called rule firing. The inference engine or rule firing as described above can be of two basic types such as: (1) composition based and (2) rule based inferences. The basic differences between them are described below.

(1) Composition based inferences: In this inference, the fuzzy relations representing the meaning of each rule are aggregated into one fuzzy relation describing

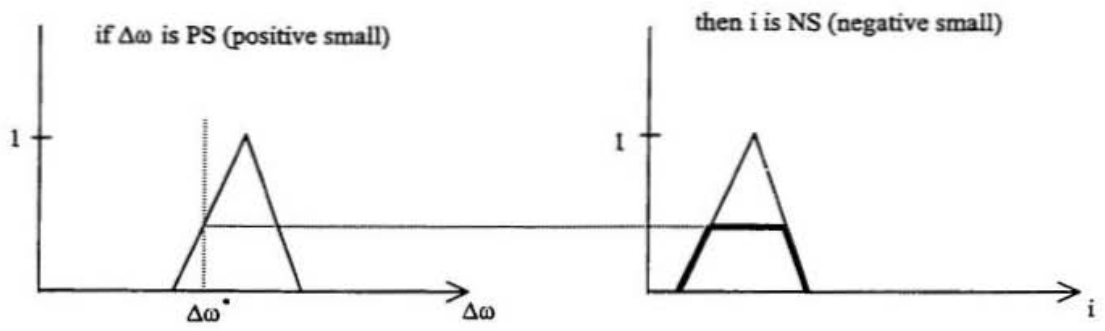

Fig.4.2 The graphical representation of the firing of a rule using Mamdani implication method.

the meaning of the overall set of rules. Then, inference or firing with this fuzzy relation is performed via the operation composition between the fuzzified crisp input and the fuzzy relation representing the meaning of the overall set of rules. As a result of the composition one obtains the fuzzy set describing the fuzzy value of the overall control output.

(2) Individual rule based inference: In this inference, first each single rule is fired. This firing can simply be described as: (a) computing the degree of match between the crisp input and the fuzzy sets describing the meaning of the rule-antecedent and (b) clipping the fuzzy set describing the meaning of the rule-consequent to which the rule-antecedent has been matched by the crisp input. Finally, the clipped values for the control output of each rule are aggregated, thus forming the value of the overall control output.

Usually, the individual rule based inference is preferred since it is computationally very efficient and saves a lot of memory. In this thesis, the individual rule based inference is used. However, the composition based inference is equivalent to the individual rule based inference in the case of Mamdani-type implication used to represent the meaning of the individual rules. In the case of individual rule based inference, the overall control output which is a combined fuzzy set from a set of rules can be mathematically expressed in [83] as

$$\mu_I(i) = \max(\mu_{CLI(1)}(i), \ldots, \mu_{CLI(n)}(i)) \tag{4.4}$$

where $\mu_{CLI(k)}$ (k=1,2,...,n) is the clipped value of the control output 'i' in the case of individual (kth) rule based inference.

$$\mu_{CLI(k)}(i) = \min(\min(\mu_{A(k)}(\Delta\omega^*), \mu_{B(k)}(\Delta e^*)), \mu_{C(k)}(i)) \tag{4.5}$$

where $\mu_{A(k)}(\Delta\omega^*)$ is the degree of membership of the crisp input $\Delta\omega^*$ in fuzzy set $\mu_{A(k)}$, $\mu_{B(k)}(\Delta e^*)$ is the degree of membership of the crisp input Δe^* in fuzzy set $\mu_{B(k)}$, and $\mu_{C(k)}(i)$ is the degree of membership of the output 'i' in fuzzy set $\mu_{C(k)}$.

4.1.3 Defuzzification:

Defuzzification is the final process of fuzzy inference in getting the control output. The input for the defuzzification process is a fuzzy set (combined output of each rule) and the output is a single number, which is non-fuzzy i.e., a crisp value. Various defuzzification methods such as center of gravity (COG), center of sums, center of largest area, first of maxima, middle of maxima, etc. are available. The center of gravity/area defuzzification method is used in this work. In the center of gravity method there are various kinds of mathematical forms but for on-line implementation of the IPMSM drive in order to reduce the computational burden the following mathematical form is used [84]

$$i = \frac{\sum_{j=1}^{NO} A_j * \mu_{C_j}(i) * Cent_j}{\sum_{j=1}^{NO} A_j} \tag{4.6}$$

Here, A_j is the area , $Cent_j$ is the centroid of the jth output set C_j, NO is the number of output fuzzy sets, $\mu_{C_j}(i)$ is the fuzzy value which scales the output set C_j.

A schematic diagram of a typical FLC which is based on the above mentioned procedure, is shown in Fig.4.3. The graphical representation of the complete fuzzy inference using two rules is shown in Fig. 4.4 where $\Delta\omega^*$ and Δe^* are two crisp inputs and 'i' is the output. It is shown that rule 1 has no dependency on input 2 but the rule 2 depends on both the inputs.

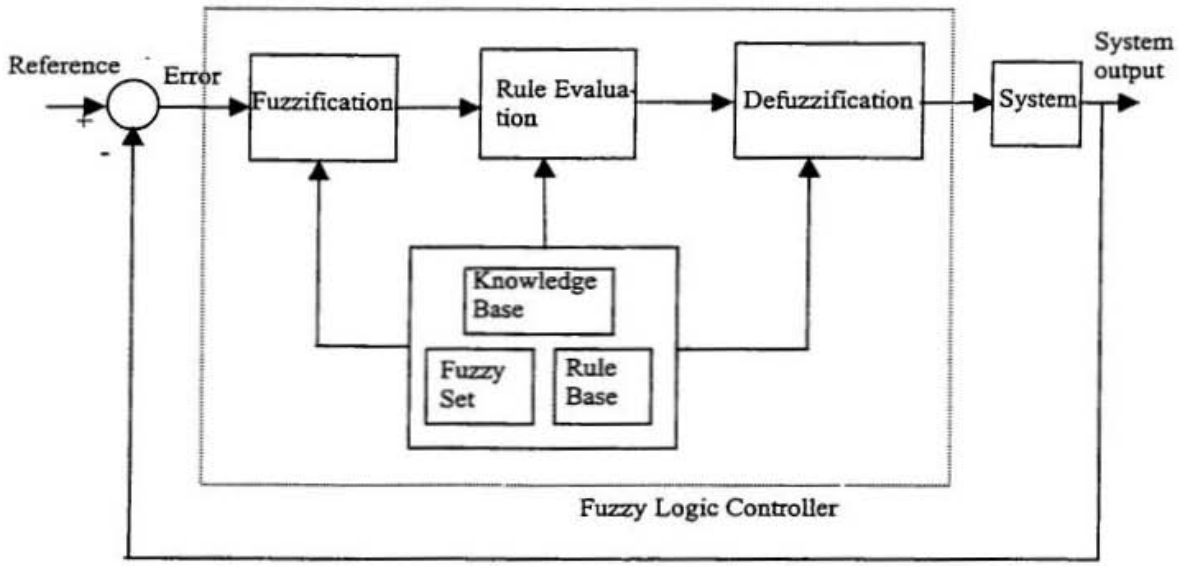

Fig.4.3. Block diagram of a general closed loop control using FLC.

4.2 Fuzzy Logic Controller for IPMSM Drive

In case of an IPMSM, the permanent magnets are buried within the rotor core that provides a smooth rotor surface and reduced air gap between the stator and the rotor. As a result, this type of motor can be used for high speed with better dynamic performances. In the case of the IPMSM, the q-axis inductance L_q is greater than the d-axis inductance L_d, and as such there exists some reluctance torque as given in Eqn.(2.26) which provides some advantages both on application and cost. However, the operation of the IPMSM drive is strongly affected by rotor magnetic saliency, core saturation and armature reaction effects due to the d-axis stator current i_d [71]. Particularly, the saturation of the rotor iron portion around the magnets produces significant distortion of the air gap flux and affects the reactance parameters. These nonlinearities

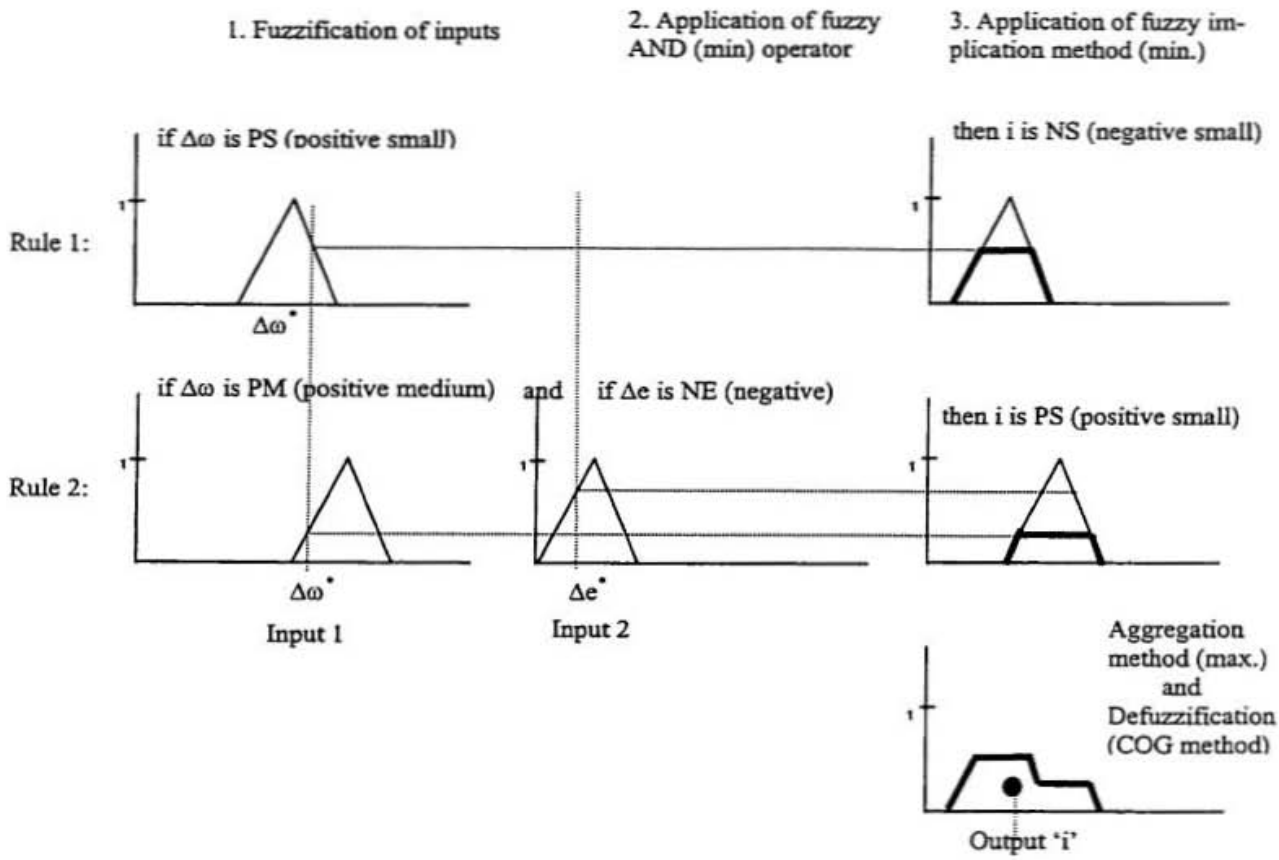

Fig. 4.4. Graphical representation of the complete fuzzy inference.

affect the performance of the drive at different dynamic operating conditions. Therefore, the optimal speed control of an IPMSM for high performance industrial drives demands special attention. In order to overcome the above mentioned difficulties of controlling the IPMSM to be used in a high performance drive system, the artificial intelligence controllers which can handle any nonlinear functions of arbitrary complexity. Some convenient features of using FLC in case of the IPMSM drive in high performance applications are given below:

(a) **System model:** As the fuzzy logic does not need any information of the exact system mathematical model and it can handle nonlinearity of any kind, the FLC is one of the best approaches in controlling an IPM motor drive where it is difficult to develop an exact system mathematical model.

(b) **Adaptability:** As the fuzzy logic is self-adaptive, the FLC is an excellent tool for optimum control of the IPMSM drive in real-time where the reactance parameters change with operating conditions, resistance may change with temperature, inertia may change with mechanical load variation and the command speed may change with demand. Therefore, the fuzzy logic controller can be used as a robust controller for the IPMSM drive. As fuzzy logic is also based on linguistic control rules and variables, it can be used for an IPMSM drive in order to make the control task simple for nonlinear systems.

(c) **Cost:** The fuzzy logic controller needs to be implemented in real-time using high speed digital signal processors. Thus, the cost may be high. But when one needs a robust controller for high performance drive applications where the quality of the performance rather than the cost is the main concern, then the fuzzy logic controller could be justified. The application of other types of intelligent controllers also needs digital signal processors to operate in real-time. Moreover, all other adaptive control schemes for HPD applications need expensive and sophisticated hardware. Thus, the use of fuzzy logic for IPMSM drives will be cost competitive considering the performance requirements.

4.3 Concluding Remarks

The fundamental ideas of fuzzy logic relating to motor control applications have been presented in this chapter. The mathematical equations and graphical representations describing the various component of fuzzy inference such as fuzzification, fuzzy inference engine and defuzzification have also been presented in this chapter. A specific fuzzy logic controller is proposed for the interior permanent magnet motor drive as a robust speed controller in order to overcome the problems caused by real-time motor parameter variations, load changes and system disturbances. Before going to implementation in real-time, it is a usual practice to predict the performance of the drive in simulation. Therefore, the simulation of a vector controlled IPMSM drive incorporating the fuzzy logic controller is given in the following chapter.

Chapter 5

Fuzzy Logic Based Vector Control of an Interior Permanent Magnet Synchronous Motor Drive

Recently, the permanent magnet synchronous motor has become popular as compared to other types of ac motors due to some of its advantageous features including high torque to current ratio, high power to weight ratio, high efficiency, low noise and robustness [4]. As mentioned in the literature review, the development of the permanent magnet synchronous motor is also related to the recent advancements of high energy permanent magnet materials, particularly neodymium-boron-iron (Nd-B-Fe) and digital signal processors with built-in interface provisions. The development of these microelectronic devices, smart power electronic converters and intelligent control algorithms offer excellent opportunity to use the IPMSM in HPD applications such as robotics, rolling mills,

air compressors, air conditioners, spindle drives and machine tools. The main criteria of HPD systems are fast and accurate speed response, quick recovery of speed from any disturbances such as load impact, step change of speed and insensitivity to parameter variations, mechanical system noise, etc. These features are important to prevent the motor driven electrical equipment from malfunctioning. However, because of some inherent difficulties of the IPMSM caused by magnetic saturation and armature reaction, it is very difficult to control the motor precisely in HPD applications. Thus, one needs to pay special attention to the speed control of IPMSM for HPD systems.

The conventional fixed gain PI and the PID controllers have been used as robust controllers due to their simplicity and easy implementation. However, these controllers are very sensitive to parameter variations, load changes and system disturbances, etc. [83]. In order to overcome some of these problems various adaptive control techniques such as MRAC, VSC, STR and SMC are utilized in modern control systems. However, the real-time implementations of these adaptive schemes are very difficult and almost all the adaptive controllers suffer from chattering, overreaching and steady-state error. Moreover, the designs of all the above mentioned controllers need an exact system mathematical model [47]. The traditional quantitative techniques of system modeling have significant limitations. It is often difficult to develop a mathematical model which describes the behavior of a nonlinear system like IPMSM. Due to unpredictable dynamics, mutual interactions and other unknown phenomena the exact mathematical model of the system may not be developed at all. Therefore, an intelligent speed controller is essential for the IPMSM to be used in HPD systems. In order to obtain more flexible and more effective capability of handling and processing the uncertainties of a complicated and ill-defined nonlinear system like IPMSM, Zadeh [56]

proposed a linguistic approach which introduced the fuzzy set and fuzzy logic theory. The FLC is developed using the fuzzy logic theory. The use of the FLC makes the control systems more robust and automatic.

This chapter contains a novel speed control scheme of IPMSM incorporating a fuzzy logic based speed controller. Based on the motor dynamics and nonlinear load characteristics a new specific fuzzy logic controller (FLC) is developed for the IPMSM. In the vector control scheme, the FLC is used in the outer loop as an optimum speed controller and the current controller is used in the inner loop. The current controller and the voltage source inverter are selected based on the performance analysis of various current controllers for the IPMSM drive in chapter 2. Systematic simulation has been done in order to predict the performances of the drive using the FLC under different dynamic operating conditions. Finally, the simulation results have been presented and discussed.

5.1 Mathematical Model of IPMSM for FLC

As mentioned in chapter 4, a FLC does not need information about the exact mathematical model of the motor. However, in order to get the specific idea of input and output linguistic variables of the FLC in a more defined and systematic way it is preferred to model the dynamics of IPMSM. As discussed in chapter 2, in the vector control scheme the stator quantities are to be transformed in the synchronously rotating rotor reference frame in order to make them constant. An IPMSM can be represented mathematically in the synchronously rotating rotor reference frame with assumed sinusoidal stator excitation as [74]

$$v_q^r = Ri_q^r + L_q \frac{di_q^r}{dt} + P\omega_r(L_d i_d^r + \psi_f) \tag{5.1}$$

$$v_d^r = Ri_d^r + L_d \frac{di_d^r}{dt} - P\omega_r L_q i_q^r \tag{5.2}$$

$$\frac{d\theta_e}{dt} = P\omega_r \tag{5.3}$$

The electromagnetic developed torque is given by,

$$T_e = \frac{3P}{2}\left[\psi_m i_q^r + (L_d - L_q) i_d^r i_q^r\right] \tag{5.4}$$

The motor dynamics can be represented by the following equation:

$$T_e = J_m \frac{d\omega_r}{dt} + B_m \omega_r + T_L \tag{5.5}$$

where T_e is the developed electric torque, T_L is the load torque, B_m is the rotor damping coefficient and J_m is the inertia constant. All the other symbols are defined in chapter 2 and the numerical values of the motor parameters are given in Appendix A. The complexity of the control arises due to the nonlinear nature of the torque equation (5.4) with i_d^r and i_q^r. In the vector control technique, in order to make the control task easier the d-axis current i_d^r is set to zero. Then the torque equation (5.4) becomes linear with i_q^r and the d-axis flux linkage depends only on the rotor permanent magnets. Now equations (5.1)-(5.5) can be simplified as,

$$pi_q^r = \frac{1}{L_q}(v_q^r - Ri_q^r - P\omega_r \psi_f) \tag{5.6}$$

$$v_d^r = -\omega_r L_q i_q^r \tag{5.7}$$

$$p\omega_r = \frac{1}{J_m}(T_e - T_L - B_m \omega_r) \tag{5.8}$$

$$T_e = K_T i_q^r \tag{5.9}$$

where $K_T = \frac{3P}{2}\psi_f$. Equation (5.9) resembles the torque equation of a separately excited dc motor where i_q^r corresponds to the armature current of a dc motor. As the FLC can handle any nonlinearity, one can consider the load as nonlinear unknown mechanical characteristics. Thus, the load torque can be modeled by using the following equation [47],

$$T_L = A\omega_r^2 + B\omega_r + C \tag{5.10}$$

From Eqn. (5.9) one can see that a precise torque control can be obtained by controlling the q-axis current i_q^r. In order to make the control task easier, the equations of an IPMSM can be expressed as a single input and single output system by combining Eqns. (5.8)-(5.10) in continuous time domain form as,

$$J_m \frac{d\omega_r}{dt} = k_T i_q^r - (B_m + B)\omega_r - A\omega_r^2 - C \tag{5.11}$$

A small incremental change Δi_q^r of the current i_q^r results in a corresponding change $\Delta\omega_r$ of the speed ω_r. Then Eqn.(5.11) can be rewritten as,

$$J_m \frac{d(\Delta\omega_r)}{dt} = k_T \Delta i_q^r - (B_m + B)(\Delta\omega_r) - A(\Delta\omega_r^2) \tag{5.12}$$

By replacing all the continuous quantities of Eqn.(5.12) by their finite differences the discrete-time small signal model of the simplified IPMSM with nonlinear load can be given as,

$$\Delta i_q^r(n) = \frac{-J_m}{k_t T_s}\Delta e(n) + (B_m + B)\Delta\omega_r(n) + A\{\Delta\omega_r(n)\}^2 \tag{5.13}$$

$$\text{Therefore, } i_q^r(n) = \int_{\text{discrete}} \Delta i_q^r(n) = f(\Delta e(n), \Delta\omega_r(n)) \tag{5.14}$$

where $\Delta e(n) = \Delta\omega_r(n) - \Delta\omega_r(n-1)$ is the change of speed error, $\Delta\omega_r(n) = \omega_r^*(n) - \omega_r(n)$ is the present sample of speed error, $\Delta\omega_r(n-1)$ is the past sample of speed

error, $\omega_r(n)$ is the present sample of actual speed, $\omega_r^*(n)$ is the present sample of command speed, T_s is the sampling time interval and f is the nonlinear function. The purpose of using the FLC is to map the nonlinear functional relationship between the q-axis current i_q^r and the speed ω_r.

5.1.1 Problem specific fuzzy logic controller (FLC)

In order to design a FLC one of the most important tasks is to determine the input and output linguistic variables. The model of the IPMSM expressed by (5.14) defines the input and output linguistic variables of FLC for the IPMSM drive. According to (5.14) the inputs of the proposed FLC are the present sample of speed error $\Delta\omega_r(n)$ and the change of speed error $\Delta e(n)$ which is the difference between present and past sample of speed errors. Thus, the input vectors of the FLC are $\Delta\omega_r(n)$ and $\Delta e(n)$ and the output vector is the q-axis command current $i_q^{r*}(n)$. The main goal of the control system is to track the command speeds by providing the appropriate torque producing current component i_q^r depending upon the operating conditions. In real-time, the rotor position information and the output of the FLC which is considered as the command q-axis current i_q^{r*}, are used to get the command phase currents i_a^*, i_b^* and i_c^* by using inverse Park's transformation [74]. The command phase currents are compared with the actual motor current in a hysteresis current controller, which provides the necessary driving pulses for the inverter. The complete control scheme for the FLC based IPMSM drive is shown in Fig.5.1. As the input, output linguistic variables are selected, the next step is to choose the scaling factors K_ω, K_e and K_i for fuzzification and to obtain the actual output of the command current. These scaling factors play a vital role for the FLC.

The factors K_ω and K_e are so chosen that the normalized values of speed error and the change of speed error $\Delta\omega_n$ and Δe_n, respectively, remain within the limit $\pm$ 1. Factor K_i is so chosen that one can get the rated current for rated conditions. In this work, the factors are taken as $K_\omega=\omega_r^*$(command speed), K_e=20 and K_i =10 in order to get the optimum drive performance based on simulation results. The next step is to choose the membership function of $\Delta\omega_m$, Δe_n and i_{qn}^*, which form the important task of the FLC. The membership functions used for the input and output fuzzy sets are shown in Fig.5.2. The trapezoidal functions are used as membership functions for all the fuzzy sets except the fuzzy set ZE (zero) of the input vectors. The triangular membership functions are used for the fuzzy set ZE of the input vectors and all the fuzzy sets of the output vector. The trapezoidal and the triangular functions are used to reduce the computation keeping in mind that the proposed method is to be implemented in real-time. The rules used for the proposed FLC algorithm are as follows:

i) if $\Delta\omega_n$ is PH (positive high), i_{qn}^* is PH (positive high).

ii) if $\Delta\omega_n$ is PL (positive low), i_{qn}^* is PM (positive medium).

iii) if $\Delta\omega_n$ is ZE (zero) and Δe is PS (positive small), i_{qn}^* is PL (positive low).

iv) if $\Delta\omega_n$ is ZE (zero) and Δe is NE (negative), i_{qn}^* is NC (no change).

v) if $\Delta\omega_n$ is ZE (zero) and Δe is ZE (zero), i_{qn}^* is NC (no change).

vi) if $\Delta\omega_n$ is NL (negative low), i_{qn}^* is NL (negative low).

vii) if $\Delta\omega_n$ is NH (negative high), i_{qn}^* is NH (negative high).

Based on the above rules the fuzzy rule base matrix is given in Table 5.1. As mentioned in chapter 4, Mamdani type fuzzy inference is used in this work [83].

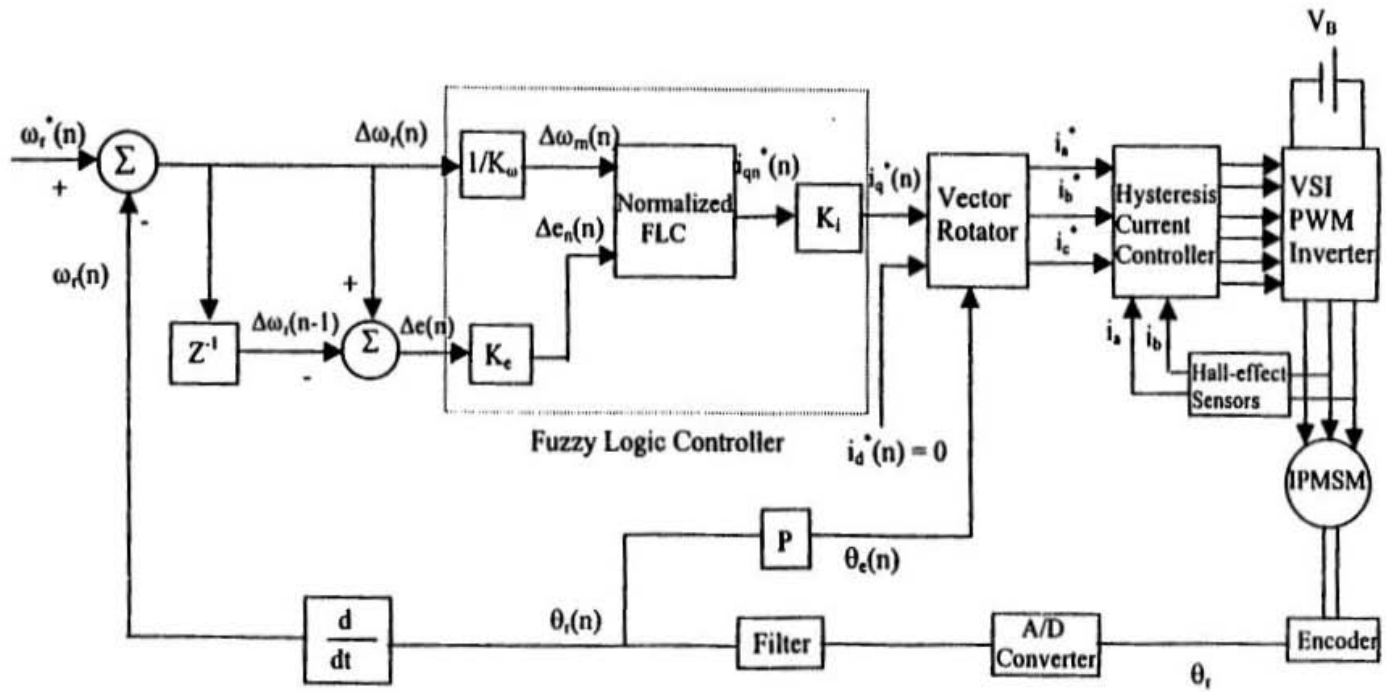

Fig.5.1. Proposed FLC based complete IPMSM drive.

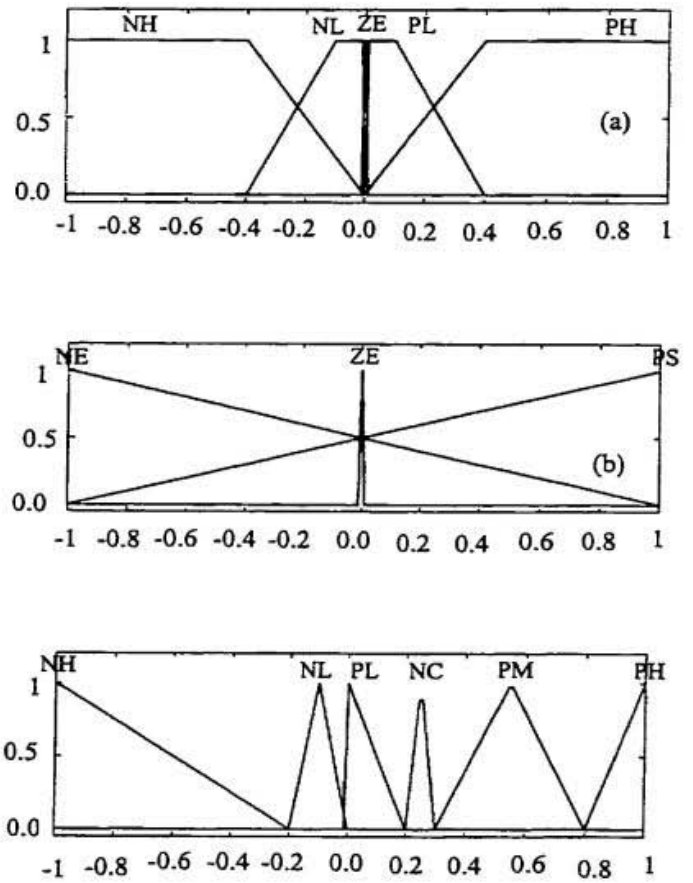

Fig.5.2 Fuzzy logic membership functions: (a) speed error $\Delta\omega_m$; (b) change of speed error Δe_n; (c) current $i_{qn}^{r}(n)$.

The values of the constants, membership functions, fuzzy sets for the input output variables and the rules used in this paper are selected by trial and error to obtain the optimum drive performance. In this work, the center of gravity method is used for defuzzification.

Table 5.1: Fuzzy rule base matrix

Δe_n \ $\Delta \omega_m$	NH	NL	ZE	PL	PH
NE	NH	NL	NC	PM	PH
ZE	NH	NL	NC	PM	PH
PS	NH	NL	PL	PM	PH

5.2 Current Controller and Voltage Source Inverter

The performances of various current controllers have been investigated both experimentally and in simulations in chapter 2. The investigation has shown that the hysteresis current controller gives better performances over the entire speed range considering the fast transient response and steady-state performance of the IPMSM drive if the inverter is made of fast switching devices like IGBTs. Therefore, the hysteresis current controller has been used in this proposed vector control technique of the IPMSM drive incorporating the fuzzy logic based speed controller. For real-time implementation an IGBT voltage source inverter and its base drive circuit have been made in the laboratory. The details of the IGBT inverter and the base drive circuit for the inverter switches are given in Appendix C. The details of the current control technique for the voltage source inverter and the principle of the hysteresis current controller have been presented in chapter 2.

5.3 Simulation Results and Discussions

An extensive simulation has been done in order to predict the performance of the proposed fuzzy logic based IPMSM drive. The simulation has been carried out using the Matlab Fuzzy Logic Toolbox [85]. Some simulation results have been presented here. The laboratory experimental 1 hp, 4-pole motor is fed by a current-controlled VSI with 2 N-m as full load. The capability of the motor to run at different loading conditions is one of the main criteria of the control system. The speed response, the corresponding command phase current, the command q-axis current and the actual steady-state 'a' phase current are shown in Figs. 5.3(a)-(d), respectively at no load and rated speed conditions. The results show that the drive follows the command speed very quickly without any overshoot and nearly zero steady-state error. The command q-axis current, which also represents the command torque, is smooth and constant at the steady-state condition. It is also shown that the actual motor current can follow the command current accurately. Figs. 5.4(a)-(d) show the responses including speed, actual phase current i_a, q-axis command current and steady-state phase currents i_a and i_b, respectively at half load and rated speed conditions. This time also the drive follows the command speed without any overshoot or steady-state error. The command q-axis current and hence the command torque is almost smooth at steady-state and also the actual current is almost sinusoidal. The similar responses of the drive at full load and rated speed conditions are shown in Figs. 5.5(a)-(d). It is shown that the drive can also follow the command speed smoothly without any overshoot and steady state error. Therefore, the proposed FLC based IPMSM drive can follow the command rated speed at various loading conditions.

The step response of command speed is applied to evaluate the performance of the IPMSM drive system in its response time, overshoot, transient or steady state

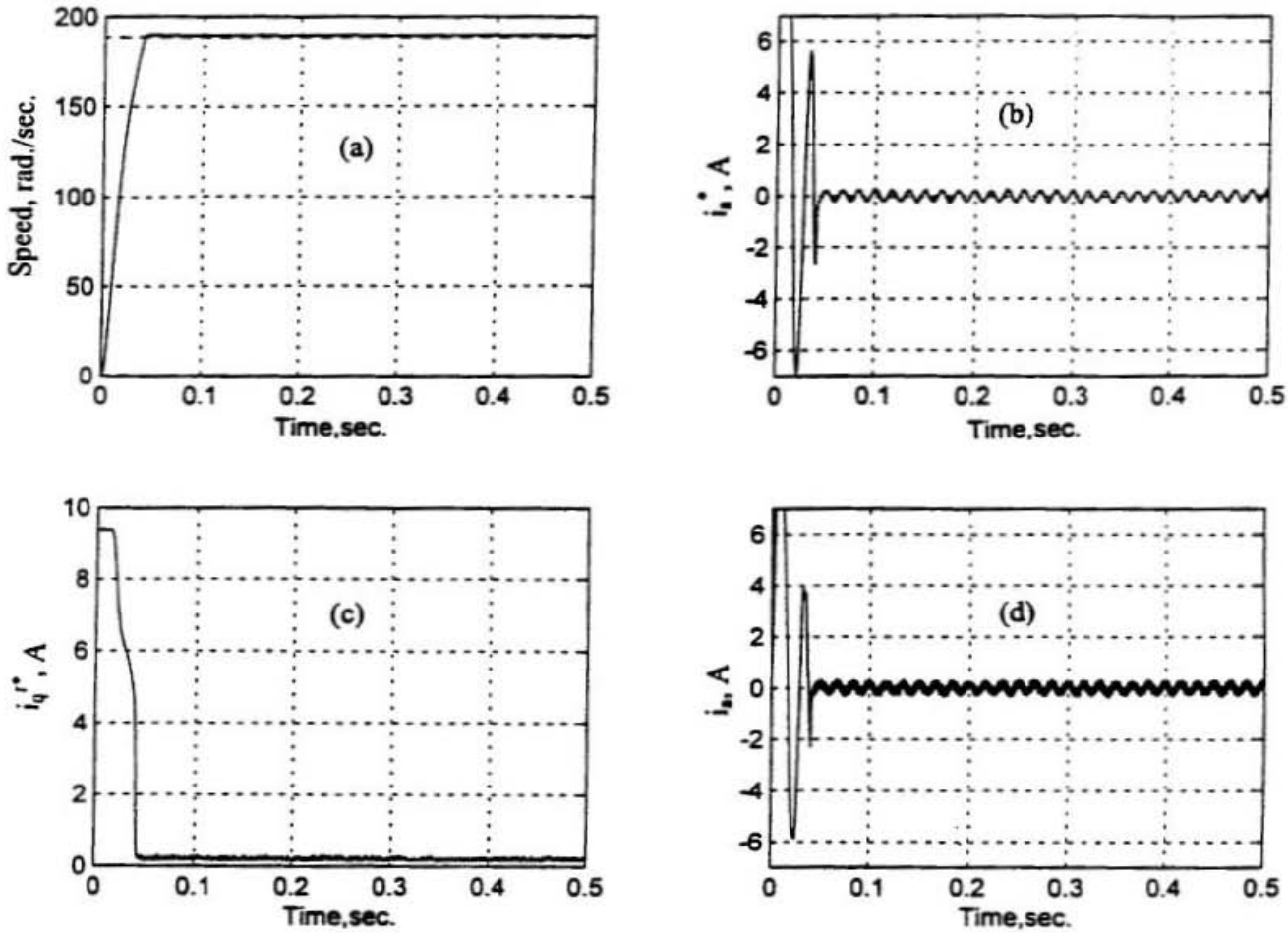

Fig. 5.3 Simulated responses of the proposed FLC based IPMSM drive: (a) speed, (b) command phase current, (c) q-axis command current and (d) steady-state actual phase current i_s at no load and rated speed conditions.

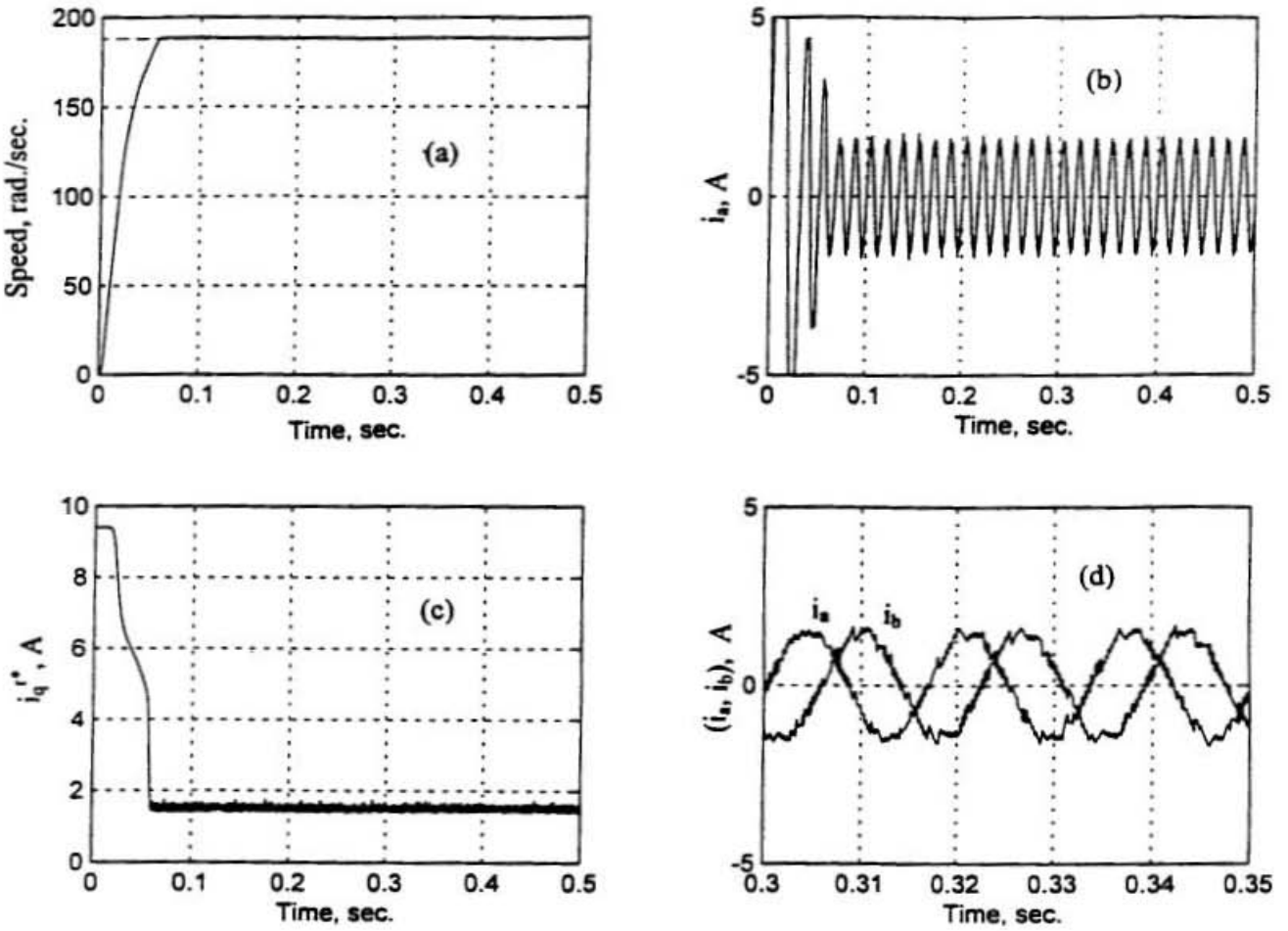

Fig. 5.4. Simulated responses of the proposed FLC based IPMSM drive: (a) speed, (b) actual phase current i_a, (c) q-axis command current and (d) steady-state actual phase currents i_a, i_b at half load and rated speed conditions.

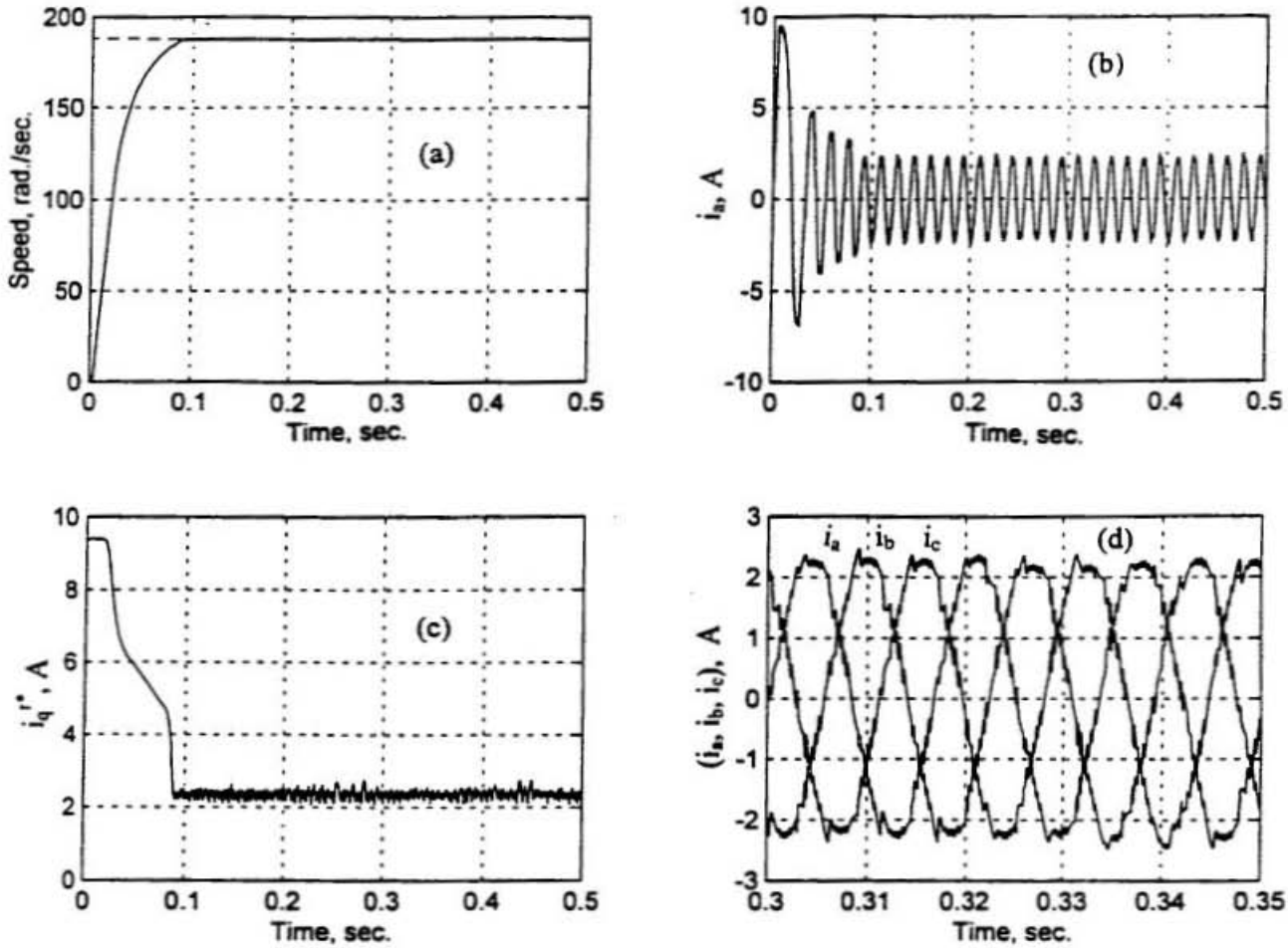

Fig. 5.5. Simulated responses of the proposed FLC based IPMSM drive: (a) speed, (b) actual phase current i_a, (c) q-axis command current and (d) steady-state phase currents i_a, i_b at full load and rated speed conditions.

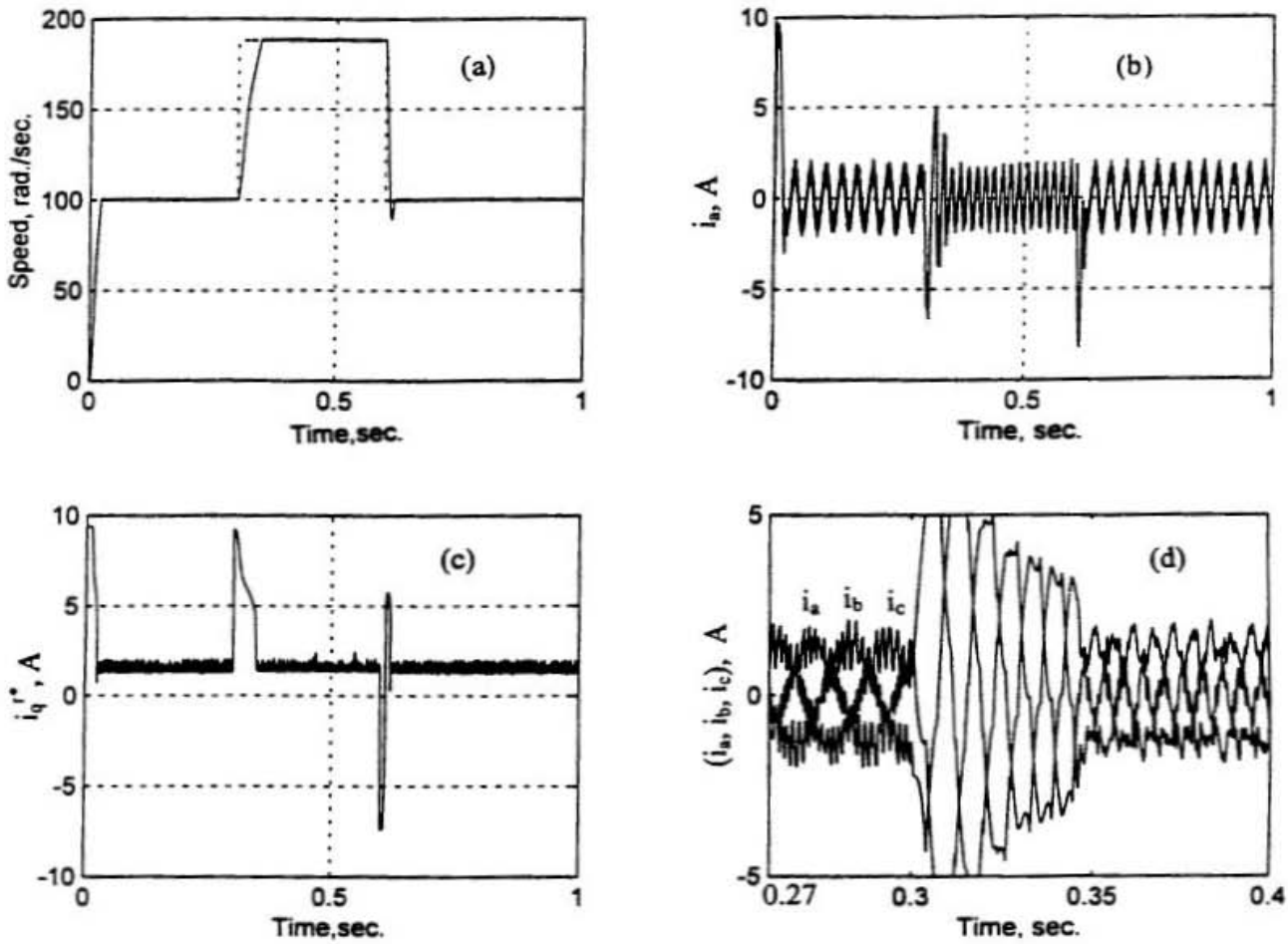

Fig. 5.6. Simulated responses of the proposed FLC based IPMSM drive: (a) speed, (b) actual phase current i_a, (c) q-axis command current and (d) steady-state actual phase current i_a at a step change of speed and half load conditions.

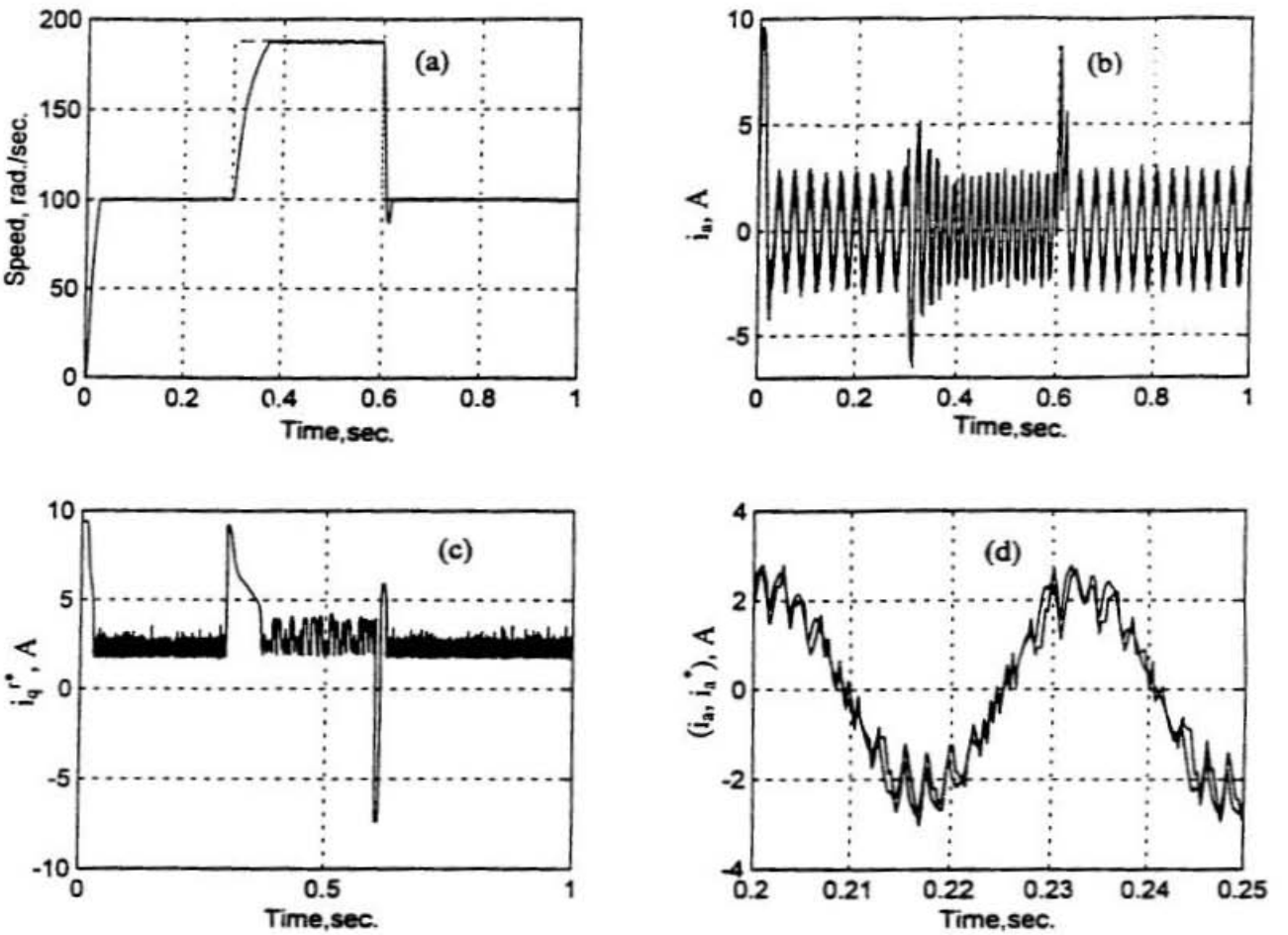

Fig. 5.7. Simulated responses of the proposed FLC based IPMSM drive: (a) speed, (b) actual phase current i_a, (c) q-axis command current and (d) steady-state actual and command phase currents i_a and i_a^*, respectively, at a step change of speed and full load conditions.

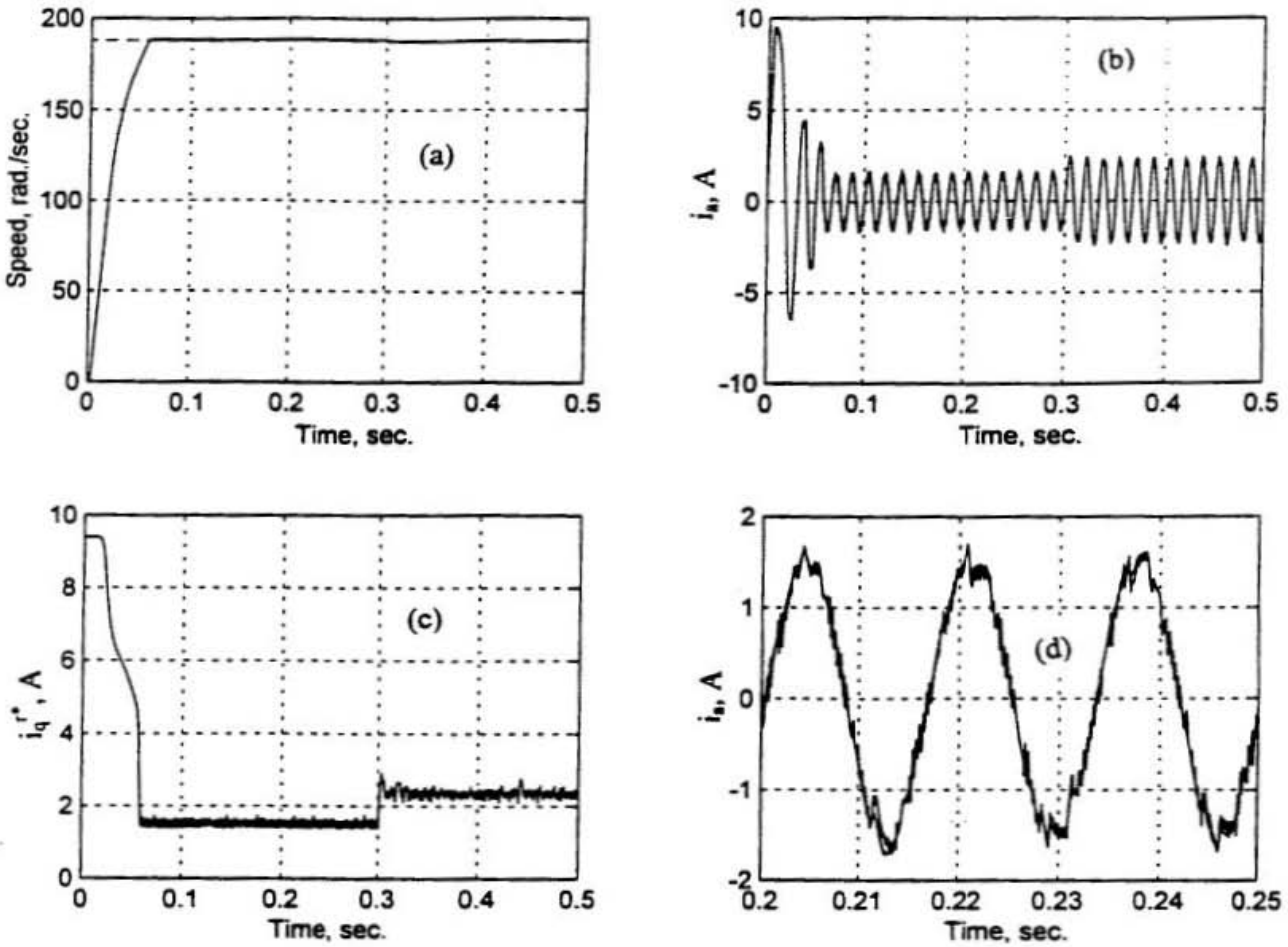

Fig. 5.8. Simulated responses of the proposed FLC based IPMSM drive: (a) speed, (b) actual phase current i_a, (c) q-axis command current and (d) steady-state actual phase current i_a for sudden increase of load (from half load to full load) at rated speed condition.

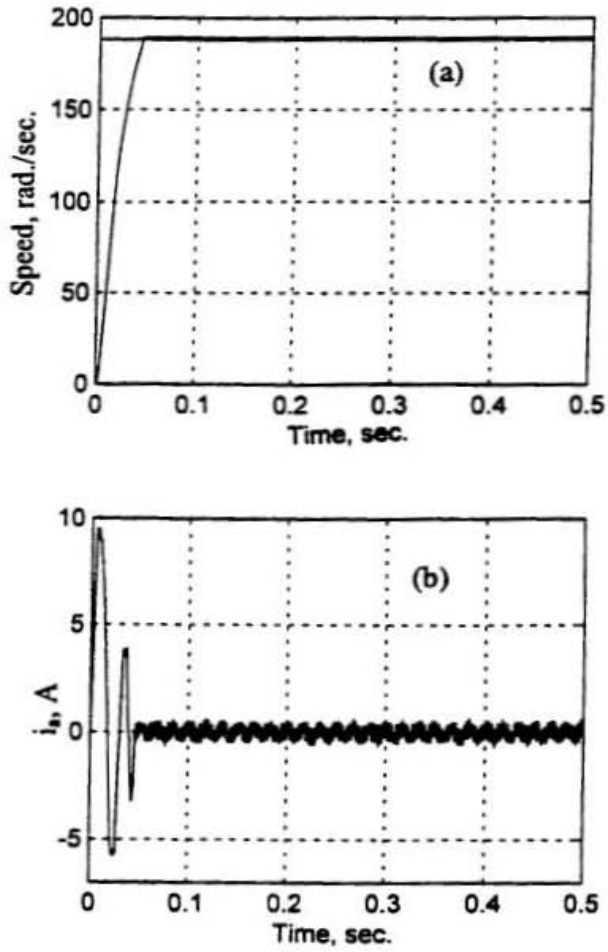

Fig. 5.9. Simulated responses of the proposed FLC based IPMSM drive: (a) speed, (b) actual phase current i_a with change in stator resistance R→2R at no load and rated speed conditions.

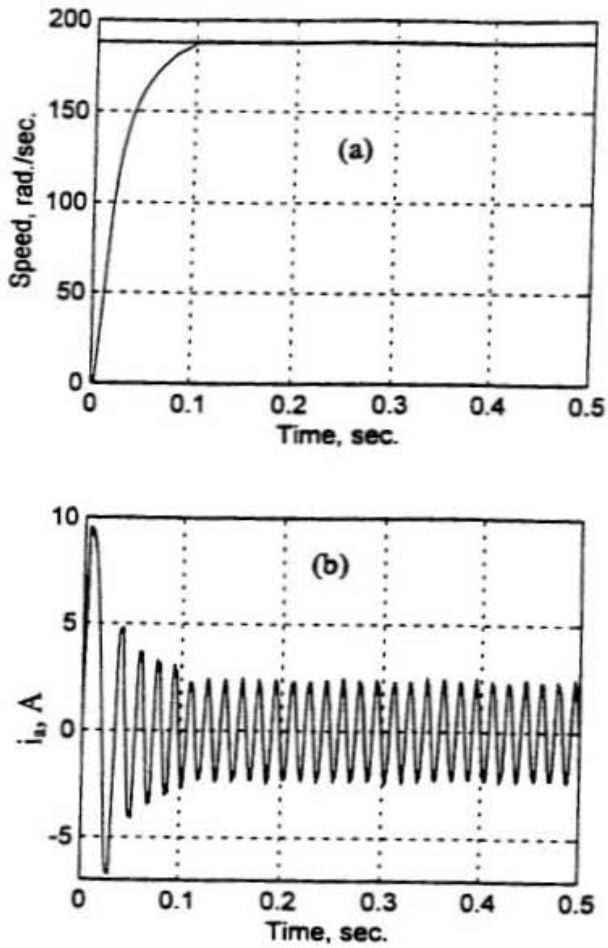

Fig. 5.10. Simulated responses of the proposed FLC based IPMSM drive: (a) speed, (b) actual phase current i_a with change in stator resistance R→2R at full load and rated speed conditions.

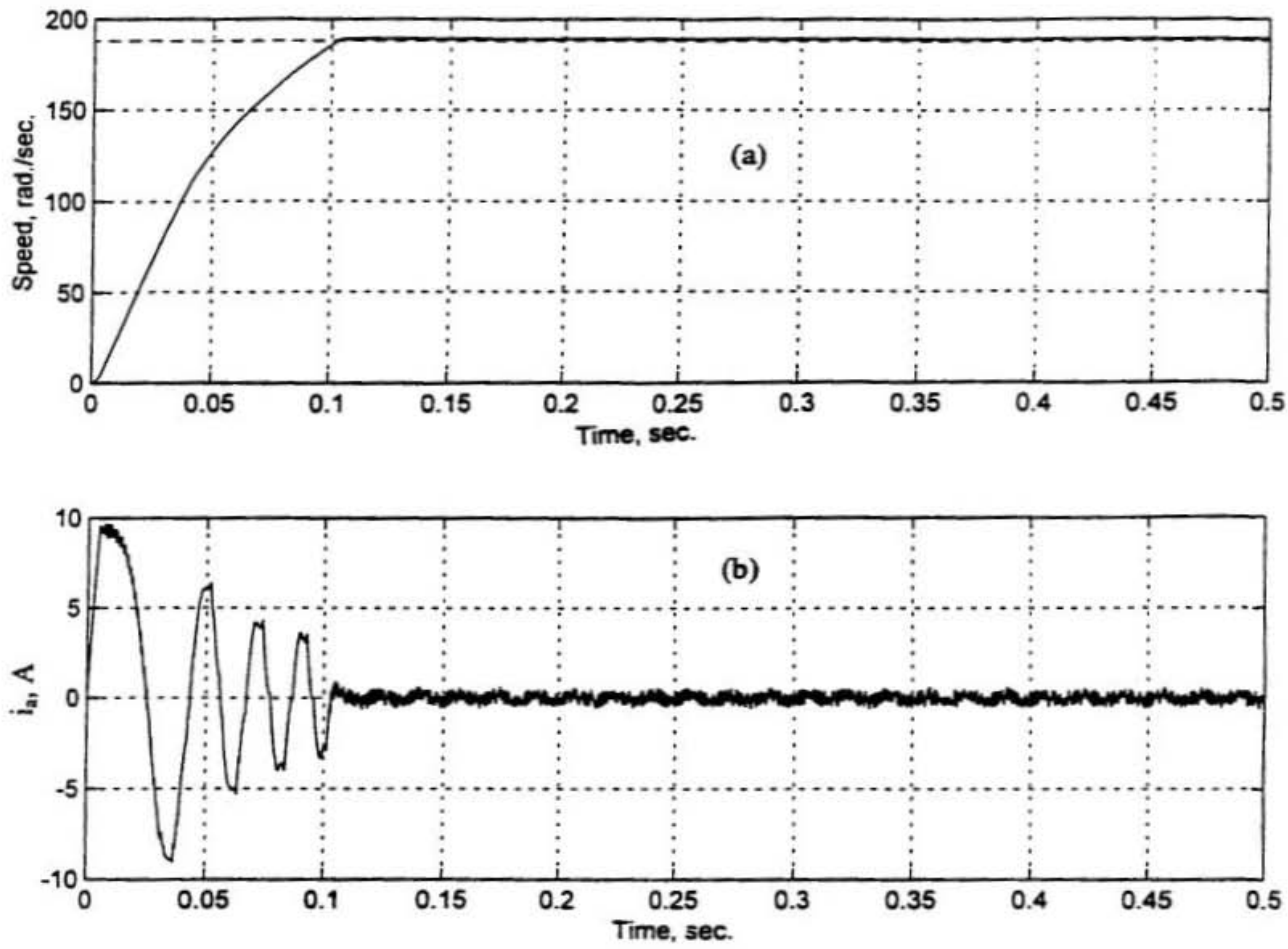

Fig. 5.11. Simulated responses of the proposed FLC based IPMSM drive: (a) speed, (b) actual phase current i_a with change in inertia J→2J at no load and rated speed conditions.

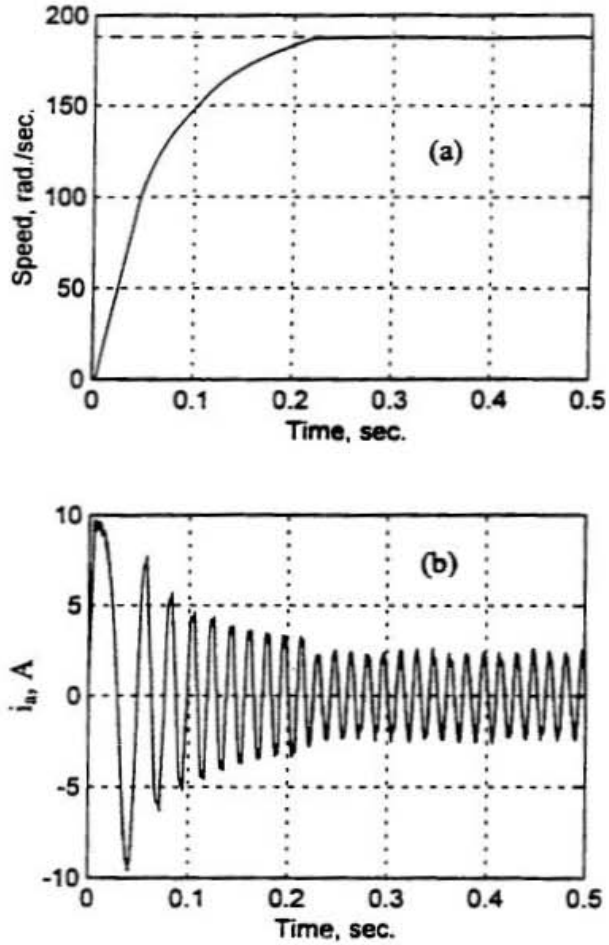

Fig. 5.12. Simulated responses of the proposed FLC based IPMSM drive: (a) speed, (b) actual phase current i_a with change in inertia J→2J at full load and rated speed conditions.

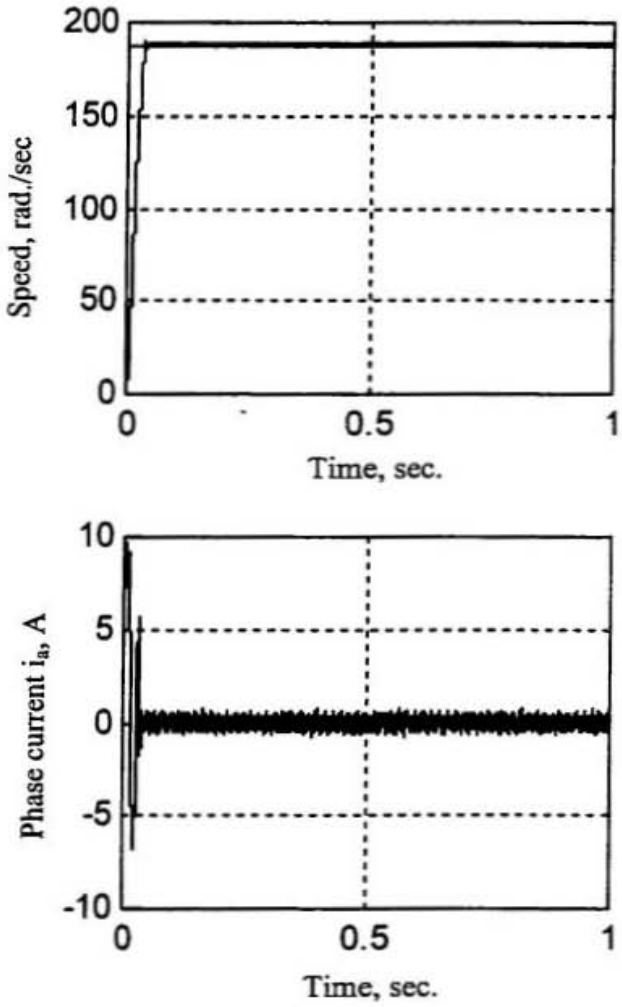

Fig. 5.13. Simulated responses of the proposed FLC based IPMSM drive: (a) speed and, (b) actual phase current i_a, with 25% decrease of L_q at no load and rated speed conditions.

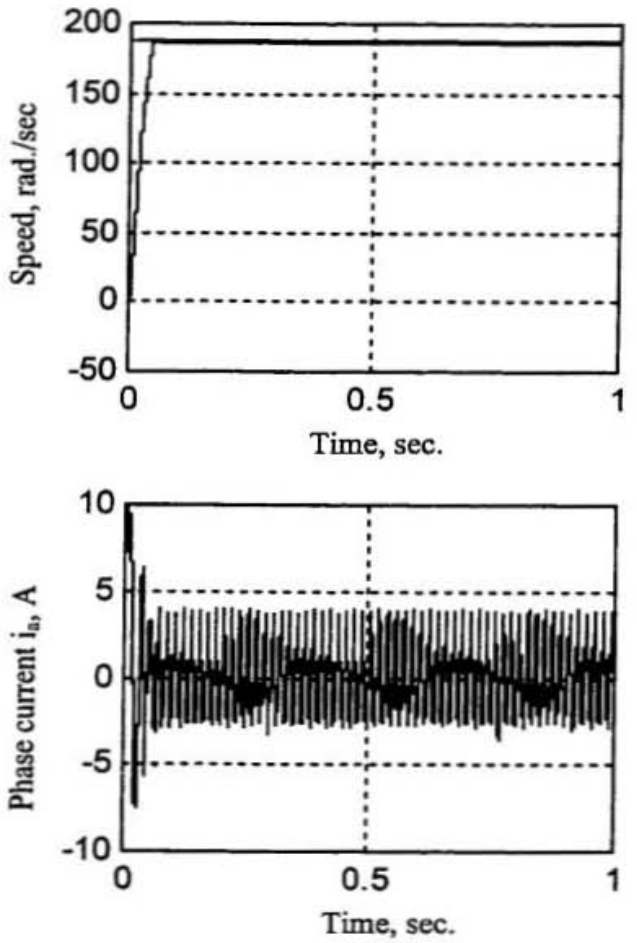

Fig. 5.14. Simulated responses of the proposed FLC based IPMSM drive: (a) speed and, (b) actual phase current i_a, with 25% decrease of L_q at full load and rated speed conditions.

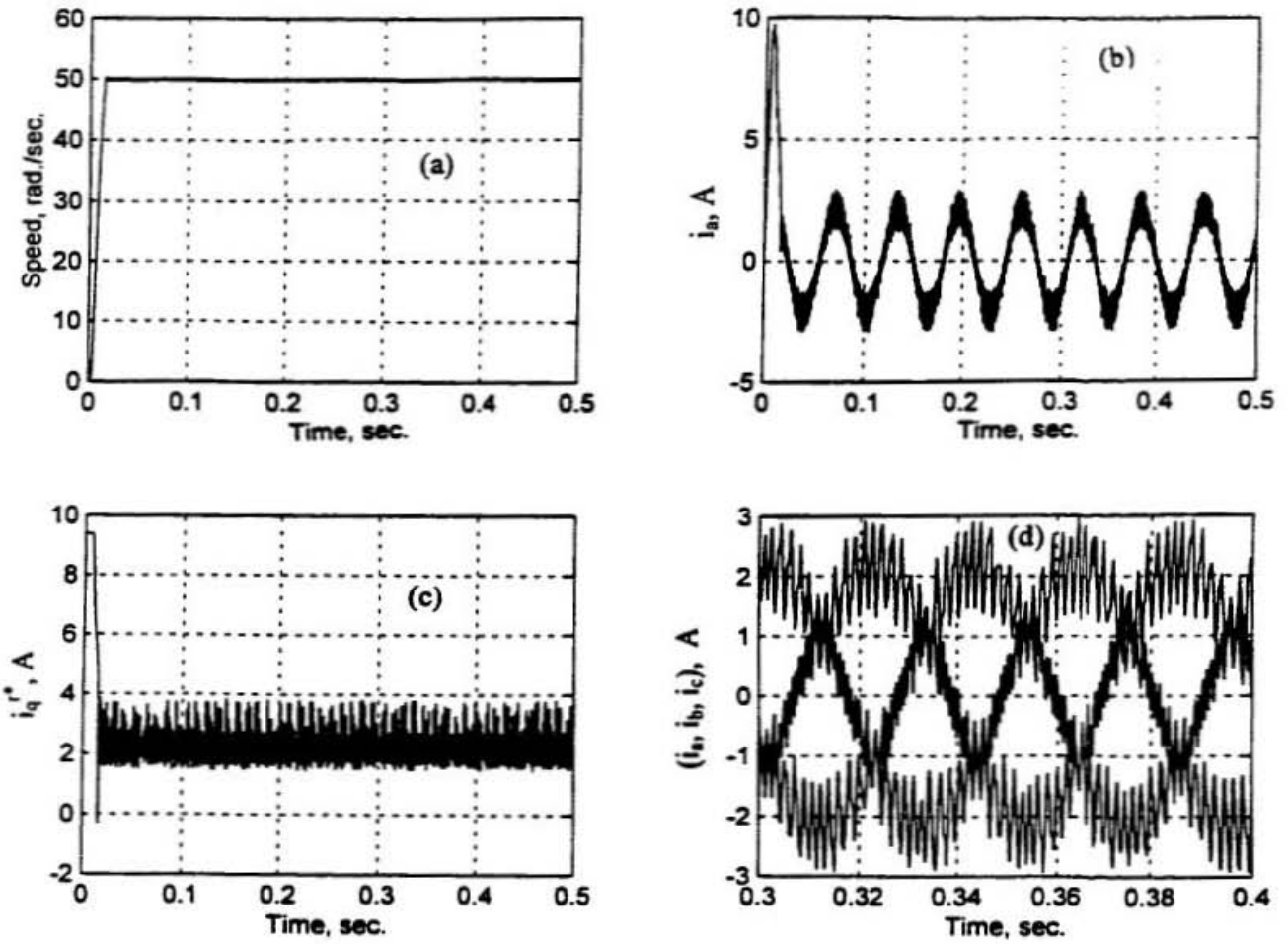

Fig. 5.15. Simulated responses of the proposed FLC based IPMSM drive: (a) speed, (b) actual phase current i_a, (c) q-axis command current and (d) the steady-state actual phase currents i_a, i_b, i_c at low speed (50 rad./sec.) and full load conditions.

errors and stability. In high performance drive applications, it is also essential to change the command speed with situational demand. The response of the drive including speed, 'a' phase actual current, q-axis command current and steady-state actual three phase currents are shown in Figs. 5.6(a)-(d), respectively for step change of command speeds at half load condition. The results show that the drive can follow the command speed without overshoot and steady-state error during a step increase of speed (100 rad./sec.→188.5 rad./sec.), but there is a small undershoot (≈10 rad./sec.) during step decrease of speed (188.5 rad./sec.→100 rad./sec.). The similar responses of the drive at the full load condition are shown in Figs. 5.7(a)-(d). The results show that the proposed drive can follow the command speed even after a step change of command speed at different loading conditions.

The ability to withstand disturbances is another important feature of the proposed FLC based control system. The change of load is a typical external disturbance and also for a high performance drive, the load change is a very common situation. The speed and the corresponding actual a-phase current of the motor, q-axis command current and steady-state actual a-phase current responses for the proposed drive are shown in Figs. 5.8(a)-(d), respectively for a sudden increase of load at the rated speed. The motor is started with half load and at t=0.3second the load is suddenly increased to full load. It is shown that the proposed FLC based IPMSM drive is almost insensitive to this step increase of load. The current response is almost sinusoidal and it follows the command current.

The ability to withstand the motor parameter variations is another important criterion of the control system, particularly for the IPMSM drive where the motor parameters are affected by saturation and temperature effects. The change of stator resistance with temperature is a common phenomenon of the machine. The speed and the corresponding actual phase current responses are shown in Figs. 5.9(a) and

(b), respectively, where stator resistance is increased by two fold, under no load and rated speed conditions. The similar responses for full load condition are shown in Figs. 5.10(a) and (b). In both cases it is shown that the drive can follow the command speed even after a change of armature resistance at different loading conditions. The inertia of the motor may change at different loading conditions so it is important to investigate the starting performance of the drive with increased inertia. Figs. 5.11(a) and (b) show the speed and the corresponding actual 'a' phase current responses, respectively with doubled rotor inertia and no load conditions. The similar responses at full load condition are shown in Figs. 5.12(a) and (b). The results show that the drive follows the rated command speed smoothly even with doubled rotor inertia. Because of increased inertia the time to reach the steady-state is slightly greater (by 0.12sec.). Among the various motor parameters the q-axis inductance parameters L_q is another important parameter as it varies significantly with the magnetic saturation. As direct axis inductance parameter L_d is assumed constant, the effect of variation of L_d is not investigated [73]. The speed and the corresponding actual 'a' phase current responses are shown in Figs. 13(a) and (b), respectively for the proposed FLC based drive system, where L_q is reduced by 25% under no load and rated speed conditions. The similar responses at the full load condition are shown in Figs. 14(a) and (b). It is shown that the proposed FLC based drive is capable of handling the variation of inductance parameters at both no load and full load conditions.

The responses of the IPMSM control system at a low speed condition also needs to be investigated in order to predict the performance of the drive for a wide speed range. The speed response and the corresponding actual a-phase current, q-axis command current and steady-state actual three-phase currents are shown in Figs. 5.15(a)-(d), respectively at a low speed of 50 rad./sec. and at rated load

conditions. The speed response shows that the drive can also follow the low command speed very quickly and smoothly without overshoot and no steady-state error. The current responses are sinusoidal and balanced. Thus, it is found that the performance of the proposed drive at a low speed condition is also satisfactory.

5.4. Concluding Remarks

A novel complete vector control scheme of the IPMSM drive incorporating the proposed FLC has been presented in this chapter. The simulation results show encouraging performances of the proposed drive. The FLC can adjust itself with different operating conditions such as load change, parameter variations and step change of command speed. Therefore, the FLC can be a good substitute for the conventional fixed gain PI or PID controllers. It is found that if the number of rules increases, better performance can be attained, but the computational burden will also be increased. This is a major limitation for real-time implementation. In order to compromise between the performance and the computational burden only seven rules have been used in the design of the FLC for the IPMSM drive in this work. The simulation results validate the robustness of the FLC in an IPMSM drive. In order to confirm the efficacy of the proposed FLC based IPMSM drive, the implementation of the complete vector control scheme of the drive is carried out in real-time as an integrated part of this work. The detailed experimental implementation procedures are described in the following chapter.

Chapter 6

Experimental Implementation of the FLC Based Vector Control of IPMSM

As mentioned in the literature review the application of the FLC has been facing some disadvantages during both hardware and software implementations due to its high computational burden [72]. Thus, real-time implementation of the FLC for the motor drives has become an engineering challenge for the control engineers. Particularly, the real-time application of the FLC for interior permanent magnet synchronous motor (IPMSM) which suffers from inherent magnetic saturation and armature reaction has not yet been reported. As an integral part of this thesis, the experimental implementation of the complete IPMSM drive incorporating the FLC is presented in this chapter. The proposed real-time implementation technique overcomes the high computational burden of the controller and gives better results than those of the conventional PI controller. In this work, the fuzzy logic calculation is on-line. Therefore, no look-up table is used. The complete vector control

scheme of IPMSM incorporating the FLC is successfully implemented in real-time using DSP controller board DS 1102 on a prototype 1 hp interior type motor. The detailed implementation through both hardware and software programming are described in this chapter. In order to validate the efficacy of the FLC, various experimental results of the drive for the proposed implementation technique carried out at different dynamic operating conditions are also presented and discussed.

6.1 Description of the Experimental Setup

The experimental setup used for the real-time implementation of the proposed FLC based IPMSM drive is shown in Fig.6.1. The test interior type permanent magnet synchronous motor is labeled as 'M'. The test motor is coupled to a dynamometer using a belt. The dynamometer is labeled as 'D' and it works as a mechanical load to the motor. The rotor position of the test motor is measured by an optical incremental encoder which is labeled as 'E'. The encoder is directly mounted to the rotor shaft using a flexible coupler. The actual motor currents are measured through Hall-effect current transducers. These transducers are labeled as 'H'. These current sensors have a good linear response over a wide range of frequencies (0-20 kHz) and currents (0-30A). A base drive circuit is used to increase the power level of the firing pulses so that these are sufficient to drive the inverter switches. The base drive circuit also provides isolation between the low power control and the high power supply circuits. In Fig.6.1 the base drive circuit is labeled as 'B'. The power circuits consist of a 3-phase (6-pulse) insulated gate bipolar transistor (IGBT) inverter, variable ac power supply and a rectifier. The 3-phase inverter module is labeled as 'I'. The dc bus voltage for the voltage source inverter (VSI) is obtained by rectifying the ac voltage. The variable ac power supply module is

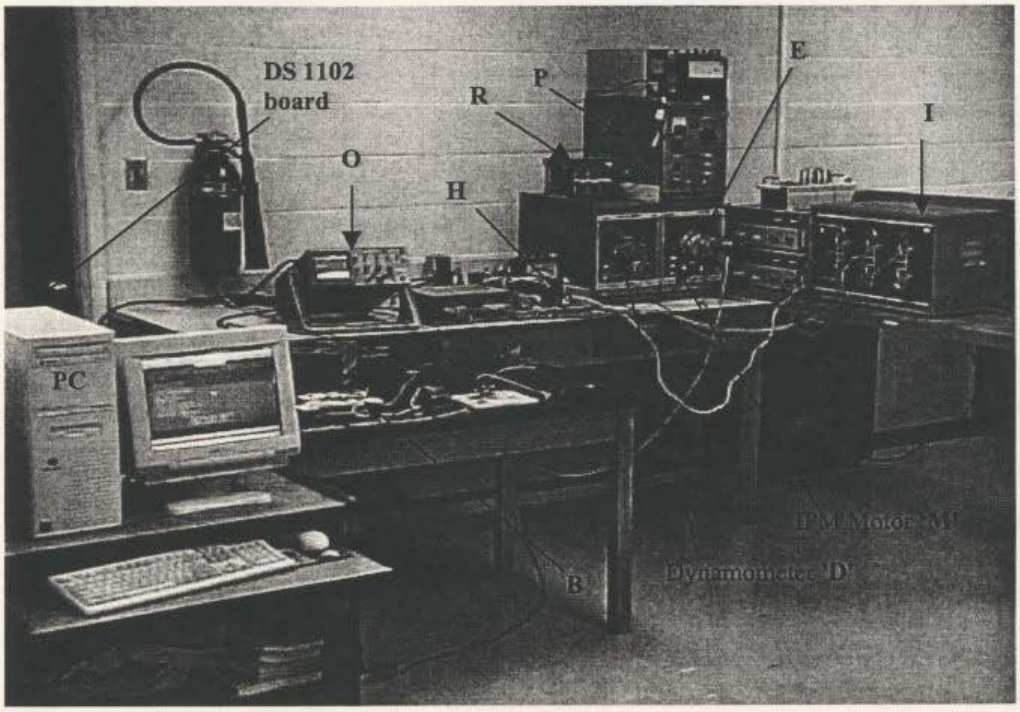

Fig. 6.1 Experimental set up for the proposed IPMSM drive. The labeled components are referred to in Section 6.1.

labeled as 'P' and the rectifier is labeled as 'R'. In order for doing safe operation of the inverter the variable supply is used. The personal computer, in which the DSP board DS1102 is installed, is labeled as 'PC'. A digital storage oscilloscope is used to capture the desired signals coming out through D/A port of the DSP board. The oscilloscope is labeled as 'O'.

6.2 DSP-Based Hardware Implementation of the Drive

As mentioned earlier, the control algorithm of the complete IPMSM drive using FLC is implemented in real-time using digital-signal-processor (DSP) board DS1102 [78]. The hardware schematic for real-time implementation of the proposed IPMSM drive is shown in Fig.6.2. The DSP board is installed in a personal computer (PC) with uninterrupted communication capabilities through dual-port memory. The DSP board is supplied with a software development system which is also installed in the PC. Therefore, the PC monitor can be used to edit and down load the software programs and also to change the command speeds and index pulses from the keyboard. The block diagram of the DSP board is shown in Fig.6.3. The DS1102 board is based on Texas Instrument (TI) TMS320C31 32 bit floating point digital signal processor. The DSP board has been supplemented by a set of on-board peripherals used in digital control systems, such as analog to digital (A/D), digital to analog (D/A) converters and incremental encoder interfaces. The DS1102 board has one 4-channel (2, 16-bit and 2, 12-bit) A/D and one 4-channel (of each 12-bit) D/A converter and two 16-bit incremental encoder subsystems. The DS 1102 is also equipped with a Texas Instruments TMS320P14 16-bit micro-

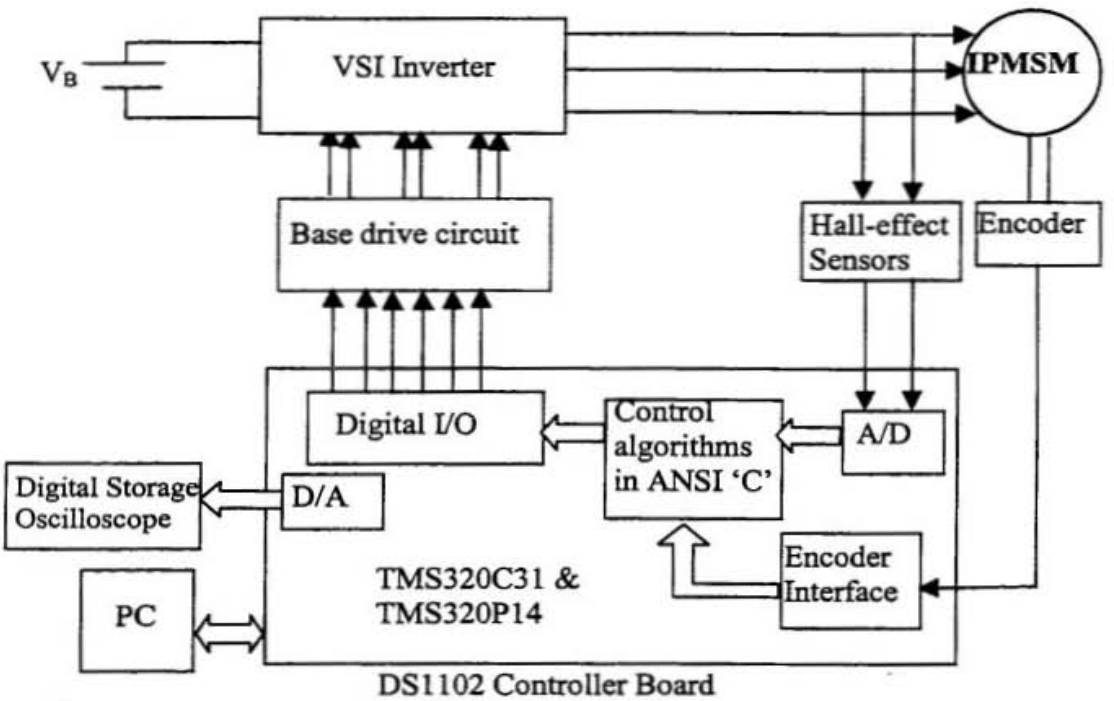

Fig. 6.2. Hardware schematic for experimental implementation of the IPMSM drive.

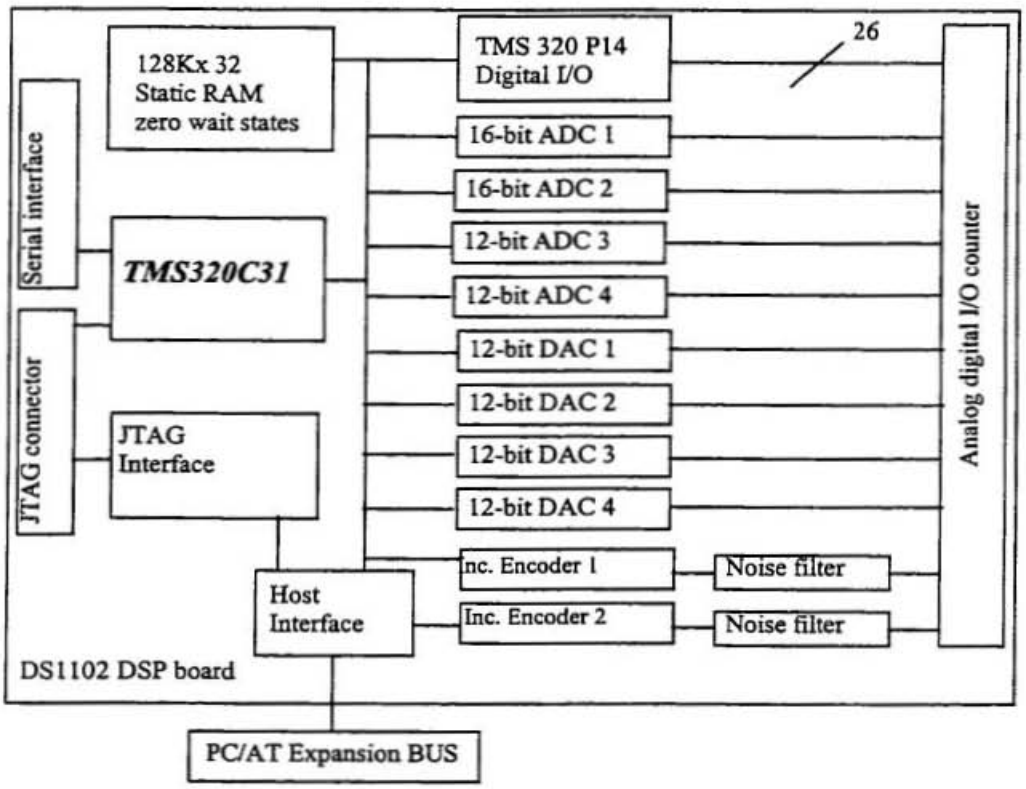

Fig. 6.3 Block diagram of the DS-1102 board.

controller DSP that acts as a slave processor and provides the necessary digital input/output (I/O) ports and powerful timer functions such as input capture, output capture and PWM waveform generation. In this work, the slave processor is used only for digital I/O configuration. The actual motor currents are measured by the Hall effect sensors, which have good frequency response and are fed to the DSP board through the A/D converter. As the motor neutral is not grounded, only two phase currents are fed back and the other phase current is calculated from them. The rotor position angle is measured by an absolute incremental encoder mounted at the rotor shaft and fed to the DSP board through the encoder interface. The encoder generates 4096 pulses per revolution, which are fed to the incremental encoder interface of the board. By using a built-in 4-fold pulse multiplication the output of the encoder is increased to 4x4096 pulses per revolution in order to get a better resolution. A 24 bit position counter is used to count the encoder pulses and is read by a calling function in the software. The counter is reset once per revolution by the index pulse generated from the encoder. The motor speed is computed from the measured rotor position angles using numerical differentiation. In order to implement the vector control algorithm, the hysteresis controller is used as the current controller. The command currents are generated from the speed controller. The hysteresis current controller compares the command currents with the corresponding actual motor currents and generates the logic signals, which act as firing pulses for the inverter switches. Thus, these six logic signals are the output of the DSP board and are fed to the base drive circuit of the insulated gate bipolar transistor (IGBT) inverter power module. The control algorithms for the fuzzy logic based speed controller and the hysteresis current controller is written in 'C' language and implemented via the controller board. Therefore, the control system becomes a

fully digital system. In addition to the routine for control algorithms, the program comprises several I/O functions to access and initialize the peripherals of the DSP board. The detailed software programming is discussed in the next section.

6.3 Software Development for Real-Time Implementation of the FLC Based IPMSM Drive

The control algorithms for the complete FLC based drive system as shown in Fig. 6.2 is implemented through software modules for two different methods described as follows [86]:

Method I: In this method the dSPACE real-time interface (RTI) unit has been used for the real-time implementation of the proposed drive. The real-time simulink graphics model is first developed and then the ANSI 'C' code is generated by the real-time workshop (RTW). The real-time simulink graphics model for the FLC based IPMSM drive is given in Appendix E. In this method, the real-time implementation is relatively easier and hence it was tried first. However, the obtained sampling frequency (162 Hz) is very low due to the high computational burden. With this low sampling frequency it was not possible to run the motor with the laboratory inverter even at low speed (50rad./sec.) condition. This is considered a major limitation for real-time implementation of Method I.

Method II: In this method a software program has been written in high level 'C' programming language for the FLC as well as the complete IPMSM drive. In Method I, 'C' codes were generated from the real-time Simulink model by the processor. Hence, Method I need larger memory space and time for the processor as compared to Method II, where 'C' codes were directly downloaded to the DSP

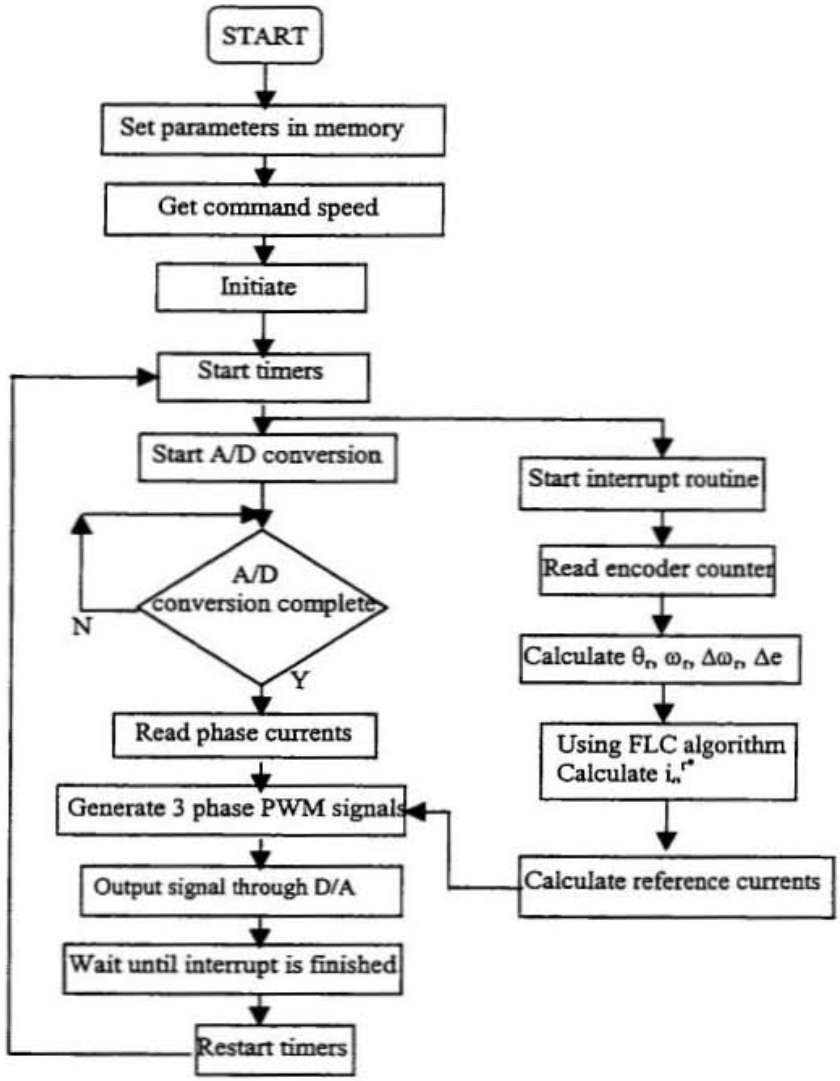

Fig. 6.4. Flow chart of the software for real-time implementation of the proposed FLC based IPMSM drive.

board. Thus, Method II reduces the computation burden greatly and hence the high sampling frequency of 5 kHz is obtained which has been found suitable for successful real-time implementation of the FLC. The flow chart of the software for real-time implementation of the complete drive is shown in Fig.6.4. In both the methods the 'C' codes are compiled by the Texas Instruments 'C' compiler first and then down loaded to the DSP board using loader program LD31 [87]. As Method-II was successful, it will be the only method discussed in the rest of this chapter. The detailed software implementation procedure for this method is described below.

6.3.1 Peripheral initialization

All the peripherals of the DSP board are to be initialized in order to access the on-board peripherals. The controller board DS-1102 is supplied with several macro functions. For example, the macro function called *init()* initializes the D/A converter subsystem of DS-1102 for output. Also, the DS-1102 interrupt request bits are reset and 16-bit A/D converters are calibrated. For real-time implementation it

Table 6.1: Peripheral initialization

```
void main()
{
 init(); /*init DAC mode, calibrate ADCs */
 init_slave_DSP_digital_i_o();
      /* initialize i/o ports for output*/
 *error=NO_ERROR;
     /* initialize overload error flag */
 dp_mem[0].f=0.0;
    /* init 1st dp-mem loc for float */
 dp_mem[1].f=0.0;
    /* init 2nd dp_mem loc for float */
 ds1102_inc_clear_counter(1);
    /* clear incr. encoder counter */
 start_isr_t0(TS);
    /* initialize sampling clock timer  */
 while(*error==NO_ERROR);
     /* background process  */
}
```

is essential to initialize the programmable timers because they require a regular sampling rate. The functions *timer*0() and *timer*1() can be used to initialize the TMS320C31's on-chip timers to generate the timer interrupts at a predefined sampling rate as given in Table 6.1. The detailed initialization and several I/O functions for A/D converters and 16 bit I/O ports are given in reference [78].

6.3.2 Interrupt service routine

After initializing all the required variables an interrupt service routine (ISR) is used to read the actual motor currents and rotor position angles every 200 μsec. The actual steps are shown in Table 6.2. The constants K_a and K_b in Table 6.2 are used to obtain the actual motor currents through A/D channels 3 and 4. These constants depend on the type of the Hall-effect sensors. The incremental gain (INCG) is used to get the actual rotor position depending on the incremental encoder. In this work, the constants K_a, K_b and INCG are 11.49, 10.93 and 3216.99049, respectively. The incremental encoder interface on the DS 1102 board consists of a 24–bit up/down counter to count the shaft encoder pulses (4096 per revolution) and expands the input to 4x4096 increments (one increment corresponding to each pulse) per revolution as mentioned earlier. The actual electrical position of the rotor can be calculated as follows [78]:

$$\theta_e = \text{Counter}\left(\frac{2^{24}}{2} - 1\right)\frac{2\pi}{4x4096}P \qquad (6.1)$$

The index pulse generated by the encoder is significant only at the startup. At the time of starting as the index pulse is generated, the counter is reset to zero so that the maximum rotor angle equals 2π. After a few seconds of starting the index pulse is disabled by a special program (start.c) as given in Appendix-E. Then the motor

Table 6.2: Interrupt service routine to read the motor currents and rotor position.

```
void  isr_t0()
 {
        .
        .
        .
   ds1102_ad_start();
   i_a = K_a*ds1102_ad(3);
   i_b = K_b*ds1102_ad(4);
   i_c = -(i_a+i_b);
   θ_r = INCG*ds1102_inc(1 or 2);
        .
        .
        .
 }
```

runs without the index pulse. Since 4096 increments correspond to an angle 2π, a maximum angle of

$$\frac{2^{24}}{4096} 2\pi = \pm 4096 * 2\pi \tag{6.2}$$

is reached before the counter changes its value from FFFFFF Hexadecimal to 0. The rotor speed is calculated by differentiation from the present and past samples of rotor positions. The q-axis command current is generated from the fuzzy logic based speed controller. The inputs to the FLC are speed error and change of speed error. The components of the FLC are fuzzification, fuzzy inference engine (rule base) and defuzzification. The implementations of these components in real-time using 'C' language are presented below [88].

Fuzzification: The process of converting a numerical variable (crisp value) into a linguistic variable (fuzzy value) is referred to as fuzzification. The normalized values of the inputs $\Delta\omega_r$ and Δe are passed to the fuzzification stage which uses preselected membership functions to convert the crisp values of $\Delta\omega_m$ (cvalue1)

Table 6.3: 'C' codes for fuzzification.

```
for (i=0; i<NS; i++)
  {
  fvalue[i] = 0;
   if( (cvalue >= b_l[i]) && (cvalue < t_l[i]))
     fvalue[i] = (cvalue - bl[i])/(tl[i] - bl[i]);
      else
       { if( (cvalue >= t_l[i]) && (cvalue <= t_h[i]))
         fvalue[i] = 1;
         else
            {
       if( (cvalue > t_h[i]) && (cvalue <= b_h[i]))
       fvalue[i] = (cvalue1 – b_h[i])/(t_h[i] – b_h[i]);
              }
         }
   }
  if (cvalue < cent[0])
        fvalue[0] = 1;
        else
           {
           if (cvalue > cent[NS-1])
              fvalue[NS-1] = 1;
           }
```

and Δe_n (cvalue2) to their corresponding fuzzy values, fvalue1 and fvalue2, respectively. In this work, the trapezoidal and triangular membership functions as shown in Fig.5.4 are used to reduce the computational burden in real-time. For fuzzification a routine (Fuzzy) for a singleton fuzzifier is written in the 'C' language. Table 6.3 contains the proposed new 'C' code for fuzzification of the IPMSM drive. In Table 6.3 NS is the number of fuzzy sets, cvalue is the crisp value, fvalue is the fuzzy value for a particular input, i denotes the ith fuzzy set of a particular input, b_l is the bottom low 'a', t_l is the top low 'b', t_h is the top high 'c', b_h is the bottom high 'd' and cent is the centroid of a trapezoidal membership function. Although the 'C' code is written for only the trapezoidal membership function, the triangular membership function can be generated from the trapezoidal membership function by setting t_l = t_h.

Fuzzy inference engine (Rule base): The fuzzy inference engine is composed of a set of conditional statements like "if-then" control rules to obtain the results of all applicable rules. According to equations (4.4) and (4.5) another routine (FuzzyEngine) for the fuzzy inference engine is written in 'C' language. Table 6.4 contains the 'C' code for rule evaluation for the proposed FLC. In Table 6.4,

Table 6.4: 'C' codes for rule evaluation.

```
for (i=0; i<NS3; i++)
                fvalue3[i] = 0.0;
  for (i=0; i<NS2; i++)
   {
    for (j=0; j<NS1; j++)
     {
      minval = fvalue2[i];
      if (minval > fvalue1[j])
            minval = fvalue1[j];
     K= RuleBase[i][j];
      if (minval > fvalue3[K])
            fvalue3[K] = minval;
     }
   }
```

NS1 (=5), NS2 (=3) and NS3 (=6) are the number of fuzzy sets for $\Delta\omega_m$, Δe_n and i_{qn}^*, respectively. RuleBase[i][j] is the two dimensional matrix corresponding to the fuzzy rule based matrix given in Table 5.1. Variable K will be an integer corresponding to the output fuzzy set given in the rule base matrix.

Defuzzification: According to the above mathematical form a routine for defuzzification is also written in 'C' language as given in Table 6.5. In this table, areas_3[i] is the area, cent_3[i] is the centroid of the ith fuzzy set of the output. After completing the FLC calculation, the command currents i_a^*, i_b^* and i_c^* are generated from the q-axis command current i_q^* and the rotor position angle θ_r using Park's

Table 6.5: 'C' codes for center of area defuzzification.

```
temp1 = 0.0;
cvalue3 = 0.0;
  for (i=0; i<NS3; i++)
    {
     temp2 = fvalue3[i]*areas_3[i];
     cvalue3 + = temp2*cent_3[i];
     temp1 + = temp2;
    }
  cvalue3 /= temp1;

i_q* = K_e * cvalue3;
```

inverse transformation. These command phase currents are compared with the actual motor currents in a hysteresis current controller, which provides the necessary driving pulses for the inverter switches. The hysteresis current controller algorithm is also written in the standard 'C' language. The digital I/O ports are configured as output ports for the six PWM logic pulses, which are fed to the base drive circuit of the inverter.

6.4 Design of PI controller for Comparison Purpose

In order to prove the superiority of the FLC, a PI controller is designed for speed control. The input to the PI controller is the speed error and the output is the torque command T_e^*. In the Laplace domain, the PI type speed controller can be described as:

$$T_e^*(s) = (K_p + \frac{K_i}{s})\,\Delta\omega_r(s) \tag{6.8}$$

where $\Delta\omega_r$ is the speed error between actual and command speeds, K_p is the proportional gain and K_i is the integral gain for the PI controller. The values of the PI

speed controller parameters are determined by tuning the parameters off-line using the transfer function of the drive for only speed control. The transfer function block of the drive with the PI speed controller is shown in Fig.6.5. For IPMSM drives, the electrical dynamics are faster than the mechanical dynamics. Usually, the mechanical time constant is ten times greater than the electrical time constant. So for the sake of simplicity the electrical dynamics are omitted and the actual currents are considered as the command currents. The PWM inverter is modeled by a delay element, $e^{-s\tau}$ with the delay time τ and unity gain, i.e., the command and phase currents are considered to be the same. Thus, the forward transfer function, $G_o(s)$ for the speed controller is given by,

$$G_o(s) = \frac{\omega_r(s)}{\Delta\omega_r(s)} = \frac{(sK_{ps} + K_{is})e^{-s\tau}}{J_m s^2 + B_m s} \tag{9}$$

Therefore, the closed loop transfer function, G(s) can be described by,

$$G(s) = \frac{\omega_r(s)}{\omega_r^*(s)} = \frac{(sK_{ps} + K_{is})e^{-s\tau}}{J_m s^2 + (B_m + K_{ps}e^{-s\tau})s + K_{is}e^{-s\tau}} \tag{10}$$

Neglecting the delay time the damping ratio ζ and undamped natural oscillation ω_n are given by,

$$\zeta = \frac{B_m + K_{ps}}{2\sqrt{K_{is}J_m}} \quad \text{and} \quad \omega_n = \sqrt{\frac{K_{is}}{J_m}} \tag{11}$$

At first, the PI controller gains are selected (K_i = 0.06 and K_p = 0.3085) for critically damping to avoid any overshoot but the controller becomes too sluggish. In order to get a reasonable settling time, the PI controller gains (K_{ps}=0.06 and K_{is}=0.628) are designed for a slightly underdamped condition (ζ=0.7). The gains of the transfer functions are normally tuned around the calculated values for best performance such as minimum overshoot, minimum settling time and zero steady state

error based on experimental results. The constants are found to be, K_p=0.06 and K_i=0.35.

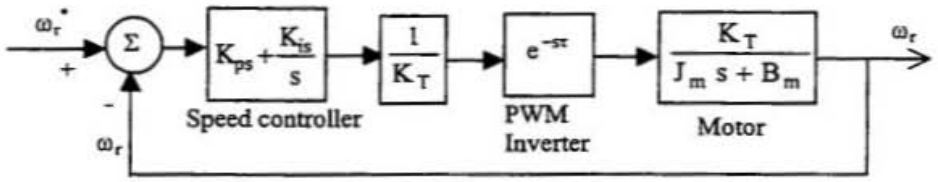

Fig.6.5. Transfer function block diagram for speed control with a PI controller.

6.5 Experimental Results and Discussions

Numerous experimental tests are carried out to verify the efficacy of the proposed FLC based IPMSM drive system. Experimental tests are also carried out for the conventional fixed gain PI controller based system in order to prove the superiority of the FLC based system. The tests are carried out at different operating conditions, such as at no load, full load, and rated and low command speeds. The tests are also carried out under certain disturbance conditions such as on-line step change in command speed, sudden change in load and parameter variations. The experimental results for the proposed FLC based IPMSM drive are also presented here to verify the simulation results shown in chapter 5. The experimental results are shown in Figs. 6.6 to 6.18.

Figures 6.6(a) and (b) show the experimental speed and the corresponding phase current response of the PI controller based IPMSM drive system, respectively, under no load and rated command speed (188.5 rad./sec.) conditions. Figures 6.7(a) and (b) show the speed and current responses of the proposed FLC based IPMSM drive system under the same operating conditions. It is shown from

Figs. 6.6 and 6.7 that the PI controller based system has an overshoot of 10 rad./sec. (95 rpm) and steady-state error which may not be acceptable for a high performance industrial drive system, whereas the proposed FLC based system can follow the command speed without overshoot and steady-state error. Moreover, the settling time of FLC is smaller by 1.0 sec. and hence it is faster than that of PI controller based system. Therefore, the FLC is superior to the conventional PI controller based system regarding the performance of the drive. Figures 6.8 and 6.9 show the speed and current responses for the PI and the FLC based system, respectively, at rated load and rated speed conditions. The experimental results in Figs. 6.8 and 6.9 show that the FLC based system is capable of running the motor following the rated command speed without overshoot and steady-state error even at rated load condition. However, for the PI controller based system the steady-state error has been increased for the full load condition as compared to the no load condition. Experimental tests are also performed to investigate the performance of the drive at low speed conditions. The speed responses of the drive for the PI and the FLC based system are shown in Figs. 6.10(a) and (b), respectively, for low command speed (50 rad./sec.) under the same operating conditions. It is shown that the FLC based IPMSM drive system also follows the low command speed without overshoot and steady-state error. However, the PI controller based system suffers from overshoot. Therefore, the efficacy of the FLC based system has been validated at various speed conditions.

The performances of the drive are also investigated for sudden change of command speed at various loading conditions. The speed and the corresponding q-axis command current responses are shown in Figs. 6.11(a) and (b), respectively for the PI controller based system for a step increase in command speed at no load

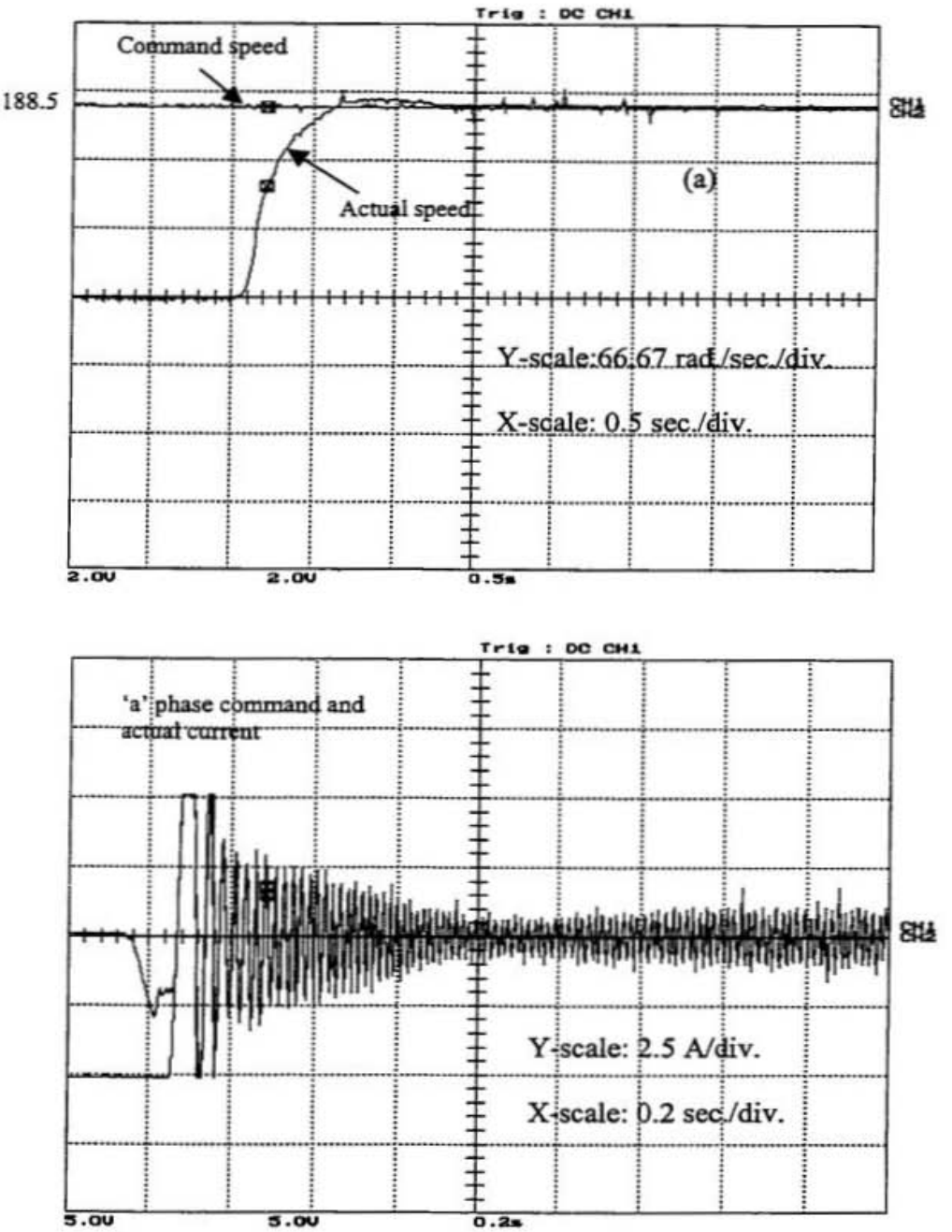

Fig. 6.6. Experimental responses of the conventional PI controller based IPMSM drive system under no load and rated speed conditions: (a) speed and, (b) current.

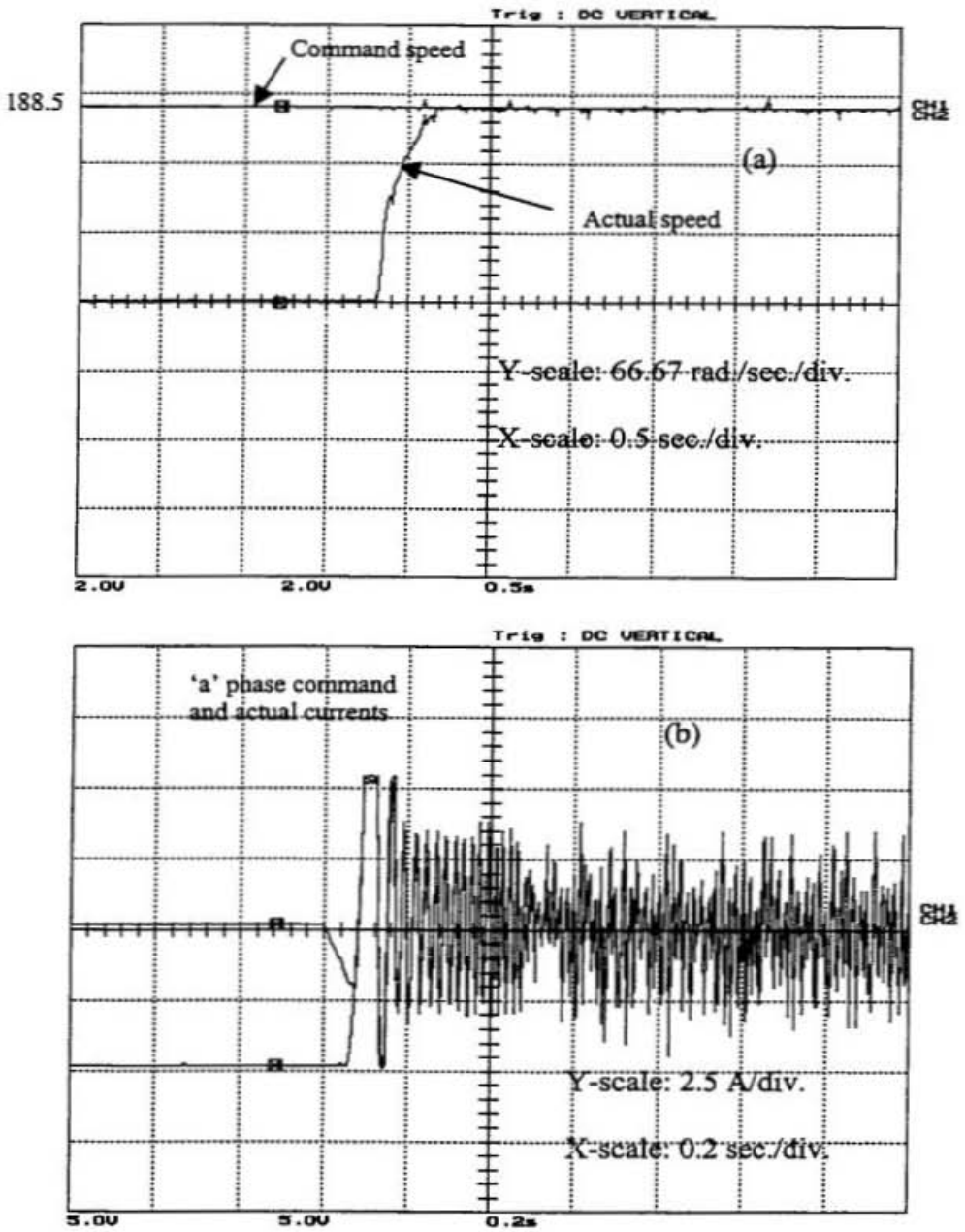

Fig. 6.7. Experimental responses of the proposed FLC based IPMSM drive system under no load and rated speed conditions: (a) speed and, (b) current.

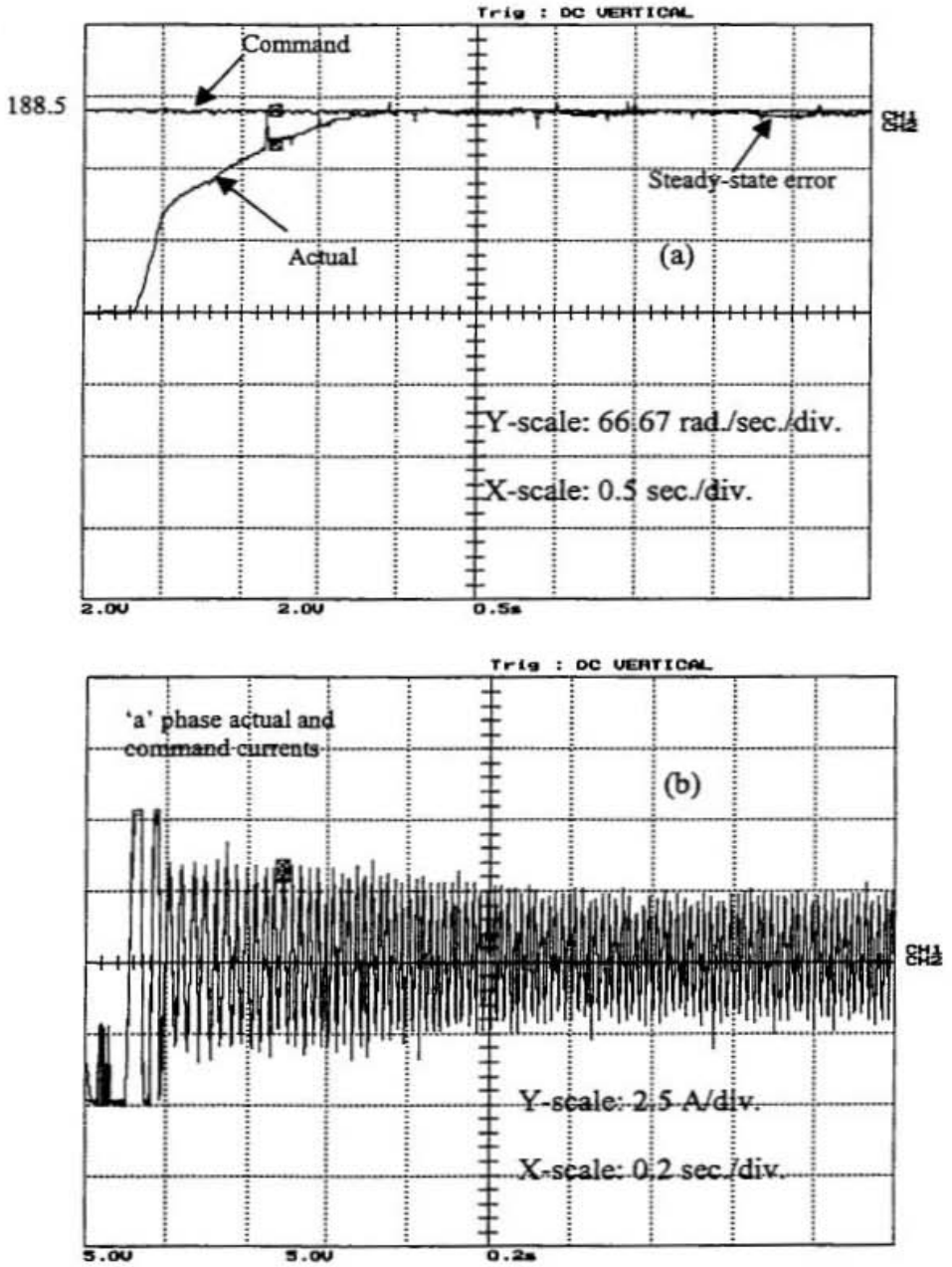

Fig. 6.8. Experimental responses of the conventional PI controller based IPMSM drive system under rated load and rated speed conditions: (a) speed and, (b) current.

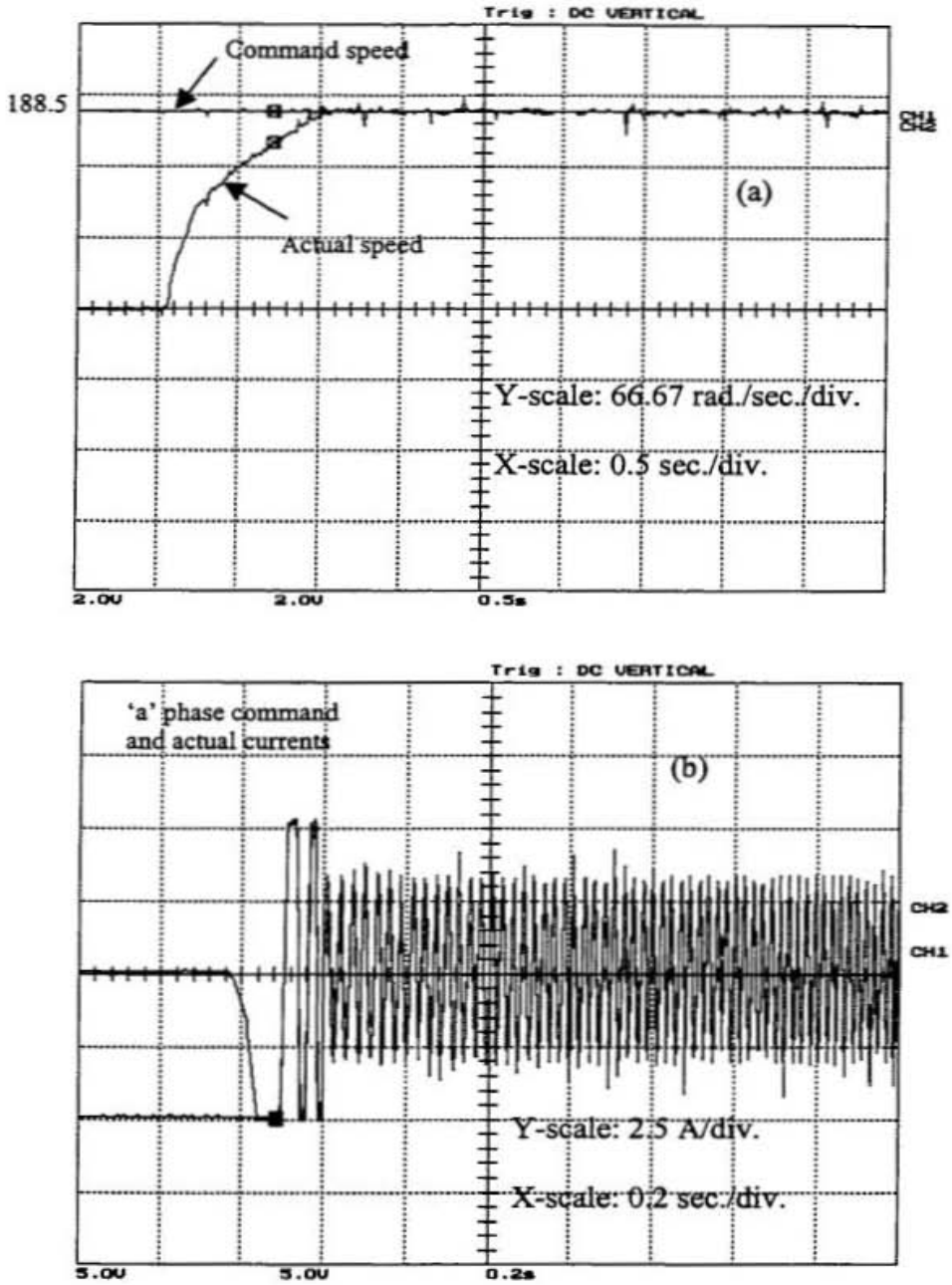

Fig. 6.9. Experimental responses of the proposed FLC based IPMSM drive system under rated load and rated speed conditions: (a) speed and, (b) current.

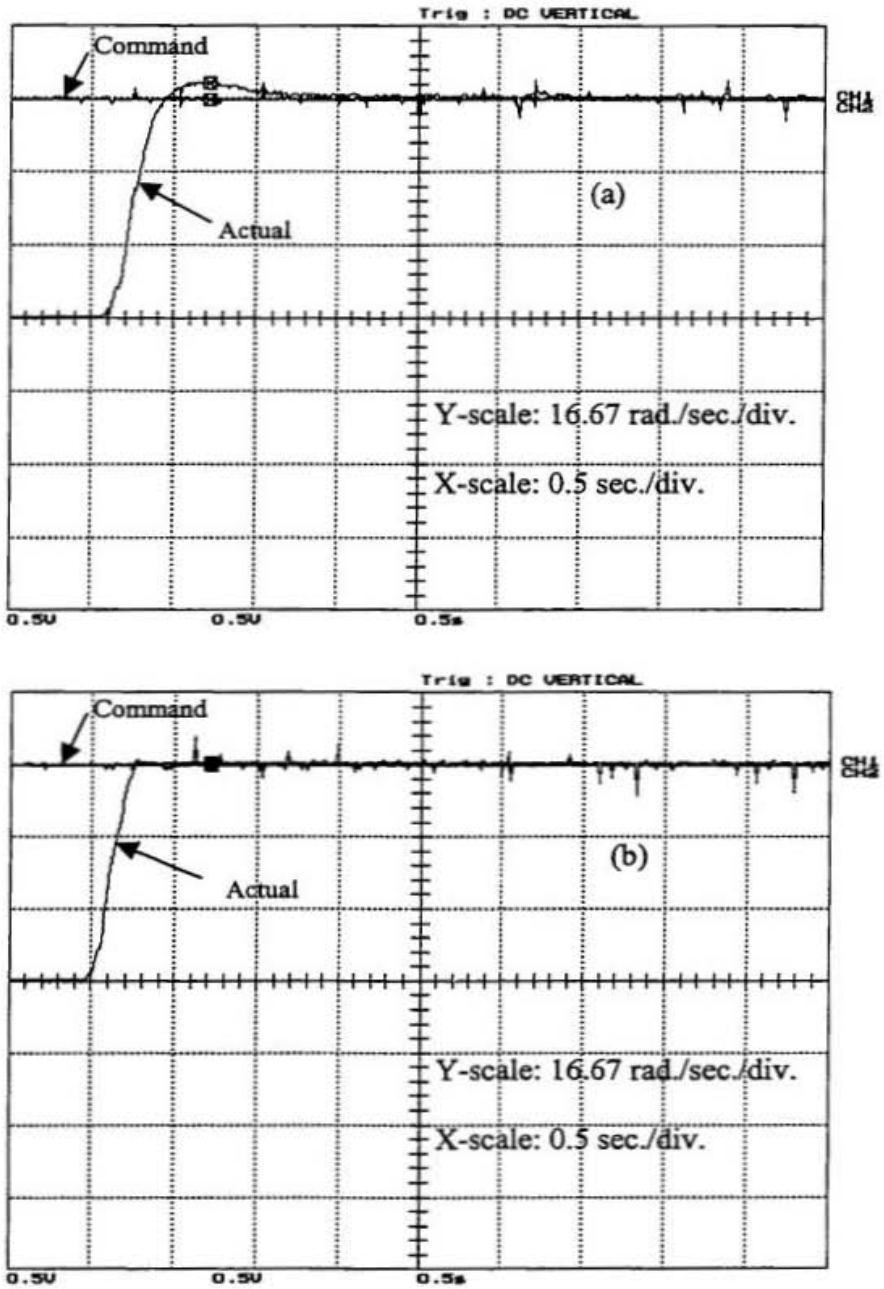

Fig. 6.10. Experimental speed responses of the IPMSM drive system under light load and low speed (50 rad./sec) conditions in the case of: (a) PI and, (b) FLC.

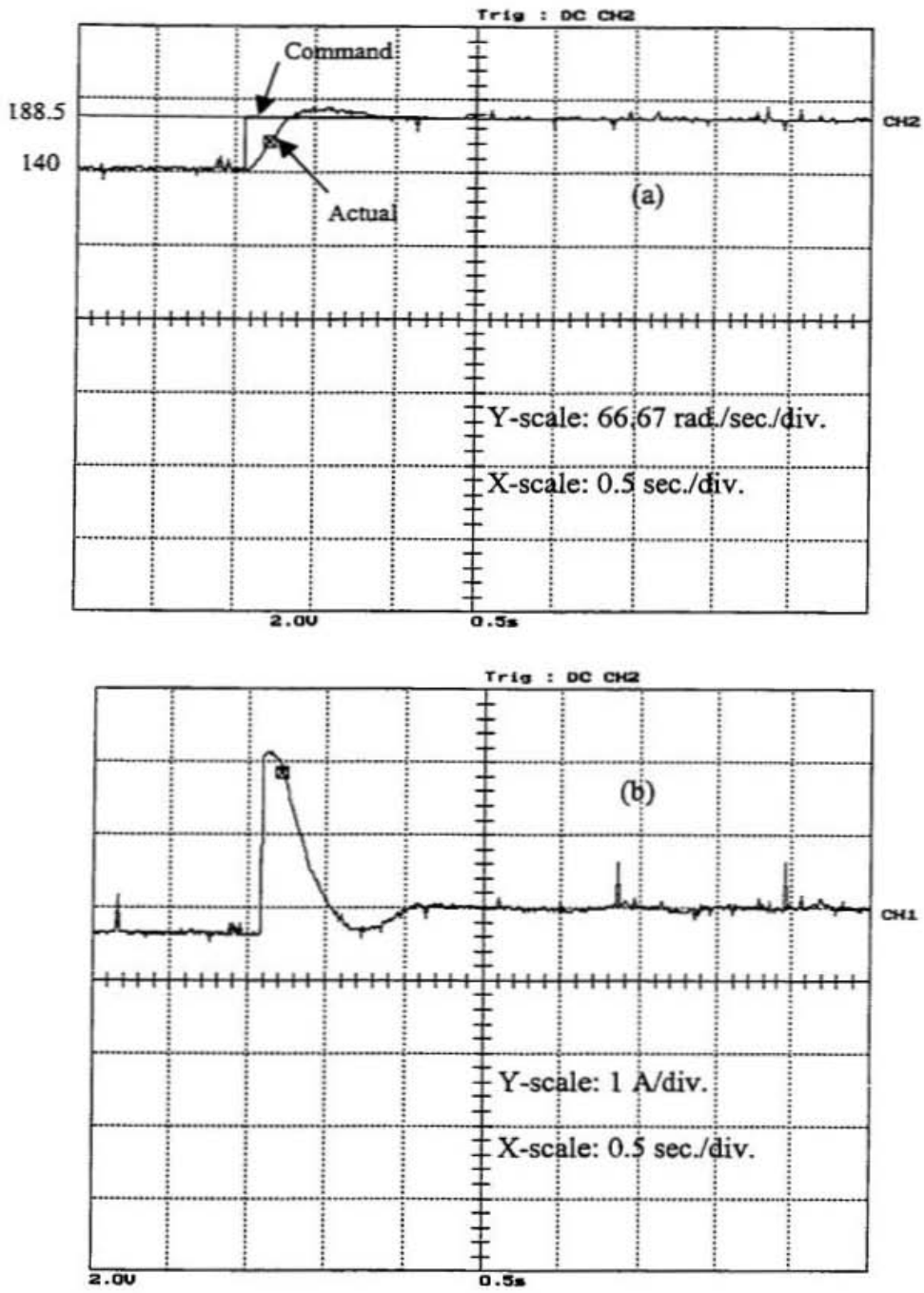

Fig. 6.11. Experimental responses of the conventional PI controller based IPMSM drive system for a sudden change in command speed at no load condition: (a) speed and, (b) q-axis command current $i_q^{r^*}$.

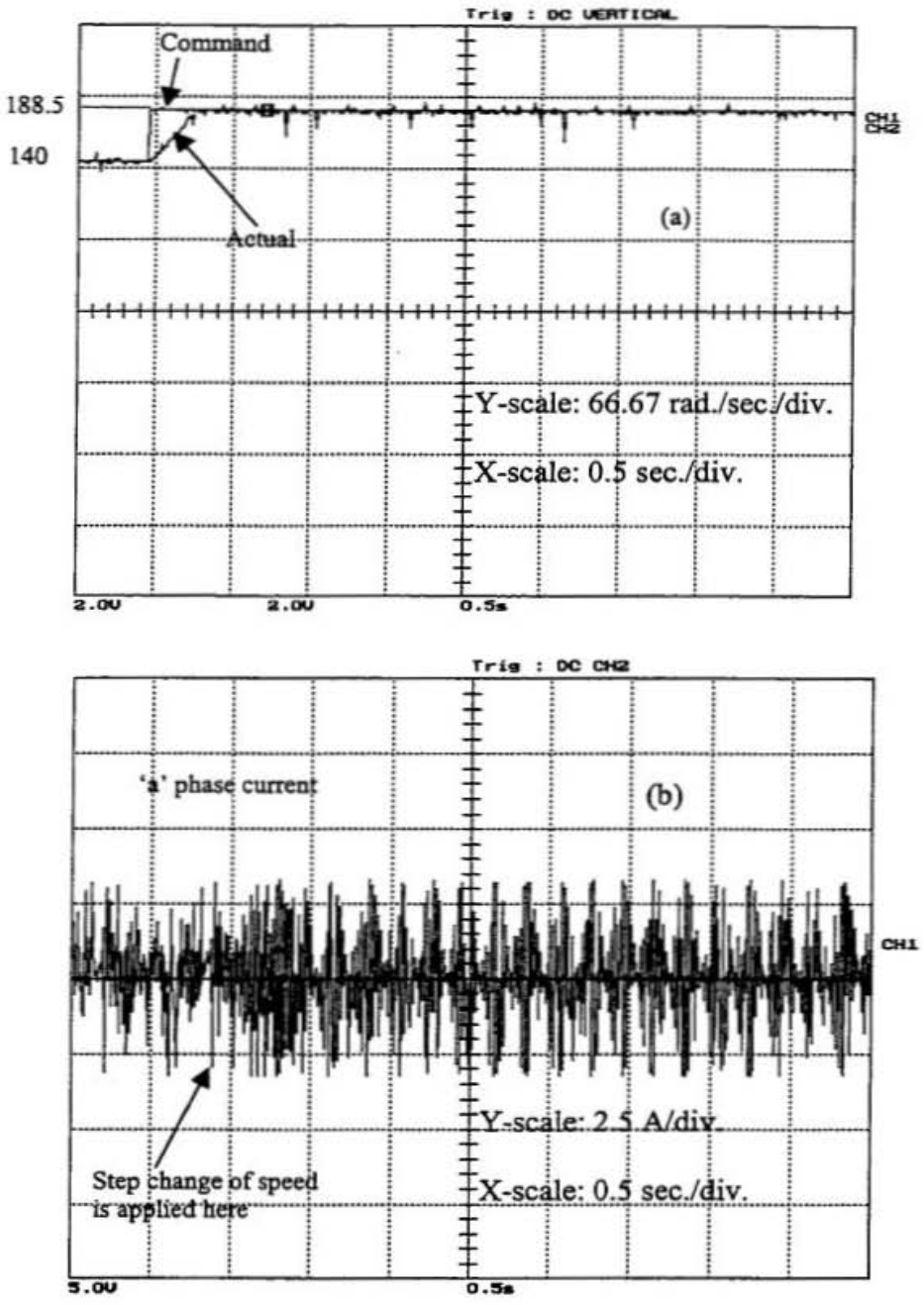

Fig. 6.12. Experimental responses of the proposed FLC based IPMSM drive system for a sudden change in command speed under no load condition: (a) speed and, (b) q-axis command current i_q^{r*}.

condition. The q-axis command current response is taken to identify the disturbance in torque as it represents the command torque. The speed and the phase current responses for the proposed FLC based drive system are shown in Figs. 6.12(a) and (b), respectively, under the same operating conditions. The command speed can be changed on-line from the keyboard using a software program (dspeed.c) given in Appendix-F. Figures 6.11 and 6.12 demonstrate that the FLC based drive system is capable of following the command speed without any overshoot and steady-state error even with the sudden change in command speed. However, the PI based IPMSM drive system has an overshoot of 10 rad./sec. at the time of change in command speed which is not acceptable for the high performance drive system. The speed responses for a sudden increase in command speed under full load condition is shown in Figs. 6.13(a) and (b) in the case of PI and FLC based system, respectively. It is shown from Figs. 6.13 (a) and (b) that for the PI controller based system the drive follows the command speed with a steady state error under full load condition, whereas, for the FLC based system the drive follows the command speed smoothly without steady-state error even under full load condition. Moreover, the FLC based system is faster than that of the PI controller based IPMSM drive system.

The ability of the drive to follow the command speed in the case of sudden decrease of the command speed is also tested experimentally. Figures 6.14(a) and (b) show such speed responses in the case of the conventional PI and the proposed FLC based IPMSM drive system, respectively, under light load condition. In the case of sudden decease of the command speed the PI controller based drive as noted in Fig. 6.14 (a) has a big undershoot (24 rad./sec.), overshoot (10 rad./sec.) and a small steady-state error which are obviously not acceptable for the high per-

formance drive systems. Whereas, the proposed FLC based IPMSM drive (Fig. 6.14 (b)) follows the command speed without undershoot, overshoot and steady-state error. Moreover, the response of the FLC based system is faster than the PI controller based system.

In practical industrial applications, the sudden change of load is a common phenomenon. Therefore, the performance of the drive is also investigated for sudden increase and decrease of load conditions. The speed responses for a sudden increase in load are shown in Figs. 6.15 (a) and (b) in the case of the PI and the FLC based system, respectively, under rated speed condition. The motor was running at no load condition and after some time suddenly the full load was applied to the motor. It is clearly evident from Figs. 6.15 (a) and (b) that the FLC based system is more robust than the PI controller based system in the case of sudden change of load. It can be seen from Fig. 6.13(a) that the motor speed drops by almost 12 rad./sec. (115 rpm) at the point of applying load in the case of the PI controller based system, whereas the FLC based system is almost insensitive to load variations due to its inherent adaptive nature with changing load conditions.

Figures 6.16 (a) and (b) show the speed responses in the case of the PI and the FLC based system, respectively, under a sudden decease in load at rated speed condition. The motor was running at full load condition and after some time suddenly the load was removed from the motor. It is shown from Figs. 6.16(a) and (b) that the PI controller based IPMSM drive has an overshoot of 10 rad./sec. at the point of removing the load, whereas, the FLC based system is completely insensitive to removing the load. Therefore, the proposed FLC IPMSM drive based system is found to be robust at various speeds and various loading conditions, for the cases of sudden change in command speed and load.

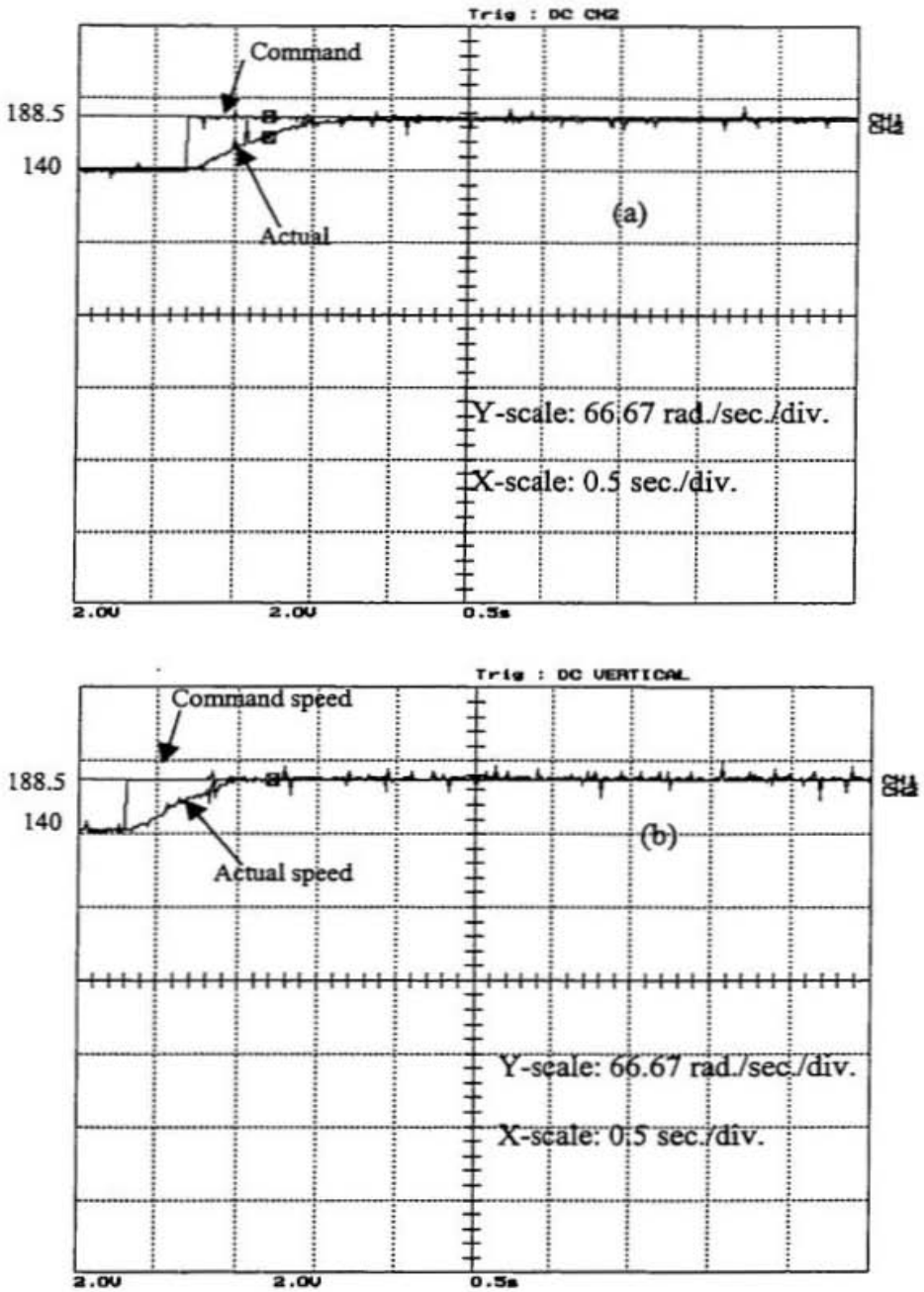

Fig. 6.13. Experimental speed responses of the IPMSM drive system for a sudden increase in command speed at full load condition in the case of: (a) PI controller and, (b) FLC.

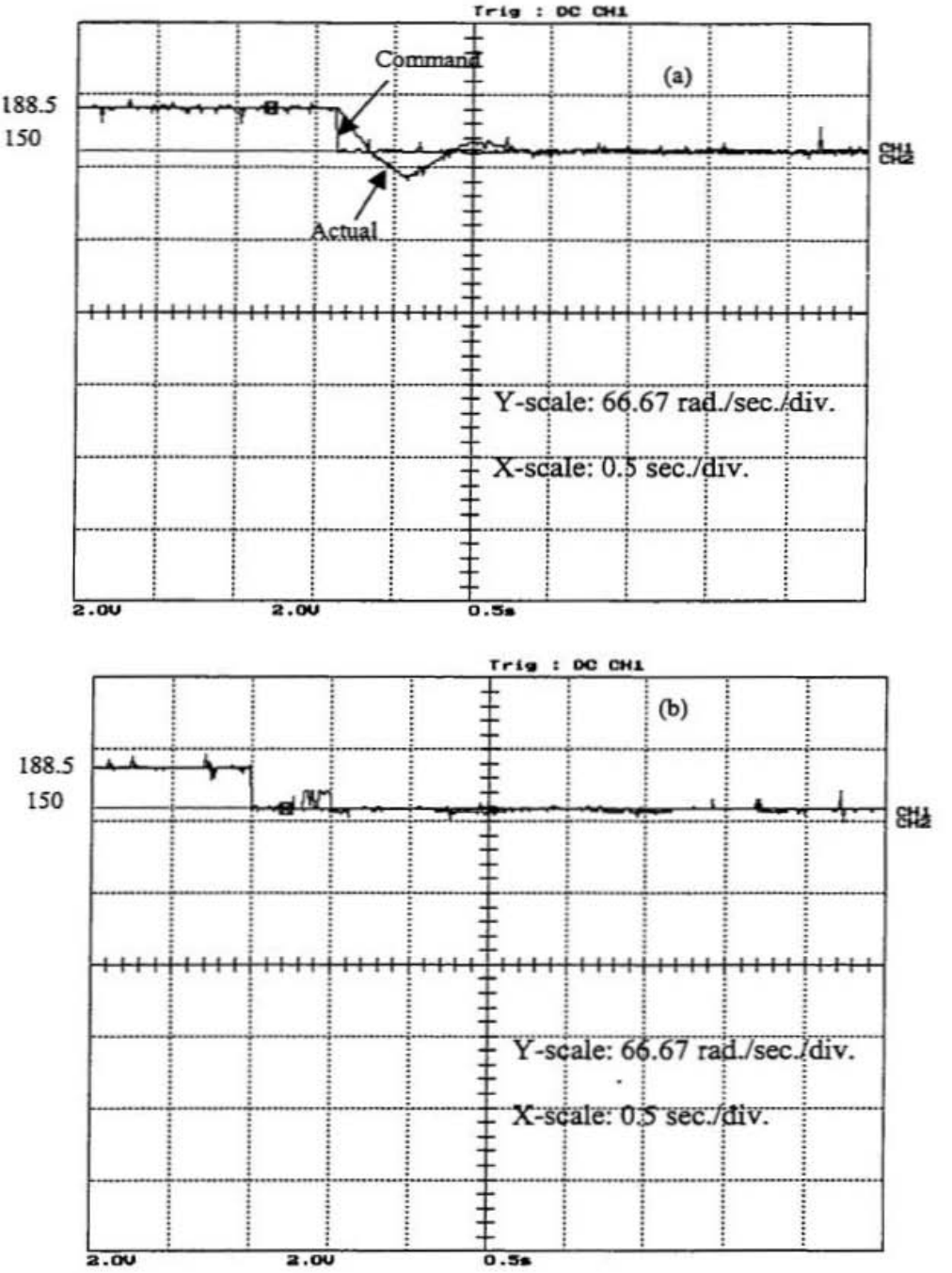

Fig. 6.14. Experimental speed responses of the IPMSM drive system for a sudden decrease in command speed at light load condition in the case of: (a) PI controller and, (b) FLC.

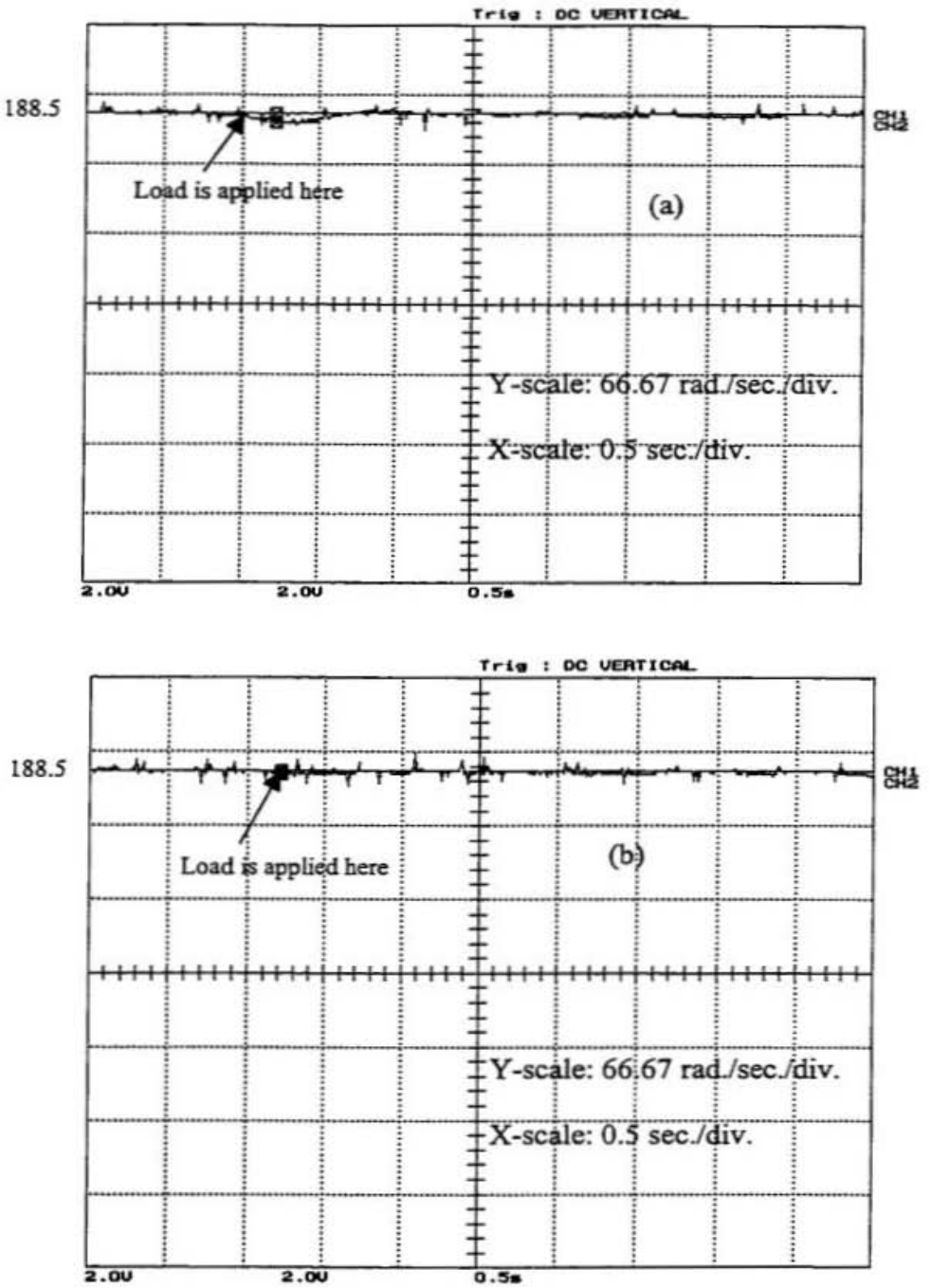

Fig. 6.15. Experimental speed responses of the IPMSM drive system for a sudden increase in load under rated speed condition in the case of: (a) PI and, (b) FLC.

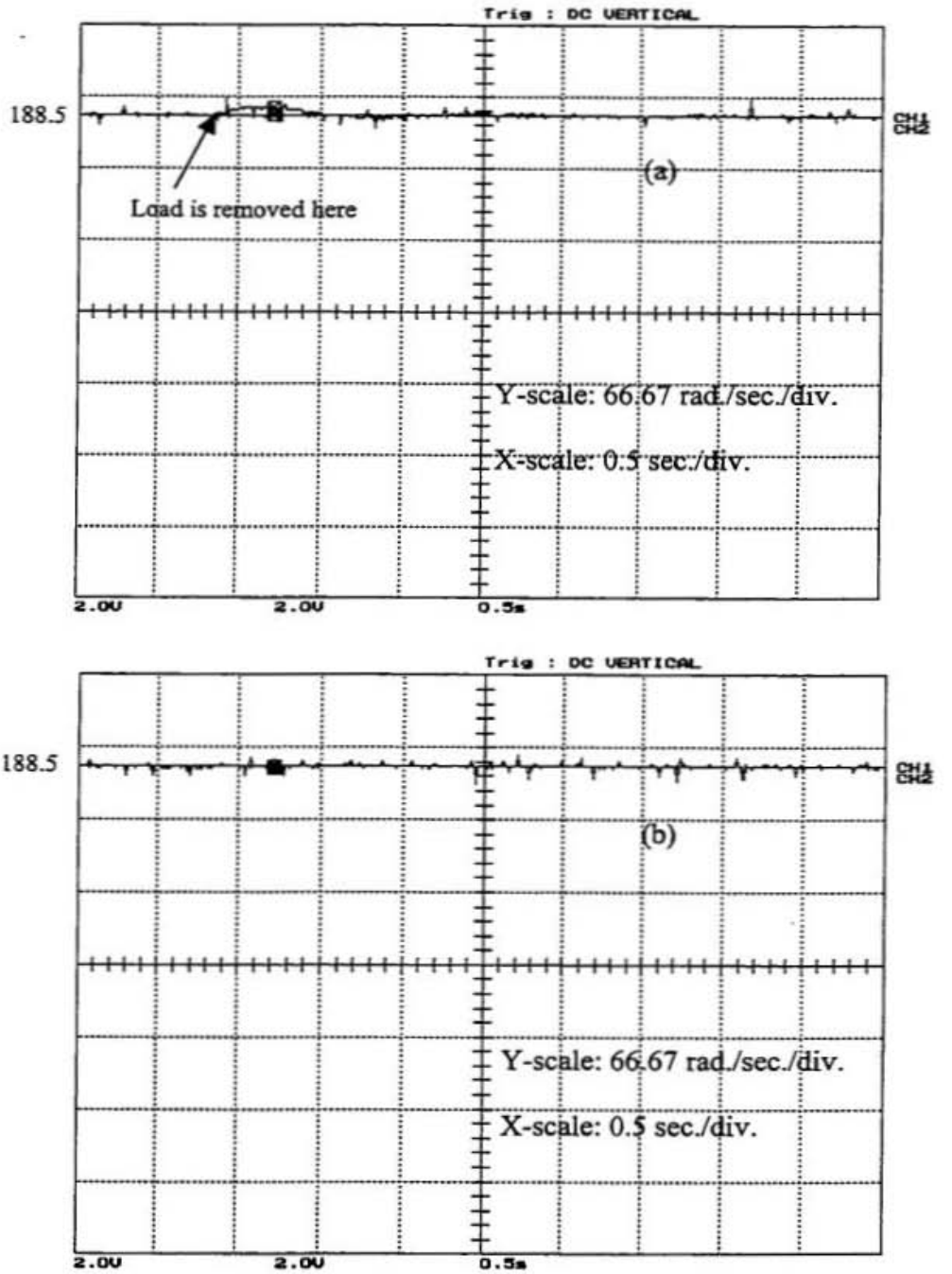

Fig. 6.16. Experimental speed responses of the IPMSM drive system for a sudden decrease in load under rated speed condition in the case of: (a) PI and, (b) FLC.

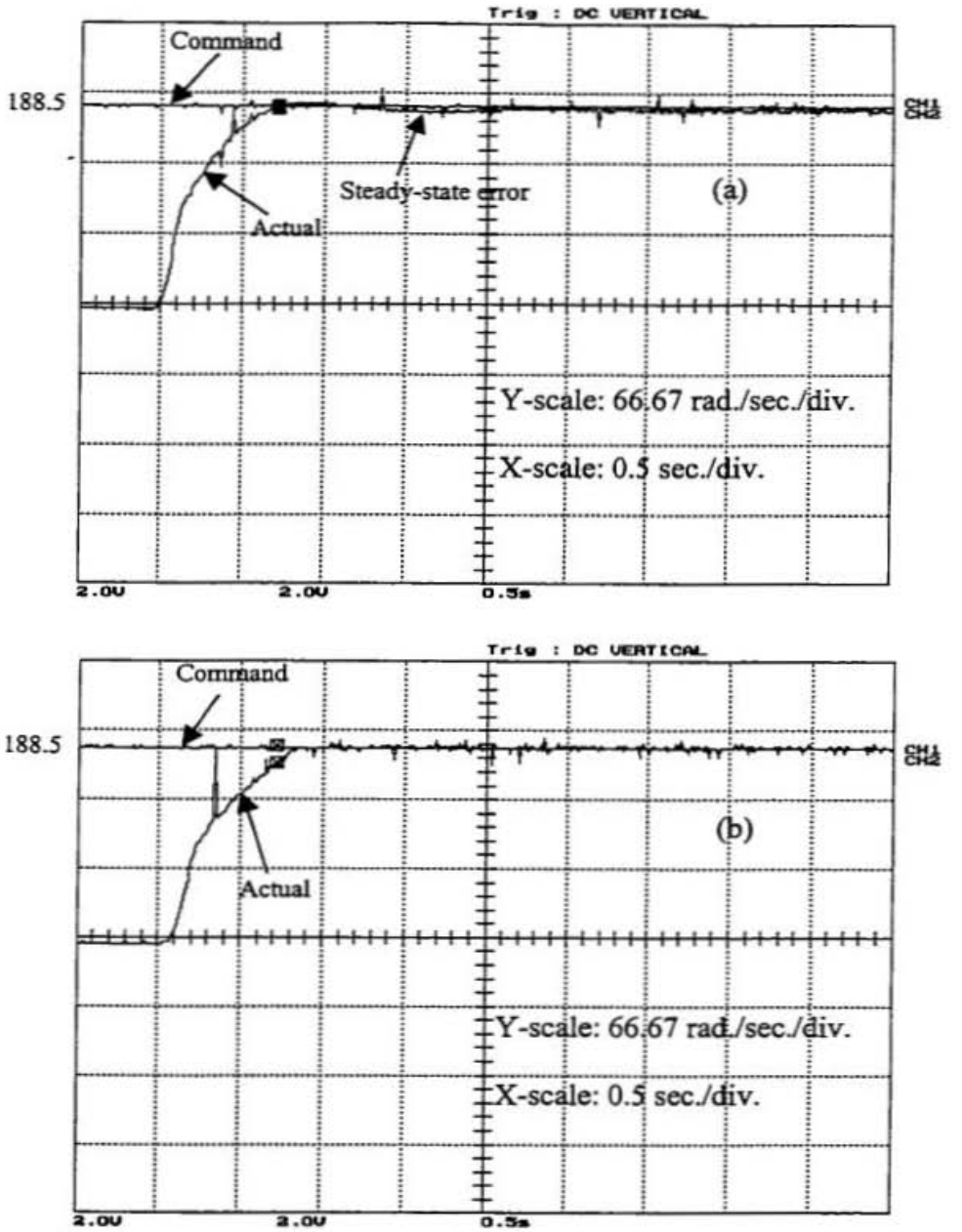

Fig. 6.17. Experimental speed responses of the IPMSM drive system with doubled inertia (J→2J) under rated speed condition in the case of: (a) PI and, (b) FLC.

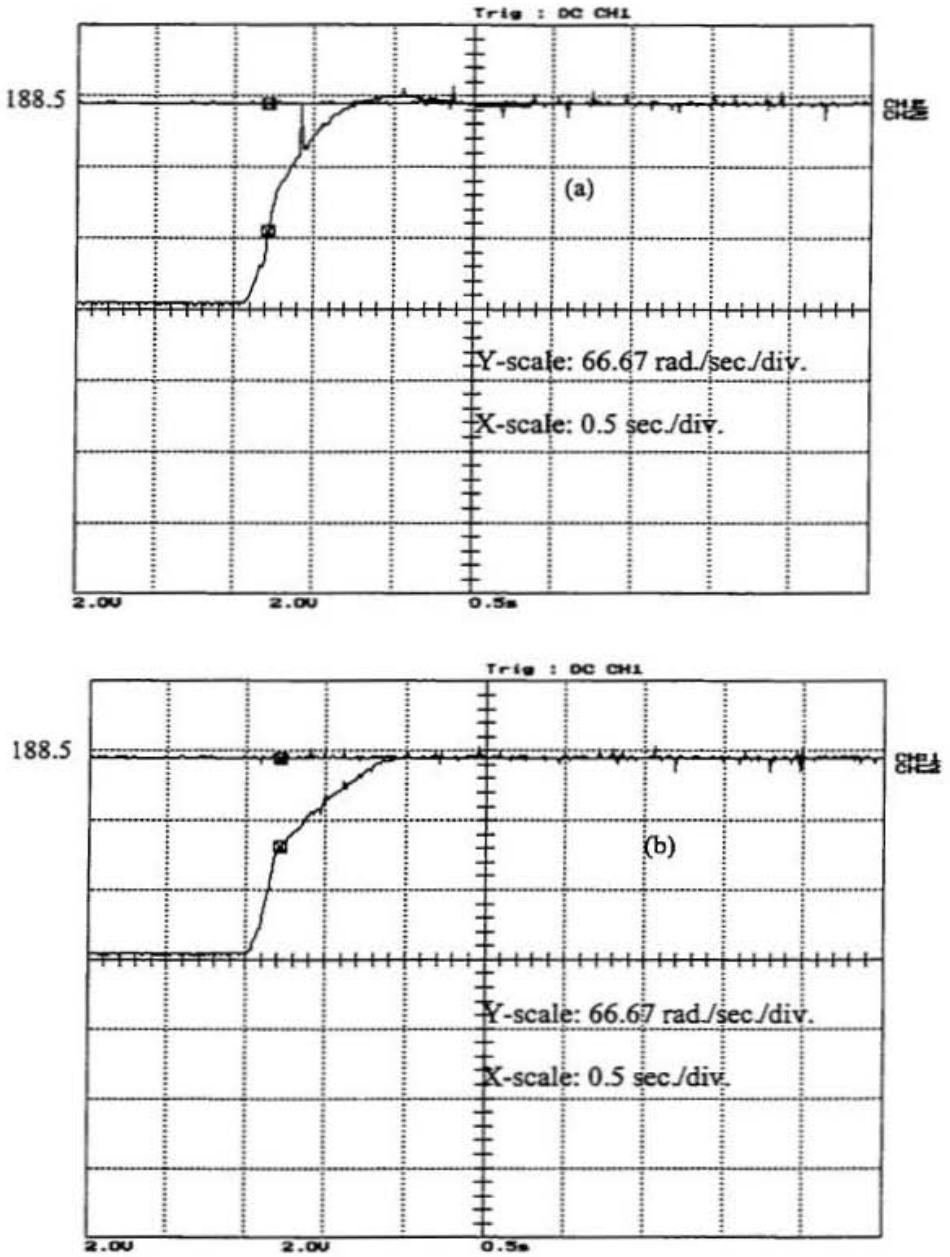

Fig. 6.18. Experimental speed responses of the IPMSM drive system with doubled stator resistances (R→2R) under full load and rated speed conditions in the case of: (a) PI and, (b) FLC.

The performances of the drive are also investigated experimentally with parameter variations for both the PI and the FLC based system. For parameter variations the rotor inertia and the stator resistances are considered. The inertia of the motor is doubled by coupling it directly with another motor of almost the same inertia as the test motor. The stator resistances are doubled by inserting external resistance to the per phase stator windings. Figures 6.17 (a) and (b) show the speed responses of the IPMSM drive in the case of the PI controller and the proposed FLC based system, respectively, with doubled inertia (J→2J) under rated speed condition. It is evident from Figs. 6.17(a) and (b) that the FLC based IPMSM drive system follows the command speed with increased inertia smoothly without overshoot and steady-state error, whereas, the PI controller based IPMSM drive does not follow the command speed smoothly and also suffers from overshoot, undershoot and steady-state error.

The drive performances with doubled the stator resistances (R→2R) are shown in Figs. 6.18(a) and (b) in the case of the PI controller and the proposed FLC based system, respectively, under rated speed and rated load conditions. These results show that the FLC based IPMSM drive can follow the command speed smoothly with zero overshoot and zero steady-state error, although the stator resistance parameter has been changed. However, the PI controller based system suffers from significant overshoot in speed.

All the comparative experimental results from Figs. 6.6 – 6.18 show that the proposed FLC based IPMSM drive can follow the command speed quickly almost without overshoot and zero steady state error at different dynamic operating conditions. As the PI controller was designed based on the available motor parameters and certain operating conditions, it is not capable of running the motor covering the

whole operating range with uncertainties like sudden load impact, parameter variations, system disturbances, etc. Thus for the PI controller, the over shoot and undershoot were significant with changing operating conditions. On the other hand, the proposed FLC based IPMSM drive system is capable of running the motor by adjusting the necessary torque with the sudden load change, parameter variations, system disturbance, etc. Thus, it is clearly established that the proposed FLC based IPMSM drive system is more robust than the conventional PI controller based system.

6.6 Concluding Remarks

In this chapter, the detailed DSP based real-time implementation procedure for the FLC based vector control of IPMSM drive has been presented. The complete drive has been implemented using a digital signal processor board DS1102 in a prototype laboratory 1 hp interior permanent magnet motor. The implementation involves both hardware and software. In order to demonstrate the superiority of the proposed FLC a PI controller is also designed and implemented in real-time. The performances of the conventional PI based and the proposed FLC based IPMSM drive have been investigated at different dynamic operating conditions such as sudden change of command speed, load change and parameter variations. The comparative experimental results establish that the FLC based IPMSM drive is more robust as compared to the PI controller based IPMSM drive system. Thus, it is found that the PI controller could successfully be replaced by the FLC in high performance industrial drive applications, where robustness is one of the prime requirements. The experimental results for the proposed FLC based IPMSM drive also validate the simulation results presented in chapter 5. The results shown in this

thesis may not be sufficient for any industry to prefer FLC. The specific industry application of the FLC needs more investigation to tune the controller parameters for smooth speed control in steady-state. However, the industry may be convinced for FLC due to some better transient responses than PI controller such as less settling time, zero overshoot, zero undershoot and zero steady-state error. The main challenge in industrial implementation of the proposed controller may be the high cost of the controller itself as compared to the motor. However, the cost of the inverter/controller and motor are comparable for those up to 5 hp motor drives. That result is found from Yaskawa Electric Co. of Japan, who is the major manufacturer of the IPMSM with matching inverters.

The proposed procedure may also be applied for real-time implementation of FLC for other dc and ac motor drives. The proposed method was applied to a laboratory 1 hp induction motor and it was found that the motor was running smoothly with the same membership functions just after adjusting the scaling factors [89]. Similar implementation techniques were developed and successfully applied to position control of the IPMSM drive in real-time for robotic applications [90]. The proposed technique can be applied to a motor of higher rating than the laboratory 1 hp by adjusting the various scaling factors, such as K_ω, K_e, K_i, etc.

Chapter 7

Conclusions

Based on the literature review in chapter 1, it is concluded that the interior permanent magnet synchronous motor (IPMSM) can be used to meet the criteria of variable speed high performance electric motor drives. However, the performance depends on the type of speed controllers. Speed controllers, constant gain types and their adaptive versions need an accurate system mathematical model. However, it is often difficult to develop such a model due to some of the system's unavoidable circumstances such as saturation, parameter variations, load impact, system mechanical noise, etc. Moreover, the fixed gain controllers suffer from overshoot, undershoot, steady-state error and occasional instability. The conventional adaptive controllers need complex circuitry to be implemented in real-time.

In chapter 1 the review of various electric motors with various control techniques has been provided. This identifies the problems of controlling the electric motors in high performance variable speed drive applications. Problems of controlling the speed accurately for an IPMSM with different dynamic operating condi-

tions have been identified and the FLC has been proposed to overcome these problems.

The in-depth literature review also indicated that recently, the FLC has become a popular choice for speed control of electric motors in variable speed drive applications. This is due to its inherent capabilities of handling nonlinearities, parameter variations, load disturbances and system noise. The FLC adjusts the control output with different dynamic operating conditions with its inherent adaptive nature. In order to verify the efficacy of the fuzzy logic based speed controller in high performance applications, a vector control scheme of the IPMSM incorporating the FLC has been implemented experimentally for a laboratory 1 hp interior type PM motor.

As an integral part of this research work the performance of various current controllers for the IPMSM drive has been simulated and experimentally investigated in order to select a suitable current controller for the vector control scheme. The mathematical formulations are presented to develop the vector control strategy of the IPMSM. Based on both the simulation and experimental results a comparison among various current controllers has been made in chapter 2. A hybrid current controller is proposed in order to take advantages from both the hysteresis and the ramp comparator controllers. However, considering the computational burden and the performance over the entire speed range the sinusoidal band hysteresis current controller has been selected along with the voltage source IGBT inverter.

In chapter 3 the control technique of the IPMSM over a wide speed range incorporating the flux weakening operation has been developed. The scheme includes the maximum torque per ampere operation in the constant torque region (i.e., below the base speed) and the flux-weakening operation in the constant power region (i.e., above the base speed). The performance of the proposed FWC technique has been

investigated both theoretically and experimentally. Finally, a comparison has also been made between the FWC and the conventional i_d =0 control techniques. The FWC technique has been found more robust than the i_d =0 control technique over a wide speed range.

Chapter 4 briefly described the fundamentals of the fuzzy logic controller (FLC) and its applications to motor control. The basic ideas of fuzzy logic, linguistic variables, fuzzy sets, membership functions, fuzzification, fuzzy inference engine (rule evaluation) and defuzzification have been presented. The detailed mathematical formulations for various processes of the FLC have also been presented in this chapter.

In chapter 5, a novel speed control scheme of the IPMSM drive using the specific fuzzy logic algorithm has been developed. Prior to laboratory implementation, the performance of the proposed FLC has been predicted through extensive simulations. The starting performances at various speed, parameters and load conditions as well as the effects of on-line load disturbances, sudden speed changes and parameter variations on both the speed and the current responses of the proposed drive have been investigated in this chapter. The FLC can adjust itself with different operating conditions such as load change, parameter variations and step change of command speed. Thus, the simulation results show encouraging performances of the proposed drive.

In chapter 6, the step-by-step real-time implementation procedures of the complete vector control scheme of IPMSM incorporating the FLC have been presented. The hardware elements including the DS-1102 board, incremental encoder, Hall-effect current sensors, base drive circuits and IGBT inverter have been presented. New software programs in 'C' language have been developed for real-time implementation of the FLC. For the complete vector control scheme the sinusoidal

band hysteresis controller is used as current controller based on the investigation of various current controllers presented in chapter 2. The performance of the proposed FLC based IPMSM drive has been experimentally investigated at different dynamic operating conditions. The experimental results validated the simulations presented in chapter 5. Finally, in this chapter, a comparison between the conventional fixed gain PI controller and the innovative FLC for the IPMSM drive has also been made. The experimental results are obtained under the same operating conditions in order to validate the superior performances of the fuzzy logic controller over the PI controller. The comparative results show that the FLC based system can follow the command speed faster than the PI controller. Moreover, the response of the FLC is free from overshoot, undershoot and steady-state error, whereas the PI controller based system suffers from overshoot, undershoot and steady-state error at different dynamic operating conditions. Thus, the FLC is found more robust and hence, a suitable replacement of the conventional PI controller. The motor has been controlled up to the base speed using the $i_d=0$ control technique in the constant torque region. In order to operate the motor above base speed, in constant power mode the flux-weakening control technique (where $i_d\neq0$) has been incorporated after calculation of the q-axis current command from the speed controller.

7.1 Major Contributions of the Dissertation

The major contributions of this dissertation are:

1. Detailed mathematical formulations for modeling the current controlled voltage source inverter (VSI) fed IPMSM drive has been presented. The vector control scheme of the VSI fed IPMSM drive has been developed. The performances of various current controllers for the IPMSM drive have been investigated both

theoretically and experimentally. A comparison has also been made among the various current controllers, particularly the hysteresis controller and the ramp comparator controller performances for the IPMSM drive in order to choose a suitable current controller before integrating it in the proposed complete IPMSM drive system.

2. A new control technique of IPMSM over a wide speed range incorporating the flux-weakening operation has been developed. The scheme incorporates the maximum torque per ampere operation in the constant torque region and the flux-weakening operation in the constant power region. The performances of this control technique have been evaluated by simulation results as well as by experimental results. A comparison between the flux-weakening control technique and the typical i_d=0 control technique has also been presented. It has been observed that for the conventional i_d=0 control, above the base speed (188.5 rad./sec.) the motor was vibrating, whereas for the FWC, the motor was running smoothly up to 400 rad./sec. Thus, the FWC technique has been found more robust as compared to the i_d=0 control technique over a wide speed range.

3. An application specific new fuzzy logic controller (FLC) for the IPMSM drive has been developed. Sets of new implementation codes have been written with a view to minimize computational burden for the practical IPMSM.

4. The new FLC has been successfully incorporated for the IPMSM drive to take into account the motor dynamics as well as nonlinear load characteristics. Prior to implementing the proposed FLC based drive in real-time, the performance of the drive has been predicted through extensive simulations carried out at differ-

ent dynamic operating conditions. Encouraging performance results in simulation have been obtained.

5. The proposed FLC based vector of IPMSM has been successfully implemented in real-time using digital signal processor (DSP) controller board DS 1102 for the laboratory 1 hp motor. The step-by-step implementation procedures for the FLC have been developed and presented. For real-time implementation of the proposed FLC based IPMSM drive, an IGBT Power Module Inverter and its associated drive circuits have been built in the Power Research Laboratory of Memorial University of Newfoundland.

6. The performance of the IPMSM drive using the new FLC have been experimentally investigated at different dynamic operating conditions such as load change, command speed change, parameter variations. It has been proved that the FLC based IPMSM drive has superior operating performances in comparison to the PI controller based drive. Finally, it is claimed that a complete IPMSM drive incorporating the FLC has been presented for the first time to the best of the author's knowledge.

7.2 Future Scope of the Work

This work mainly involves the use of different current and speed controllers for the IPMSM drive to be used in high performance drive systems. Particularly, the successful real-time implementation technique for the complete vector control scheme of IPMSM incorporating the FLC has been developed for the first time. It has been observed experimentally that the torque response of the developed FLC has a significant pulsation. That is why, the speed responses given in Chapter 6 showed spikes in steady-state. As a future recommendation of this work, it is suggested that the proposed FLC can be modified in order to reduce the torque pulsation by making it more adaptive with the change of membership functions, fuzzy sets and fuzzy rule based matrix on-line. By reducing the torque pulsation it is possible to run the motor smoothly at steady-state. Thus, the speed response will be free from spikes. However, the same implementation technique presented in this work can be used. For on-line adaptation the neuro-fuzzy technique may also be used.

A systematic development of the IPMSM drive using efficient artificial neural network (ANN) controllers should be undertaken. The comparative efficacy of the IPMSM in high performance drive applications should be presented for the FLC, ANN and neuro-fuzzy speed controllers in the future scope of intelligent controllers.

Stability analysis using Lyapunov's function can be attempted in line with the recent work [91].

7.3 Conclusions

The main points of the conclusions of this work are:

- The sinusoidal band hysteresis controller can be used as a suitable current controller for the current controlled VSI-fed IPMSM drive to be used in high performance drive systems.

- The flux-weakening control technique presented in this thesis can be used for the high performance of IPMSM drive over a wide speed range covering both the constant torque and constant power regions.

- The developed FLC can be effectively used for the speed control of IPMSM as well as for other ac and dc motors in order to provide robust performance at different dynamic operating conditions such as load change, command speed change and parameter variations.

- The proposed FLC is found more robust as compared to the conventional fixed gain PI controller, and hence, the conventional PI controller could be successfully replaced by the developed FLC.

- Rather than using a look-up table, the on-line calculation of the fuzzy logic algorithms provides the critically damped speed response for the IPMSM drive. The proposed implementation technique overcomes the high computation burden of the FLC and makes the drive system suitable for high performance applications.

References

[1] P. C. Sen, "Electric Motor Drives and Control – Past, Present and Future", *IEEE Trans. on Industrial Electronics*, vol. 37, no. 6, Dec. 1990, pp. 562-575.

[2] M. A. Rahman, "Modern Electric Motors in Electronic World", *IEEE/IECON'93 Conference Record*, (Hawaii), pp.644-648.

[3] M. A. Rahman, "Permanent Magnet Synchronous Motors- A Review of the State of Design Art", *Proceedings of International Conference On Electric Machines, Athens*, 1980, pp. 312-319.

[4] G. R. Slemon, *Electric Machines and Drives*, Addison-Wesley Publishing Company, 1992.

[5] B. K. Bose, *Power Electronics and AC Drives*, Englewood Cliffs, NJ: Prentice Hall, 1986.

[6] P. C. Sen, *Principles of Electric Machines and Power Electronics*, New York: Wiley, 1988.

[7] M. H. Rashid, *Power Electronics-Circuits, Devices and Applications*, Englewood Cliffs, NJ: Prentice Hall, 1996.

[8] F. Blaschke, "The Principle of Field Orientation as Applied to the New Transvector Closed-Loop Control System for Rotating Field Machines", *Siemens Review*, Vol. 34, May 1972, pp. 217-220.

[9] A. V. Gummaste and G. R. Slemon, "Steady State Analysis of a Permanent Magnet Synchronous Motor Drive with Voltage Source Inverter", *IEEE Trans. on Industrial Applications*, vol. IA-17, no. 2, March/April 1981, pp.143-151.

[10] G. R. Slemon and A. V. Gummaste, "Steady State Analysis of a Permanent Magnet Synchronous Motor Drive with Current Source Inverter", *IEEE Trans. on Industrial Applications*, vol. IA-19, no. 2, March/April 1983, pp. 190-197.

[11] P. C. Krause, R. R. Nucera, R. J. Krefta and O. Wasynczuk, "Analysis of a Permanent Magnet Synchronous Machine Supplied from 180° Inverter with Phase Control", *IEEE Trans. on Energy Conversion*, vol. EC-2, no. 3, Sept. 1987, pp.423-431.

[12] T. H. Liu, C. M. Young and C. H. Liu, "Microprocessor Based Controller Design and Simulation of Permanent Magnet Synchronous Motor Drive", *IEEE Trans. on Industrial Electronics*, vol. 35, no. 4, Nov. 1988, pp. 516-523.

[13] P. Pillay and R. Krishnan, "Modeling of permanent magnet motor drives", *IEEE Trans. on Industrial Electronics*, vol. 35, no. 4, Nov. 1988, pp. 537-541.

[14] P. Pillay and R. Krishnan, "Modeling, Simulation and Analysis of Permanent Magnet Motor Drives, Part I: The Permanent-Magnet Synchronous

Motor Drive", *IEEE Trans. on Industry Applications*, vol. 25, no. 2, March/April 1989, pp. 265-273.

[15] P. Pillay and R. Krishnan, "Modeling, Simulation and Analysis of a High Performance Vector Controlled Permanent Magnet Synchronous Motor Drive", *IEEE/IAS Annual Meeting Conference Record*, 1987, pp 253-261.

[16] P. Pillay and R. Krishnan, "Control Characteristics and Speed Controller Design for High Performance Permanent Magnet Synchronous Motor Drive", *IEEE Trans. on Power Electronics*, vol. 5, no. 2, April 1990, pp.151-159.

[17] P. Pillay, C. R. Allen and R. Budhabhathi, "DSP-Based Vector Control and Current Controllers for Permanent Magnet Synchronous Motor Drive", *IEEE/IAS Annual Meeting Conference Record*, Seattle, Washington, 1990, pp. 539-544.

[18] B. K. Bose, "A High Performance Inverter Fed Drive System of an Interior Permanent Magnet Synchronous Machine", *IEEE Trans. on Industry Applications*, vol. IA-24, no. 6, 1988, pp. 987-997.

[19] H. Le-Huy and L. A. Dessaint, "An Adaptive Current Control Scheme for PWM Synchronous Motor Drive: Analysis and Simulation", *IEEE Trans. on Power Electronics*, vol. 4, no. 4, Oct. 1989, pp. 486-495.

[20] H. Le-Huy, K. Silmani and P. Viarouge, "Analysis and Implementation of a Real-Time Predictive Current Controller for Permanent Magnet Synchronous Servo Drives", *IEEE Trans. on Industrial Electronics*, vol. 41, no. 1, Feb. 1994, pp. 110-117.

[21] B. K. Bose and P. M. Szczesny, "A Microcomputer-Based Control and Simulation of an Advanced IPM Synchronous Machine Drive System for Electric Vehicle Propulsion", *IEEE Trans. on Industrial Electronics*, vol. 3, no. 4, Nov. 1988, pp. 547-559.

[22] T. M. Jahns, G. B. Kilman and T. W. Neumann, "Interior Permanent Magnet Synchronous Motors for Adjustable Speed Drives", *IEEE Trans. on Industry Applications*, vol. IA-22, no. 4, July/August 1986, pp. 738-747.

[23] T. M. Jahns, "Flux-Weakening Regime Operation of an Interior Permanent Magnet Synchronous Motor Drive", *IEEE Trans. on Industry Applications*, vol. IA-23, no. 4, 1987, pp. 681-689.

[24] S. Morimoto, Y. Takeda and T. Hirasha, "Current Phase Control Methods for Permanent Magnet Synchronous Motors", *IEEE Trans. on Power Electronics*, vol. 5, no. 2, April 1990, pp. 133-139.

[25] S. Morimoto, Y. Takeda, T. Hirasa and K. Taniguchi, "Expansion of Operating Limits for Permanent Magnet Motor by Current Vector Control Considering the Inverter Capacity", *IEEE Trans. on Industry Applications*, vol. 26, no. 5, Sept./Oct. 1990, pp.866-871.

[26] S. Morimoto, Y. Takeda, K. Hatanaka, Y. Tong, and T. Hirasa, "Design and Control System of Permanent Magnet Synchronous Motor for High Torque and High Efficiency Operation", *IEEE/IAS Annual Meeting Conference Record*, 1991, pp. 463-468.

[27] S. Morimoto, K. Hatanaka, Y. Tong, Y. Takeda and T. Hirasa, "Servo Drive System and Control Characteristics of salient Pole Permanent Magnet Syn-

chronous Motor", *IEEE Trans. on Industry Applications*, vol. 29, no. 2, March/April 1993, pp. 338-343.

[28] S. Morimoto, Y. Takeda, and T. Hirasa, "Flux Weakening Control Method for Surface Permanent Magnet Synchronous Motors", *IPEC Conference. Record, Tokyo, Japan,* 1990, pp. 942-950.

[29] S. Morimoto, M. Sanda and Y. Takeda, "Effects and Compensation of Magnetic Saturation in Flux-Weakening Controlled Permanent Magnet Synchronous Motor Drives", *IEEE Trans. on Industry Applications*, vol. 30, no. 6, Nov./Dec. 1994, pp. 1632-1637.

[30] M. F. Rahman, L. Zhang and K. W. Lim, "A Direct Torque-Controlled Interior Permanent magnet Synchronous Motor Drive Incorporating Field Weakening", *IEEE Trans. on Industry Applications*, vol. 34, no. 6, Nov./Dec. 1998, pp. 1246-1253.

[31] S. Vaez, V. I. John and M. A. Rahman, "An On-Line Loss Minimization Controller for Interior Permanent Magnet Motor Drives", *IEEE Trans. on Energy Conversion*, Paper No. PE-I345-EC-0-07-1998.

[32] T. S. Radwan, M. A. Rahman, A. M. Osheiba and A. E. Lashine, "Performance of a Hybrid Current-Controlled VSI Permanent Magnet Synchronous Motor Drive", *IEEE/PESC Conference Record*, 1996, pp.951-957.

[33] R. Krishnan, "Control and Operation of PM Synchronous Motor Drives in the Field Weakening Region", *IEEE/IECON'93 Conference Record, Hawaii*, 1993, pp. 745-750.

[34] S. R. Macminn and T. M. Jahns, "Control Techniques for Improved High–Speed Performance of Interior PM Synchronous Motor Drives", *IEEE Trans. on Industry Applications*, vol. 27, no. 5, Sep./Oct. 1991, pp. 997-1004.

[35] R. Dhanuadi and N. Mohan, "Analysis of Current-Regulated Voltage Source Inverters for Permanent Magnet Synchronous Motor Drives in Normal and Extended Speed Range", *IEEE Trans. on Energy Conversion*, vol. 5, no. 1, March 1990, pp. 137-147.

[36] A. Kumamoto and Y. Hirame, "A Flux-Weakening Method for a Buried Permanent Magnet Motor with Consideration of Parameter Detuning on System Performance", *IPEC Conference Record, Tokyo, Japan*, 1990, pp. 950-955.

[37] I. Choy, T. Yoon, K. Kim, and M. Park, "Microprocessor-Based Permanent Magnet Synchronous Motor Drives using MRAC", *IPEC Conference Record, Tokyo, Japan*, 1990, pp. 481-488.

[38] E. Cerruto, A. Raciti and A. Testa, "A Robust Adaptive Controller for PM Motor Drives in Robotic Applications", IEEE Trans. on Power Electronics, vol. 10, no. 1, Jan. 1995, pp. 62-70.

[39] Y. Sozer and D. A. Torrey, "Adaptive Flux Weakening Control of Permanent Magnet Synchronous Motors", *IEEE/IAS Annual Meeting Conference Record*, 1998, pp. 475-482.

[40] C. Namudri and P. C. Sen, "A Servo-Control System using a Self-Controlled Synchronous Motor (SCSM) with Sliding Mode Controller", *IEEE/IAS Annual Meeting Conference Record*, 1987, pp. 283-295.

[41] A. Consoli and Antonio, "A DSP Based Sliding Mode Field Oriented Control of an Interior Permanent Magnet Synchronous Motor Drive", *IPEC Conference Record, Tokyo, Japan*, 1990, pp. 263-303.

[42] M. Ghirby and H. Le-Huy, "Optimal Control and Variable Structure Combination using Permanent Magnet Synchronous Motor", *IEEE/IAS Annual Meeting Conference Record*, 1994, pp. 408-415.

[43] A. A. El-Samahy, M. A. El-Sarkawi, and S. M. Saraf, "Adaptive Multi-Layer Self-Tuning High Performance Tracking Control for DC Brushless Motor", *IEEE Trans. on Energy Conversion*, vol. 9, no. 2, June 1994, pp.311-316.

[44] R. B. Sepe and J. H. Lang, "Real Time Adaptive Control of the Permanent Magnet Synchronous Motor", *IEEE/IAS Annual Meeting Conference Record*, 1990, pp. 545-552.

[45] Siri Weerasooriya and M. A. El-Sarkawi, "Identification and Control of a DC Motor Using Back Propagation Neural Networks", *IEEE Trans. on Energy Conversion*, vol. 6, no. 4, Dec. 1991, pp. 663-669.

[46] F. M. Khouly, A.S. A. Gaffar, A. A. Mohammed and A. M. Sharaf, "Artificial Intelligent Speed Control Strategies for Permanent Magnet DC Motor Drives", *IEEE/IAS Annual Meeting Conference Record*, 1994, pp. 379-385.

[47] M. A. Rahman and M. A. Hoque, "On-Line Self-Tuning ANN Based Speed Control of a PM DC Motor", *IEEE/ASME Trans. on Mechatronics*, vol. 2, No. 3, Sept. 1997, pp. 169-178.

[48] M. T. Wishart and R. G. Harley, "Identification and Control of Induction Machines using Artificial Neural Network", *IEEE/IAS Annual Meeting Conference Record*, 1993, pp. 703-709.

[49] B. Burton, R. G. Harley, G. Diana and J. L. Rodgerson, "Implementation of a Neural Network to Adaptively Identify and Control of VSI-Fed Induction Motor Stator Currents", *IEEE Trans. on Industry Applications*, vol. 34, no. 3, May/June 1998, pp.580-588.

[50] A. Ba-razzouk, G. Olivier and A. Cheriti, "A Neural Networks Based Field Oriented Control Scheme for Induction Motors", *IEEE/IAS Annual Meeting Conference Record*, 1997, pp. 804–811.

[51] L. Ben-Brahim, K. Shimane, T. Kudor and H. Naitoh, "Implementation of an Induction Motor Estimator using Neural Network", *IPEC Conference Record, Japan*, 1997, pp. 52-57.

[52] B. Burton, F. Kamran, R. G. Harley, G. T. Habetter, M. Broike and R. Poddar, "Identification and Control of Induction Motor Stator Currents using Fast On-Line Random Training of a Neural Network", *IEEE/IAS Annual Meeting Conference Record*, 1995, pp. 1781-1787.

[53] M. A. El-Sarkawi, A. A. El-Samahy and M. L. El-Syed, "High Performance Drive of dc Brushless Motors Using Nerural Network", *IEEE Trans. on Energy Conversion*, vol. 9, no. 2, June 1994, pp. 317-322.

[54] C. Shiguo, D. G. Holmes and W. A. Brown, "Digital Control of a Servo System using Neural Network", *IEEE/IAS Annual Meeting Conference Record*, 1995, pp. 129-133.

[55] M. A. Rahman and M. A. Hoque, "On-Line Adaptive Artificial Neural Network Based Vector Control of Permanent Magnet Synchronous Motors", *IEEE Trans. on Energy Conversion*, vol. 13, no. 4, 1998, pp. 311-318.

[56] L. A. Zadeh, "Outline of a new approach to the analysis of complex system and decision processes", *IEEE Trans. on Syst, Man and Cybern.*, vol. SMC-3, 1973, pp.28-44.

[57] G. S. Buja, "Neural Network Implementation of a Fuzzy Logic Controller", *IEEE/IECON Conference Record*, 1993, pp. 414-417.

[58] G. S. Buja, and F. Todesco, "Neural Network Implementation of Fuzzy Logic Controller", *IEEE Trans. on Industrial Electronics*, vol. 41, no. 6, 1994, pp. 663-667.

[59] P. Lin, S. Hwang and J. Chou, "Comparison on Fuzzy Logic and PID controls for a dc motor position control", *IEEE/IAS Annual Meeting Conference Record*, 1994, pp. 1930-1935.

[60] B. Singh, V. K. Sharma, and S. S. Murthy, "Performance Analysis of Adaptive Fuzzy Logic Controller for Switched Reluctance Motor Drive System", *IEEE/IAS Annual Meeting Conference Record*, 1998, pp. 571-579.

[61] S. Bolognani and M. Zigliotto, "Fuzzy Logic Control of a Switched Reluctance Motor Drive", *IEEE Trans. on Industry Applications*, vol. 32, no. 5, Sept./Oct. 1996, pp. 1063-1068.

[62] H. Henao, G. A. Capolino and M. Poloujadoff, "A Fuzzy Logic Approach to Current Control of Switched Reluctance Motors", *Proceedings of International Conference on Electric Machines, Istanbul, Turkey*, 1998, pp. 131-136.

[63] E. Cerruto, A. Consoli, A. Raciti and A. Testa, "Fuzzy Adaptive Vector Control of Induction Motor Drives", *IEEE Trans. on Power Electronics*, vol. 12, No. 6, Nov. 1997, pp. 1028-1039.

[64] S. A. Mir and D. S. Zinger, "Fuzzy Controller for Inverter Fed Induction Machines", *IEEE/IAS Annual Meeting Conference Record*, 1992, pp. 464-471.

[65] B. K. Bose, N. R. Patel and K. Rajashekara, "A Neuro-Fuzzy Based On-Line Efficiency Optimization Control of a Stator Flux-Oriented Direct Vector-Controlled Induction Motor Drive", *IEEE Trans. on Industrial Electronics*, vol. 44, no. 2, April 1997, pp. 270-273.

[66] I. Miki, N. Nagai and S. Nishiyama and T. Yamada, Vector Control of Induction Motor with Fuzzy PI Controller", *IEEE/IAS Annual Meeting Conference Record*, 1991, pp.341-346.

[67] C.Y. Won, S.C. Kim and B.K. Bose, "Robust Position Control using Fuzzy Logic Control", *IEEE/IAS Annual Meeting Conference Record*, 1992, pp.472-481.

[68] K. Inoue, Y. Takakado and M. Nakaoka, "Auto Tuning Technology for Fuzzy Algorithms Based DC Brushless Servo Systems", *IEEE/PESC Conference Record*, 1993, pp. 446-450.

[69] K. Erenay, I. Ciprut, L. Tezduyar, Y. Istefanopulos, "Application of Fuzzy Algorithms to the Speed Control of Washing Machines with Brushless DC Motors", *Proceedings of International Conference on Electric Machines, Istanbul, Turkey*, 1998, pp. 1231-1236.

[70] Z. Koviac, S. Bogdan and P. Crnosija, "Fuzzy Rule-Based Model Reference Adaptive Control of Permanent Magnet Synchronous Motor", *IEEE/IECON Conference Record*, 1993, pp. 207-212.

[71] F. J. Lin, R. J. Wai and H. P. Chen, "A PM Synchronous Servo Motor Drive with an On-Line Trained Fuzzy Neural Network Controller", *IEEE Trans. on Energy Conversion*, vol. 13, no. 4, December 1998, pp. 319-325.

[72] S. Bolognani and M. Zigliotto, "Hardware and Software Effective Configurations for Multi-Input Fuzzy Logic Controllers", *IEEE Trans. on Fuzzy Systems*, vol.6, no.1, Feb. 1998, pp.173-179.

[73] M. A. Rahman and Ping Zhou, " Field Circuit Analysis of Brushless Permanent Magnet Synchronous Motors", *IEEE Trans. on Industrial Electronics*, vol.43, no.2, April 1996, pp. 256-267.

[74] P. C. Krause, *Analysis of Electric Machinery*, McGraw-Hill Inc., 1986.

[75] T. Sebastian, G. R. Slemon and M. A. Rahman, "Modelling of Permanent Magnet Synchronous Motors", *IEEE Trans. on Magnetics*, vol. MAG-22, no. 5, 1986, pp. 129-134.

[76] D. M. Brod ad D. W. Novotny, "Current Control of VSI-PWM Inverters", *IEEE Transactions on Industry Applications*, Vol. IA-21, No. 4, May/June 1985, pp. 562-570.

[77] Simulink User Guide, The Math Works Inc., 1997.

[78] dSPACE, "Digital Signal Processing and Control Engineering", Manual Guide, Gmbh, Paderborn, Germany, 1997.

[79] M. N. Uddin, T. S. Radwan, G. H. George and M. A. Rahman, "Performance of Current Controllers for VSI-Fed IPMSM Drive", *IEEE Trans. on Industry Applications*, vol. 36, no. 6, paper # MSDAD-S-00-14.

[80] M. A. Rahman, M. N. Uddin, T. S. Radwan and M. A. Hoque, "Intelligent Speed Control of Interior Permanent Magnet Synchronous Motors", *IEEE/IAS Annual Meeting Conference Record*, 1998, pp. 364-370.

[81] B. Sneyers, D. W. Novotny and T. A. Lipo, "Field-Weakening in Buried Permanent Magnet AC Motor Drives," *IEEE Trans. on Industry Appliactions*, vol. IA-21, pp. 398-407, March/April 1985.

[82] M. N. Uddin, T. S. Radwan and M. A. Rahman, "Performance of Interior Permanent Magnet Motor Drive over Wide Speed Range", *Proceedings of IEEE International Electric Machines and Drives Conference*, Seattle, USA, May 1999, pp. 546-548.

[83] D. Driankov, H. Hellendoorn and M. Reinfrank, *An Introduction to Fuzzy Control*, Springer, 1996.

[84] H.T. Nguyen, M. Sugeno, R. Tong and R.R. Yager, *Theoretical Aspects of Fuzzy Control*, John Wiley & Sons, Inc., 1995.

[85] Fuzzy Logic Toolbox User Guide, The Math Works Inc., 1997.

[86] M. N. Uddin and M. A. Rahman, "Fuzzy Logic Based Speed Control of an IPM Synchronous Motor Drive", *Journal of Advanced Computational Intelligence*, vol. 4, no. 2, 2000, paper # JACI-CCECE-S-05.

[87] *LD31 User's Guide*, dSPACE, Paderborn, Germany, Ver. 2, 1996

[88] M. N. Uddin and M. A. Rahman, "A Real-Time Implementation of Fuzzy Logic Controller for Interior Permanent Magnet Synchronous Motor Drive", *Submitted to the IEEE Transaction on Power Electronics for review and publication.*

[89] M. N. Uddin, T. S. Radwan and M. A. Rahman, "Digital Implementation and Performance Analysis of Fuzzy Logic Based vector Control of an Induction Motor Drive", *Proceedings of the IEEE/IAS Annual Meeting Conference*, Rome, Italy, October 8-12, 2000, pp. 1225-1231.

[90] M. N. Uddin, T. S. Radwan and M. A. Rahman, "Fuzzy Logic Based Position Control of Permanent Magnet Synchronous Motor", *Proceedings of the Canadian Conference on Electrical and Computer Engineering (CCECE)*, Halifax, Canada, 2000, pp. 93-97.

[91] M. Vilathgamua, M. A. Rahman and K. J. Tseng, "Nonlinear control of Interior Permanent Magnet Synchronous Motor", *Proceedings of the IEEE/IAS Annual Meeting Conference*, Rome, Italy, October 8-12, 2000, pp. 1115-1120.

APPENDIX- A

IPMSM Parameters

Number of phases = 3

Number of poles = 4

Rated frequency = 60 Hz

Rated power = 1 hp

Rated input line to line voltage = 208 V

q-axis inductance L_q = 0.07957 H

d-axis inductance L_d = 0.04244 H

Stator resistance per phase r_s = 1.93 Ω

Inertia constant J_m = 0.003 Kg.m^2

Rotor damping constant B_m = 0.0008 (N-m)/rad./sec.

Permanent magnet flux linkage ψ_m = 0.314 volts/rad./sec.

Magnet type = Samarium Cobalt

APPENDIX- B

Simulink Subsystems

The details of the subsystem blocks for the simulink schematic of the complete current-controlled voltage source inverter (VSI) fed IPMSM drive as shown in Fig.2.8 have been presented in this appendix. The inputs of the command current generator subsystem (B.1) are command speed ω_r^* and the feedback actual speed of the motor ω_r. The outputs are the command currents IAC, IBC and ICC. The PID controller is used to represent actual PI controller by setting derivative term to zero. The command currents act as inputs to the current controller subsystems (B.2) and (B.3). In current controller subsystems, the relays are used to represent the hysteresis band. The actual motor currents also act as inputs to this subsystem. The outputs of this subsystem are the logic signals NA, NB and NC which are used to turn the inverter switches on and off. The inputs of the inverter subsystem (B.4) are logic signals NA, NB, NC and the dc bus voltage V_B. The outputs of this subsystem are the d-q axis voltages in the stationary reference frame. The coordinate transformation subsystem (B.5) transforms d-q axis voltages from stationary frame to the synchronously rotating rotor reference frame. The d-q axis currents generation subsystem (B.6) generates d-q axis currents in the rotating reference frame from the synchronously rotating d-q axis voltages and motor parameters. The actual current generation subsystem (B.7) generates actual currents ia, ib and ic from the synchronously rotating d-q axis currents and the rotor position angle. The motor output subsystem (B.8) generates the rotor position angle th_e and the motor speed ω_r from the synchronously rotating d^r-q^r axis currents and the motor parameters using the motor dynamics.

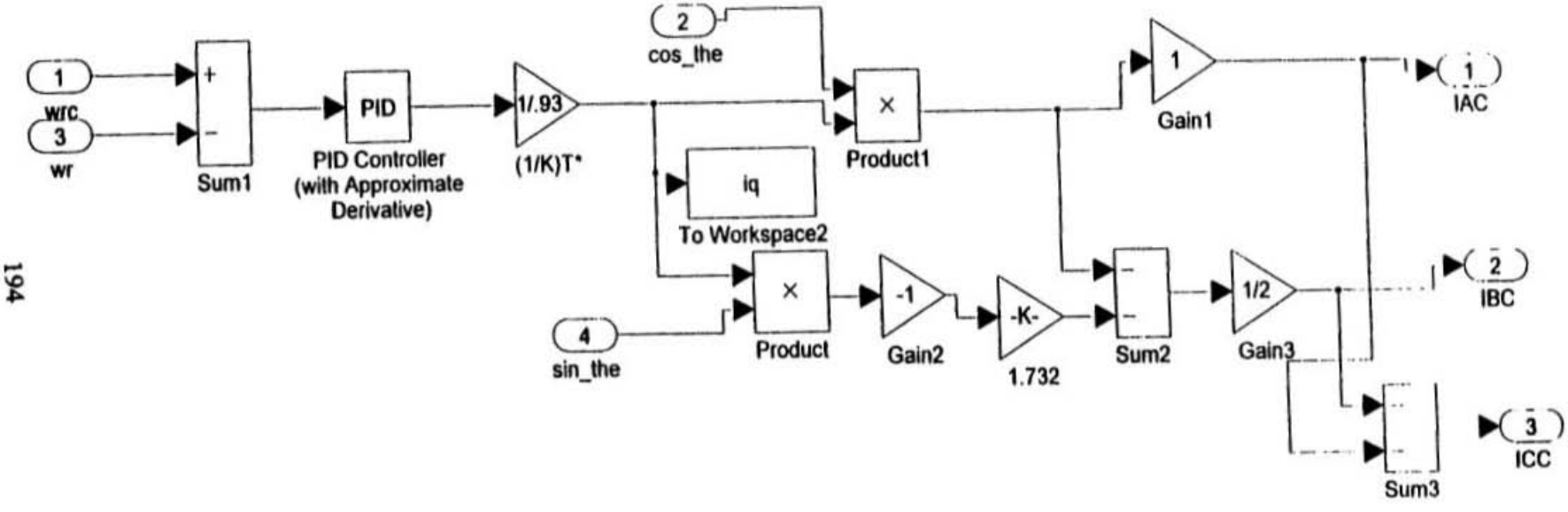

B.1 Command Current Generator Subsystem

B.2 Hysteresis Current Controller Subsystem

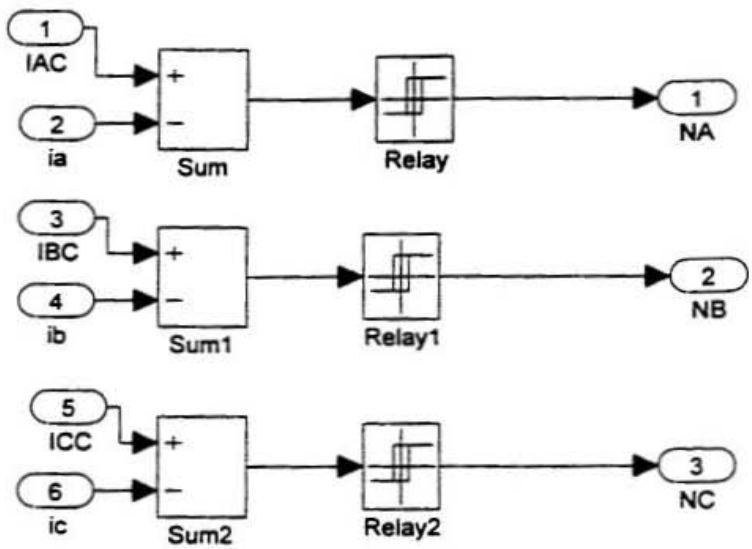

B.3 Ramp Comparator Controller Subsystem

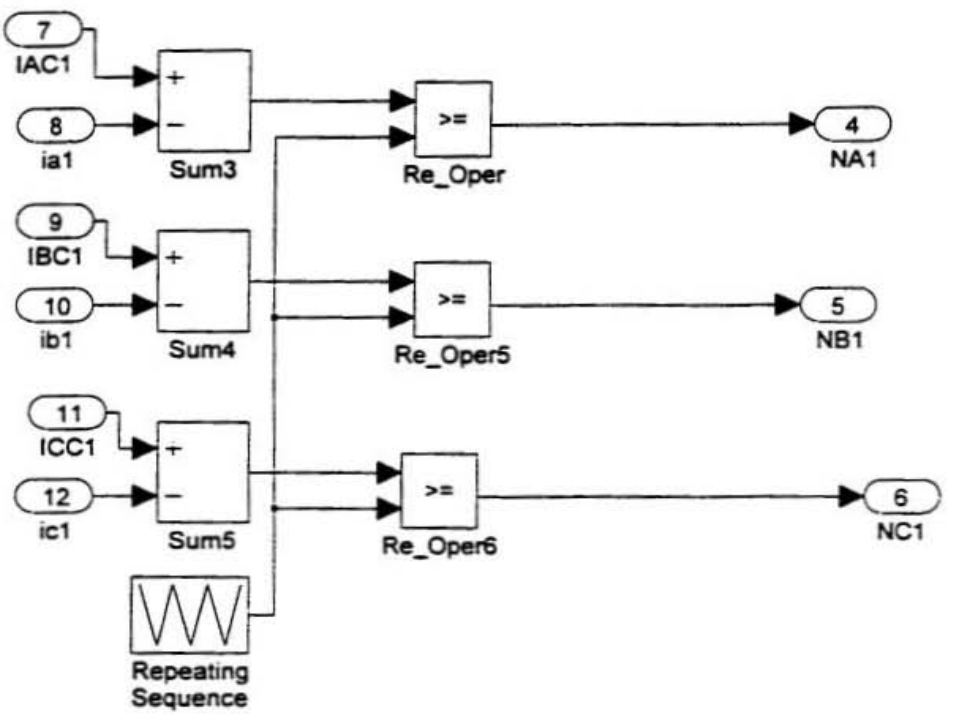

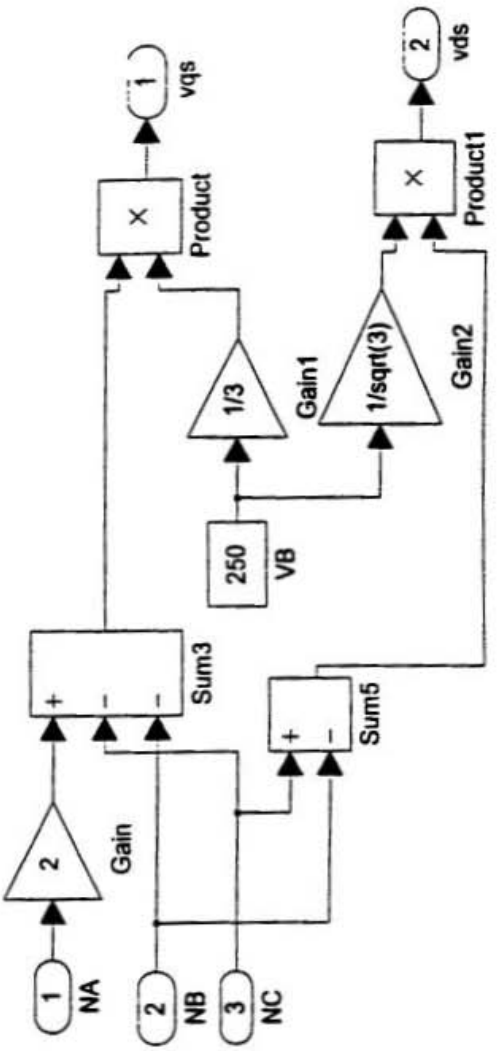

B.4 Inverter Subsystem

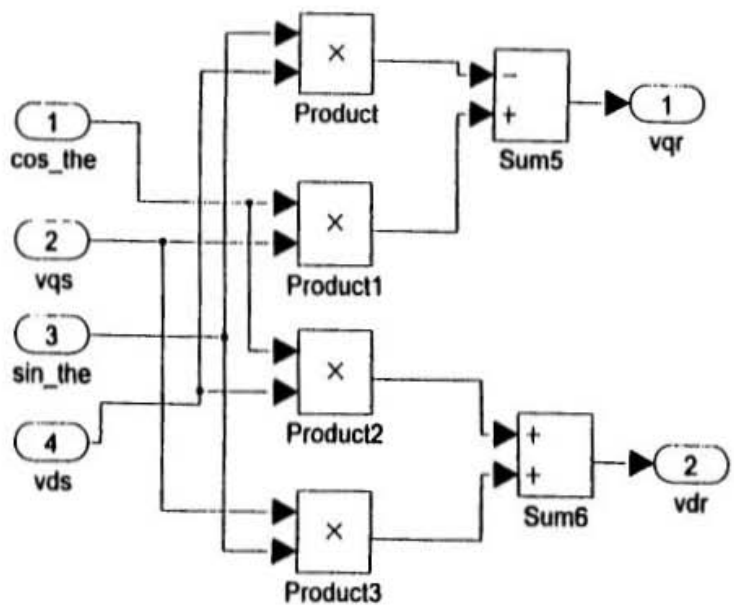

B.5 Coordinate Transformation Subsystem

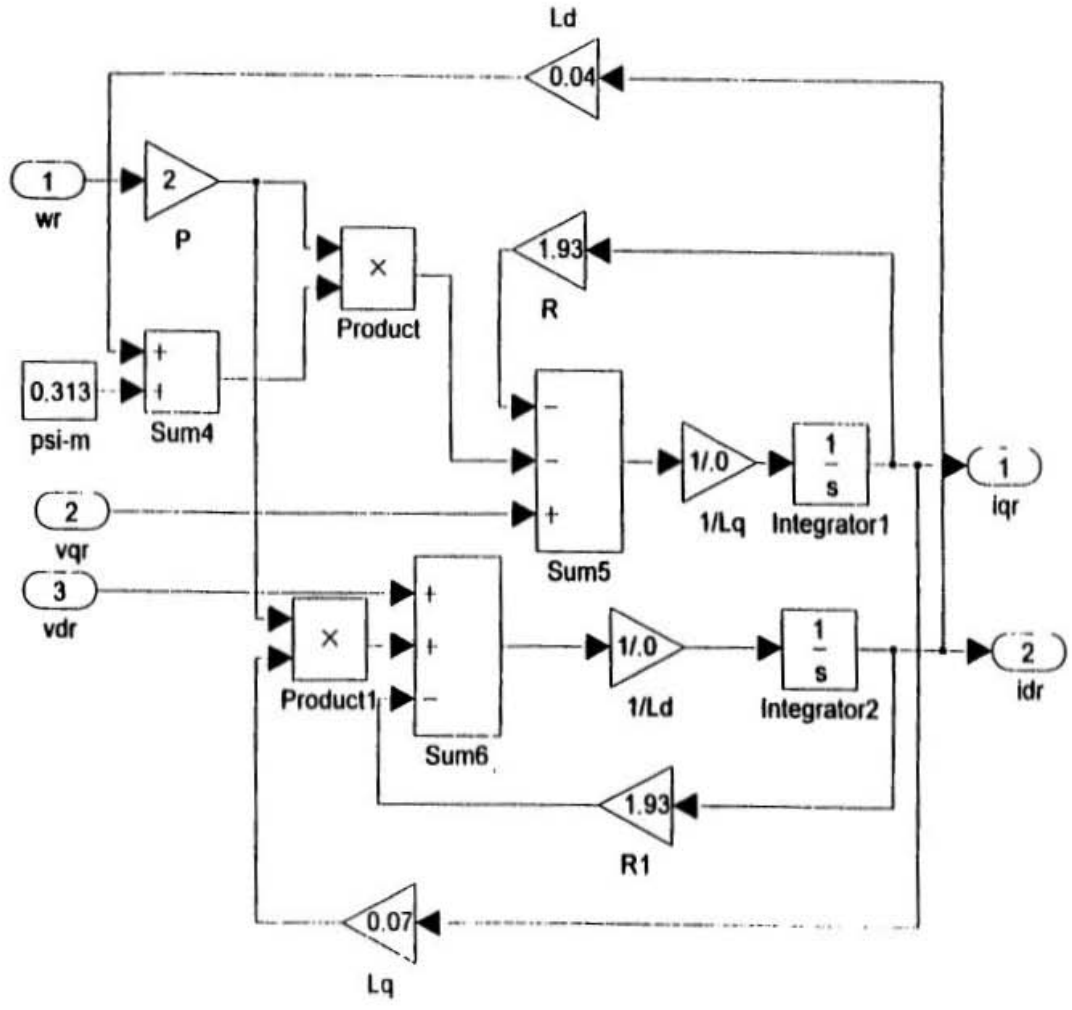

B.6 d-q axis Currents Generation Subsystem

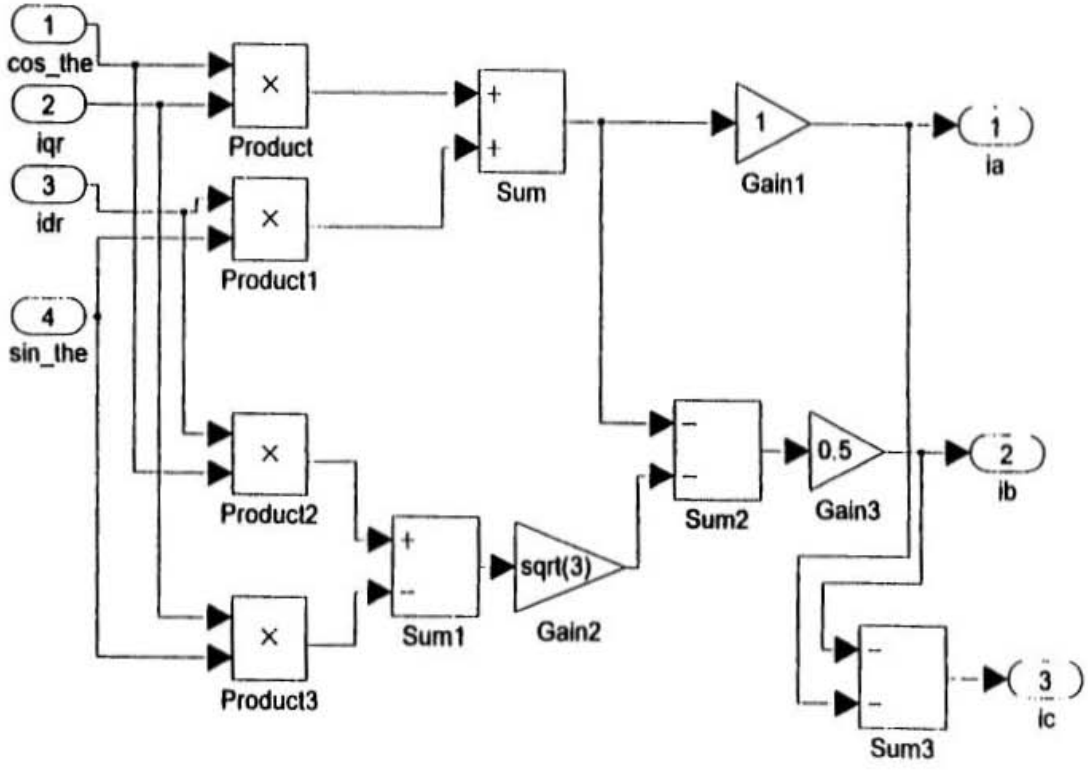

B.7 Actual Current Generation Subsystem

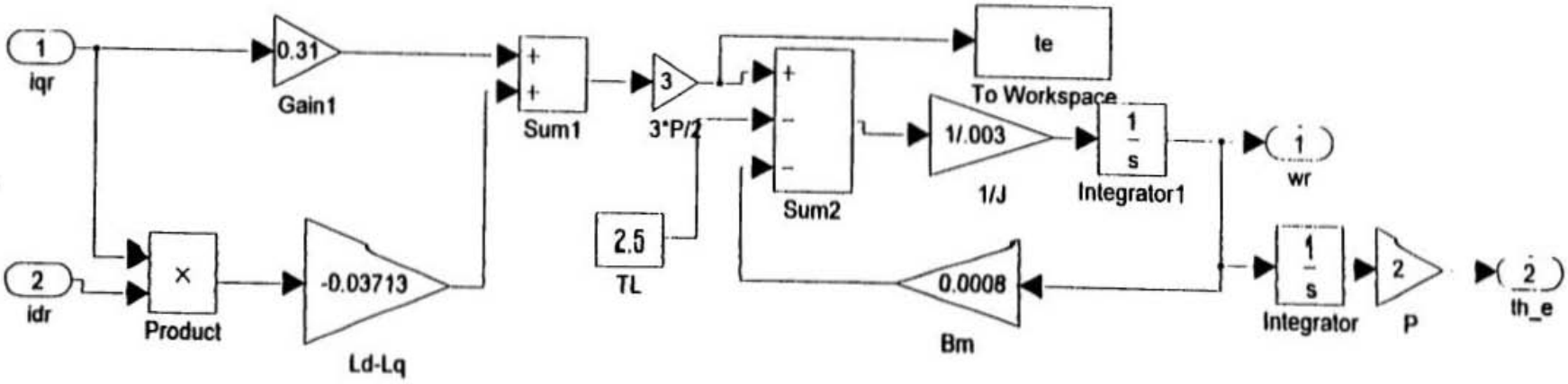

B.8 Motor Output Subsystem

APPENDIX- C

IGBT Inverter

The advantages of bipolar junction transistors (BJTs) and metal-oxide-semiconductor field-effect transistors (MOSFETs) are combined in an insulated gate bipolar transistor (IGBT). An IGBT has high input impedance like MOSFETs and low conduction losses like BJTs. Because of high input impedance the gate draws a very small leakage current. An IGBT has no second breakdown problem like the BJT. An IGBT is made of four alternate PNPN layers. The performance of IGBT is closer to that of a BJT than a MOSFET. A BJT is a current controlled device and requires base current for flowing current in the collector. Since the collector current is dependent on the base current so the current gain is highly dependent on the junction temperature. However, an IGBT is a voltage-controlled device like a power MOSFET. It has lower switching and conduction losses while sharing many of the appealing features of power MOSFETs, such as ease of gate drive, peak current capability and ruggedness. An IGBT is inherently faster than a BJT but slower than a power MOSFET. An IGBT is a three terminal device which are gate, collector and emitter. The current and voltage ratings of a single IGBT can be up to 400 A, 1200 V and the switching frequency can be up to 20 kHz. In order to implement the proposed control scheme an IGBT inverter module has been made in the Power Research Laboratory of Memorial University of Newfoundland (MUN). The schematic of the IGBT inverter module with its snubber circuit is shown in Fig. C.1. Although the IGBT is capable of handling both soft and hard switching but still a snubber circuit has been used to limit the rate of change of voltage across the inverter legs because of unpredictable transient behavior of interior permanent magnet synchronous motor (IPMSM).

R = 25 Ω, 50 W

C = 450 V (D.C), 450 μF

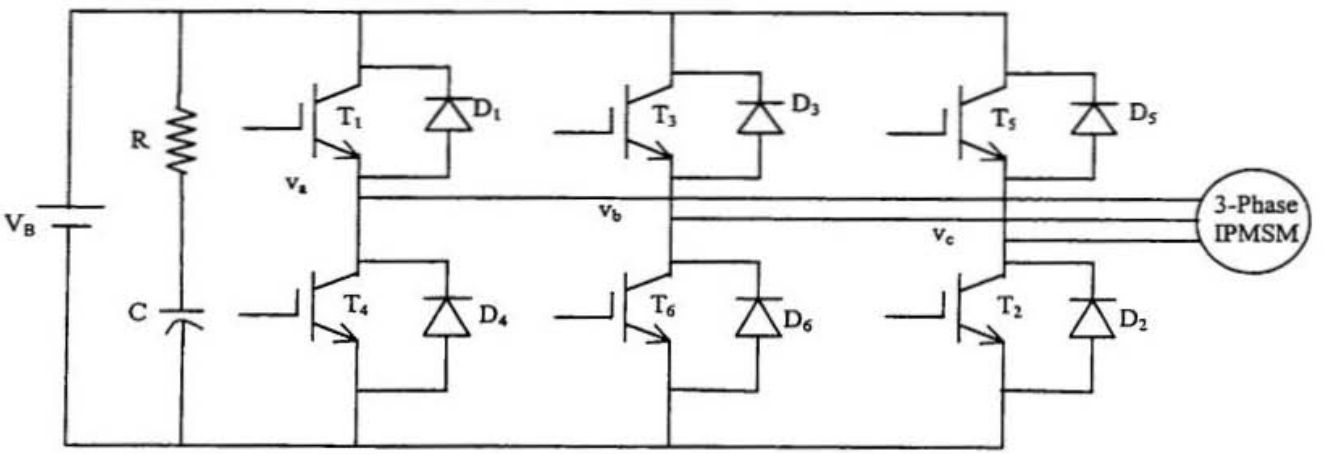

Fig. C.1. Basic circuit of an IGBT inverter module.

C.1 Base Drive Circuits

For operating IGBTs as switches the gate voltage must be appropriate so that the IGBTs are into the saturation for low on-state voltage. The main function of the base drive circuit is to generate six pulses having proper voltage level for the six IGBTs of the inverter. The outputs of the digital I/O subsystem of the DSP board DS 1102 are six pulses having magnitude of 5 V that is not sufficient for the gate drive of IGBTs. Moreover, isolation is needed between the logic circuits and the IGBTs because the logic signal should be applied between the gate and the emitter. So for the high transistors (T_1, T_3 and T_5) the ground of the logic pulses will not be common. Thus a base drive circuit is essential for the inverter to provide an isolation and appropriate voltage to the gate of IGBTs. The base drive circuit, which has been built up in Power research Laboratory of MUN, is shown in Fig. C.2. The chip SN7407N has been used as level shifter that shifts the voltage level from +5V to +15V. The chip HP2531 is an optocoupler, which has been used to provide isolation between the logic circuit and the power circuit of the inverter. The chip IR2130 is the main driver, which provides six driving pulses for the six switches of the inverter. In order to provide +20V isolated power to the optocoupler and the driver an isolated power supply has been built which is also shown in Fig. C.2.

Resistance and capacitor values:

$R_{18\text{-}23} = 22\ \Omega$, $R_{12\text{-}17} = 680\ \Omega$, $R_{5\text{-}10} = 3.3\ \Omega$, $R_{11} = 3.3\ k\ \Omega$

$C_{3\text{-}5} = 10\ \mu F$, $C_{6\text{-}11} = 180\ pF$, $C_{12} = 100\ \mu F$, $C_{13} = 47\ \mu F$

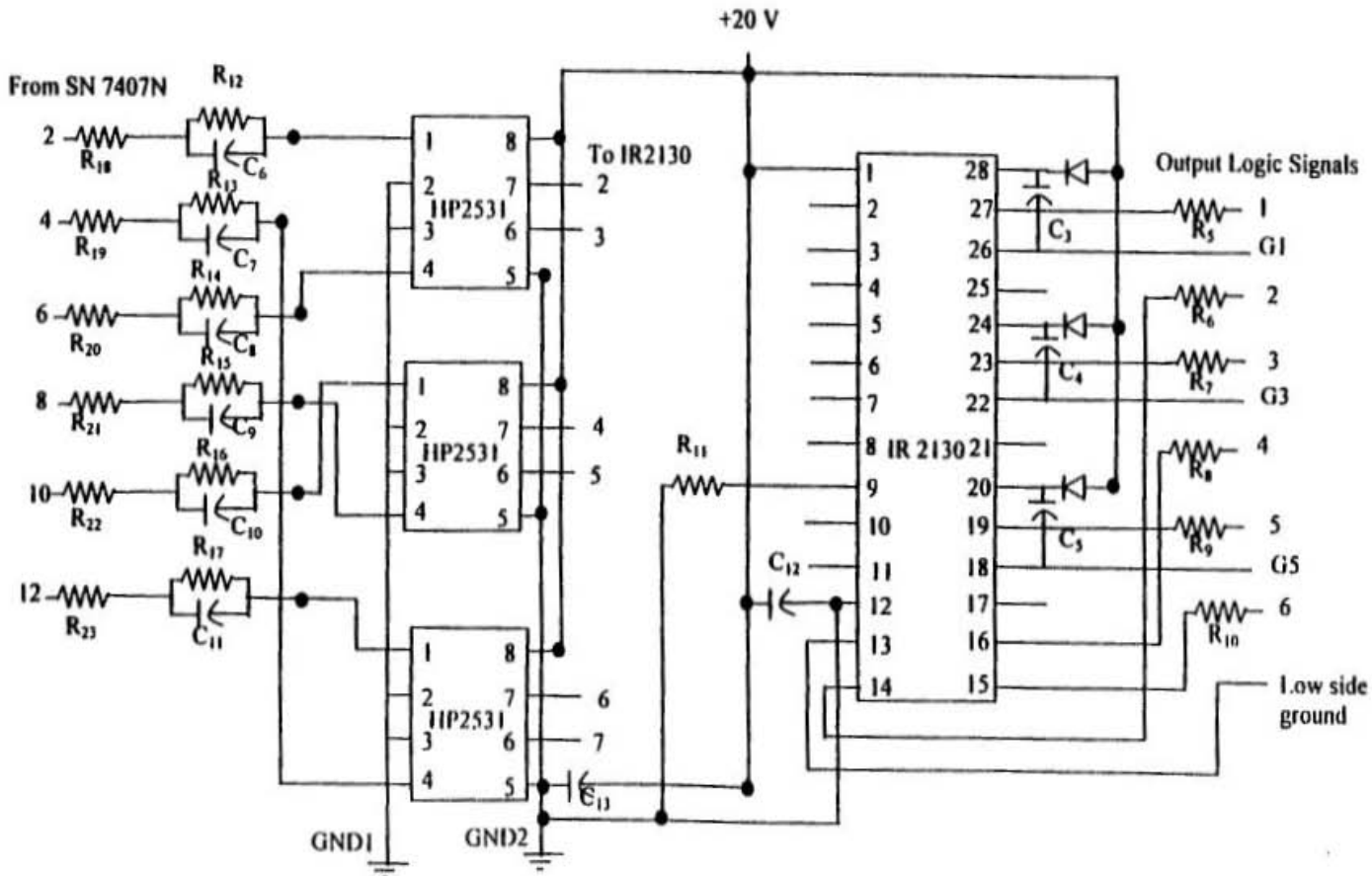

Fig. C.2. Base drive circuits.

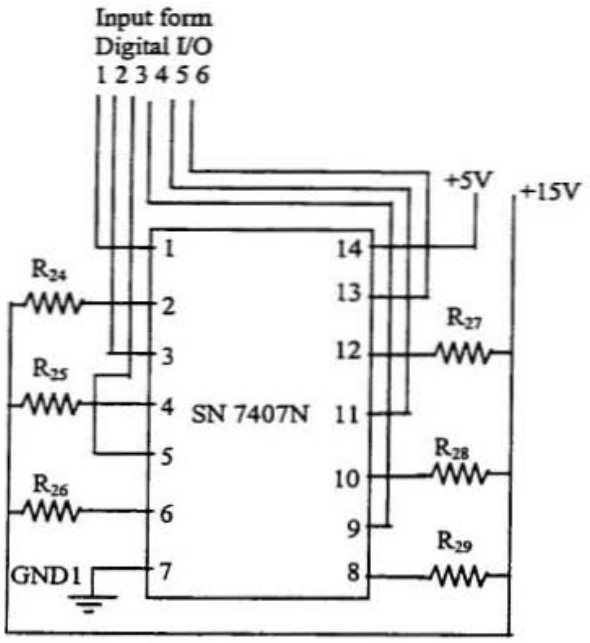

Resistance and capacitor values:

$R_{24\text{-}29} = 1.5\ k\Omega$, $R_1 = 1.1\ k$, $R_4 = 3.3\ k\Omega$

$C_1 = 2200\ \mu F$, $C_2 = 10\ \mu F$

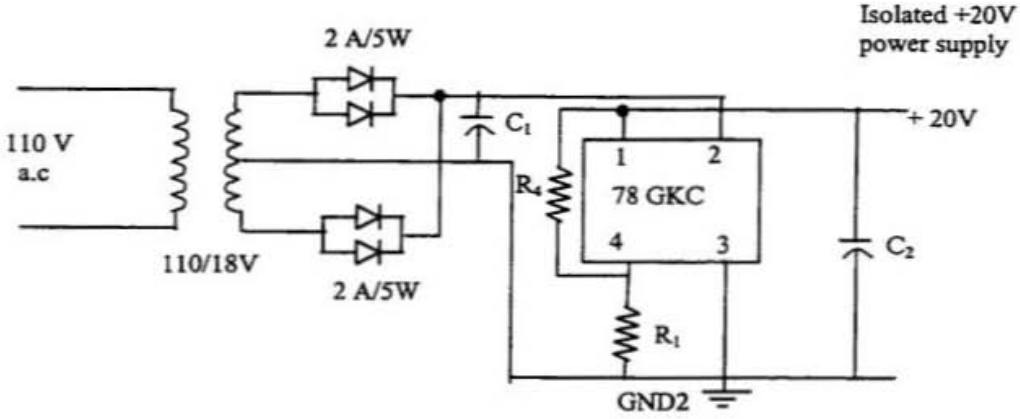

Fig. C.2. Base drive circuits. (Continued)

APPENDIX-D

Real-Time Simulink Model for IPMSM Drive

The Simulink model can be directly used for real-time applications using the software real-time interface (RTI) supplied by the dSPACE. The RTI's board library provides Simulink blocks representing the dSPACE I/O hardware. The complete system Simulink diagram is shown in Fig. D.1. It is shown in this figure that the board DS1102 has two incremental encoders but encoder 1 is used in this work. The encoder 2 is terminated by a terminator. The subsystem representing the fuzzy logic controller is shown in Fig. D.2. This is a subsystem within the main subsystem Ref_curr (reference currents generator). The other subsystems are similar to the subsystems given in Appendix-B. The A/D converters 3 and 4 are used to read the actual motor currents from phase 'a' and 'b'. The other two A/D converters are terminated. The logic signals which are the outputs of the Hys_cnt (hysteresis current controller) subsystem are coming out through the digital I/O ports. The output ports are used from the RTI library and the number of channel is selected according to the configuration desired. The signals to be captured by the stored oscilloscope are fed to the D/A ports of the board.

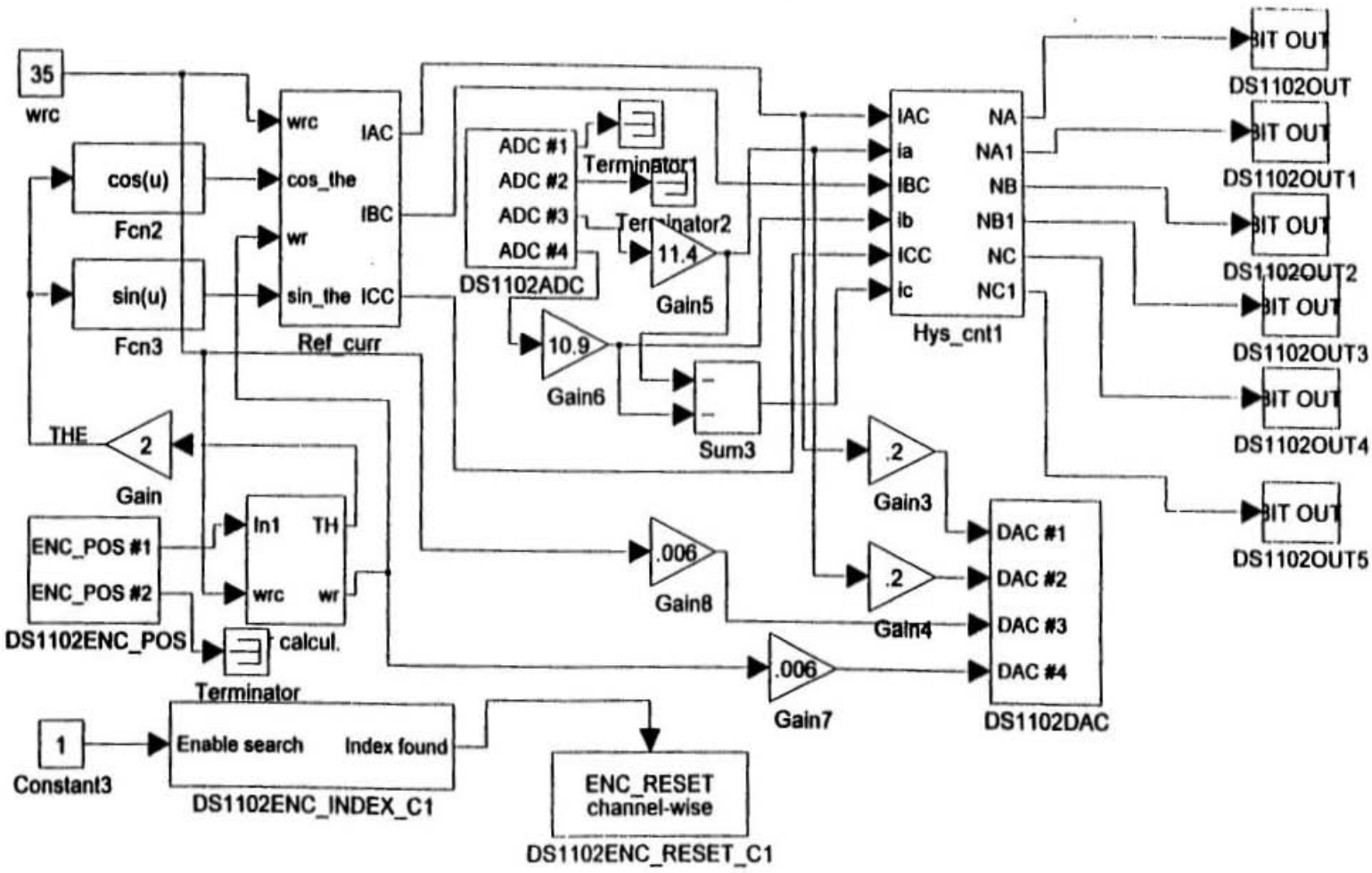

Fig. D.1. Real-Time Simulink Model for the FLC based vector control of IPMSM drive.

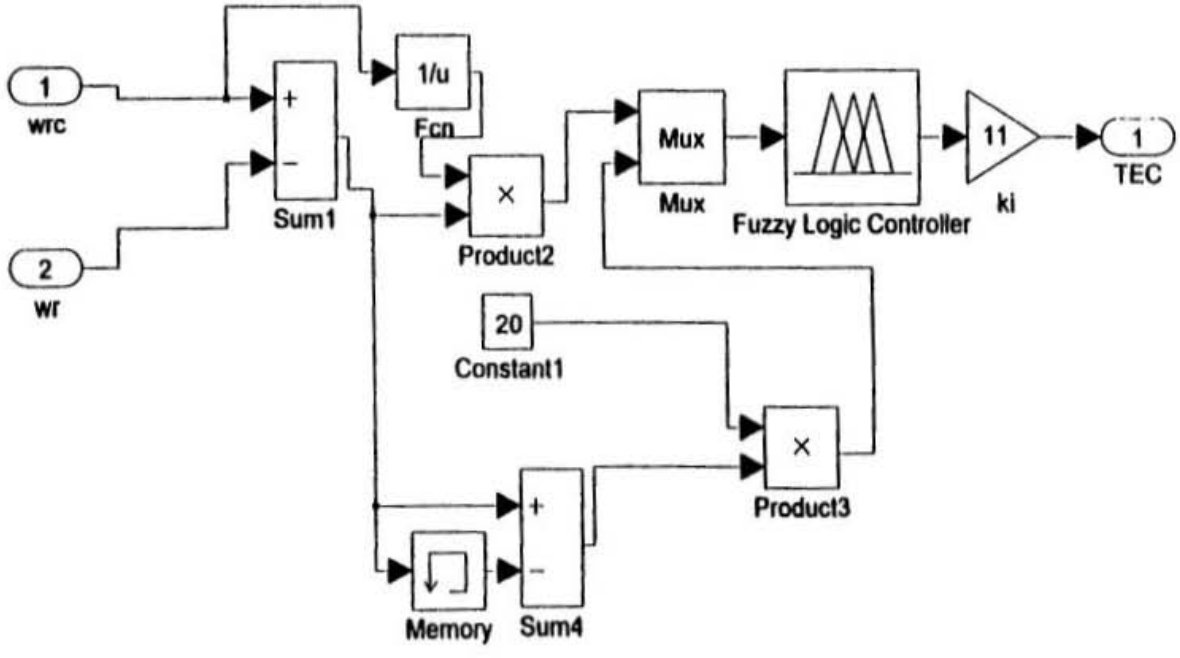

Fig. D.2. Simulink subsystem representing the fuzzy logic controller.

APPENDIX-E

START.C

```
/* start.c ********************************************************
          Instruction to compile with Borland C: bus version:
                    bcc /ml start.c bcdclib.lib
*****************************************************************/

#include <stdlib.h>
#include <stdio.h>
#include <clib.h>      /* Host-DSP interface library include file */
#define DP_MEM_OFFS 1 /* use first dual-port memory address */

float number;
unsigned int board_index;
void close_and_exit (int error_code)
{
    DSP_unregister_host_app();
    exit(error_code);
}

void write_dual_port_memory (UInt32 address, UInt32 value)
{
    int error;
    error = DSP_lock_board(board_index);
    if(error != DSP_NO_ERROR)
    {
      printf("Error: can't lock board  error = %d.\n\n",error);
      close_and_exit(5);
    }
   error = DSP_write_dual_port_memory(board_index, address, value);
    DSP_unlock_board(board_index);
    if(error != DSP_NO_ERROR)
    {
printf("Error %d writing the DSP board's dual-port memory !\n\n",
              error);
      close_and_exit(5);
    }
}

void main (int argc, char *argv[])
{
    int error;

    printf("\n start  ``The motor allready started...''\n\n");

    if(argc != 2)
    {
```

```
        printf("Usage: start board\n\n");
        exit(1);
      }

      error = DSP_register_host_app("start");
      if(error != DSP_NO_ERROR){
        switch(error){
          case DSP_DEVICE_DRIVER_NOT_FOUND:
            printf("\nDevice Driver not installed.\n");
            break;
          case DSP_VXD_NOT_LOADED:
            printf("\nVirtual device driver not installed.\n");
            break;
          case DSP_NO_FREE_HOST_APP_IDX:
            printf("\nNo free host application index.");
            break;
#ifdef NET
          case DSP_NET_ERROR:
            printf("\nNetwork error.");
            break;
#endif
          default:
            printf("\nDSP_register_host_app: error code %d\n",error);
            break;
        }
        exit(1);
      }

      error = DSP_board_index(argv[1],&board_index);
      if(error != DSP_NO_ERROR)
      {
        printf("\nBoard %s not registered, error = %d.\n",
               argv[1],error);
        close_and_exit(2);
      }

      /* initialize output signal with 0.0 */
      write_dual_port_memory(DP_MEM_OFFS,
                             DSP_cvt_ieee_to_ti((Float32) 0.0));

      /* set output signal to start */
printf("\n please enter any number except 0 to finsh starting proc-
ess...\n");
      scanf("%f", &number);
      write_dual_port_memory(DP_MEM_OFFS,
               DSP_cvt_ieee_to_ti((Float32) number));

      printf("Press RETURN to abort ...\n");
      rewind(stdin);
      getchar();

      close_and_exit(0);
}
```

APPENDIX-F

DSPEED.C

```
/* dspeed.c ************************************************************
       Instruction to compile with Borland C: bus version:
              bcc /ml dspeed.c bcdclib.lib
**********************************************************************/
#include <stdlib.h>
#include <stdio.h>
#include <clib.h>     /* Host-DSP interface library include file */
#define DP_MEM_OFFS 0  /* use first dual-port memory address */
unsigned int board_index;
float speed,delta_speed;
void close_and_exit (int error_code)
{
    DSP_unregister_host_app();
    exit(error_code);
}

void write_dual_port_memory (UInt32 address, UInt32 value)
{
    int error;
    error = DSP_lock_board(board_index);
    if(error != DSP_NO_ERROR)
    {
      printf("Error: can't lock board  error = %d.\n\n",error);
      close_and_exit(5);
    }
   error = DSP_write_dual_port_memory(board_index, address, value);
    DSP_unlock_board(board_index);
    if(error != DSP_NO_ERROR)
    {
printf("Error %d writing the DSP board's dual-port memory !\n\n",
              error);
      close_and_exit(5);
    }
}

void main (int argc, char *argv[])
{
    int error;
printf("\n dspeed "change speed reference from key board...
''\n\n");
    if(argc != 2)
    {
      printf("Usage: dspeed board\n\n");
      exit(1);
    }
```

```
    error = DSP_register_host_app("dspeed");
    if(error != DSP_NO_ERROR){
      switch(error){
        case DSP_DEVICE_DRIVER_NOT_FOUND:
          printf("\nDevice Driver not installed.\n");
          break;
        case DSP_VXD_NOT_LOADED:
          printf("\nVirtual device driver not installed.\n");
          break;
        case DSP_NO_FREE_HOST_APP_IDX:
          printf("\nNo free host application index.");
          break;
#ifdef NET
        case DSP_NET_ERROR:
          printf("\nNetwork error.");
          break;
#endif
        default:
          printf("\nDSP_register_host_app: error code %d\n",error);
          break;
      }
      exit(1);
    }

    error = DSP_board_index(argv[1],&board_index);
    if(error != DSP_NO_ERROR)
    {
      printf("\nBoard %s not registered, error = %d.\n",
             argv[1],error);
      close_and_exit(2);
    }

    /* initialize output signal with 0.0 */
    write_dual_port_memory(DP_MEM_OFFS,
                           DSP_cvt_ieee_to_ti((Float32) 0.0));

    /* set output signal to speed */
    do{
    printf("\n please enter the delta_speed in rpm...\n");
    scanf("%f", &delta_speed);
    speed=delta_speed*0.104719755;
    write_dual_port_memory(DP_MEM_OFFS,
                           DSP_cvt_ieee_to_ti((Float32) speed));
    } while (delta_speed!=0.0);
    printf("Press RETURN to abort ...\n");
    rewind(stdin);
    getchar();

    /* reset output signal to 0.0 */
    write_dual_port_memory(DP_MEM_OFFS,
                           DSP_cvt_ieee_to_ti((Float32) 0.0));

    close_and_exit(0);
}
```